Phytochemical analysis of Baby Banana peels (*Musa acuminata*) in relation with a hyperpigmentation phenomenon

Von der Fakultät für Lebenswissenschaften

der Technischen Universität Carolo-Wilhelmina

zu Braunschweig

zur Erlangung des Grades

einer Doktorin der Naturwissenschaften

(Dr. rer. nat.)

genehmigte

D i s s e r t a t i o n

von Marcela Elizabeth Castro Benitez
aus Bogotá /Kolumbien

1. Referent: Prof. Dr. Peter Winterhalter
2. Referent: apl. Professor Dr. Ulrich Engelhardt
eingereicht am: 28.01.2015
mündliche Prüfung (Disputation) am: 26.03.2015

Druckjahr 2015

Vorveröffentlichungen der Dissertation

Teilergebnisse aus dieser Arbeit wurden mit Genehmigung der Fakultät für Lebenswissenschaften, vertreten durch den Mentor der Arbeit, in folgenden Beiträgen vorab veröffentlicht:

Tagungsbeiträge

Castro-Benitez, M. and Winterhalter, P.: Preparative spiral coil (LSRCCC) application method for the phytochemical analysis of Baby banana peels (*Musa acuminata)* with hyperpigmentation. (Oral Presentation). XV Congreso Latinoamericano de Cromatografia y Técnicas Afines. Cartagena. Colombia. Septiembre 29th al Octubre 3rd (2014). Proceeding abstract Part 1, O-IN-04.

Castro-Benitez, M. and Winterhalter, P.: Optimization of the solvent system for the separation of chlorophylls and derivatives by means of High-Speed countercurrent chromatography in Baby banana peels, spinach and grass. (Oral Presentation) XV Congreso Latinoamericano de Cromatografia y Técnicas Afines. Cartagena. Colombia. Septiembre 29th al Octubre 3rd (2014). Proceeding abstract Part 1, O-PN-05.

Poster

Castro-Benitez, M. and Winterhalter, P.: The role of chloroform and dichloromethane as stationary phase in the solvent system for the isolation of chlorophylls and xantophylls in plants by High Speed Countercurrent Chromatography. (Poster) 8th International Conference on Countercurrent Chromatography, London, UK, July 23-25 (2014). Proceeding abstract p.195.

Castro-Benitez, M. and Winterhalter, P.: Preparative Spiral Coil-LSRCCC Application Method for the Phytochemical Analysis of Baby Banana Peels (*Musa acuminata)* with Hyperpigmentation. (Poster) 8th International Conference on Countercurrent Chromatography*,* London, UK, July 23-25 (2014). Proceeding abstract p.194.

Castro-Benitez, M. and Winterhalter, P.: In the search of chlorophylls in Baby banana peels and plants by means of High-Speed Countercurrent Chromatography. (Poster) 8th International Conference on Countercurrent

Chromatography, London, UK, July 23-25 (2014). Proceeding abstract p. 167.

Castro-Benitez, M., Burmeister, A., Wilde, A., Winterhalter, P.: Partial isolation of chlorophyllase enzyme and proteins in Baby banana peels (*Musa acuminata*) from Colombia. (Poster). 5. Jahrestreffen Seniorexperten Chemie. Braunschweig 6.-8. Mai (2014).

Castro-Benitez, M. and Winterhalter, P.: In the search of chlorophylls in Baby banana peels and plants by means of High-Speed Countercurrent Chromatography (Poster). Doktoranden-Kolloquium des Fachbereichs Chemie an der TU Braunschweig. (Poster). 5. Braunschweiger Jungchemiker Tagung. Braunschweig, 15. April (2014). Proceeding abstract p. 33

Castro-Benitez, M., Timpe, M., Winterhalter, P.: Isolation of Phospholipids, Glycolipids and Fatty acids from Baby Banana Peels (*Musa acuminata*) on a Preparative Scale by Means of High-Speed Countercurrent Chromatography. (Poster). Regionalverbandstagung Nord der Lebensmittelchemischen Gesellschaft. Hamburg School of Food Science, Hamburg, 24./25.3. 2014.

Castro-Benitez, M., Willeke, O., Timpe, M., Wilde, A., Winterhalter**.** P.: High Speed countercurrent chromatography for analysis of Chlorophylls *a/b* ratio and their derivates in plants. (Poster). 42. Deutscher Lebensmittelchemikertag. Braunschweig, 16.-18.9. (2013). Abstract in Kurzreferate-Band ANA 045, 151 (2013)

Castro-Benitez, M., Muñoz-Ortuño, M., Winterhalter P.: Isolation of Chlorophyll *a*, Chlorophyll *b* and Pheophytin a on a Preparative Scale using High Speed Countercurrent Chromatography. (Poster). 41. Deutscher Lebensmittelchemikertag. Westfälische Wilhelms-Universität Münster, 10.-12.9. (2012). Abstract in Lebensmittelchemie 67(5), 114 (2013).

Castro-Benitez, M., Jerz, G., Winterhalter, P.: Isolation of cycloartane-type triterpenes from fruit peel of baby banana (*Musa acuminata*) by means of High-Speed countercurrent chromatography (Poster). 39. Deutscher Lebensmittelchemikertag. Stuttgart-Hohenheim, 20.-22.9. (2010). Abstract in Lebensmittelchemie 65(2), 31 (2011), erratum Lebensmittelchemie 65(4) 81 (2011).

Danksagungen

Die vorliegende Arbeit wurde im Rahmen des länderbezogenen Stipendienprogramms ALECOL durchgeführt und gründet sich auf die Kooperationsvereinbarung zwischen dem Deutschen Akademischen Austauschdienst (DAAD) und der Pontificia Universidad Javeriana Bogotá, Kolumbien (Stipendium-Kennziffer: A/06/32945).

Ich möchte auf Deutsch schreiben: **Dankeschön**; weil Deutschland **meine „Akademische Heimat"** ist. Ich lernte, als Doktorandin, im Institut für Lebensmittelchemie, TU-Braunschweig, was das Wort „Wissenschaft" bedeutet. Ein großer Dank gilt allen, die mich während dieser Zeit unterstützt haben.

Lieber Herr Prof. Dr. Peter Winterhalter, meinen herzlichsten Dank, dass ich bei Ihnen meine Dissertation anfertigen durfte. Vielen Dank für das entgegengebrachte Vertrauen und die Unterstützung.

Le agradezco mucho Profesor Dr. P. Winterhalter por permitirme ser parte de su grupo de investigación y por darme la posibilidad de aprender. Usted es un gran ejemplo para mi de cómo debe ser un buen Profesor. Me llevo esta enseñanza en mi corazón y la voy a difundir en Colombia. Gracias por todo. Nunca olvidaré mis gratos momentos en el Instituto. Gracias a usted Alemania es maravillosa y siempre deberá recordar que para usted y mi afectuosa Evelyn, nuestro hogar en Colombia es vuestro hogar, por siempre.

Ein besonders großes Dankeschön an Frau Carola Balcke für ihre Hilfsbereitschaft, die vielen Korrekturen während der Jahre und die sorgfältige Durchsicht meiner schriftlichen Arbeit. Ich könnte nicht, ohne Ihre Unterstützung, hier etwas erreichen. Liebe Frau Balcke, ich danke auch für Ihre Freundschaft und Geduld.

Meinen Dank gilt ebenfalls Prof. Dr. Petra Mischnick und ihrer Arbeitsgruppe, inbesondere Frau Qimeng Zhang, Frau Julia Cuers, Herrn Marko Rother, Herrn Christian Bork, Frau Kristin Voiges und Frau Sheetal Gangula für die Unterstützung bei der Charakterisierung der Glycolipide und konstruktive Diskussionen.

Dem Arbeitskreis Winterhalter und dessen Ehemaligen gilt mein Dank für die nette Arbeitsatmosphäre. Vielen Dank Dr. Sebastian Tolle, Dr. Andreas Juadjur, Dr. Fabian Weber und Dr. Kathrin Ronneburg für Eure Geduld mit meinen Fragen!!

Ein besonderer Dank geht an Frau Stefanie Kuhnert, Frau Anne-Katrin Tschira, Herrn Ulf Stodt, Dr. Nils Kaiser und Frau Claudia Thräne für die vielseitige Unterstützung und tolle Zeit, insbesondere Dr. Tuba Esatbeyoglu, Dr. Stephanie Trebst, Dr. Yumen Hilal, Dr. Andrea Wilkens, Dr. Inga Unterieser, Dr. Christian Laue für die schönen Momente außerhalb der Uni. Frau Eva Schmalfuß, Frau Margret Brüggemann, Frau Rouba Horanni, Herrn Philipp Ewald, Herrn Recep Gök, Dr. Sebastian Macke und Frau Annika Burmeister danke ich für Eure Hilfe und vor allem Eure Begleitung.

Frau Tille-Lauckner, Frau Beate Maiwald, Frau Marita Baum, Frau Monika Messerer und Frau Silke Lehmann danke ich für die schnelle Lösung aller Probleme und auch für Eure besondere Freundschaft. Sie bleiben in meinem Herz.
Besonders hervorheben möchte ich:
- Dr. Peter Fleischmann danke ich für die konstruktiven Gespräche.
- NMR-Spektren: Dr. Kerstin Ibrom und Frau Petra Holba Schultz danke ich für die große Unterstützung.
- Herrn Oliver Willeke, Frau Amelie Wilde und Frau Mira Timpe danke ich für die praktische Unterstützung dieser Arbeit.
- Gäste: Un especial agradecimiento por el entusiasmo e invalubale apoyo que me brindaron durante vuestra estancia en el Instituto a Maria Muñoz (mi Maria), Aida Mezquida (mi Aida), Dr. Fernanda das Neves Costa (mi querida amiga y consejera), Dr. Monica Schwarz y Dr. Ana Maria Sanchez.
- Braunschweiger Wach- und Schließgesellschaft: Herr Thomas Kötz

Meiner lieber Familie: los adoro, y te agradezco **mi Umañosky** que me hayas apoyado en este camino, gracias a ti he llegado al final. Mi amor lindo, **Diego**, gracias por existir en nuestra vida. **Noche**, **Tobita y Mitsu**, nuestra amorosa y cálida compañía en Alemania. **Gracias.**

Zusammenfassung und Ausblick

Der Grad der Grünfärbung einer Banane wird durch Chlorophyll-Pigmente bestimmt und ist wichtig, um die Qualität im Zeitraum nach der Ernte festzustellen. Deshalb wurde in der vorliegenden Studie das Phänomen der Hyperpigmentierung, die an Schalen einiger Babybananen (*Musa acuminata AA Simmonds cv. Bocadillo*) aus Kolumbien beobachtet wurde, untersucht.

Wenn die Frucht das Stadium der grünen Reife erreicht, erscheinen schmale, grüne Streifen, die wieder verschwinden, sobald die Carotinoide zu den Hauptbestandteilen der Schale werden. Dieses Verschwinden kann mit einem Abbau des Chlorophylls in Zusammenhang gebracht werden, wie die Ergebnisse der vorliegenden phytochemischen Untersuchung zeigen.

Aus den Schalen von Babybananen wurden Chlorophyll *a* (Chl *a*), Chlorophyll *b* (Chl *b*) und Pheophytin *a* (Phy *a*) mittels Hochgeschwindigkeits-Gegenstromverteilungschromatographie (engl. High-speed countercurrent chromatography, HSCCC) und einem neuentwickelten Fließmittelsystem bestehend aus Hexan/EtOH/CH_2Cl_2/H_2O (6:2:4:2 *v/v/v/v*) isoliert. Dieses Fließmittelsystem ermöglicht die Ermittlung des Verhältnisses der Chlorophylle *a/b* sowie ihrer Derivate sowohl in Bananenschalen als auch in Gras und Spinat. Die Ergebnisse zeigten einen erheblichen Unterschied in der Pigmentzusammensetzung zwischen Babybananen mit Hyperpigmentierung und einer Babybananen-Kontrollgruppe.

Die Verhältnisse zwischen Chl *a/b* und Phy *a/b* in der Kontrollgruppe und in den hyperpigmentierten Bananen lassen darauf schließen, dass die Babybananen-Kontrollgruppe während des Abbauprozesses eine umgekehrte Chl-*b*-Biosynthese nutzt, um ausschließlich Chl-*a* zu produzieren, wohingegen Bananen mit Hyperpigmentierung kein Chl-*a* aufweisen und stattdessen Chl-*b* anreichern.

Laut aktuellen Veröffentlichungen finden Abbaumechanismen des Chlorophylls nicht nur in Chloroplasten/Gerontoplasten statt, sondern durch die Phäophorbid-*a*-Oxygenase (PaO) auch im Cytosol und in Vakuolen. Dieser

Vorgang führt zu einer Produktion von fluoreszierenden (Mc-FCC) und nicht-fluoreszierenden (NCCs) Chlorophyll-Kataboliten. Die Bevorzugung des Phäophorbids *a* gegenüber Phäophorbid *b* als Substrat von PaO liegt darin begründet, dass Phäophorbid *b* ein kompetitiver Inhibitor des PaO ist. Deshalb ist die Umsetzung des Chlorophylls *b* nötig, um Chlorophyll *a* zu erhalten.

Diese Ergebnisse könnten die Akkumulation von Chl-*b* in Babybananenschalen mit Hyperpigmentierung sowie das mit 0.86 geringere Verhältnis von Phy *a/b* im Vergleich zu 3.06 in der Kontrollgruppe erklären. Der Unterschied im Verhältnis von Phy *a/b* resultiert aus dem geringeren Anteil Phy *b* in der Babybananen-Kontrollgruppe verglichen mit dem hohen Gehalt von Phy *b* in den hyperpigmentierten Bananen.

Enzyme spielen während des Chlorophyllabbaus eine entscheidende Rolle, weshalb eine Methode zur Isolierung von Chlorophyllase-Enzym und- Proteinen in Babybananen angewandt wurde (siehe 4.3.6). Mittels SDS/PAGE wurden in den Extrakten aus Babybananenschalen ohne Hyperpigmentierung Proteinbanden in einem Bereich von 20 kD bis 37 kD gefunden. Aufgrund der Übereinstimmung sowohl mit der in der Literatur beschriebenen 25 kDa-Proteinbande als auch dem 35 kDa-Molekulargewicht des erhitzten Enzym-Proteins können diese der Chlorophyllase zugeordnet werden (Harpaz-Saad et al. 2007, Trebitsh et al. 1993). Weitere Studien sind nötig, um diese Ergebnisse mit dem Protein-Screening eines Extraktes aus hyperpigmentierten Babybananen zu vergleichen.

Mittels Spiral-Coil LSRCCC konnten 17 g eines Hexanextraktes aus hyperpigmentierten Babybananenschalen unter Verwendung des Fließmittelsystems Acetonitril/Hexan (1:1 *v/v*) fraktioniert werden. Chlorophyllderivate wurden im Elution-Extrusion-Modus eluiert (polar→unpolar). Diese Extraktionsmethode erhöht die Phäophytinisierung. Ferner zeigten Messungen mittels APCI-HPLC-MS, dass die Methode für derartige Inhaltsstoffe mit polaren und unpolaren Gruppen geeignet ist.

Weitere Untersuchungen via Spiral-Coil LSRCCC erscheinen sinnvoll, um bewerten zu können, wie sich das Verhältnis von Chlorophyll *a/b* unter

Anwendung der zweiten Extraktionsmethode verhält, die den vollständigen Chlorophyllabbau durch das neue Fließmittelsystem Hexan/EtOH/CH_2Cl_2/H_2O (6:2:4:2 *v/v/v/v*) verhindert.

Die Strukturaufklärung der in Fraktion 14 der Spiral-Coil LSRCCC-Trennung von hyperpigmentierten Babybananenschalen enthaltenen Tocotrienole durch 1D- und 2D-NMR ist wichtig, da diese Substanzen in der Kontrollgruppe nicht vorkommen.

Die vorläufigen Vermutungen wurden bekräftigt durch die Detektion der Hauptderivate des Chlorophylls in hyperpigmentierten Babybananenschalen während der Untersuchungen mittels Spiral-Coil LSRCCC. Hierbei handelte es sich um Pyrophäophorbide, welche mit Sterinen/Sterolen verestert waren (siehe 2.3.3). Während des Chlorophyll-Abbaus findet eine Abspaltung von Phytol statt, welches angereichert wird und gemäß den Veröffentlichungen von Collakova und DellaPenna (2003) sowie DellaPenna und Pogson (2006) zu Tocopherolen und Tocotrienolen umgewandelt werden kann. Eine Synthese von Tocopherolen findet ausschließlich in Organismen statt, die Photosynthese betreiben.

Die Anwesenheit von Triterpenalkohol-ferulaten in Reiskleieöl wurde nach einer Fraktionierung durch HSCCC bereits in der Literatur beschrieben (Angelis et al. 2011; Liu et al. 2013). In der Spiral-Coil LSRCCC Fraktion 14 konnten mit Hilfe von APCI-HPLC-MS sowohl 25-Hydroxy-24-methylcycloartenylferulat sowie mittels 1D- und 2D-NMR-Experimenten Cycloartenyl-*trans*-ferulat identifiziert werden (siehe 2.3.4.1, 2.3.4.2). Die oben genannten Quellen berichten weiterhin, dass unter dem Namen γ-Oryzanol ein funktionelles Speiseöl vertrieben wird, welches als Nebenprodukt der Reiskleie hohe Gehalte an Sterinen/Sterolen, Triterpenalkohol-ferulaten und Vitamin E (Tocopherole und Tocotrienole) aufweist. Demzufolge stellen Babybananenschalen mit Hyperpigmentierung ein wertvolles Ausgangsmaterial für Produkte mit antioxidativen und hypocholesterinämischen Eigenschaften dar (Scavariello und Arellano 1998; Islam et al. 2008).

Bei der phytochemischen Analyse von Babybananenschalen wurde das Glycolipid O-α-D-Gal*p*(1''→6')-O-β-D-Glu*p*(1'→3)-2,1-diacyl-L-glycerol entdeckt, welches damit zum ersten Mal in einer höheren Pflanzenart nachgewiesen wurde (siehe 2.1.2). Des Weiteren wurden die Strukturen von Phosphatidylcholin (Lecithin), Phosphatidylethanolamin, Sulphoquinovosyldiacylglycerol sowie molekulare Spezies des Glucocerebrosids mit Hilfe von 1D-, und 2-D-NMR-Spektroskopie aufgeklärt. Diese Verbindungen wurden im Rahmen dieser Arbeit erstmalig in Bananen nachgewiesen.

Es ist wichtig zu beachten, dass Carotinoide keine bedeutende Rolle in Bezug auf das Phänomen der Hyperpigmentierung spielen, da sich ihre Gehalte in beiden Bananenarten ähneln. Allerdings ermöglicht das zweite neue Fließmittelsystem Hexan/EtOH/$CHCl_3$/H_2O (6:2:4:2 *v/v/v/v*) die Isolierung von Xanthophyllen aus Früchten und Pflanzen, wovon weitere Forschungsarbeiten profitieren könnten.

Forschungsansätze für die nahe Zukunft bestehen in der gründlichen Analyse weiterer Bestandteile der HSCCC-Fraktionen, welche aus methanolischen Extrakten der hyperpigmentierten Babybananenschalen und der Kontrollgruppe gewonnen wurden. Hierdurch soll das Vorkommen polarer Derivate des Chlorophylls, wie z. B. ein roter Chlorophyllkatabolit (engl. red chlorophyll catabolite, RCC), neue fluoreszierende Chlorophyllkatabolite (engl. fluorescent chlorophyll catabolites, FCCs) und nicht-fluoreszierende Chlorophyllkatabolite (engl. nonfluorescent chlorophyll catabolites, NCCs), erklärt werden. Anschließend sollte der Fokus auf die Erforschung des Hyperpigmentierungsphänomens an frischen kolumbianischen Babybananen mittels HSCCC und Spiral-Coil LSRCCC und unter Anwendung der im Rahmen dieser Arbeit entwickelten Methoden gelegt werden.

"May all being find peace, joy, and liberation"

H.H. Gyalwa Karmapa Orgyen Trinley Dorje

To Prof. Emeritus Eliezer E. Goldschmidt,
Camilo and Diego

TABLE OF CONTENTS

List of Figures

List of Tables

List of Abbreviations

1D NMR	One dimensional NMR measurement
2D NMR	Two dimensional NMR measurement
APCI	Atmospheric Pressure Chemical Ionization
CCC	Countercurrent Chromatography
cm	Centimeter
d	Doublet
DAD	Diode array detector
DEPT	Distortionless enhancement by polarization transfer
El-MS	Electron Ionization Mass Spectrometry
ESI/MS	Electrospray Ionization Mass Spectrometry
Exp	Experimental
Fig	Figure
g	Gramm
GC	Gas Chromatography
GC-EI/MS	Electron ionization mass spectrometry coupled to gas chromatography
h	Hours
HMBC	Heteronuclear Multiple Bond Correlation
HPLC	High Performance Liquid Chromatography
HSCCC	High-Speed Countercurrent Chromatography
HSQC	Heteronuclear Single Quantum Coherence
Hz	Hertz
J	Coupling constant
kg	Kilogram
l	Column length (cm)
L	Liter
LSRCCC	Low-Speed Rotary Countercurrent Chromatography
M	Molar mass

m	Multiplet
m/z	mass-to-charge ratio
mg	Milligram
μM	Micro-Molar
MHz	Megahertz
min	Minutes
mM	Milli-Molar
mm	Millimeter
MPLC	Medium Pressure Liquid Chromatography
MS	Mass spectrometry
nd	Not detected
nm	Nanometer
NMR	Nuclear Magnetic Resonance
º C	Degree Celsius
pH	Hydrogen ion concentration
ppm	Parts per million
RP	Reversed Phase
rpm	Revolutions per minute
Rt	Retention time
s	Singlet
TLC	Thin Layer Chromatography
t	Triplet
UV	Ultraviolet
v	Volume
vs	Versus
WL	Wave length (nm)

INTRODUCTION

The Baby Banana fruit (*Musa acuminata*) is cultivated in Colombia, Ecuador, Costa Rica, Venezuela, Costa Rica and Kenya, however Colombia is the main country in Latin-American which has developed the marketing for exporting fruit to Europe and USA. Colombia exports not only Baby Banana but also other tropical fruits, e.g. *Physalis peruviana* (known as Uchuva) and *Hylocereus undatus* mentioned as white Pitahaya or dragon fruit, and they are classified as "exotic fruits".

The tropical fruit is collected from different regions of Colombia and during the last years increasing experience has been gained to maintain the postharvest quality during exporting the fruit. Since climatic changes influence rainfalls, temperature and water availability, the traders of baby banana in Colombia confirmed the presence of an irregular ripening in several Baby Banana peels during the post-harvest stage that they called "hyperpigmentation" (HP). The occurrence of visible small green bands in the peels during the ripening showed that degradation of chlorophyll was abnormal in comparison with control bananas. Consequently, those Baby Banana fruits with hyperpigmentation were not suitable for export because they did not meet the overall standards of quality and both farmers and traders were affected economically. Farmers strictly classified the fruits during the postharvest stage before offering them for export and the fruit traders contacted the researcher in order to explore the phenomenon of hyperpigmentation in Baby Banana fruits.

Thus, two groups of Baby Banana (with hyperpigmentation and without hyperpigmentation) have been studied under the hypothesis that the degradation of chlorophylls could play a role in the occurrence of the abnormal green bands on Baby bananas peels with hyperpigmentation.

Therefore, the main objective of this study was the analysis of the hyperpigmentation phenomenon in relation with the chlorophyll degradation in Baby Banana peel. Thus, the three specific objectives were: (i) the isolation of chlorophyll and derivatives by means of High Speed Countercurrent Chromatography (HSCCC); (ii) the comparison between Baby Banana peel without hyperpigmentation (control) vs. Baby Banana with hyperpigmentation by application of HSCCC; and (iii) to set up a phytochemical profile of Baby Banana peel.

The optimization of a solvent system for the separation of chlorophylls by means of High-Speed Countercurrent Chromatography (HSCCC) was performed and the proposal of using additional samples such as grass and spinach during the trials could enable the understanding of the role of chlorophylls in plants and fruits.

Finally, a scale-up by means of Spiral Coil-Low Speed Rotary Countercurrent Chromatography (Spiral Coil-LSRCCC) is presented which has proven to be a suitable system for large-scale fractionations of extracts obtained from Baby Banana peel with hyperpigmentation.

1. GENERAL CONCEPTS

1.1 Baby Banana (*Musa acuminata* AA Simmonds cv. Bocadillo)

1.1.1 Taxonomic Classification of Bananas (*Musa acuminata*)

The first edition of Linnaeus' Species Plantarum in 1753 established the botanical nomenclature of genus *Musa*, familiy *Musaceae* and divided bananas and plantains (*Musa* ssp.) according to the consumption, in dessert bananas (*Musa sapientum* L.) being eaten raw, and plantain (*Musa Paradisiaca* L.) being processed by cooking before consumption. APG II system (Angiosperm Phylogeny Group II system) in 2003, assigned *Musaceae* to the order *Zingiberales* in the clade *Commelinids* in monoctos[1]. A third version of APG (The angiosperm Phylogeny Group) in 2009, established an additional criteria of classification based on the genome.[2]

Bananas and plantains have originated in Southeast Asia where they were domesticated by selection from wild species more than 5.000 years ago and now are known as hybrids of polyploids progenies of two wild banana species- *Musa acuminata* and *Musa balbisiana*- according to a genome-based system introduced by Ernest Cheesman, Norman Simmonds, and Ken Sherpherd, which indicates the degree of genetic inheritance from the two wild parents and the number of chromosomes (ploidy). Therefore, Linnaeus' *Musa sapientum* is now identified to be the hbrid Latundan cultivar (M. x *paradisiaca* AAB Group 'Silk'), *Musa paradisiaca* AAB, *Musa balbisiana* ABB and *Musa acuminata* AA and AAA.

---

[1] APG II 2003. An update of the Angiosperm Phylogeny Group classification for the orders and families of flowering plants: APG II. The Angiosperm Phylogeny Group. *Botanical Journal of the Linnean Society*, 2003, 141, 399-436.
[2] APG III 2009. An update of the Angiosperm Phylogeny Group classification for the orders and families of flowering plants: APG III. The Angiosperm Phylogeny Group. *Botanical Journal of the Linnean Society,* 2009, 161, 105-121.

Actually, banana cultivars or clones are named e.g. *Musa* AAB *Simmonds*, clon Cachaco Cardeñosa, a species from Colombia and in case of Baby Banana from Colombia, its official designation is *Musa acuminata* AA Simmonds, cv. "Bocadillo".[3]

The Baby Banana is known in English as “Lady Finger”, “Singer bananas”, “Date banana”, “Fig banana” or “Sucrier”, depending on the region where it is cultivated.

1.1.2 Plant morphology

The banana plant is the largest herbaceous flowering plant. Cultivated bananas are parthenocarpic, fruits in which the flesh swells and ripens without its seeds being fertilized and developing. The propagation is vegetative due to the lacking of viable seeds and farmers remove and transplant part of the underground stem (corm) from which all the above-ground part of the banana plant grow. The external part of the plant consists in a vertical shoot that develops from the base of the banana plant called "pseudostem" or " false stem". The edges of the sheath meet when it is first produced, make it look tubular. As new growth occurs in the centre of the pseudostem the edges are forced apart. Cultivated banana plants vary in height depending on the variety and growing conditions between 5 to 7 m. Leaves are spirally arranged and grow 2.5 metres long and 50 cm wide (Robinson 1996; Simmonds 1995; Ortiz et al. 1995) (Zeller 2005).

[3] Belalcázar, C., S., 1991. *Manual de asistencia técnica N° 50: El cultivo del plátano en el trópico.* ICA, CIID, INIBAP y Comité de Cafeteros del Quindío. Armenia, Quindío, p.56.

After 10 to 15 months the banana plant is mature and the corm stops producing new leaves. Then a stem develops which grows up inside the pseudostem, carrying the immature inflorescence until eventually it emerges at top. This inflorescence is known as "banana heart". The flowers appear in group (hands) along the stem and are covered by purplish bracts which roll back and shed as the fruit stem develops. The first hands to appear contain female flowers which will develop into bananas. The female flower appears in rows and varies from a few to more than 10, further up the steam from the rows of male flowers that are in the bottom of the inflorescence. The ovary is inferior, meaning that the tiny petals and other flowers parts appear at the tip of the ovary. Male and female flowers are morphologically indistinguishable until the inflorescence is about 12 cm long. At this point the ovary in the male flower fails to develop any further (Simmonds, 1953a). Flowers have a 3-lobed stigma and style and an inferior ovary fused from 3 loculi. Each loculus of a female flower contains two rows of ovules embedded in a strip of mucilage (Simmonds, 1953). There are 5 stamens in male flowers; these are reduced to staminodes in female flowers (Simmonds, 1953a).

Each fruit is a berry and is known as a "finger". Each cluster of fruits at a node is known as a "hand" and the entire collections of hands are known as a "bunch". The number of hands varies with species and cultivar. The outer protective layer of each fruit, known as the "skin" or "peel", is a fusion of the hypanthium (florar receptacle) and outer layer (exocarp) of the pericarp (fruit wall derived from the ovary wall). This peel is easily removed from the fleshy pulp that originates mainly from the endocarp (innermost layer of the pericarp), (Simmonds, 1953). During the development of the fruit from the ovary, the tepals, style and staminodes abscise leaving a characteristic calloused scar at the tip of the fruit. Color, size, texture and flavour of common cultivated *Musa* fruits vary with cultivar (Australian Government, 2008).

Figure 1-1 depicts the cultivation of Baby banana in Colombia. The fruits are berries between 8-13 cm in length and 1.5 to 1.3 cm in width. Fruits turn from green to yellow during the ripening. The flesh, ivory-white is firm, astringent,

even gummy with latex when is unripe, turning tender and slippery, soft and mellow, rather dry, mealy or starchy when ripe **(Figure 1-2).**

Figure 1-1. Baby Banana cultivation in Cundinamarca, a central region of Colombia (South America).

Figure 1-2. Baby Bananas (*Musa acuminata AA Simmonds cv*." Bocadillo") from Colombia at different stages of ripening after being harvested.

1.1.3 Pre-harvest

Baby Banana is cultivated in Colombia in different regions whose height oscillate between 1.000 and 2.000 meters above sea level with a temperature between 16-30 °C. The average rainfall of the area changes between 1.800 and 2.800 mm. The main growing areas are in western Antioquia department, known as Uraba, in eastern Santander department and in the Central part of Colombia where the major of department are located in a mountainous area.[4] **(Figure 1-3)**

The cultivation of Baby Banana in Colombia regularly belong to farmers more than to multi-national giant corporation like today´s Chiquita Brands International and Dole. The first trader for Baby banana fruit export begun in the 80´s.

Banana represents 244 US $ millions of global exportations of Colombia and currently ranks third in the exportation in comparison with coffee and flowers in first and second ranking, respectively. The major countries in Europe that receive banana are Belgium, United Kingdom and Germany.[5] **(Figure 1-4)**

[4] Belalcázar, C., S., 1991. *Manual de assistência técnica N° 50: El cultivo del plátano en el trópico.* ICA, CIID, INIBAP y Comité de Cafeteros del Quindío. Armenia. Quindío. p.56
[5] Ministerio de Comercio, Industria y Turismo de Colombia. Estadísticas e Informes. –DANE-DIAN. 2013 (http://www.minicit.gov.co/publicaciones.php?id=15815)

Figure 1-3. Commercial Baby Banana growing areas in Colombia, in western Antioquia Department, in central territory, and in the eastern Santander Department (Belalcázar, 1991).

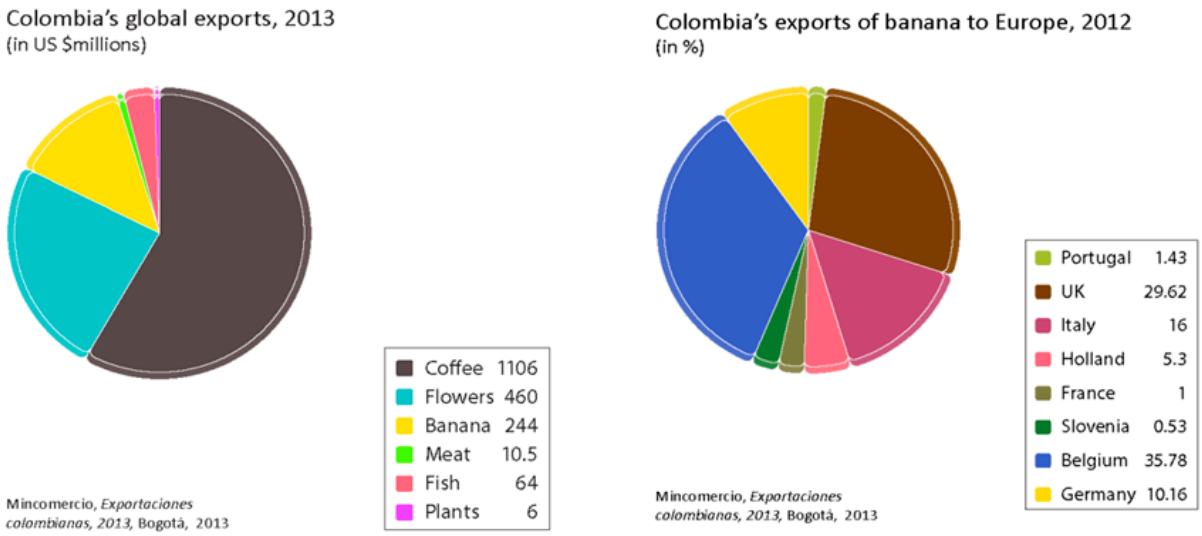

Figure 1-4. Exportations from Colombia ranking in US $ (millions) for 2013 (left) and receiving countries in Europe (right).

1.1.4 Post-harvest

The mature bunch is harvested after one year of planting by vegetative propagations. Since then plant produce a bunch each four months. Therefore, the growers implement farm management for obtaining harvests in sequence during the year. In this way they can adequate the marketing according to the supply and demand. The period between flowering and harvest varies from 6 to 10 weeks depending on the stage of ripening that is necessary according to the marketing either national or international.[6] In most commercial operations, the banana bunches are covered in plastic or cloth bags to prevent blemishes from mechanical and bird/plying and sugar glider damage.

Commercially, harvesting takes place when the fruit on the upper hands are just changing to light green and during the post-harvest it is monitored with a color chart **(Figure 1-5).** Because of the ripening process could be halted due to an inadequate temperature, the fruit should kept between 13.5 and 15 °C.

Figure 1-5. Post-harvest of Baby Bananas in green stage before being exported (left).
Control color chart of Bananas used during the post-harvest marketing.

[6] Corporación Colombiana Internacional, Departamento de Planeación. *Análisis internacional del sector hortifrutícula para Colombia* (1994).

The critical temperature of storage is 12 °C at 70% humidity and the optimal time is two weeks for prolonging four week of shelf-life of fruits.[7] When the Baby Banana fruit is exposed to 2 °C and 7 °C damage occurs due to variation in the respiratory activity with a low level of carboxylic acids and sugars in comparison with a control at 20 °C. The peel shows black spots and a high contamination by fungi. The organoleptic characteristics as flavour and color are altered.[8]

Short treatment post-harvest (15% CO_2, 2% O_2, 83% N_2) were applied during 48 h to Baby Banana fruits after harvesting, and the climateric peak was delayed by 21 days without chemical and sensorial changes. Extraction and enzymatic activity of chlorophyllase was performed in Baby Banana peels both with treatment and without treatment (control) and the apparent Michaelis-Menten kinectics (Km) was reported. The substrate concentration at which the reaction rate is half of V_{max} (361 µM-Chl *a*/min/mg) was 0,034 µM-Chl *a* at 37 °C and pH 7.0. The results depict a stable enzyme-substrate complex with a high affinity for chlorophyll *a.* SDS-PAGE experiments were applied to protein extracts from Baby Banana peel and molecular mass between 12 and 35 kD were reported for chlorophyllase.[9]

---

[7] Díaz, R., Porras, G., *Determinación de la temperatura crítica de almacenamiento del banano bocadillo* (*Musa paradisiaca* L.). Trabajo de grado. Santafé de Bogotá. Universidad Nacional de Colombia. Departamento de Química (1998).
[8] Bustos, Y., *Estudio preliminar del efecto de las bajas temperaturas en el almacenamiento del banano bocadillo* (*Musa paradisiaca* L.). Trabajo de grado. Santafé de Bogotá. Universidad Nacional de Colombia. Departamento de Química (1995).
[9] Castro, B. M., *Efectos de tratamientos postcosecha en la actividad enzimática de la clorofilasa del Banano Bocadillo* (*Musa acuminata*). Trabajo de grado. Mención meritoria. Título Maestría. Santafé de Bogotá. Universidad Nacional de Colombia. Departamento de Química. Departamento de Agronomía (2001).

1.1.4.1 Hyperpigmentation phenomenon

The hyperpigmentation phenomenon in Baby Banana peel was observed for first time in Colombia during the recollection of fruits for export around the 90´s and this fact was confirmed when the sanity control in the European Union was applied to the fruits due to the occurrence of green band in the peels **(Figure 1-6).** The fruits were rejected as a consequence that fruit with hyperpigmentation were excluded into the international marketing. The farmers learned to do a strict classification during the post-harvest stage and fruits with hyperpigmentation were addressed to the local marketing. The label of "hyperpigmentation" was assigned by the traders to identify the fruit with the quality problem.

Figure 1-6. Baby Banana with hyperpigmentation (HP) (left), and without hyperpigmentation (Control), (right).

The green bands are visible when the fruit is in the green stage (1-3 point according to the control color chart), more than in yellow stage. Even though this fact does not mean that fruit develops a normal stage of ripening. The effect of the hyperpigmentation was monitored during 10 days postharvest in fruit, hence the influence of the phenomenon on the peels could be observed. The green bands could be related to the degradation of chlorophyll since the hyperpigmentation shows green veins through the peels especially in the posterior view that could depict chlorophyll accumulation on the peels. The control usually turn on green to yellow on the peels without intermediate stage as it is illustrated in the control color chart, except for stage 5 where only the upper and button area maintain a green color **(Figure 1-7.)**

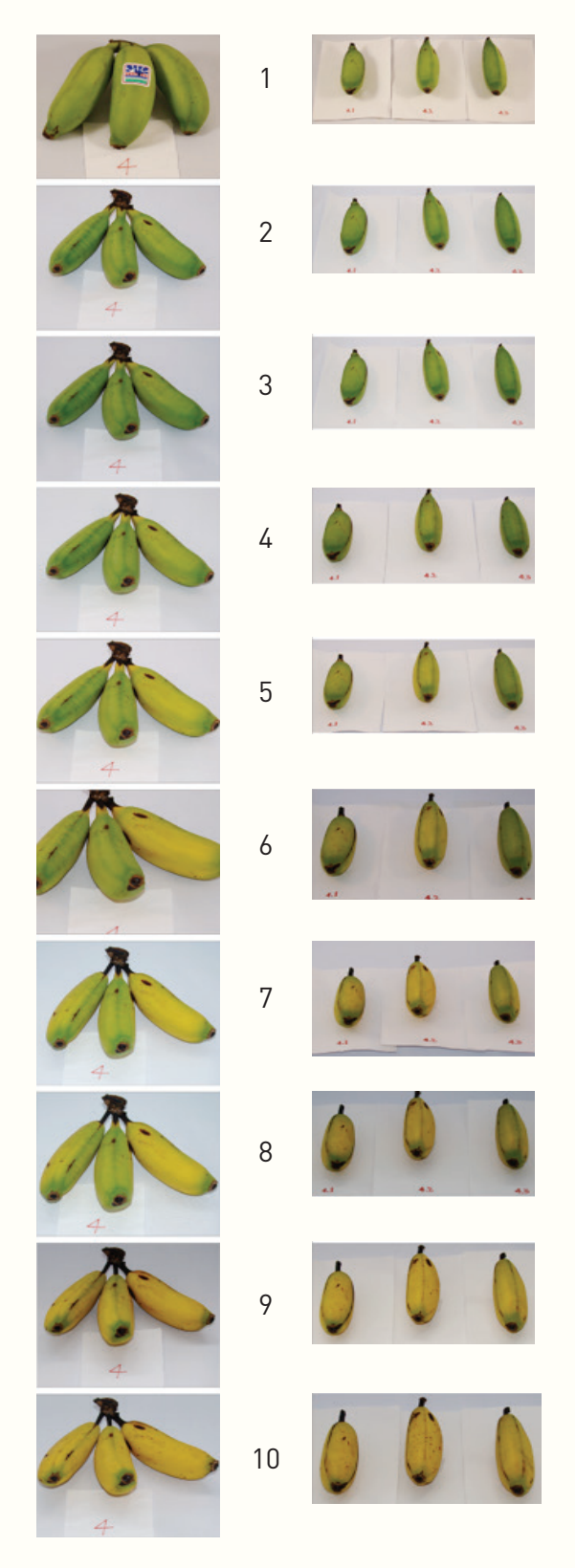

Figure 1-7. Baby Banana with hyperpigmentation at different stages of ripening during 10 days after being harvested.

1.2 Chlorophyll degradation

The knowledge on chlorophyll degradation has grown considerably nowadays due to relevant reports about chlorophyll catabolites in higher plants and fruits which reveal a path of chlorophyll breakdown not only in chloroplast but also in both cytosol and vacuole (Kräutler et al. 2012).

The controversy about whether chlorophyll catabolism occurs either *in vivo* via oxidase or peroxidase (Minguez-Mosquera and Garrido-Fernandez 1996; Thomas & Janave 1992) or via the pheophorbide *a* oxigenase (PaO) pathway proposed by Hörtensteiner (1999) and Kräutler at al (1997) has been clarified in favor of the PaO pathway (Pružinská et al. 2005; Berghold et al. 2006; Moser et al. 2012).

The first step in chlorophyll *a* catabolism corresponds to a loss of phytol by chlorophyllase enzyme and subsequently chlorophyll derivatives are formed such as pheophytin *a*, pheophytin *b*, pyropheophytin *a,* pyropheophytin *b*, pheophorbide *a*, pheophorbide *b*, chlorophyllide *a*, chlorophyllide *b*. Structural isomers of chlorophyll *a* and *b*, such as chlorophyll derivatives, are shown in **Figures 1-8, 1-9.**

Chlorophyllase was one of the first plant enzymes described by Willstätter and Stoll in 1913. Studies of biochemistry and molecular biology concluded that the enzyme is a serine lipase-type esterase (Jakob-Wilk et al. 1999) Additional results in Citrus (C*itrus sinensis*) suggest that chlorophyllase functions as a rate-limiting enzyme in chlorophyll catabolism controlled via posttranslational regulation (Harpaz-Saad et al. 2007; Ginsburg 1993).

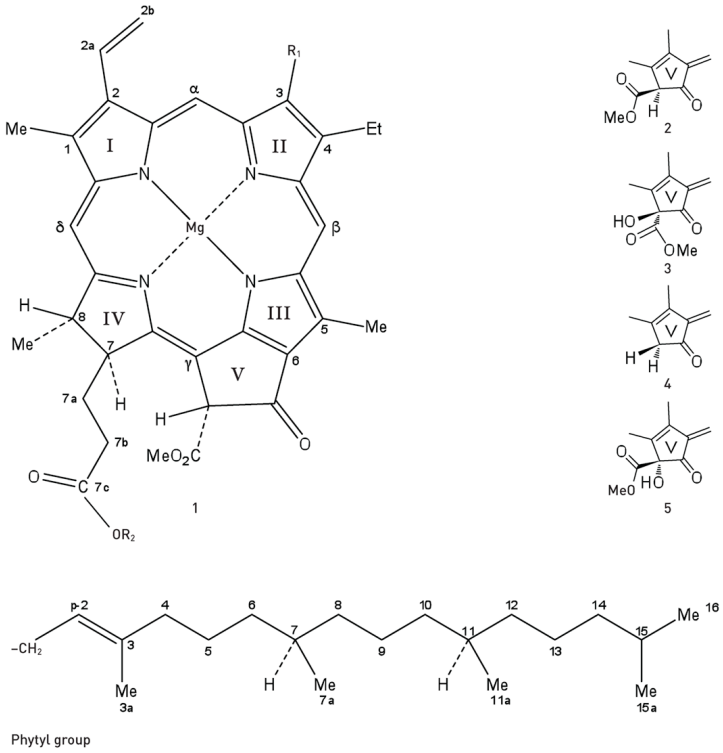

Compound	**Mg***	**R_I**	**R_2**	**Isocycling Ring (V)**
Chlorophyll *a*	+	CH3	Phytyl	1
Chlorophyll *b*	+	CHO	Phytyl	1
Chlorophyll *a'*	+	CH3	Phytyl	2
Chlorophyll *b'*	+	CHO	Phytyl	2
Hydroxypheophytin a	–	CH3	Phytyl	3
Hydroxypheophytin *a'*	–	CH3	Phytyl	5
Pheophytin *a*	–	CH3	Phytyl	1
Pheophytin *a'*	–	CH3	Phytyl	2
Hydroxypheophytin *b*	–	CHO	Phytyl	3
Hydroxypheophytin *b'*	–	CHO	Phytyl	5
Pheophytin *b*	–	CHO	Phytyl	1
Pheophytin *b'*	–	CHO	Phytyl	2
Hydroxychlorophyll *a*	+	CH3	Phytyl	3
Hydroxychlorophyll *b*	+	CHO	Phytyl	3
Pyropheophytin a	–	CH3	Phytyl	4

*Mg is represented by 2H in pheophytins.

Figure 1-8. Structural formulas and nomenclature of chlorophylls and their derivatives (Huang et al. 2008).

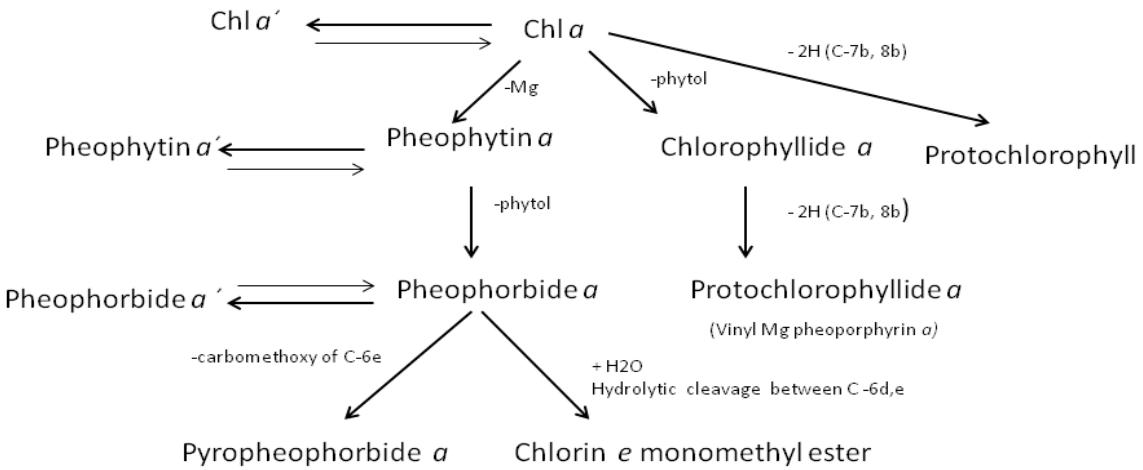

Figure 1-9. Nomenclature of the porphyrins related to Chl a and the isomer Chl a' (Aronoff 1966).

Subsequent studies have been reported by Hörtensteiner and support that chlorophyll *a* is converted to chlorophyll *b* in order to be catabolised by the pathway where enzymes such as Chl *b* reductase, Mg dechelatase, pheophorbide a oxigenase and RCC reductase are involved (Hörtensteiner 1999, 2006; Pružinská et al. 2003; Thomas et al. 2001).

The chlorophyllide is formed by activity of chlorophyllase as well as pheophorbide by Mg dechelatase and both chlorophyllide and pheophorbide are green **(Figure 1-10).** They are intact in the plastids but when chlorophylls and their derivatives are moved to chloroplasts or gerontoplasts, the tetrapyrrole ring of the pheophorbide is opened due to the activity of pheophorbide a oxygenase and a red metabolite (RCC) is produced. A redox reaction is necessary involving O_2 and Fe. The spectrum of RCC is distinguished by a peak at ca. 485 nm (Hörtensteiner 1999, 2006; Moser et al. 2012) **(Figure 1-11).**

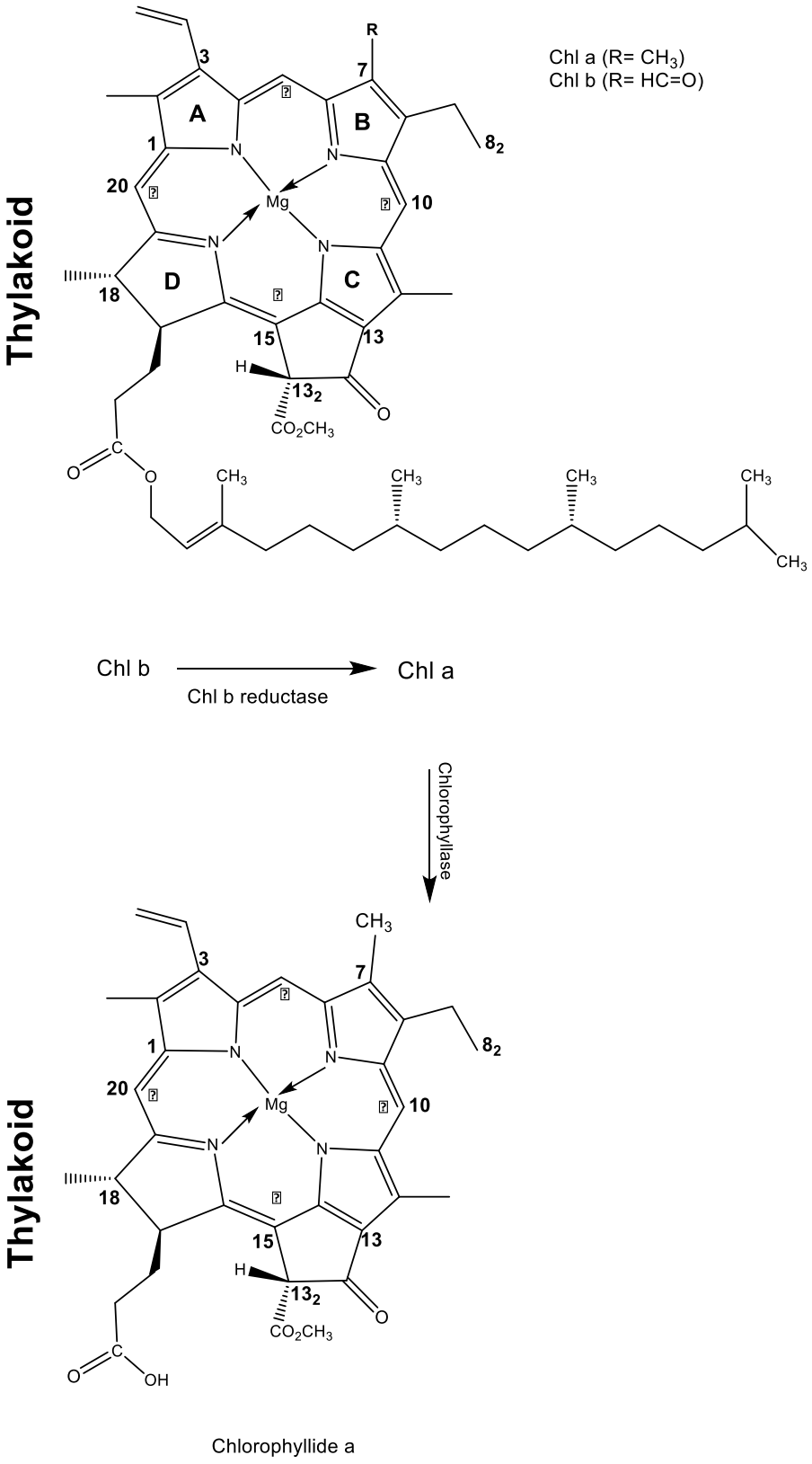

Figure 1-10. Chlorophyll breakdown pathway in higher plants (first stage) (Hörtensteiner 2006).

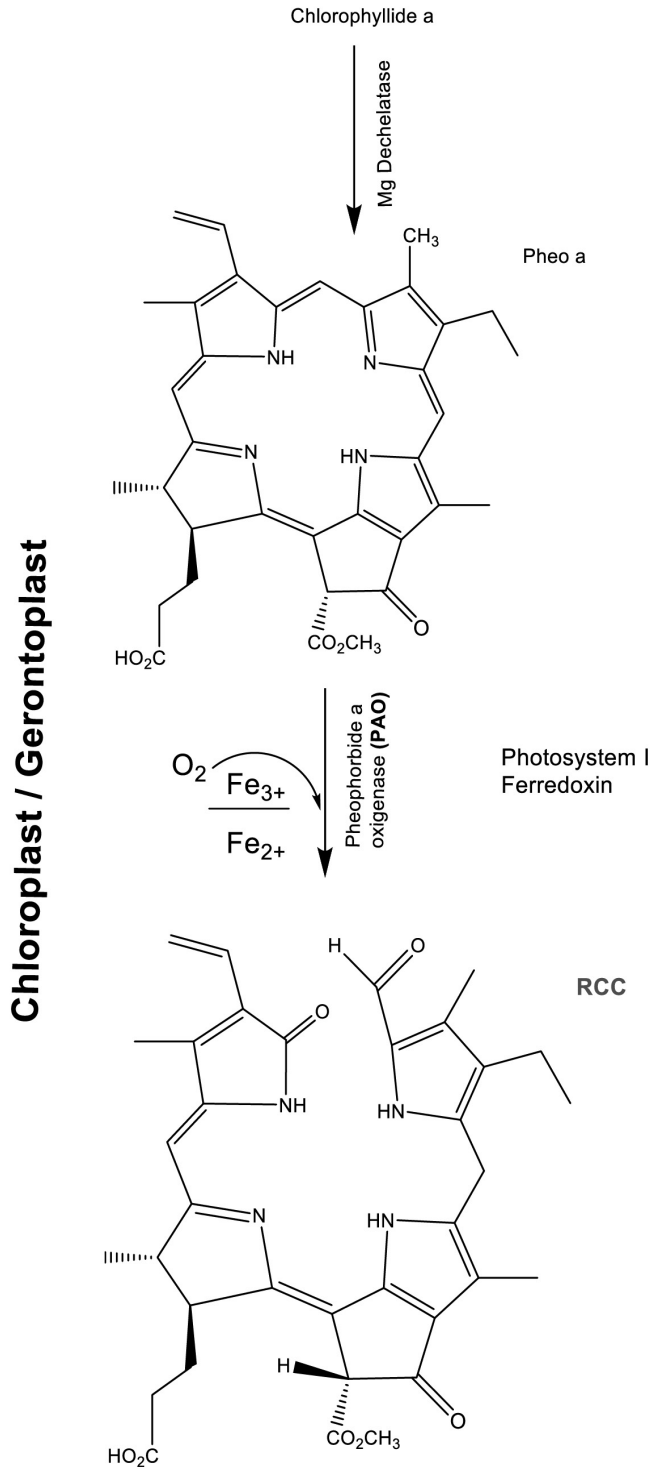

Figure 1-11. Product of the pheophorbide a reaction to red chlorophyll catabolite (RCC). (Kräutler et al. 1991, 1992, 2012).

Hörtensteiner et al. (1995) sugggested that pheophorbide *b* is a competitive inhibitor of PAO and for these reasons pheophorbide *a* is used as substrate. Therefore, catabolism of chlorophyll *b* is required to yield chlorophyll *a* (Folly and Engel 1999).

Chl *b* is a component of the antenna complex in the photosystems and occurs at variable ratios to Chl *a*. All catabolites of chlorophyll so far characterised in higher plant as nonfluorescent chlorophyll catabolites (NCCs), however, have a methyl group attached to C-7 on the B pyrrole ring, the characteristic methyl of chlorophyll *a*.

Hörtensteiner explains that the reason for this behavior is found in the specificity of PAO for pheophorbide *a*, and consequently conversion to the *a*-forms is a prerequisite of Chl b breakdown via PAO (Hörtensteiner 2006).

Red derivatives of chlorophyll corresponding to RCC are also known to be produced in *Chlorella protothecoides* during enforced degreening under N-deficiency and heterotrophic metabolism (Engel et al. 1996; Oshio and Hase 1969). In these green algae, RCCs represent the final step of Chl breakdown which are excreted into the medium whereas in higher plant the final catabolites are exclusively derived from chlorophyll a and identified as nonfluorescent chlorophyll catabolites (NCCs).

RCC reductase is the enzyme that catalyses the ferredoxin-dependent reduction of a double bond in the pyrrole system of RCC to produce an almost colorless tetrapyrrole with a strong blue fluorescence at 321 and 361 nm. All three remaining mesopositions are fully reduced, resulting in the complete disruption of the double-bonding system of chlorophylls. The "primary" fluorescent chlorophyll catabolites *p*FCC, or its C1 epimer, *epi-p* FCC has been identified (Kräutler et al. 1991, 2012) **(Figure 1-12).**

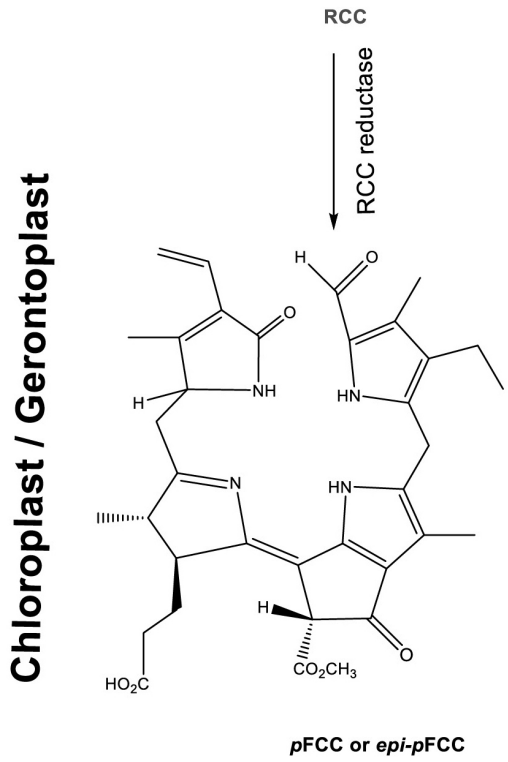

Figure 1-12. Reduction of red chlorophyll catabolite (RCC) to produce the "primary" fluorescent chlorophyll catabolite (*p*FCC or its C1 epimer, *epi*-*p*FCC) in senescent leaves and ripening fruit (Kräutler and Hörtensteiner 2006).

The following step resembles the biochemistry undergone by xenobiotics and other harmful chemical (Kreuz et al. 1996). The *p*FCC is expulsed into the vacuole and tautomerised to accumulate there as nonfluorescent chlorophyll catabolites (NCCs). This behavior of the cell could be understood as a treatment of chlorophylls derivatives as dangerous products, which must be detoxified.

14 new NCCs from tobaco, *Arabidopsis,* spinach, and maize have been structurally caracterized (Berghold et al. 2004; Berghold 2005; Oberhuber et al. 2001). All NCCs structurally analyzed so far are derived from Chl *a* and share a common basic tetrapyrrolic structure.

The degradation of chlorophyll in ripening bananas revealed a stunning variety of colorless chlorophyll catabolites, as a result of a surprisingly complex break-down path. Four persistent FCCs (Mc-FCCVs) which accumulated in the peels of ripe bananas were identified (Kräutler et al. 2012; Moser et al. 2008, 2009a, 2009b).

The different of FCCs in banana in comparison with other species is the persistence of the compounds and the ester function at the propionate side-chain. In other species they exist only "fleetingly" and they are hard to observe (Moser, et al. 2012) **(Figure 1-13).**

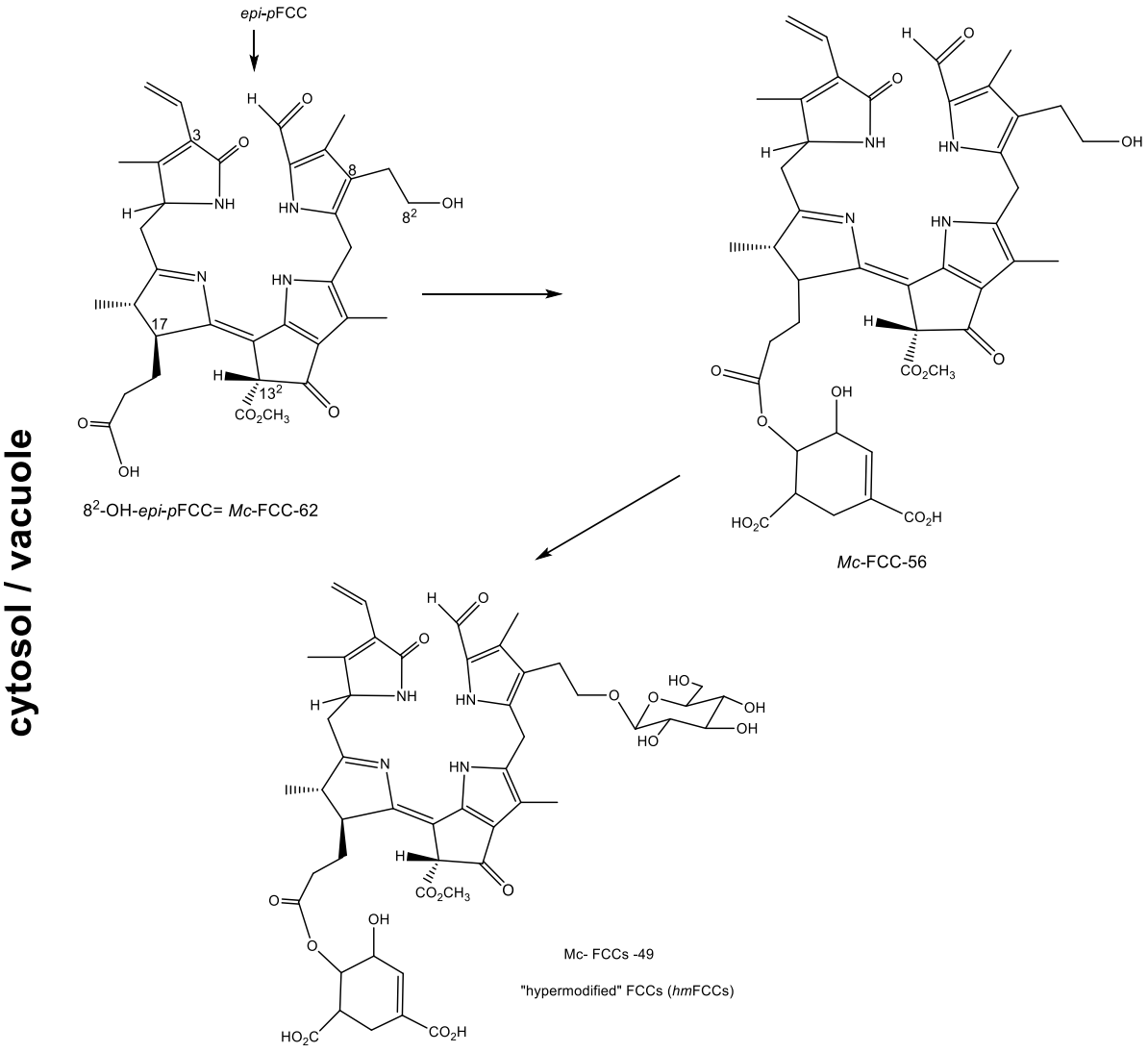

Figure 1-13. Fluorescent catabolites (*Mc*-FCCs) in extract of the peels of freshly ripe bananas (Thomas et al. 1989; Moser et al. 2012).

The Mc-FCCs step of chlorophyll breakdown begins with *epi-p*FCCC-62 and is proposed as a common precursor of the following catabolites. Mass spectrometric analysis indicated only one oxygen atom more than a primary FCC (*p*FCC). The elucidation confirmed the hydroxyl group at the terminal position of the ethyl substituent at C8. Thus Mc-FCC-62 was revealed to be a 8^2-hydroxy-13^2-(methoxycarbonyl)-3^1,3^2-didehydro-1,4,5,10,17,18,20,22-octahydro-4,5,seco-(22H)-phytophorphyrin (Moser et al. 2008, 2009ab).

The most polar compound is the "hyper-modified" (*hm*FCCs) Mc-FCC-49 due to a glucose bound at C-8^2 together with the complex propionate ester function. Modified FCC (*m*FCC) with a free propionic acid group are not present and may only exist transiently (Moser et al. 2012). They are imported into the vacuole, where they are isomerized rapidly to the corresponding NCCs by acid catalyzed reactions (Pružinská et al. 2005).

Nonfluorescent catabolites (Mc-NCCS) were detected by analytical HPLC and classified tentatively, based on their UV spectra. Seven of ten compounds were isolated by preparative HPLC, and further analyzed by mass spectrometry and NMR spectroscopy. They differ from each other by modifications of peripheral side chains, which are restricted to three positions **(Figure 1-14).**

Six reactions can be distinguished: dihydroxylation of the vinyl group of pyrrole A (R_1), hydroxylation at C8^2, followed by glucosylation and/or malonylation (R_2), C13^2 demethylation (R_3), finally, tautomerization of FCCs to NCCs. Except for the C8^2-hydroxylation and tautomerization, which are reactions common to all investigated species, other side chain modifications occur in a species-specific manner (Matile et al. 1999).

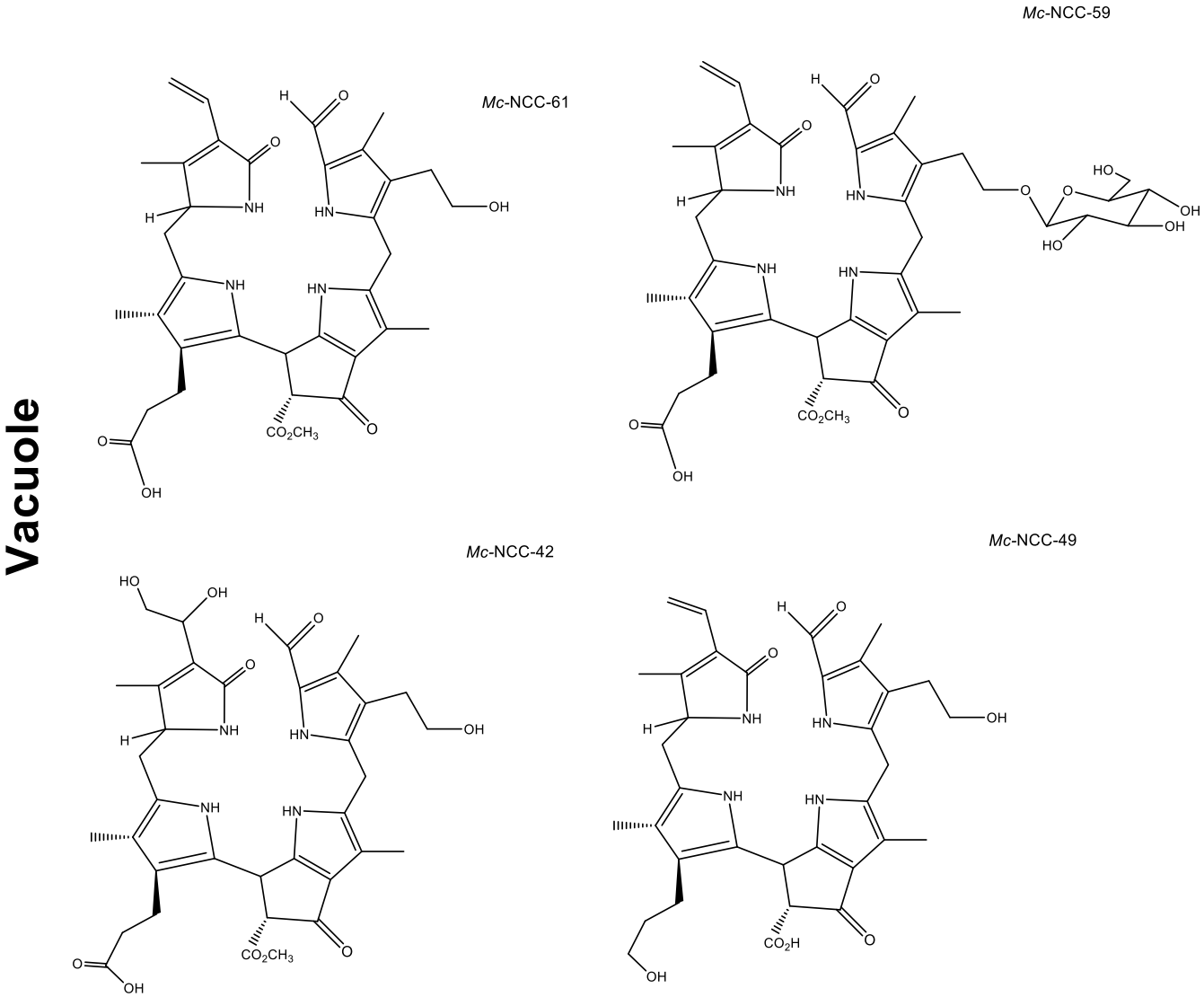

Figure 1-14. Nonfluorescent catabolites (*Mc*-NCCs) identified in an extract of the peels of ripe banana (Moser et al. 2012; Mühlecker and Kräutler 1996; Mühlecker et al. 1997).

In banana peels, *hm* FCC accumulate in freshly ripening tissue and in still viable, senescent cells in the transition region from intact, ripened to dead peel tissue. Persisten fluorescent chlorophyll catabolites, which are endogenously provided by chlorophyll breakdown, may hence commend themselves as natural molecular *in-vivo* reporters of senescence and senescence-associated cell-death symptoms (Moser et al. 2012).

1.3 High-Speed Countercurrent Chromatography

The preparative method called counter-current chromatography (CCC) provides an advantage over the conventional column chromatography by eliminating the use of a solid support where dangers of irreversible adsorptions from the support are inevitably present (Ito 2005) The technique is based on liquid-liquid partitioning of two immiscible liquid phases identified as mobile and stationary phases.

The High-Speed Countercurrent Chromatography (HSCCC) mechanism consists in a multilayer coil separation column which holder rotates about its own axis and revolves around the centrifuge axis at the same angular velocity (ω) in the same directions. This planetary motion prevents twisting the bundle of flow tubes allowing continuous elution through a rotating column without leakage and contamination. **Figure 1-15** illustrates a system with three coils of a High-Speed Countercurrent Chromatography (HSCCC).

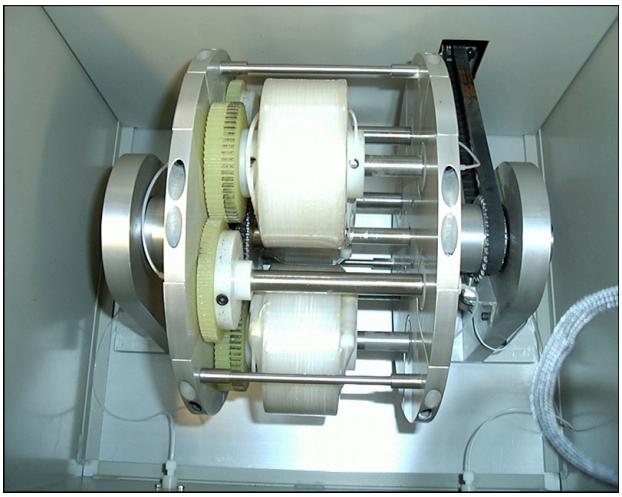

Figure 1-15. Preparative triple-coil planetary motion of separation column in High-Speed Countercurrent Chromatography (HSCCC).

The motion and distribution of the two phases in the rotating coil is based on the Archimedean screw force. When two immiscible solvent phases are introduced in an end-closed coiled column, the rotation separates the two phases completely along the length of the tube where the lighter phase occupies one end called the “head” and heavier phase, the other end called the “tail”. The

head and tail are defined according to Archimedean screw effect: all objects with differents densities, either lighter or heavier than the suspending medium, present in the rotating coil are driven toward the head of the coil.

The columns are divided in two zones: mixing zone near the center of the centrifuge and settling zone in the rest of the area. Motion of the mixing zones through the stretched spiral column shows that the mixing zone travels through the spiral column at a rate of round per one revolution of the column. Consequently, it indicates a high partition efficiency of the system that the solutes present at any portion of the column are subjected to a partition process of mixing and settling at an extremely high frequency of 13 times per seconds at 800 rpm (Ito 2005).

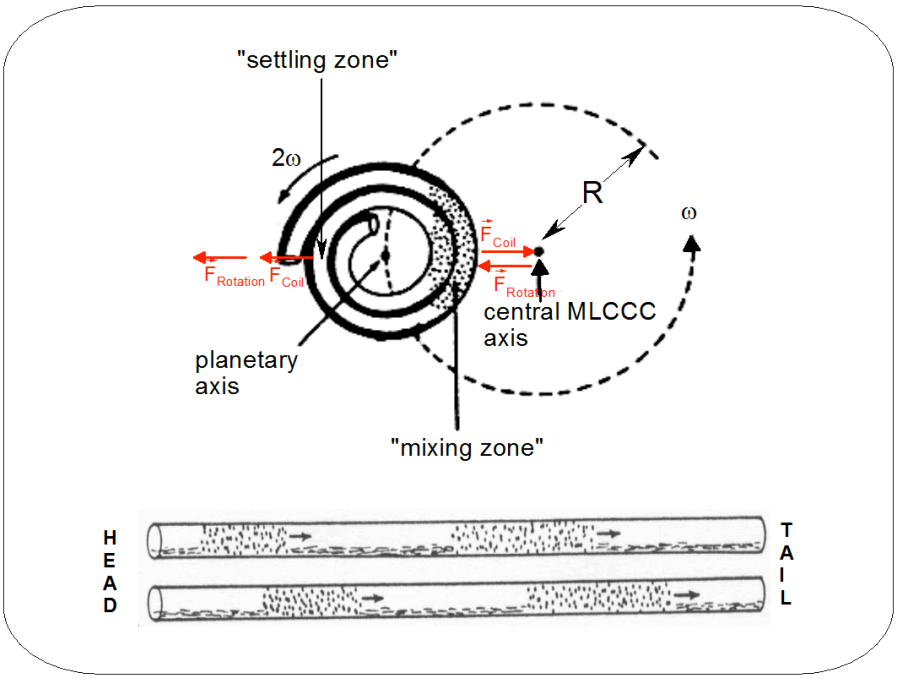

Figure 1-16. Schematic drawing of motion and distribution of two phases in the spiral column undergoing type J- planetary motion in High-Speed Counter Current Chromatography (Ito and Conway 1996).

The selection of the two phase solvent system for the target compounds is the most important step in HSCCC where searching for a suitable two-phase solvent system may be estimated as 90% of the entire work in HSCCC. The consulting of literature is essential before beginning with the experiment and several monographs, review articles and books chapters in the cited references

describe various two-phase solvent systems to be applied (Ito 2005; Sticher 2008; Friesen and Pauli 2005, das Neves and Guimarães Leitão, 2010).

Figure 1-17 depicts the components in a High-Speed Countercurrent Chromatography system. The HPLC-pump transports the system phase towards the coil and between the coil and the pump the injection port is installed. The sample is transported into the coil through the column which contains the solvent system and then is going out in direction to the detector. Then, the fraction are gathered by a fraction collector. The acceleration of the coils is ejected by a motor with capacity to get 800 or 900 rpm.

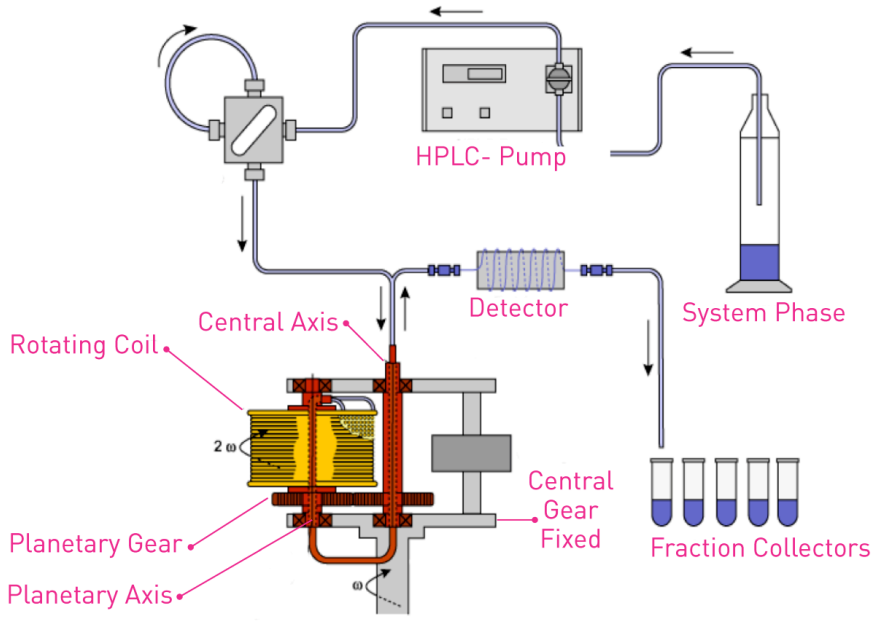

Figure 1-17. Schematic drawing of a High-Speed Countercurrent Chromatography (Sutherland, 1987)

1.4 Spiral-Coil Low-Speed Rotary Countercurrent Chromatography (Spiral-Coil LSRCCC)

The spiral-coil low speed rotary countercurrent chromatography is a versatile and gentle all liquid partition chromatographic method, which has been used for several applications in natural product isolation. The prototype has become a powerful tool in enrichment and isolation of target compounds in large quantities and consists of three spiral layers connected in series with a total volume of 500 mL. The column is composed of convoluted PTFE tubing (8.5 mm I. D) of 9.7 m length. The assembly is mounted onto a seal-less flow-through centrifuge, which is operated by speed control. The pitch of the spiral was ca.3.7 cm. The spiral starts at 6.7 cm and ends at 22.0 cm from the center of rotation, forming nearly four-spiral turns. A pair of flow tubes (standard–wall 0.85 mm ID Teflon tubing) from each terminal of the spiral column was led through the central axis of the apparatus, supported by a hollow plastic guide pipe, and then rigidly held at the stationary exit spot. The rotary speed of the column was regulated with a speed control. The solvents were delivered by an HPLC pump (Waters, model 515, Milford, MA; Köhler et al. 2004).

Figure 1-18. Assembly of Spiral-Coil Low Speed Rotary Countercurrent chromatography (Spiral-Coil LSRCCC).

As a comparison between the preparative techniques is realized, the spiral-coil avoids the long separation time that is necessary for the scale-up experiments with LSRCCC. Therefore, the CCC prototype combines two advantages, such as short separation time and large sample load. **Table 1-1** describes the features of each CCC technique.

Table 1-1. Comparative features between scale-up Spiral-Coil Low-Speed Rotary-CCC, Low-Speed Rotary CCC and High-Speed CCC.

	HSCCC	LSRCCC	Spiral-Coil-LSRCCC
Capacity	50 mL – 850 mL (2000 mL)	5.5 L (40 L)	5.5 L
Sample load	< 5 g (30 g)	50 g (500 g - kg)	50 g
	analytical - preparative	preparative – semi-industrial scale	preparative – semi-industrial scale
rpm	800 - 1000	50 - 80	50 - 200
Application	all (problems with polymeric samples in hydrophilic solvent systems)	nearly all (restrictions to some solvent systems) ideal for hydrophilic applications	designed for polar samples (hydrophilic solvent systems) and faster separations

The form of tubes plays an important role in the scale-up preparative technique since the form is convoluted in comparison to the bare-tube used in HSCCC. An additional characteristic, such as the gravitational force, increases the separation of the target compounds into the coil of LSRCCC, however, the Spiral-Coil Rotary-CCC performs a broadly distribution of the target compound into the coil due to the spiral conformation. Therefore not only the gravitational force is involved but also the spiral force.

The Spiral-Coil Rotary CCC increases the retention of stationary phase in comparison with the Low-Speed Rotary CCC and this demonstrates the meaningful effect of the scaled-up separation of target compounds (Köhler et al. 2004)

2. RESULTS AND DISCUSSION

2.1 Phytochemical profile of Baby Banana control peels

Introduction: Isolation of Phospholipids and Glycolipids from Baby Banana peels

Preparation of an extract from Baby Banana peels (20 mg) was carried out with with N, N-dimethylformamide and the filtrates were treated with hexane in a decantation funnel in order to extract and separate the carotenoids present in the samples. The phase of N, N-dimethylformamide retained polar and nonpolar compounds.

A total of eight extractions with hexane were needed to collect 405.5 mg of Baby Banana peel's extract that was injected for a preparative separation by HSCCC. The elution mode used in the separation was *'head-to-tail'* and the solvent system was hexane/CH_2Cl_2/EtOH/H_2O (2:1:3:1, v/v/v/v). The flow rate of the mobile ethanol/water phase was set to 3.5 mL/min; for detection λ 440 nm was used. A total of 13 fractions were collected during the elution mode and 3 additional fractions resulted in the extrusion mode **(Figure 2-1).**

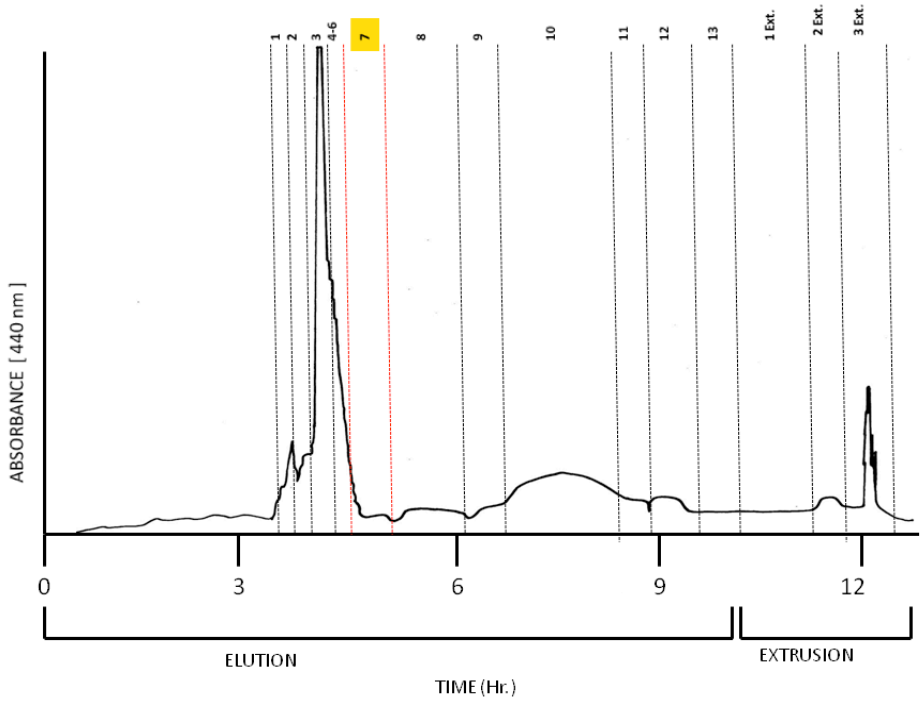

Figure 2-1. HSCCC chromatogram of 405.5 mg of an extract from Baby Banana peels monitored at 440 nm using elution and extrusion mode.

The preliminary phytochemical screening was analysed by means of TLC that revealed the presence of phytoconstituents, not previously identified, in fraction 7 (62.2 mg) from the HSCCC separation. Consequently, an additional preparative HPLC-reversed-phase separation was carried out using MeOH/EtOH (70:30, v/v) as isocratic eluent with a Phenomenex Luna 5 µ column, (250 x 15 mm) and 11 fractions were collected and monitored by TLC (RP-18) **(Figure 2-2) (c.f.4.2.1.7.1).**

2.1.1 Phosphatidylcholine (Lecithin)

The compound 1,2-dilinoleoyl glyceryl-phosphorylcholine was isolated in fraction 11 from the preparative HPLC-reversed phase system and the pure phosphatidylcholine structure was elucidated by 1D/2D-NMR spectroscopy ($^{1}H^{1}H$, ^{13}C, $^{1}H/^{1}H$-COSY, HSQC, HMBC, NOESY) and complemented by mass spectrometry, data were in agreement with previously published data (Sobolev et al. 2005; Willmann et al. 2011; Duarte et al. 2009) **(Figure 2-3).**

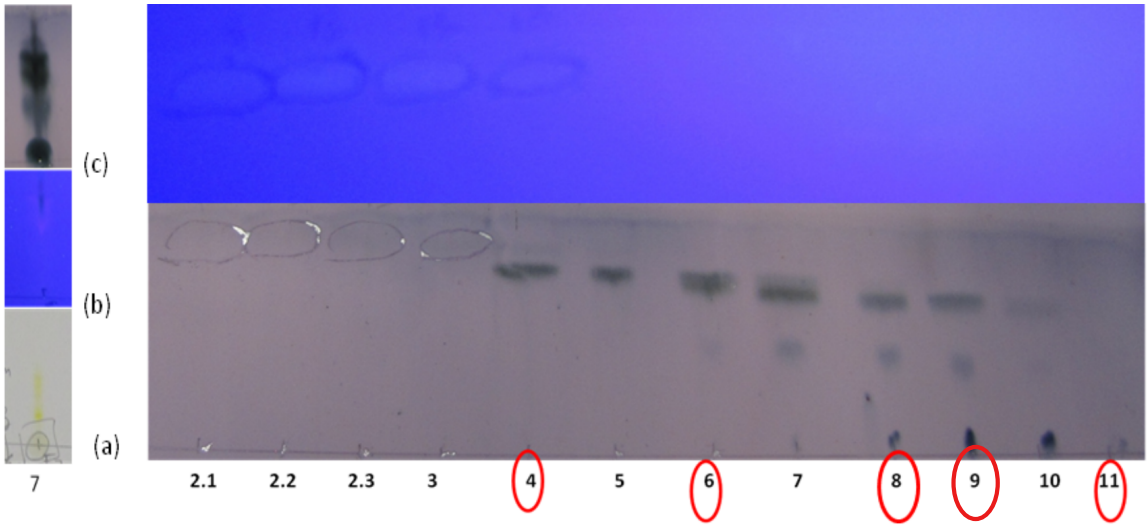

Figure 2-2. Fraction 7. Left: RP-18 TLC and Silica gel screening of target fraction 7 from HSCCC elution phase containing 62.25 mg of lipids. (a) Silica gel TLC. (b) RP-18 TLC 363 nm. (c) RP-18 TLC developed plate with p-anisaldehyde stain. Right: Separation of fraction 7 by HPLC-reversed phase system.

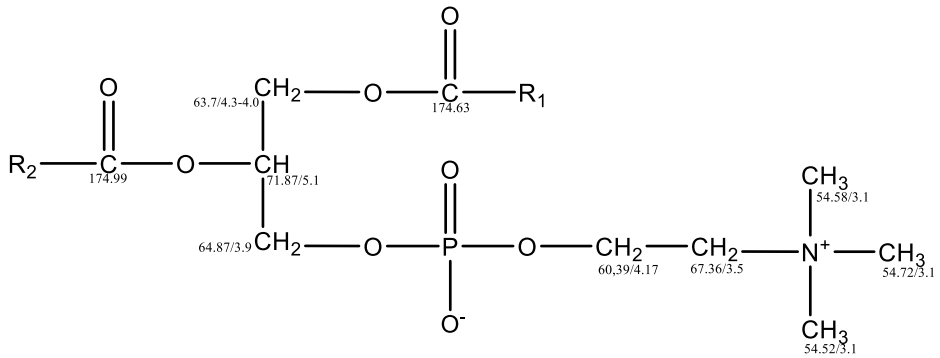

Figure 2-3. Chemical structure of phosphatidylcholine. Chemical shift of HSQC correlation shows numbered carbons and protons that confirm the elucidated data.

Table 2-1. ^{1}H-NMR and ^{13}C-NMR spectroscopic data of phosphatidylcholine (PTC) and assignments of resonances in the 600 MHz ^{1}H-NMR and 150 MHz ^{13}C-NMR in CD_3OD.

Assignment	**δ ^{1}H (ppm)**	**Multiplicity J/ Hz**	**δ^{13}C (ppm)**
CH_2*sn*-1	4.3_a	*dd* [12.0;6.9]	63.7
	4.0_b	*dd* [12.0;3.1]	
CH*sn*-2	5.1	*m*	71.8
CH_2 *sn*-3	3.9	*t* [5.9]	64.8
CH_2OP	4.17	*m*	60.3
CH_2N	3.5	*m*	67.3
$(CH_3)_3N$	3.1	*s*	54.5

The ^{13}C-NMR spectrum of phosphatidylcholine contained a fatty acid region with lipid signals of CH_3 at δ 14.39 and of CH_2 from δ 23.64 to 35.19 that correspond to allylic region; also, carbonyl signals of two esters at δ 174.9 and 174.6 corresponding to chains esterified at sn-1 and sn-2 of glycerol. The hydrophilic region of the structure is represented by the glycerol moiety at sn-3 esterified with a phosphate group which itself is esterified with the OH-group of choline **(Figure 2-4).**

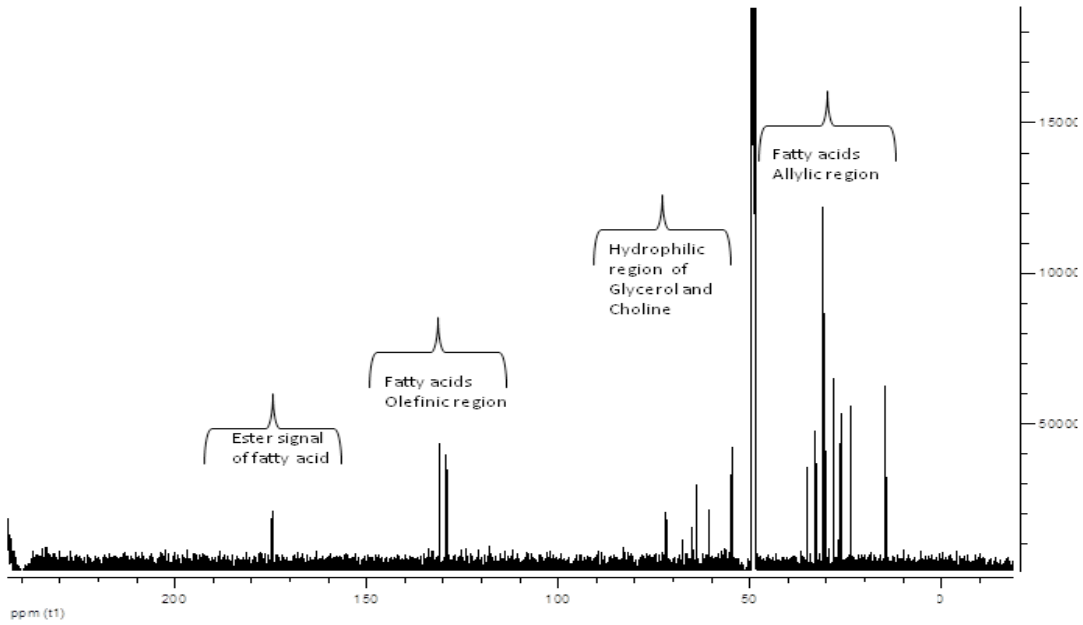

Figure 2-4. 600 MHz ^{13}C-NMR spectrum of phosphatidylcholine in CD_3OD.

The most characteristic ^{1}H signals of phosphatidylcholine or lecithin is the singlet at 3.1 ppm from $(CH_3)_3N$ and the multiplet at 3.5 ppm, due to CH_2N. Moreover, the multiplet at 4.17 ppm shows the correlation with the ^{13}C resonance of 60.39 ppm corresponding to CH_2OP **(Figure 2-5).** Furthermore, the ^{31}P spectrum showing the resonances at 0.729 ppm determinates the Phosphorous in the structure (Kaffarnik et al. 2013) **(Figure 2-6).**

Comparison of resonances in ^{13}C and DEPT NMR spectra confirmed the presence of methyl and methylene from the choline moiety, whose signal of CH_3 at δ 54.5 had three resonances linked to each other and a correlation with the singlet at 3.1 ppm from $(CH_3)_3N$**, (Figure 2-7);** also resonances of CH_2OP and CH_2N at δ 60.3; and at 67.3, respectively, in correlation with the multiplet at 4.17 and 3.5 ppm **(Table 2-1).**

Two linoleic fatty chains were elucidated in the ^{13}C spectrum of phosphatidylcholine which showed ester carbonyl signals at δ 174.6 and 174.9,methylene and methine signals between δ 23.64 and 35.19 with predominant signals of CH_2 at δ 30.84, δ 30.86 and CH_3 at δ 14.5. Also double bond lipids were detected with several signals at δ 129.2, 129.0, δ 130.8 and 131.0, which correspond to two unsaturated linoleic fatty acid chains. The DEPT NMR spectrum

showed inverted CH_2 signals in the carbohydrate region from δ 30.07 to 30.41 matching eight CH_2 in the allylic region, between CH_2 4-7. Further signals were at δ 34.8 and 34.9 representing CH_2-2, and signals from δ 23.8 to 28.1 that belong to CH_2-3, 11, 14, 17 and confirm the presence of two fatty acids. COSY and NOESY spectra allowed the assignment of proton signals and HMBC spectra, which was then used for assigning ^{13}C-NMR signals **(Table 2-2).**

Examination of linoleic acid using COSY, NOESY and HMBC gave information to confirm that the fatty acid could be an unsaturated omega-6 fatty acid. The 2D NMR correlation displayed a proton signal between CH_3-18 and CH_2-17, CH_2-16 and also a resonance between CH_2-14 and CH_2-15 is apparent.

The glycerol moiety was confirmed by 1D and 2D NMR spectra which sustained proton signals at δ 3.9, 5.1 and 4.0-4.3 for CH_2 *sn*3, CH_2 *sn*2 and CH_2 *sn*3, respectively, and their correlation with ester carbonyl signals from the fatty acid and the distribution of them related to the structure of PTC. Linoleic acid with C-1 signal at δ 174.9 showed correlation resonance in the HMBC spectrum with δ 4.0-4.3 proton equivalent to CH_2 *sn* 1. Similarly, C-1 signal at δ 174.63 had a correlation resonance with δ 5.1 equivalent to CH_2 *sn* 2 of the glycerol part.

Table 2-2. 1H-NMR and 13C-NMR spectroscopic data of two linoleic acids (18:2Δ9, 12) as part of the structure of PTC and assignment of resonances in the 600 MHz 1H-NMR and 150 MHz 13C-NMR in CD3OD. The full assignments of the structures were based on 2D experiments and literature data (Sassaki et al. 1999; Gunstone 1990; Zamora et al. 2002; Vlahov 2009).

Assignment	**δ^{1}H (ppm) R1-R2**	**Multiplicity J/ Hz**	**δ^{13}C (ppm) $^{\delta}$R1-R2**
CH_2-1	---	---	174.9-174.6
CH_2-2	2.20	*m*	34.8-34.9
CH_2-3	1.50	*m*	26.0-26.9
CH_2-4, 7	1.20	*m*	30.0-30.4
CH_2-8	1.97	*t* [6.80]	28.1-28.1
CH_2-9	5.20	*m*	130.9
CH_2-10	5.20	*m*	129.0
CH_2-11	2.60-2.20	*m*	26.5-26.0
CH-12	5.20	*m*	129.2
CH-13	5.20	*s*	130.8
CH_2-14	2.00	*m*	28.1-28.1
CH_2-15	1.18	*t* [7.60]	30.8
CH_2-16	1.25	---	32.6-33.0
CH_2-17	1.30	---	23.8-23.7
CH_3-18	0.89	---	14.5

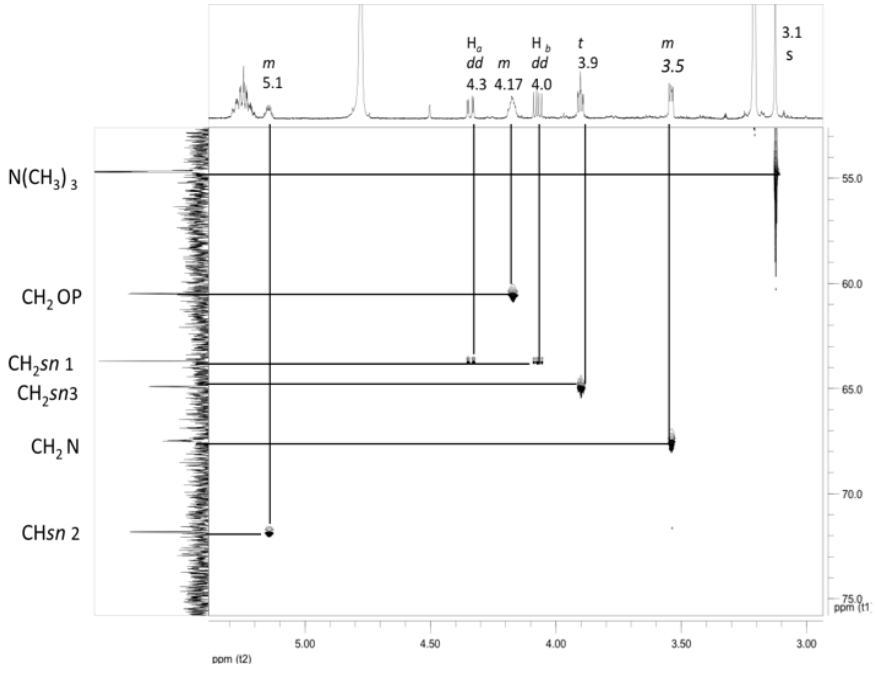

Figure 2-5. ^{1}H-NMR and ^{13}C-NMR HSQC spectra of phosphatidylcholine (hydrophilic region). The spectral region of hydrophilic portion between 50-75 ppm resonances of ^{13}C and the ^{1}H signals represents the phosphate group esterified with the OH-group of choline.

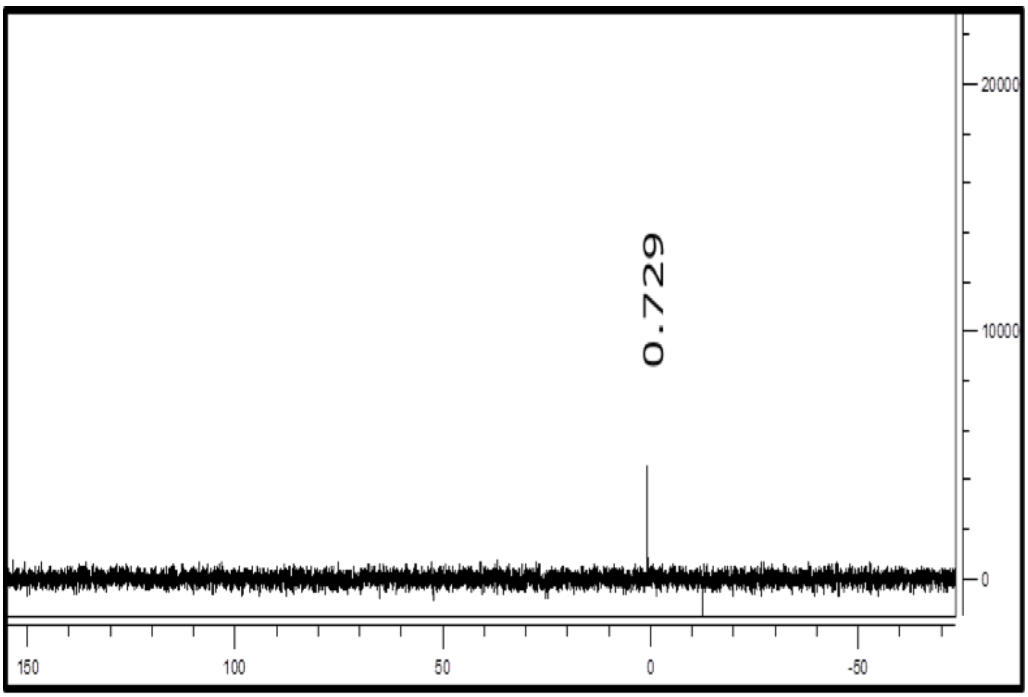

Figure 2-6. One dimensional ^{31}PNMR spectra of phosphatidylcholine (PTC).

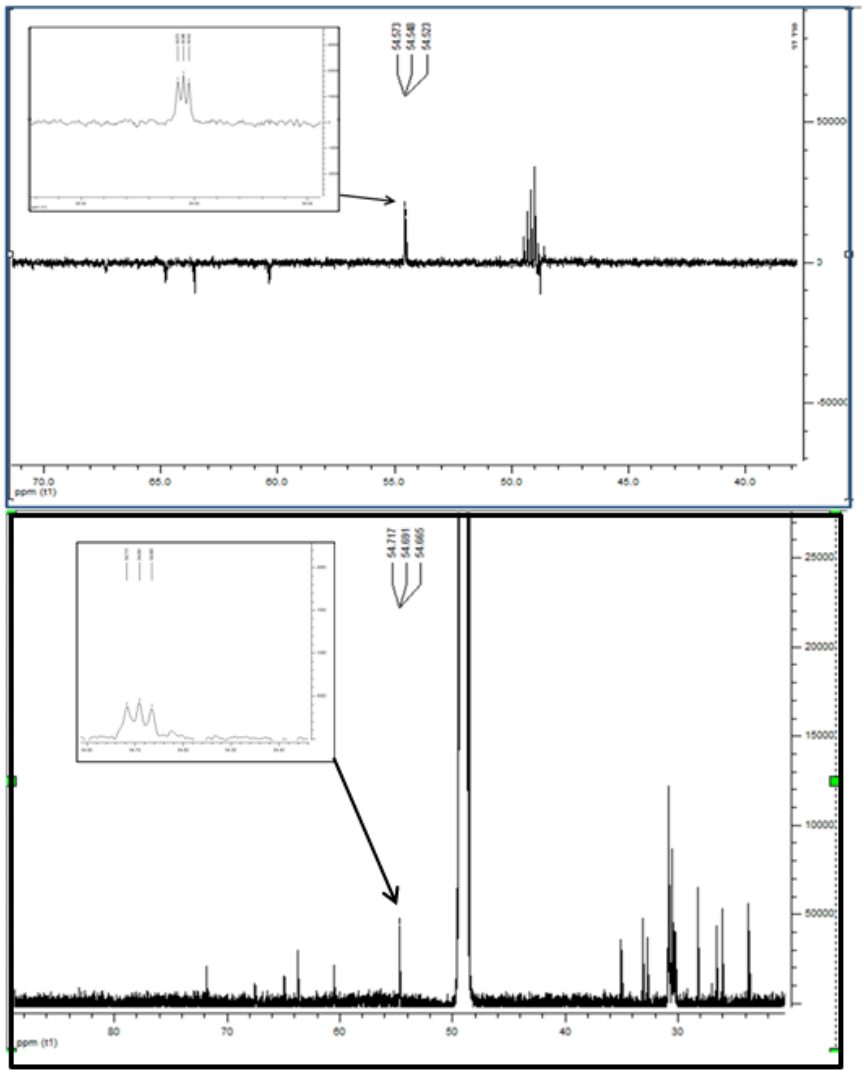

Figure 2-7. ^{13}C and DEPT NMR spectra of methyl belongs to hydrophilic section of the PTC corresponding to $(CH_3)_3N$.

High performance liquid chromatography/atmospheric pressure chemical ionization mass spectrometry (HPLC-APCI-MS/MS) was applied to identify and confirm the structure of phosphatidylcholine in positive (+) mode. The APCI is the most frequently ionization technique used in HPLC-MS analysis of diacylglycerides and triacylglycerides because it enables – in addition to the molecular mass (Mr) determination – the identification of the individual acyl moieties from the $[M+H\text{-}RCOOH]^+$ ions.

In the phosphatidylcholine spectrum **(Figure 2-8)** the molecular ion peak was identified as *m/z* 780.4, which confirms a structure of 1-2-dilinoleyl glyceryl-

phos-phorylcholine and a ion at *m/z* 663.2, as a base peak. The ions *m/z* 618.4, 607.1 are interpreted as a result of extensive rearrangements involving the expulsion of the phosphate group as it is described for other Phosphorous-containing molecules. The other ions in this group are suggested as arising from the choline moiety (Klein 1971; Ismaiel et al. 2008; Jensen et al. 1986). The linoleic acid is represented in the spectrum at *m/z* 297.9 as [M+H_2O].

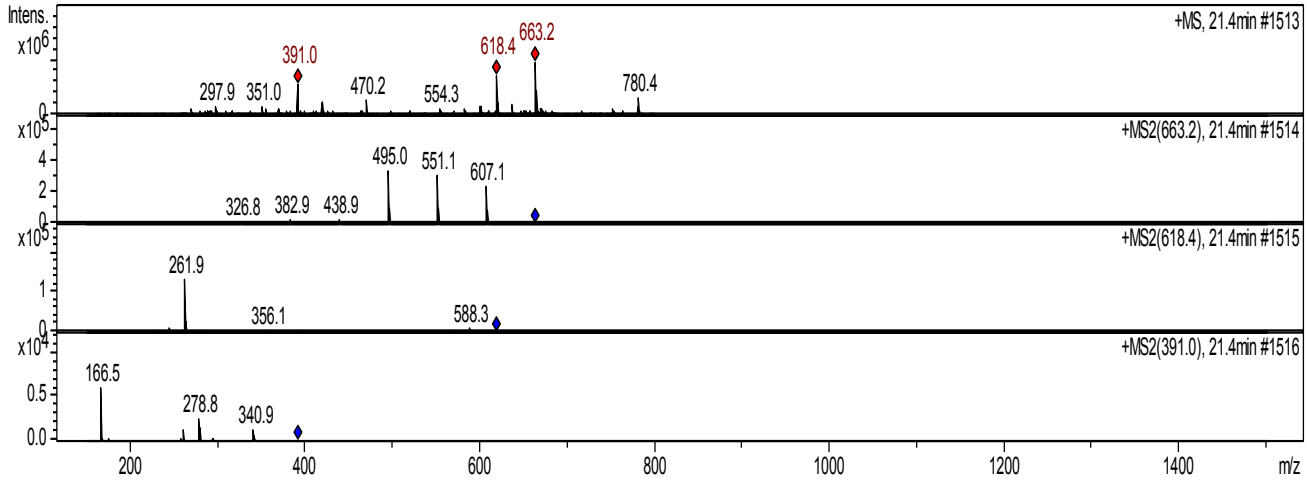

Figure 2-8. Positive-ion APCI mass spectra of 1-2-dilinoleyl glyceryl-phosphorylcholine. Intensity [mAU] depicts the percentage relative abundance plotted against *m/z* values between 150 and 1500. The peak *m/z* 780.4 was identified as the molecular ion peak and three daughter ions at *m/z* 663, *m/z* 618.4 and *m/z* 391.0 result from the loss of choline and Phosphorous moieties and the fragmentations of the linolenic acid.

2.1.2 Glycosyldiacylglycerolipids

Previous analysis reported the presence of glycosylglycerides in Banana but these compounds have not been fully characterized (Aghofack-Nguemezi and Manka`abiengwa 2012); Blackbourn et al. 1990). Galactosyl-glucosyl-diacylglycerol (GGDG) (*O*-α-*D*-Gal*p (1''→ 6')*- *O*-*β*-*D*-Glu*p (1'→ 3)*- 2, 1-*L*-diacyl-glycerol was isolated in fraction 4 of a preparative HPLC-reverse phase RP-18 system which came from the fraction 7 of HSCCC separation of Baby Banana peels **(Figure 2-2).** The compound was pure in fraction 4 and gave only one band in the TLC screening of the RP-18 preparative HPLC. 1 mg of GGD was sufficient to elucidate the structure by 1D/2D NMR experiments. The relevant correlations are summarized in **Table 2-3.**

Table 2-3. ^{1}H-NMR and ^{13}C-NMR spectroscopic data of *O*-α-D-Gal*p* (1''→ 6')- O-β-D-Glu*p* (1'→ 3)- 2, 1-diacyl-L-glycerol-GGDG and assignment of resonances in the 600 MHz ^{1}H-NMR and 150 MHz ^{13}C-NMR in CD_3OD. The full assignments of the structures were based on 2D experiments and literature data (Sassaki et al. 1999; Sobolev et al. 2005; Colson and King 1976).

Assignment Glycolipid GGDG	**δ^{13}C (ppm)**	**δ^{1}H (ppm)**
C-1''	100.63	4.70
C-2''	70.24	3.67
C-3''	71.48	3.63
C-4''	71.13	3.79
C-5''	72.60	3.74
C-6''	62.87	3.612_a-3.62_b
C-1'	105.35	4.14
C-2'	72.40	3.41
C-3'	74.69	3.38
C-4'	70.02	3.77
C-5'	74.62	3.638
C-6'	67.80	3.58_a-3.80_b
C-1', Gly	63.97	4.1_a-4.3_b
C-2', Gly	71.46	5.15
C-3', Gly	68.74	3.62_a-3.88_b

2.1.2.1 O-α-D-Gal*p* (1''→ 6')- O-β-D-Glu*p* (1'→ 3)- 2, 1-diacyl-L-glycerol (GGDG)

The GGDG showed in the ^{1}H and ^{13}C NMR spectra two anomeric signals at δ 4.14/105.35 for a single βGlu*p* unit and at δ 4.7/100.63 for a single αGal*p* unit. HMBC examination gave useful information for the ^{1}H and ^{13}C NMR assignments, and confirmed signals that correspond to a glycerol, to an *O*-substituted C-6' of β-Glu*p* unit (δ 67.8) and a non-substituted C-6'' signal at δ 62.87 belonging to αGal*p.* Characteristic coupling constants afforded the configuration of the glycosidic bonds: $^{3}J_{1''\text{-}2''}$= 3.8 Hz for the anomer H-1'' (δ 4.7), together with ^{13}C chemical shift (δ 100.63), indicated the α-galactopyranosidic linkage to the aglycone moiety, and a value of $^{3}J_{1'\text{-}2'}$ = 7.0 Hz for the anomeric H-1' (δ 4.14) with HSQC correlation ^{13}C chemical shift (δ 105.35) and relevant chemical shift data identified the unit of the β-glucopyranoside (Hansen 1981; Hansen et al. 1981)

The combined use of homonuclear and heteronuclear two-dimensional NMR has provided support to establish the arrangement of substituents in the structures, according to the determination of the ^{1}H-^{1}H coupling constants, and in addition of COSY and NOESY observations of the resonances. Vicinal, geminal and long distance coupling for glucose and galactose structures were assigned and summarized in **Table 2-4**.

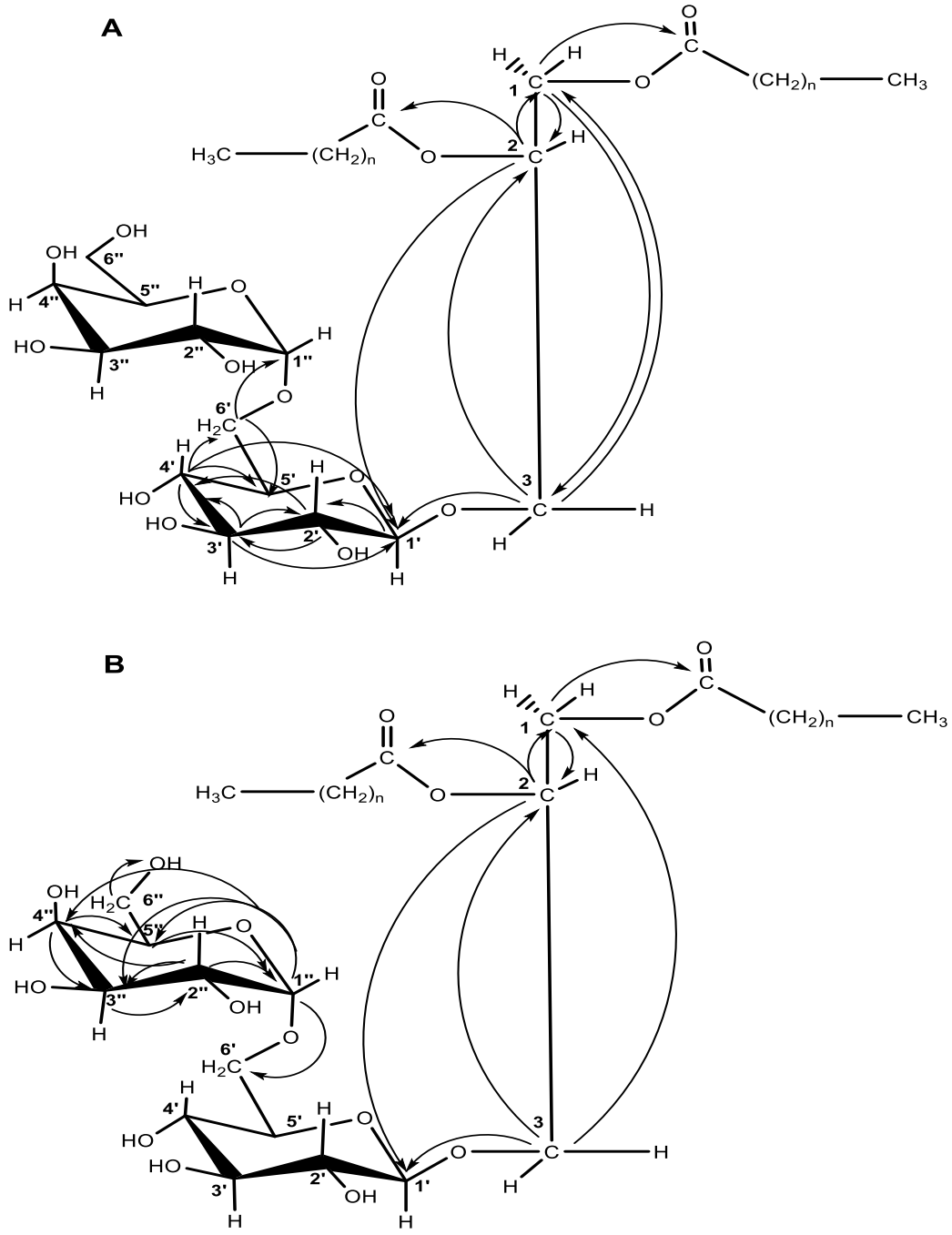

Figure 2-9. Structure relevant long-range HC-correlation in the HMBC of *O*-α-D-Gal*p* (1''→ 6')- *O*-β-D-Glu*p* (1'→ 3)- 2, 1-diacyl-L-glycerol. (A) Glucose HMBC; (B) Galactose HMBC.

The application of the COSY and NOESY technique in spectral assignments demonstrated the power of the technique to illustrate the assignments of the substituents and also confirmed that the lower sugar unit was glucose. **Figure 2-10** shows the coupling information contained in the spectrum. The ^{1}H-^{1}H connectivities in the homonuclear chemical shift correlation spectrum (COSY) allowed a straightforward assignment of the proton resonances.

Table 2-4. COSY correlations of *O*-α-D-Gal*p* (1''→ 6')- *O*-β-D-Glu*p* (1'→ 3)- 2, 1-diacyl-L-glycerol.

Glucose (A) Methanol-d4 99, 96% ^{1}H(ppm) J=Hz		**Galactose(B) terminal sugar moiety Methanol-d4 99, 96% ^{1}H (ppm) J=Hz**	
H'-1	4.14 (*dd, 1H,* $^{4}J_{1\text{-}Sn3\text{-}Hb}$= 3.0 Hz $^{3}J_{1'\text{-}2'}$= 7.0 Hz)	H''-1	4.75 (*d*, 1H, $^{3}J_{1''\text{-}2''}$=3.8 Hz)
H'-2	3.41 (*dd,* 1H, $^{3}J_{2'\text{-}1'}$ =7.3 Hz, $^{3}J_{2'\text{-}3'}$ = 9.8 Hz)	H''-2	3.68 (*dd*, 1H, $^{3}J_{2''\text{-}1''}$=3.8 Hz, $^{3}J_{2''\text{-}3''}$=10.1 Hz)
H'-3	3.38 (*dd,* 1H, $^{4}J_{3'\text{-}1'}$ 3.2 Hz, $^{3}J_{3'\text{-}4}$ = 9.6)	H''-3	3.62 (*dd*, 1H, $^{3}J_{3''\text{-}4''}$=2.7 Hz, $^{4}J_{3''\text{-}5''}$=3.9 Hz
H'-4	3.77 (*dd,* 1H, $^{4}J_{4'\text{-}6'Ha'}$ =1.0 Hz, $^{4}J_{4'\text{-}5'}$ 3.2 Hz	H''-4	3.79 (*dd*, 1H, $^{3}J_{4''\text{-}3''}$=2.6 Hz, $^{3}J_{4''\text{-}5''}$=3.7 Hz)
H'-5	3.63 (*m,*1H)	H''-5	3.75 (*m*, 1H)
H'-6_a	3.58 (*d,*1H, $^{2}J_{H6a'\text{-}6Hb'}$=6.9 Hz,	H''-6_a	3.62 (*m*, 1H)
H'-6_b	3.8 (*d,*1H, $^{2}J_{H6b'\text{-}6Ha'}$= 6.2 Hz,	H''-6_b	3.61 (*m*, 1H)

The COSY correlation between H'-1 and H'-2 with a vicinal coupling constant $^{3}J_{1'\text{-}2'}$= 7.0 Hz confirms how the βGlu trans-arrangement is supported by the coupling constant of H'-2, whose values match the vicinal coupling $^{3}J_{2'\text{-}1'}$ =7.3 Hz and $^{3}J_{2'\text{-}3'}$ = 9.8 Hz. In addition, the COSY correlations between H'-3 and H'-4 can be reflected by the vicinal coupling of H'-3, $^{3}J_{3'\text{-}4'}$ =9.6 Hz, which shows a trans-arrangement between H'3 and H'4. Moreover, the axial position of H'4 and the confirmation of the glucose pyranose as the sugar moiety connected to the glycerol moiety could be demonstrated (Iida-Tanaka et al. 2002; Inagaki et al. 1987). The meaningfully information of the COSY correlation and the coupling constants are illustrated **(Figure 2-11; Table 2-4).**

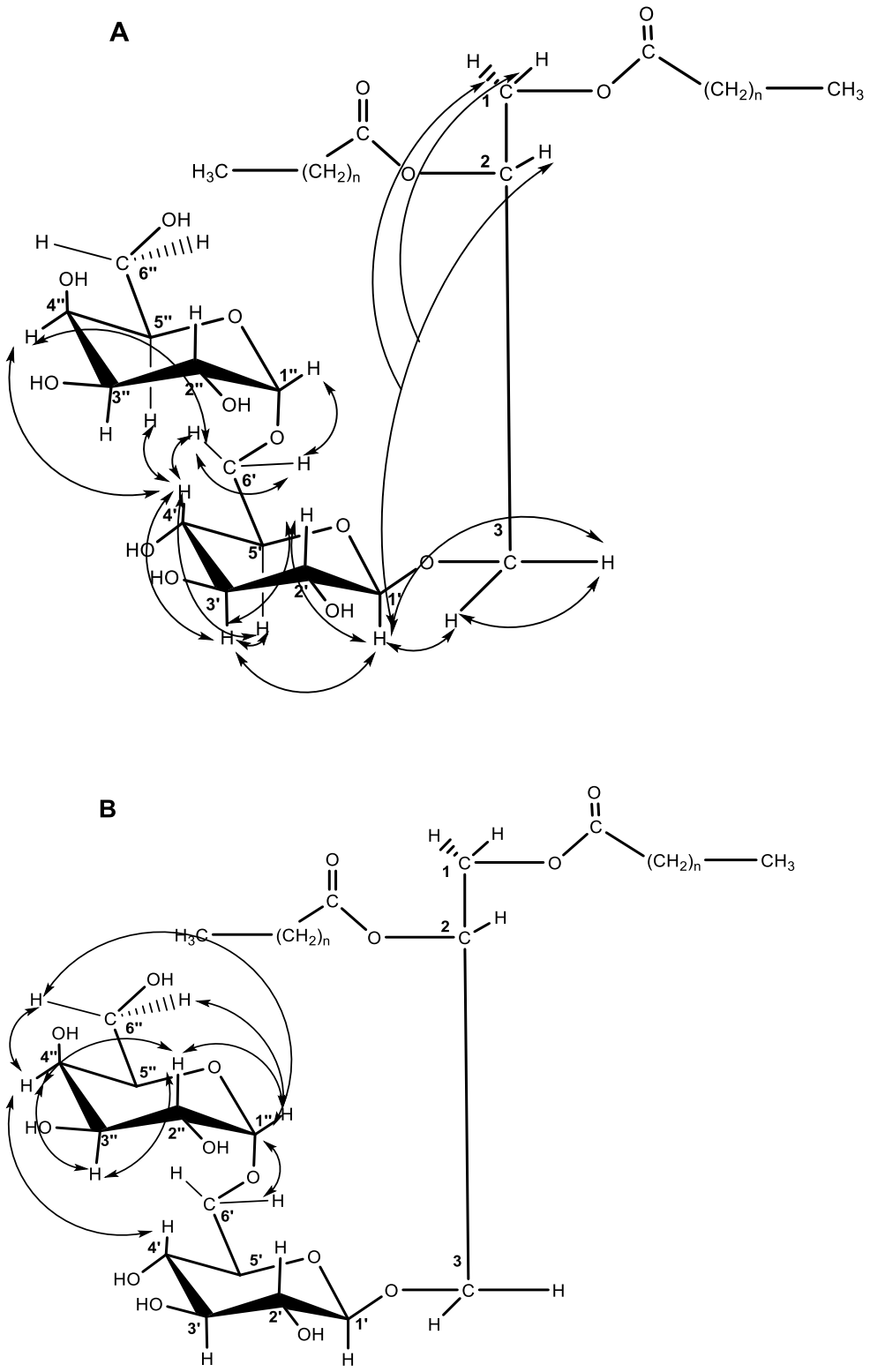

Figure 2-10. Structure relevant correlation in the COSY of *O*-α-D-Gal*p* (1''→ 6')- *O*-β-D-Glu*p* (1'→ 3)- 2, 1-diacyl-L-glycerol in CD_3OD. (A) Glucose COSY; (B) Galactose COSY.

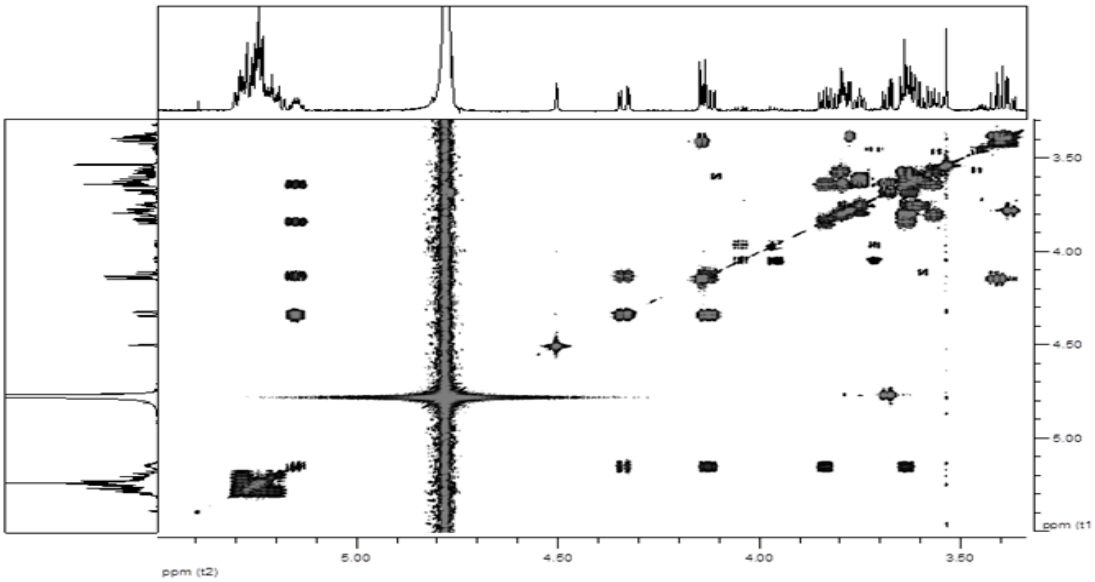

Figure 2-11. The 600 MHz COSY spectrum of *O*-α-D-Gal*p* (1''→ 6')- *O*-β-D-Glu*p* (1'→ 3)- 2, 1-diacyl-L-glycerol in CD_3OD.

The cis-arrangements of two adjacent protons in position C''-3 and C''-4 are depicted by the coupling constant of H''3 which corresponds to (*dd*) $^3J_{3''\text{-}4''}$=2.7 Hz, $^3J_{3''\text{-}5''}$=3.9 Hz) where the vicinal coupling $^3J_{3''\text{-}4''}$= 2.7 Hz shows a typical equatorial arrangement. Likewise, the value of coupling constant 2.7 Hz is found in the result of coupling constant calculation for H''-4, which supports the equatorial arrangements for the H''-4. Thus, the COSY correlation evidences the coupling constants calculation for the terminal sugar moiety in the structure and therefore it is possible to conclude that a galactosyl pyranose could correspond to the terminal sugar moiety in the structure **(Figure 2-11; Table 2-4).**

The stereochemistry *O*-α-D-Gal*p* (1''→ 6')- *O*-β-D-Glu*p* (1'→ 3)- 2, 1-diacyl-L-glycerol was determined through 600 MHz 2D NOESY experiments and played a crucial role in defining relationships among those molecules which share close proximity. **Figure 2-12** shows a close proximity between C''-4 and C''-3 with C'-4, which supports the arrangement of the substituents, thus proving the lower sugar moiety to be Glu*p* and the upper to be Gal*p.*

Observation of strong NOEs resonances **(Figure 2-12)** of Gal*p* between protons H''-4''-5''-3''-2'', clearly indicated that all interfering protons are located on the same side of the cyclohexane plane. Similarly, the NOEs effect from H'-5 (δ 3.638) and H'-4 (δ 3.77) linked to Gal*p* — with the protons H'' 3-4-5 from Glu*p* — supports the spatial proximity between protons and also between the sugars besides their stereochemistry. It is relevant that NOE enhancements from H'-5 (δ 3.638) belong to Glu*p* and are related to the majority of protons coming from Glu*p* and Gal*p*. This indicates that the free rotation of the ring could be restricted and that it is occupying a fixed position related to the Glu*p* sugar. The close proximity among the nuclear protons from glycerol moiety with H''1 and H'1-2, in Glu*p* and Gal*p* respectively, illustrates how these protons share close proximity.

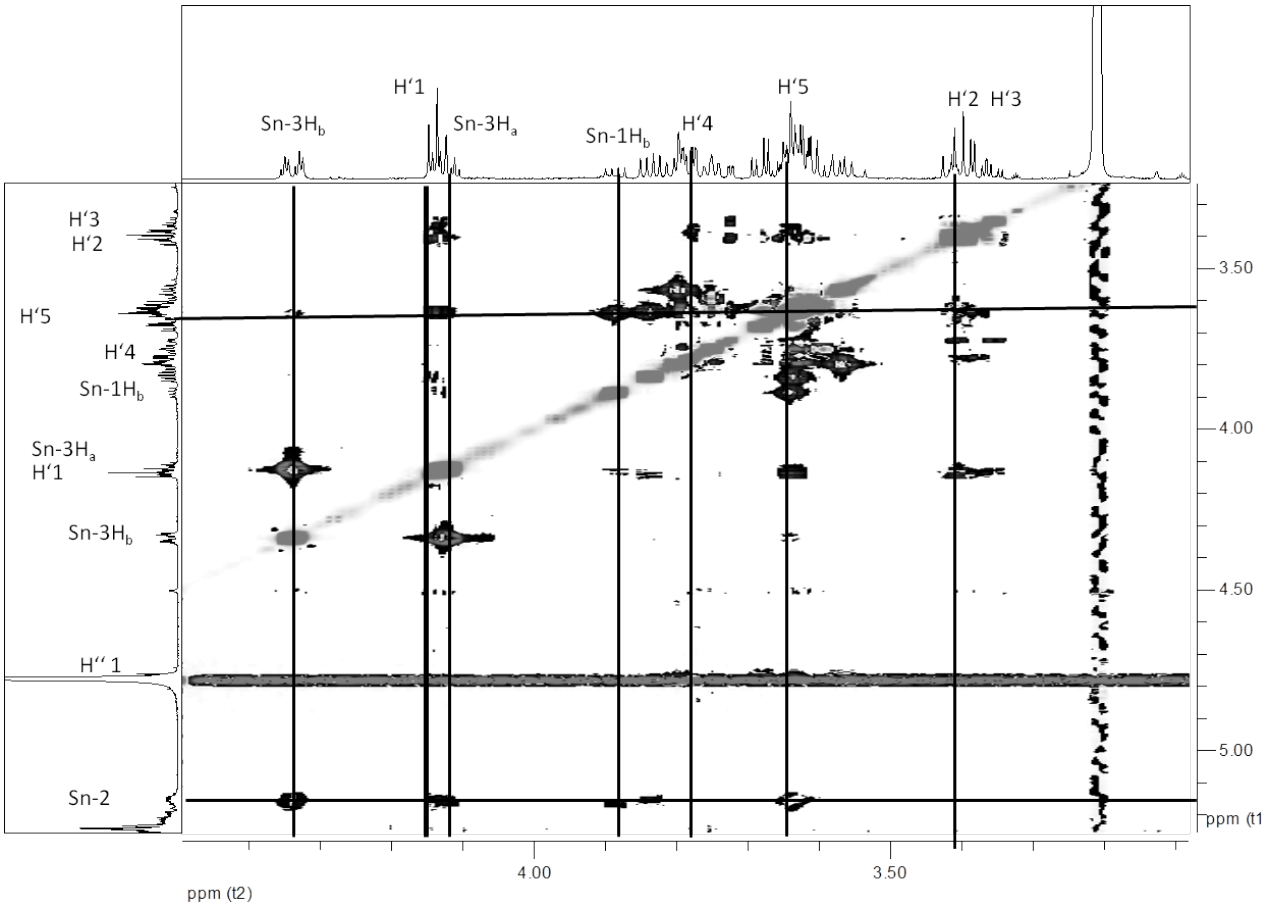

Figure 2-12. The 600 MHz 2D NOESY spectrum of O-α-D-Gal*p* (1''→ 6')- O-β-D-Glu*p* (1'→ 3)- 2, 1-diacyl-L-glycerol in CD_3OD with relevant enhancements used to define the stereochemistry of the molecule.

The L-glycerol molecule was established in the GGDG as part of HMBC experiments whose results stated the multiple-bond correlation 3 of the glycerol moiety, in the right side of the GGDG molecule, between C-1, C-2 and C-3 **(Figure 2-13)**. It is evident now that the fatty acid linked to the chiral center of the glycerol moiety is pointing to the left. Hence, the top carbon of the glycerol is then denoted C-1.

The ^{13}C NMR spectrum showed two lipid signals at δ 14.44 and δ 14.69, as well as ester carbonyl signals at δ 175.08 and δ 174.72. Lipids containing double bonds were indicated by three signals in a range between δ 128.29-129.24 and three signals between δ 130.76-132.73. Moreover, the HMBC spectrum corroborated the linkage of δ 175.08 and δ 174.72 signals at the C-1, C-2, respectively, of the glycerol moiety. The DEPT and ^{13}C NMR experiments enabled the complete determination of the -CH_2 chain carbons of the allylic region with signals of CH_2 from δ 21.54 to δ 36.50, with predominancy at 26.46 corresponding to C-11 and linked to the fatty acids. With these NMR results, the structures of the fatty esters are linolenic (18:3Δ 9, 12, 15) and palmitic acid (16:0) **(Table 2-5).**

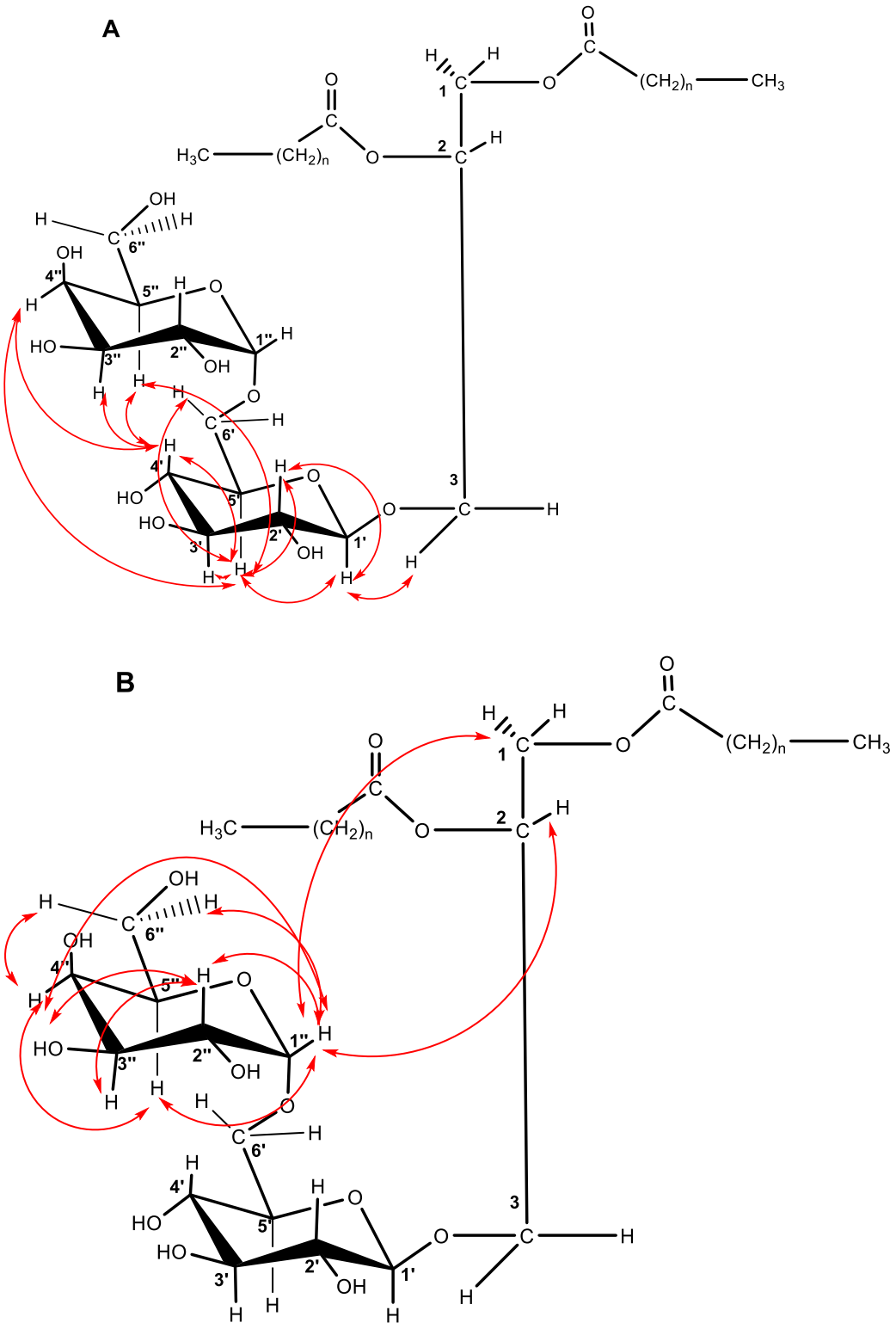

Figure 2-13. Relevant NOEs enhancements used to define the stereochemistry of *O*-α-D-Gal*p* (1''→ 6')-*O*-β-D-Glu*p* (1'→ 3)- 2, 1-diacyl-L-glycerol in CD_3OD (A) Glucose NOESY (B) Galactose NOESY.

Table 2-5. ^{1}H-NMR and ^{13}C-NMR spectroscopic data of ω-3 linolenic acid (18:3 Δ9, 12, 15) and palmitic acid (16:0) as part of the structure of O-α-D-Gal*p* (1''→ 6')- O-β-D-Glu*p* (1'→ 3)- 2, 1-diacyl-L-glycerol (GGDG) and assignment of resonances in the 600 MHz ^{1}H-NMR and 150 MHz ^{13}C-NMR measured in CD_3OD. The full assignments of the structures were based on 2D experiments and literature data (Sassaki et al. 1999; Gunstone 1990; Zamora et al. 2002; Vlahov 2009).

LINOLENIC ACID **Assignment**	**δ^{1}H (ppm)-R1**	**Multiplicity *J*/ Hz**	**δ^{13}C (ppm)-R1**
CH_2-1	---	*q* [7.6]	175.08
CH_2-2	2.22	*dd*[6.6]	35.15
CH_2-3	1.51	[12.4]	26.08
CH_2-4,7	1.23	*m*	30.04-30.47
CH_2-8	1.99	*m*	28.26
CH_2-9	5.28	*m*	131.03
CH_2-10	5.24	*m*	128.91
CH_2-11	2.71	*t* [6.0]	26.46
CH -12	5.24	*m*	129.24
CH -13	5.24	*m*	130.76
CH_2-14	2.71	*m*	26.46
CH_2-15	5.21	*m*	128.29
CH_2-16	5.28	*m*	132.73
CH_2-17	1.98	*m*	21.54
CH_3-18	0.87	*t* [7.5]	14.71
PALMITIC ACID **Assignment**	**δ^{13}C (ppm) δ-R2**	**Multiplicity J/ Hz**	**δ^{13}C (ppm)-R1**
CH_2-1	---	m	174.72
CH_2-2	2.09	*dd*[6.9]	36.50
CH_2-3	1.50	[13.1]	26.08
CH_2-4	1.23	m	30.04
CH_2-5-12	1.19	m	30.43-30.65
CH-13	1.23	m	30.27
CH_2-14	1.18	m	33.21
CH_2-15	1.21	m	23.79
CH_2-16	0.80	*t* [6.8]	14.44

In order to complement the compositional analysis of fatty acid and their chemical structure, a diluted sample was used for the methanolysis and an analysis was carried out by means of gas chromatography–MS of the methyl esters **(c.f 4.3.3.1).** The mass spectrum confirmed the occurrence of methyl linolenolate as the majority peak *m/z* 292, and in a lower proportion, the presence of methyl palmitoleate at *m/z* 270. The incidence of a small peak could be explained as a glycerol moiety **(Figure 2-14)**.

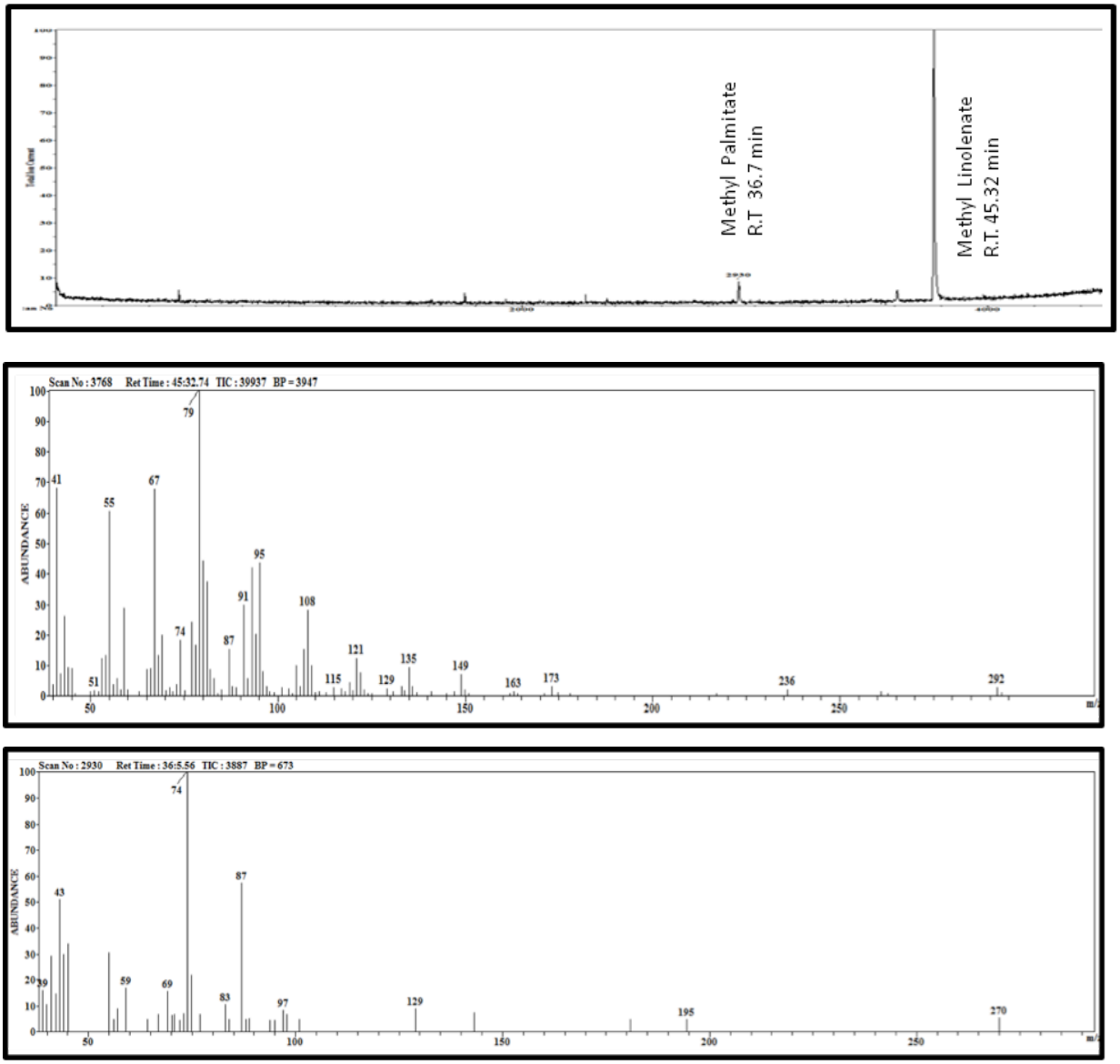

Figure 2-14. GC-MS chromatogram and mass spectrum from the acyl moiety from *O*-α-D-Gal*p* (1''→ 6')-*O*-β-D-Glu*p* (1'→ 3)-2, 1-diacyl-L-glycerol after the derivatization. The resulting methyl ester derivatives corresponded to a linolenic acid (*m/z* 292) and to a palmitic acid (*m/z* 270), and retention times of 45.32 and 36.07 min, respectively. The chromatogram of the methyl ester derivatives depicted the occurrence of few other peaks possibly corresponding to oleic and linoleic acids in low proportion.

For sensitive detection of the of *O*-α-D-Gal*p* (1''→ 6')- *O*-β-D-Glu*p* (1'→ 3)- 2, 1-L-diacyl-glycerol, atmospheric pressure chemical ionization mass spectroscopy (LC-APCI-MS) is operated in positive mode in accordance with the conditions described **(c.f 4.2.2).** The LC-APCI-MS spectrum emitted abundant and complex signals with Na^+ adduct $[M+Na]^{\cdot+}$ and fragment ions at *m/z* 613, corresponding to diacylglycerol moiety $[CH_2(OCOR^1)CH(OCOR^2)CH_2OH_2OH_2]^{\cdot+}$, as

well as at *m/z* 335 corresponding to monoacylglycerol moiety $[CH_2(OCOR^1)CH(OH)CH_2]^{\cdot+}$ in agreement with literature data (Yamauchi et al. 2001, Yamauchi 2005).

The APCI–MS data shows two linolenic acids in the acyl moiety as a prominent daughter ion at *m/z* 613 (100% percentage relative intensity) and its fragmentation at *m/z* 522 $[R^1]^{+\cdot}$ $[R^2]^+$ corresponding to two molecules of linolenic acid $2[M]^+$-H_2O. The sugar moieties fragmentation is depicted at *m/z* 423 by means of two sugars in addition to glycerol, and the addition of a low mass fragment at *m/z* 198 which could be represented as a sugar moiety $[M]^+$-H_2O **(Figure 2-5)**.

A daughter peak at *m/z* 683 (47.90% percentage of relative intensity) could be the result of the loss of a palmitoyl group at *m/z* 236, in that case the precursor ion at *m/z* 942 could be detected, this is because the ion extraction does not happen in the current spectrum (Benning et al. 1995). **Table 2-6** and **Figure 2-15a-b** summarize the APCI-MS analysis of the *O*-α-D-Gal*p* (1''→ 6')-*O*-β-D-Glu*p* (1'→ 3)-2, 1-L-diacyl- glycerol (GGDG) being in agreement with literature data (Yamauchi et al. 2001, Yamauchi 2005; Benning et al. 1995; Holcapek et al. 2003).

Table 2-6. APCI-MS data of O-α-D-Gal*p* (1''→ 6')- O-β-D-Glu*p* (1'→ 3)-2, 1 -L-diacyl- glycerol (GGDG) separated by Reversed-Phase HPLC and the prominent daughter ions representing the GGDG in the spectrum according to literature data (Yamauchi et al. 2001, Yamauchi 2005; Benning et al. 1995; Holcapek et al. 2003).

ION	**PEAK (*m/z*)**
$[M+Na].^+$ $[M-Na].^+$	973 950
Diacylglycerolmoiety $[CH_2(OCOR^1)CH(OCOR^2)CH_2OH_2OH_2].^+$	613
Monoacylglycerol $[CH_2(OCOR^1)CH(OH)CH_2].^+$,	335
Acyl moiety (18:3 /18:3) $[R_1]$	278
$[R_1]$ and $[R_2]$-H_2O $[R_{1\text{-}2}]$ Linolenic acid	522

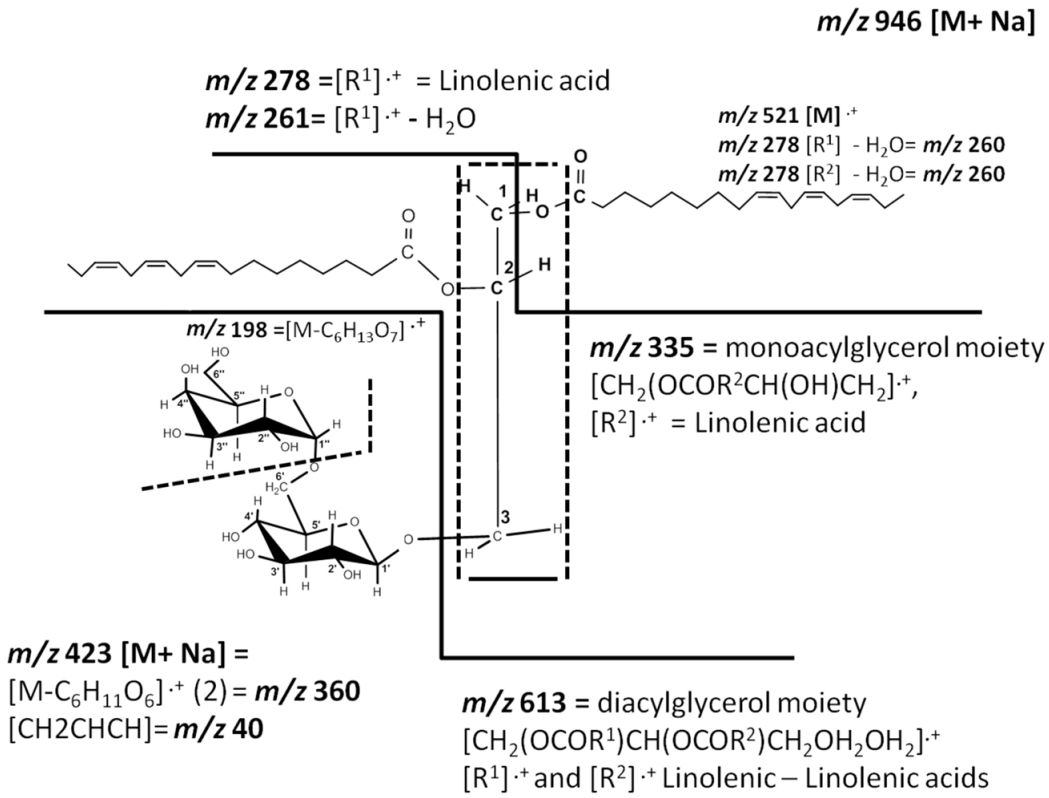

Figure 2-15 a. Proposed fragmentation for O-α-D-Gal*p* (1''→ 6')- O-β-D-Glu*p* (1'→ 3)-2, 1 -L-diacyl-glycerol (GGDG) based on HPLC-APCI-MS.

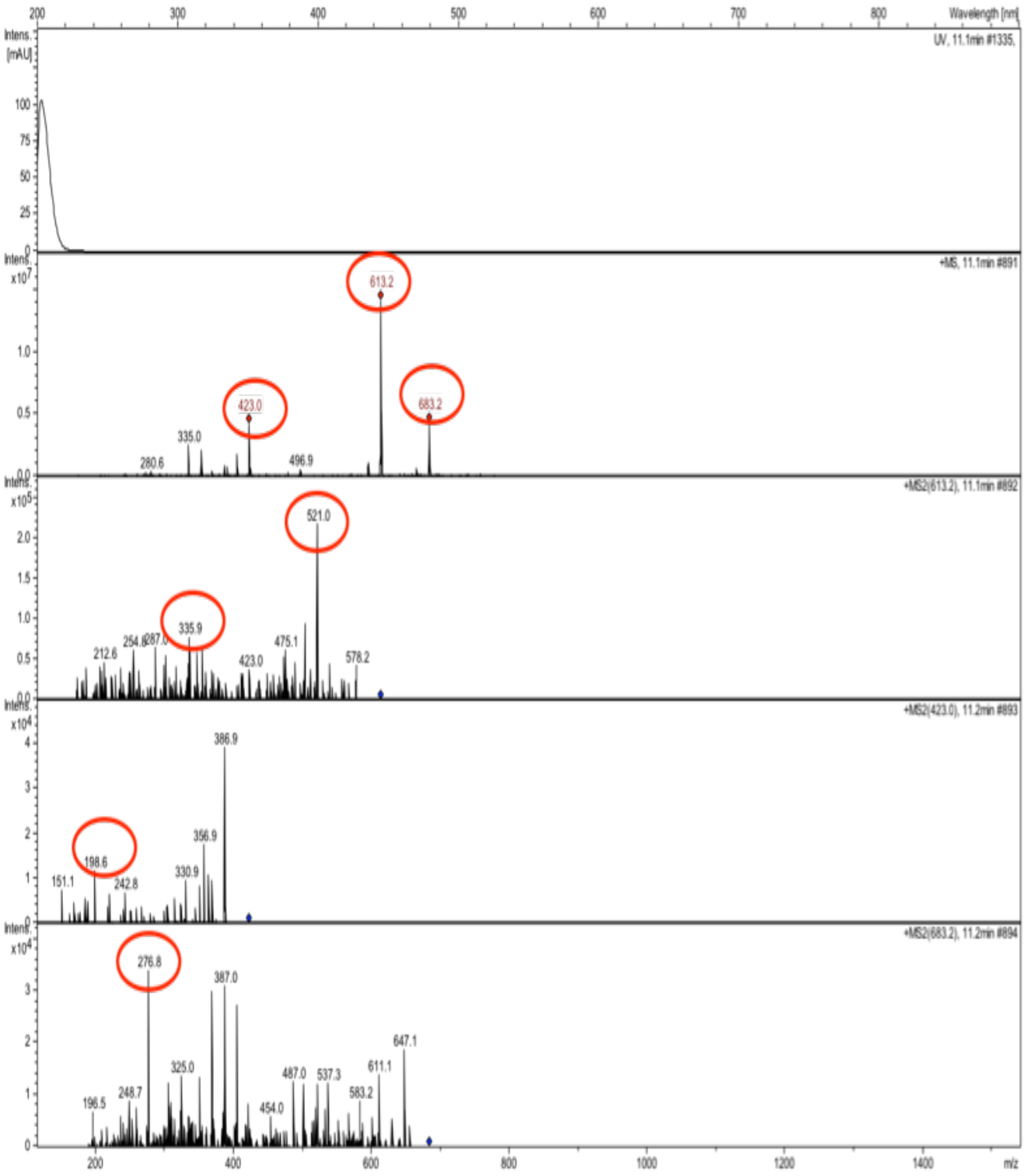

Figure 2-15 b. The mass spectra for O-α-D-Gal*p* (1''→ 6')- O-β-D-Glu*p* (1'→ 3)-2, 1 -L-diacyl- glycerol (GGDG) by HPLC-APCI-MS and the proposed fragmentation schema with 18:3/18:3 linolenic acid as acyl moieties (Yamauchi et al. 2001; Yamauchi 2005; Benning et al. 1995) (Figure 2-15a).

The results obtained with different methods like gas chromatography-MS and APCI-MS, could explain the occurrence of both linolenic and palmitic fatty acids and support the presence of lower traces of linoleic and oleic acids. The APCI-MS chromatogram depicts a prominent peak, two minor minor peaks, and three minor peaks between 10.9 and 11.3 min. However, the result of both methods indicated that linolenic fatty acid species were predominant in the digalactosyl-glucosylglycerol in fraction 4. The total ion APCI –MS chromatogram matches literature data (Yamauchi et al. 2001, Yamauchi 2005).

Although the result of mass spectrometry (APCI-MS) may be seen in contradiction with the NMR spectrum, specifically related to the acyl moiety, the sensitivity and accuracy of NMR 1D/2D procedures detected the existence of two type of methyl signals at δ 14.44 and δ 14.71 derived from palmitic and linolenic acid respectively. Nevertheless, the predominance of linolenic acid as main species in the structure is indicated in the spectrum since the chemical shift at δ 0.87 from linolenic acid has a higher intensity in comparison with the chemical shift at δ 0.8 from palmitic acid. It is also remarkable that the linolenic acid resonance split into two smooth signals at the bottom of the peaks **(Figure 2-16).**

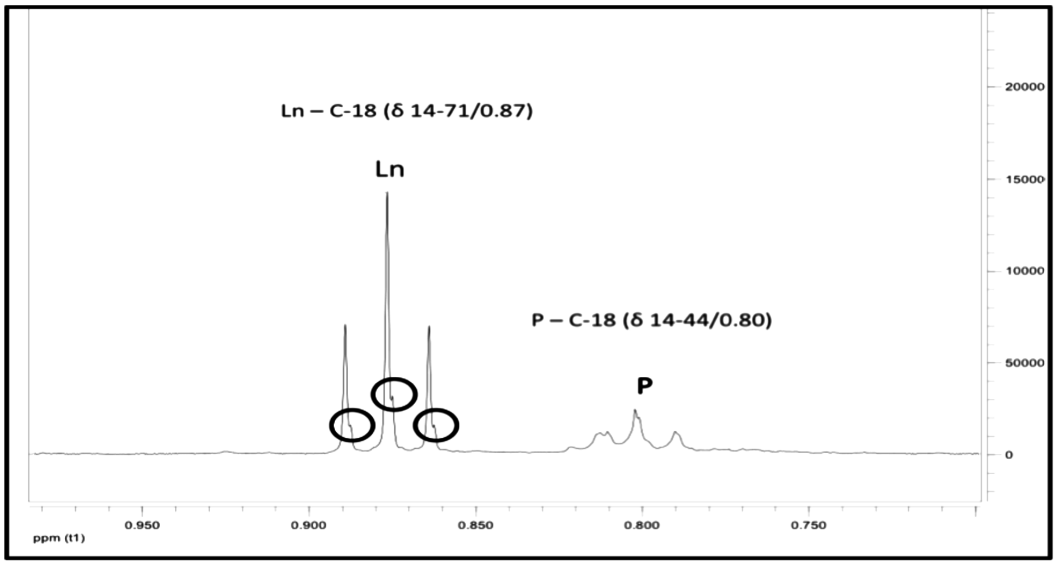

Figure 2-16. The identification of resonances corresponding to methyl signals at δ 14.44/0.80 and δ 14.71/0.87 ppm from palmitic and linolenic acid, respectively, in the ^{1}H spectrum of O-α-D-Gal*p* (1''→ 6')- O-β-D-Glu*p* (1'→ 3)-2, 1 -L-diacyl-glycerol (GGDG) in fraction 4.

The 2/D NOESY and COSY spectra were used to define the stereochemistry of the linolenic acids in the GGDG. Relevant assignments show an omega-3 linolenic acid with cis-double bonds (18:3$\Delta^{9, 12, 15}$) and a palmitic acid (16:0).

The NOEs resonances of the linolenic acid bond to C-2 Gly confirm the orientation of the structure with a skew because H-11 has multiple resonances assignments with glucose and galactose molecules. Likewise, the palmitic acid bond to C-1 Gly shows NOESY enhancements between H-16 with H-3; Hb-1-Gly, respectively **(Figure 2-17)**.

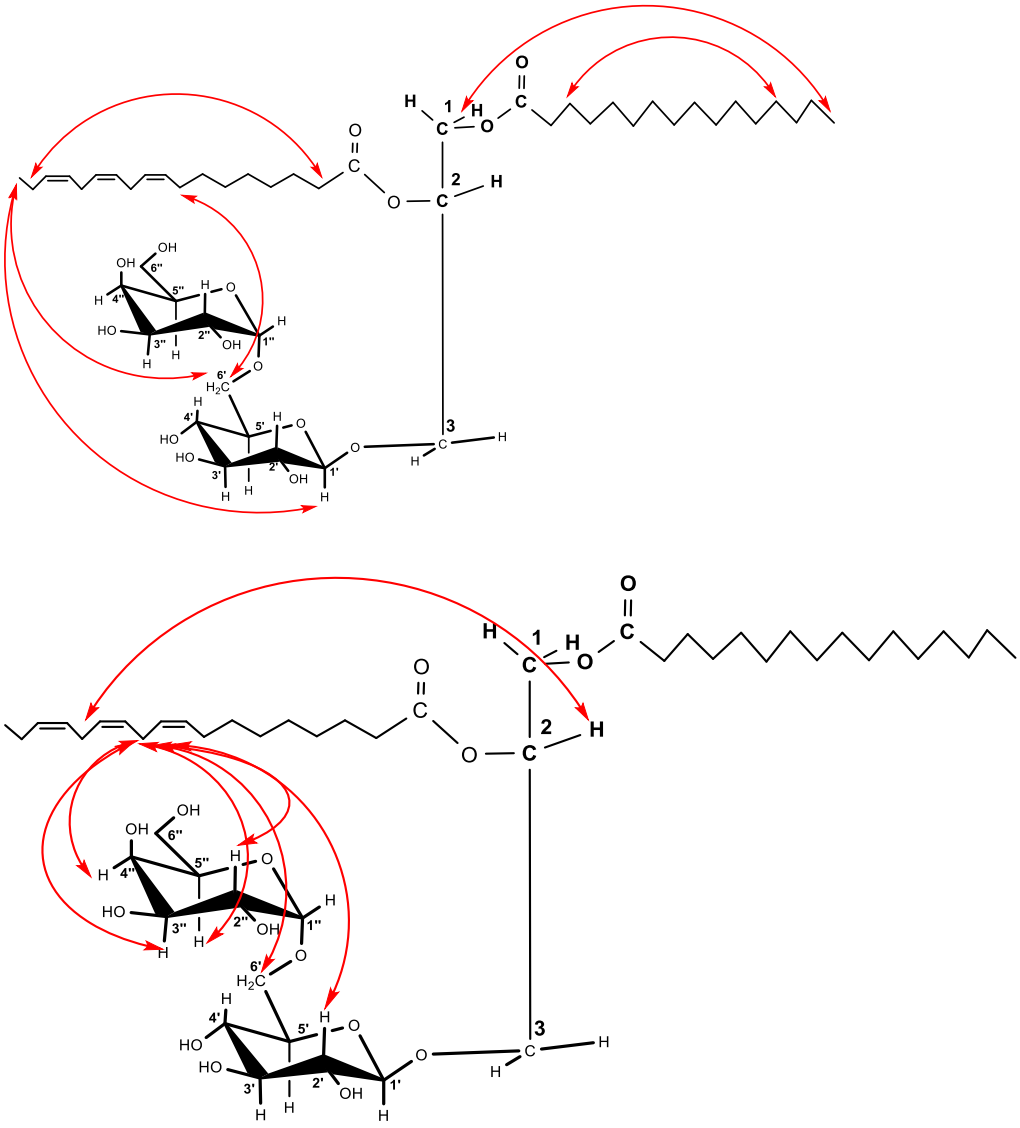

Figure 2-17. Relevant NOEs enhancements used to define the stereochemistry of ω-3 linolenic acid and palmitic acid in the GGDG structure.(Above) Linolenic acid-C-2 Glycerol and palmitic acid-C-1-Glycerol NOEs enhancements. (Below) Relevant NOEs enhancements of H-11 from linolenic acid-C-2-Glycerol.

The tentative arrangement of the two fatty acids after the 1D/2D NMR analysis of the of O-α-D-Gal*p* (1''→ 6')-O-β-D-Glu*p* (1'→ 3)-2-linolenoyl-1-palmitoyl-L-glycerol is illustrated in **Figure 2-18**.

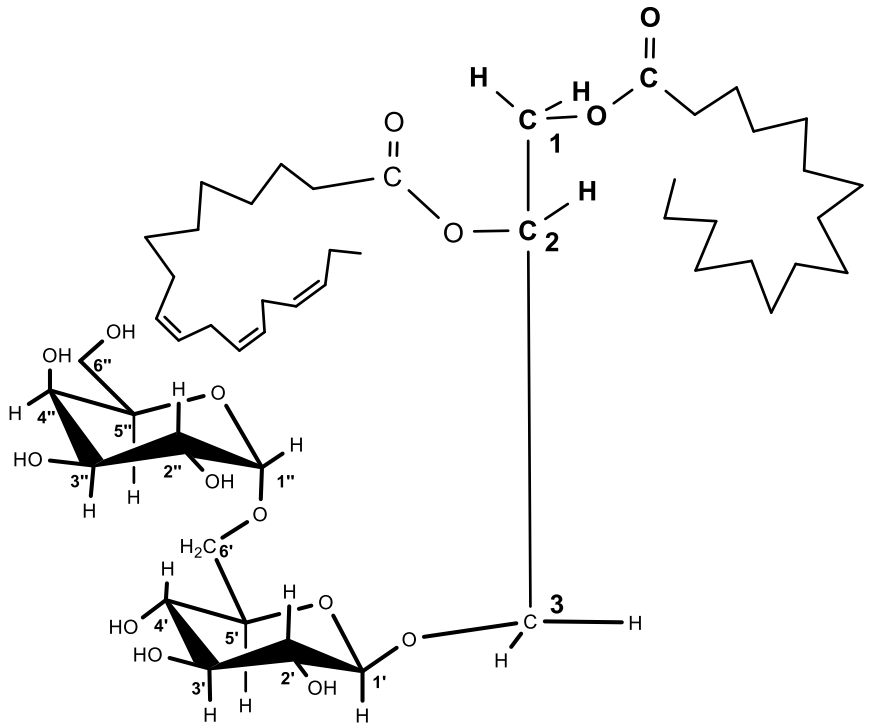

Figure 2-18. Possible arrangement of the substituents in *O*-α-D-Gal*p* (1''→ 6')- *O*-β-D-Glu*p* (1'→3)-2-linoleyl, 1-palmitoyl-L-glycerol according to 2D NOESY and COSY spectra.

2.1.2.2 O-β-D-Galp(1‴-3)-2, 1 diacyl-L-glycerol (MGDG)

Monoglucosyl diacylglycerol (MGDG) (*O*-β-D-Gal*p*(1‴-3)-2, 1-diacyl-L-glycerol) was isolated in fraction 6 of a preparative HPLC-reversed phase RP-18 system. The RP-18 TLC plate showed a broad band in fraction 6 that contained 5.8 mg of both MGDG and GGDG. The GGDG has been identified previously in fraction 4 (cf. 2.1.2.1). Structural elucidation of these glycosyldiacylglycerolipids was performed by heteronuclear NMR correlation HSQC, HMBC, COSY and NOESY, that corroborated the glycosidic linkages of sugars as well lipids and glycerol signals **(Table 2-7)**.

^{1}H and ^{13}C NMR spectra from compound MGDG showed one signal in the C_1 region corresponding to a single Gal*p* unit in the β-glycosidic configuration at a low field (δ 105.39), and displayed a typical H-1 of dublet signal at δ 4.12, with a coupling constant of $^{3}J_{1\text{-}2}$=7.2 Hz (Hansen 1981). NOESY and COSY spectra allowed the assignment of proton signals; DEPT and HMBC spectrum were used for assigning ^{13}C NMR signals. Once it was known that a β-Gal*p* unit was linked (1‴↔3) to glycerol, C-2‴ to C-6‴, H-2‴ to H-6‴ of *β*-Gal*p,* and C-1 to C-2 of glycerol could be assigned. The DEPT NMR spectrum showed inverted CH_2 signals in the carbohydrate region at δ 62.48, which corresponded to C-6‴ of Gal*p*‴ unit, indicating that its carbon was not *O*-substituted and that those at δ 68.74, δ 71.82 and δ 63.97, respectively, arise from C-3 (downfield *O*-glycosylation), C-2, and C-1 of glycerol moiety **(Figure 2-19).**

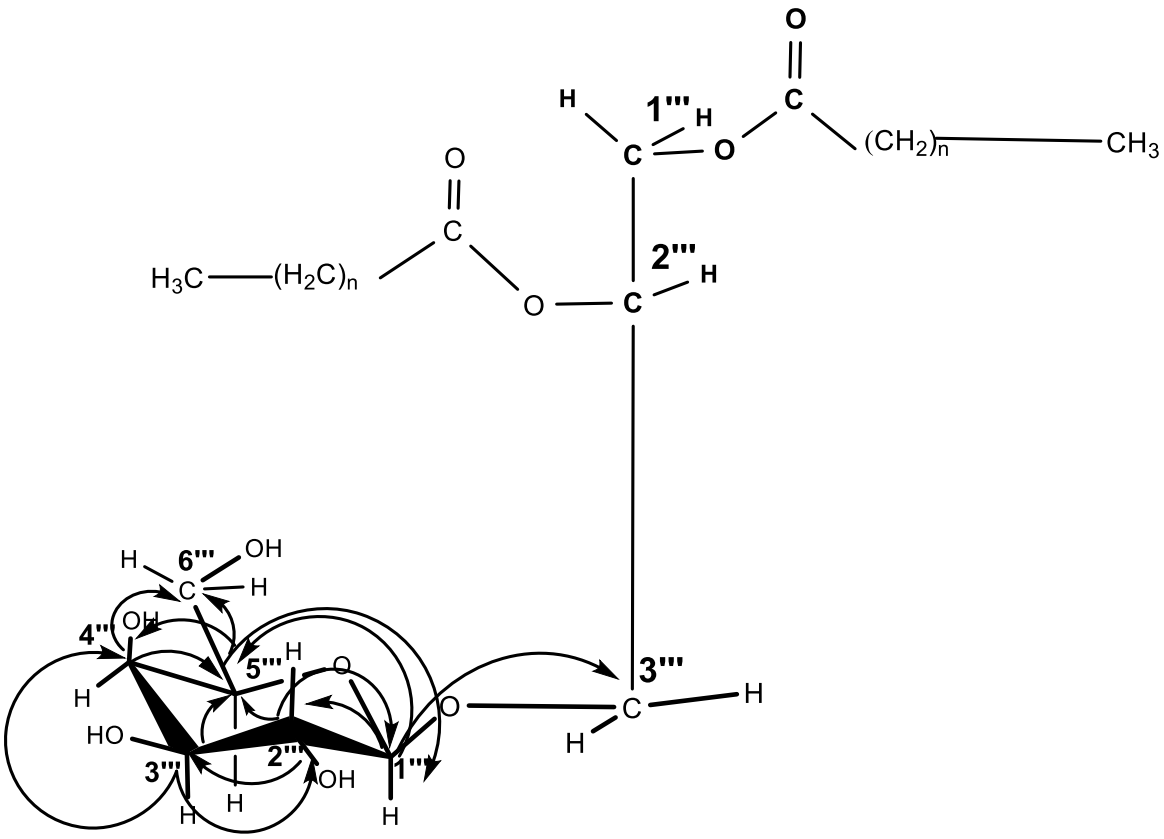

Figure 2-19. Structure relevant long-range HC-correlation in the HMBC of *O*-β-D-Gal*p* (1‘’’-3)-2, 1 diacyl-L-glycerol (MGDG).

By means of a heteronuclear single–quantum correlation (HSQC) and the correlation coupling homonuclear spins (COSY), the experiments identified the occurrence of an extra glycerol molecule (MGDG) due to the presence of double shift signals at δ 71.79-71.82, corresponding to C-2, Gly’ (GGDG) and C-2, Gly’’’ (MDGD) respectively. Likewise, a triplet resonance with an overlapped peak in ^{1}H spectrum was detected at δ 4.33-4.34 and corresponds to Hb’- Hb’’’’ in the methylene C-1Gly’ and C-1Gly’’’ at δ 63.97 **(Figure 2-20).** The resonance in HSQC represents the relationship with partner protons Ha-2’- Ha-2’’’ and also a relationship with the methine (CH) singlet from C-2, Gly’’’-Gly’.

The signal at δ 68.74 from C-3’- C3’’’Gly shows a resonance with δ 3.83-3.88 as a double doublet (dd) which represents the interaction between Hb’-Hb’’’ from GGDG **(Figure 2-20).** Besides, relevant signals in the HSQC spectrum were identified in the assignments of C1’’’-C6’’’ and H1’’’-H6’’’ in the MDGD **(Figure 2-20).**

The results of the 2D experiment analysis with HMBC, COSY and NOESY provided assignment for MGDG, with significant differences when compared with GGDG. **Table 2-7** illustrates the assignments of both glycolipid occurrences in the fraction 6 of the preparative RP-18 and these GGDG results are in accordance with the O-α-D-Gal*p* (1’’→ 6’)-O-β-D-Glu*p* (1’→ 3)-2, 1-dilinoleyl-L-glycerol, isolated from fraction 4.

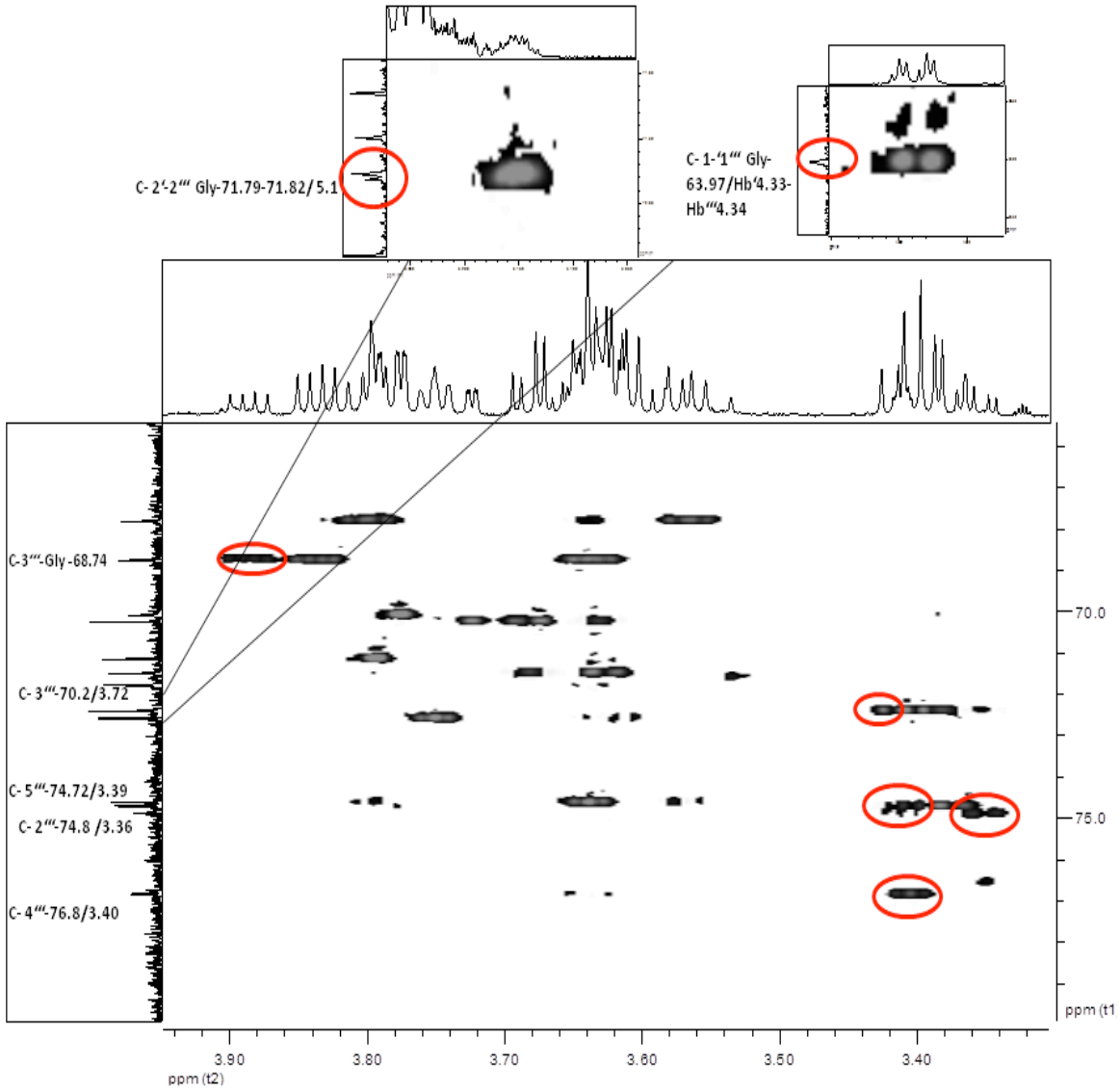

Figure 2-20. The HSQC long-range correlation spectrum shows the relevant resonances of the structure (1) *O*-β-D-Gal*p*(1'''-3)-2, 1 diacyl-L-glycerol (MGDG) such as the signals of C-2'-2''' Gly 71.79 and 71.82, respectively (upper left); C-1'-1''' Gly 63.97 overlapped peak (upper right) and C-3'''gly into the spectrum (The assignments from C-1''' to C-6''' are pointed with red circles).

Table 2-7. ^{1}H-NMR and ^{13}C-NMR spectroscopic data of O-*ß*-D-Gal*p* (1‴→ 3)-2, 1-diacyl-L-glycerol-MGDG and the O-α-D-Gal*p* (1″→ 6′)- O-β-D-Glu*p* (1′→ 3)- 2, 1-diacyl-L-glycerol assignment of resonances in the 600 MHz ^{1}H-NMR and 150 MHz ^{13}C-NMR in CD_3OD. The full assignments of the structures were based on 2D experiments and literature data (Sassaki et al. 1999; Sobolev et al. 2005; Colson and King 1976).

Assignment Glycolipid MGDG	**δ^{13}C (ppm)**	**δ^{1}H (ppm)**	**Assignment Glycolipid GGDG**	**δ^{13}C (ppm)**	**δ^{1}H (ppm)**
(1)	**(1)**		**(2)**	**(2)**	
C-1‴	105.39	4.12	C-1″	100.63	4.70
C-2‴	74.80	3.36	C-2″	70.24	3.67
C-3‴	70.24	3.72	C-3″	71.48	3.63
C-4‴	76.86	3.40	C-4″	71.13	3.79
C-5‴	74.72	3.39	C-5″	72.60	3.74
C-6‴	62.48	3.62a-3.65b	C-6″	62.87	3.612_a-3.62_b
C-1, Gly‴	63.97	4.1-4.3	C-1′	105.35	4.14
C-2, Gly‴	71.82	5.15	C-2′	72.40	3.41
C-3, Gly‴	68.74	3.62-3.83	C-3′	74.69	3.38
			C-4′	70.02	3.77
			C-5′	74.62	3.638
			C-6′	67.80	3.58_a-3.80_b
			C-1, Gly′	63.97	4.1-4.3
			C-2, Gly′	71.79	5.15
			C-3, Gly′	68.74	3.62_a-3.88_b

The coupling constants in the structure β-D-Galp (1‴→3)-2,1-diacyl-L-glycerol (MGDG) were calculated with ^{1}H spectrum, COSY and NOESY resonances, in order to confirm the conformation and the arrangement of the substituents. According to the results, the couplings between the protons support the CIS arrangements to the extent that the majority of the coupling constant values are between 0.9 and 4.0 Hz with the exceptions of H‴-1, $^{3}J_{1‴\text{-}2‴}$=7.5 Hz; H‴ 2, $^{3}J_{2‴\text{-}3‴}$=11.8 Hz and H‴-4, $^{3}J_{4‴\text{-}6‴}$=6.7 Hz‴ **(Table 2-8).**

The application of COSY and NOESY experiments support the position of the substitutes in the structure and clearly indicated that the majority of interfering protons are located on the same side of the cyclohexane plane. This implies an equatorial orientation for C‴- 4 and C‴5 meaning that the H‴-4 is arranged as equatorial in the same way that the enhancements in NOEs illustrate the interaction of H‴-4 with all the adjacent protons. **Figure 2-21** shows the NOEs enhancements between the protons in the molecule of β-D-Gal*p* (1‴→ 3)-2,1-diacyl-L-glycerol and depicts an approximation about the stereochemistry of the molecule.

Table 2-8. ^{1}H-NMR chemical shift and coupling constants for *O*-β-D-Gal*p* (1‴-3)-2, 1 diacyl-L-glycerol (MGDG).

Glucose-(A)	**Methanol-d4 99, 96%**
H‴-1	4.12(1H.*d*, $^{3}J_{1‴\text{-}2‴}$=7.5 Hz)
H‴-2	3.35 (*dd*, 1H, $^{6}J_{2‴\text{-}6‴}$=2.0 Hz, $^{3}J_{2‴\text{-}3‴}$=11.8 Hz)
H‴-3	3.72 (*dd*, 1H, $^{4}J_{3‴\text{-}5‴}$=0.9 Hz, $^{3}J_{3‴\text{-}4‴}$=3.3 Hz)
H‴-4	3.41 (*dd,* 1H, $^{3}J_{4‴\text{-}5‴}$=1.2 Hz, $^{4}J_{4‴\text{-}6‴}$=6.7 Hz)
H‴-5	3.38 (1H, *m*)
H‴-6a	3.62 (1H, *d*, ^{2}J $H_{6a‴\text{-}6Hb‴}$=3.9)
H‴-6b	3.65 (1H, *d*, $^{2}J$$H_{6b‴\text{-}H6a‴}$=3.6)

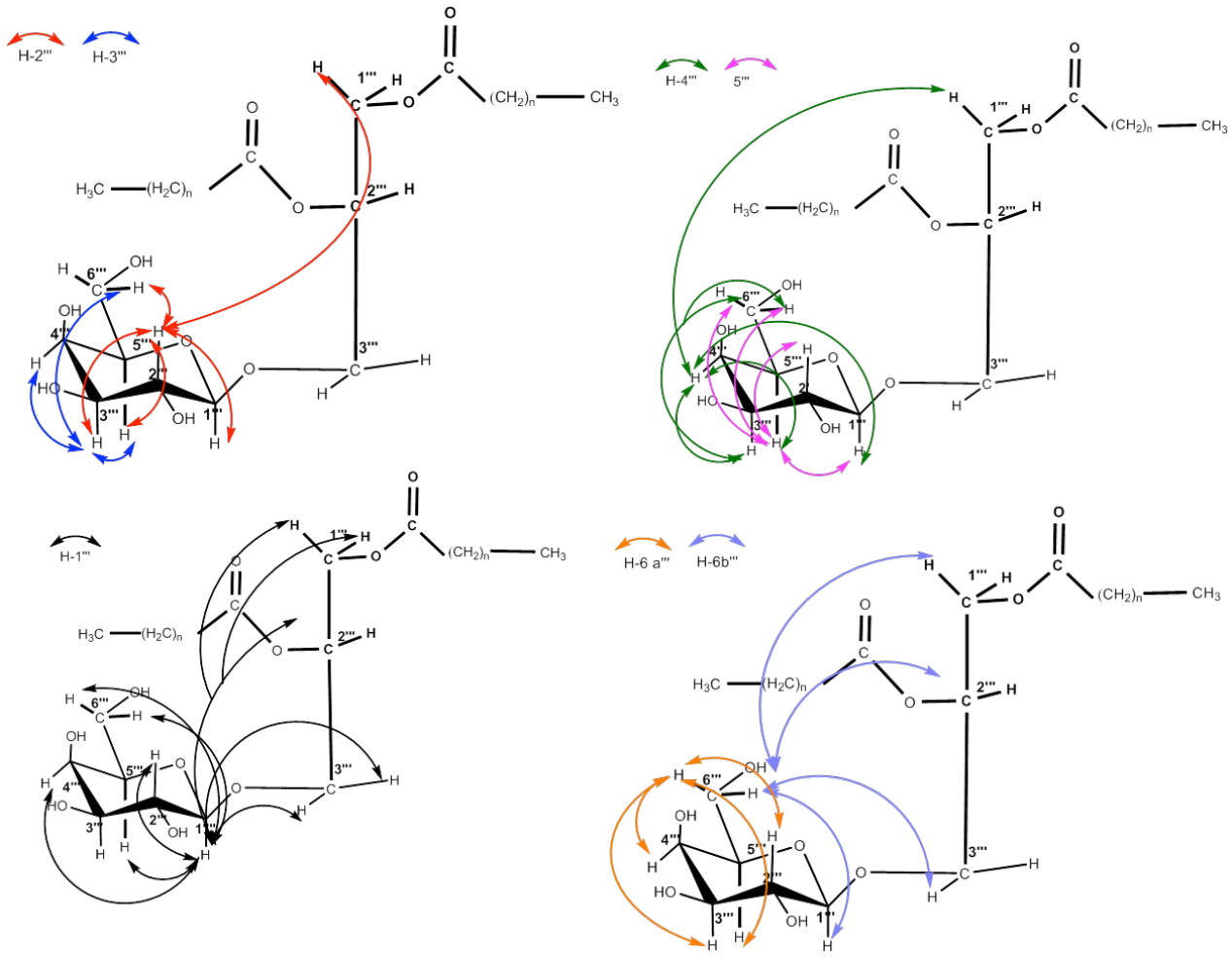

Figure 2-21. Relevant NOEs enhancements used to define the stereochemistry of the β-D-Gal*p* (1'''→ 3)-2, 1-diacyl-L-glycerol in fraction 6 of the preparative RP-18 –HPLC separation from fraction 7 of HSCCC in Baby Banana peels.

The acyl glycerol moiety was defined through ^{13}C spectrum, HSQC, and HMBC experiments. Additional support was obtained by a linoleic acid standard, already isolated in this current research. According to the NMR spectrum, four ester carbonyl signals were detected at δ 175.83, δ 175.04, δ 174.74, and δ 174.72, and four methyl signals at δ 14.72, δ 14.48, δ 14.46 and δ 14.26 were useful to determinate the occurrence of four fatty acids. Complementary information using the HSQC and HMBC experiments indicated the coupling between the sn-1 glycerol ^{1}H signal at δ 4.3-4.1 with ^{13}C signals at δ 175.83, δ 175.04 and the sn-2 glycerol ^{1}H at δ 5.1.

The olefinic region shows ^{13}C chemical shifts resonances in a range between 128.27 and 132.76 with the result that two clusters of intensities are grouped. The first cluster displayed six strong signals (δ 132.76, δ 131.08, δ 130.98, δ 129.23, δ 128.92, δ 128.27); the second cluster had eight signals of middle intensities (δ 130.98, δ 130.93, δ 130.89, δ 130.87, δ 129.17, δ 129.11, δ 129.09, δ 129.07). The HSQC experiment provides the meaning of the groups as a result of the enhanced correlations of the olefinic carbons with two proton cluster of strong and medium signal at δ 5.28; δ 5.24 for the first cluster and at δ 5.21 and δ 5.24 overlapped medium enhancements for the second cluster. The significance of a correlation between both proton and ^{13}C chemical shifts resonances evidenced the presence of double bonds and also a relationship with the number of carbons for each group, thus corroborating the fact that the first cluster with six carbons belongs to the three double bonds fatty acid (ω-3) and the second cluster with eight carbons to the two fatty acids, each one of those provided with two double bonds (ω-6).

Lipid signals in the ^{13}C spectrum from 21.51 to 34.99 ppm of $CH_{2,}$ with a predominant one at δ 26.58, were detected and in concordance to the HSQC correlation experiment, the CH_2 carbons were grouped in four clusters, according to its resonances, with the chemical shift of ^{1}H protons at δ 1.98, δ 1.21, δ 1.23 and δ 1.19. Consequently, the range between δ 1.19 and δ 1.23 chemical shift of ^{1}H showed a significant enhancement with CH_2 between δ 30.35 and δ 30.65 which corresponded to CH_2 range between CH_2-4 to 7 from

linolenic and linoleic acid, as well as the range between CH_2-5 and 12 from palmitic acid.

An unusual ^{13}C chemical shift of CH_2 at δ 21.51 was noted, with a resonance at δ 1.98 proton signal, besides a strong and unusual HMBC enhancement between carbon atom at δ 132.76, with δ 0.87 proton signal. This HSQC resonance corresponds to C-18 (14.72 ppm). These unusual results confirm the occurrence of a linolenic acid as a fatty acid in the acyl moiety, due to that it is a standard characteristic of any ω-3 linolenic acid holding of a C-17 with a ^{13}C chemical shift near 21.5 ppm. Moreover, a HMBC resonance ^{13}C chemical shift at δ 132.76 with C-16 supports the ω-3 conformation of the linolenic acid. The NMR data is in accordance to published references (Gunstone 1990; Sobolev et al. 2005; Hatzakis et al. 2011).

The ^{13}C chemical shift at C-18 splitted into two signals at δ 14.48 and δ 14.46 that depicts a strong resonance with proton signal at δ 0.80, whilst C-18 at δ 14.72 is represented as a unique peak and shows a HSQC resonance at δ 0.87. The coupling constant at δ 0.80 provided a relevant information about the occurrence of more than one carbon (δ 14.48 and 14.46) derived from the doublet of a triplet (*td*) with *J*=6.7 Hz and J=13.1 Hz. In contrast, the coupling constant at δ 0.87 result is a triplet (*t*) *J*=7.5 Hz. The relevant information coincides with the occurrence of two ω-6 linoleic acids and one ω-3 linolenic acid in the acyl moiety. A ^{13}C chemical shift at δ 14.12 with a low intensity shows a HSQC resonance with proton signal at 0.80 and it may support the occurrence of palmitic acid. **Table 2-9** summarizes the ^{1}H- and ^{13}C-NMR spectroscopic chemical shift of the unsaturated fatty acids in fraction 6 **(Figure 2-22).**

In spite of the chemical shift of the linoleic acids which appear near each other, the assignment was clearly elucidated due to the appropriate reproducibility of the assignment between the fatty acids during the elucidation experiment using 1D/2D NMR. An example illustrates it in the ^{13}C spectrum C-1 (A) and C-2 (B) in each of the fatty acid in this following sequence: linolenic, linoleic, and palmitic acids **(Figure 2-22).**

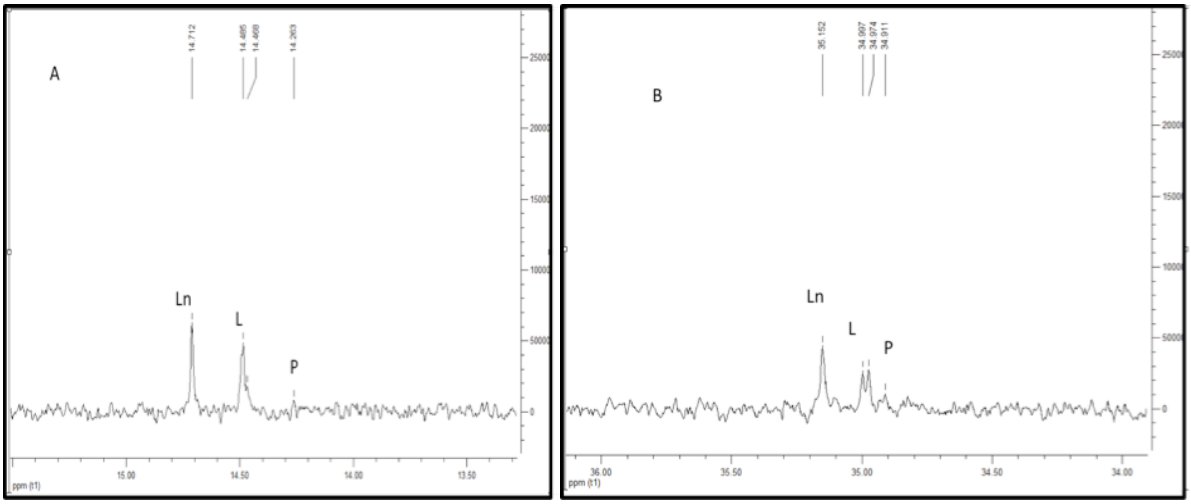

Figure 2-22. ^{13}C chemical shift resonances corresponding to C-1 (A) and C-2 (B) of the linolenic acid (Ln), linoleic acid (L) and palmitic acid (P) to illustrate as the sequence of the distance was constant during the 1D/2D NMR experiments.

The 1D/2D NMR experiments proved to be a powerful multinuclear technique able to determine in qualitative manner the full pattern of the complex structure in the fraction 6. Equally by comparing the NMR spectrum of fraction 4 and fraction 6, concerning the region of acyl moieties, it was possible to confirm that two new fatty acid resonances occurring in the spectrum could correspond to two linoleic acid linkages to the *O*-β-D-Gal*p*(1‴-3)-2, 1 diacyl-L-glycerol (MGDG). The linolenic and palmitic acid would correspond to the structure previously elucidated as *O*-α-D-Gal*p* (1″→6′)- *O*-β-D-Glu*p* (1′→3)- 2, 1-diacyl-L-glycerol (GGDG) in fraction 4 **(Table 2-9)**.

In spite that two glycolipids (GGDG and MGDG) have been found in fraction 6, the elucidation was possible because the MGDG signals are not overlapped with the GGDG resonances. The absence of an additional signal from C-1 at a low field, with a typical high-field H-1 signal at δ 4.0, excluded an additional glycosidic bond from the GGDG with a third sugar terminal moiety. Instead, the HMBC, NOESY and COSY experiments showed the linkage between the MGDG and the glycerol moiety **(Figure 2-23)**.

Table 2-9. ^{1}H-NMR and ^{13}C-NMR spectroscopic data of ω-3 linolenic acid, two ω-6 linoleic acids and palmitic acid assignment of resonances in the 600 MHz ^{1}H-NMR and 150 MHz ^{13}C-NMR in CD_3OD. The full assignments of the structures were based on literature data (Gunstone 1990; Sobolev et al. 2005; Hatzakis et al. 2011).

Assignments	**δ^{1}H (ppm)**	**Multiplicity J/ Hz**	**δ^{13}C (ppm)**
LINOLENIC FATTY ACID ω-3 (GGDG)			
C-1	---	---	175.04
CH_2-2	2.22	*dd* [7.6]	35.15
CH_2-3	1.51	*dd* [6.6][12.4]	26.08
CH_2-4-7	1.23	*m*	30.04-30.47
CH_2-8	1.99	*m*	28.26
CH-9	5.28	*m*	131.08
CH-10	5.24	*m*	128.91
CH_2-11	2.71	*t* [6.0]	26.46
CH-12	5.24	*m*	129.23
CH-13	5.24	*m*	130.90
CH_2-14	2.71	*m*	26.46
CH-15	5.21	*m*	128.27
CH-16	5.28	*m*	132.76
CH_2-17	1.98	*m*	21.51
CH_3-18	0.87	*t* [7.5]	14.72
LINOLEIC FATTY ACID * ω-6 (MGDG) *	**(1) - (2)**		**(1) - (2)**
C-1	---	---	175.83-174.74
CH_2-2	2.22	*q* [7.6]	34.99-34.97
CH_2-3	1.50	*dd* [6.6][12.4]	26.05-26.05
CH_2-4-7	1.23	*m*	(30.04-30.47)
CH_2-8	1.96	*m*	28.21-28.15
CH-9	5.22	*m*	130.98-130.89
CH-10	5.21	*m*	129.17-129.09
CH_2-11	2.67	*t* [6.0]	26.58-26.55
CH-12	5.24	*m*	129.11-129.07
CH-13	5.24	*m*	130.93-130.87
CH_2-14	1.96	*m*	28.15-28.21
CH_2-15	1.22	*m*	23.78-23.76
CH_2-16	1.19	*s*	33.123-33.094
CH_2-17	1.23	*m*	23.78
CH_3-18	0.8	*td* [6.7][13.1]	14.46-14.48
PALMITIC ACID (GGDG)			
C-1	---	----	174.72
CH_2-2	2.09	*m*	36.50
CH_2-3	1.50	*dd* [6.9][13.1]	26.08
CH_2-4	1.23	*m*	30.04
CH_2-5-12	1.19	*m*	30.43-30.65
CH-13	1.23	*m*	30.27
CH2-14	1.18	*m*	33.21
CH2-15	1.21	*m*	23.79
CH3-16	0.80	*t* [6.8]	14.12

*Linoleic fatty acids bonded to C-1,C-2 of glycerol in MDGD.

In order to complement the compositional analysis of fatty acid and their chemical structure, a dilution of the sample was used for the methanolyzation and then the analysis by means of gas chromatography –MS of the methyl esters was carried out **(cf. 4.3.3.1).** The mass spectrum confirms the occurrence of the methyl linolenoate at *m/z* 292 (45.33 min) methyl linoleate at *m/z* 294 (43.45 min) and methyl palmitate at *m/z* 270 (36.4 min).

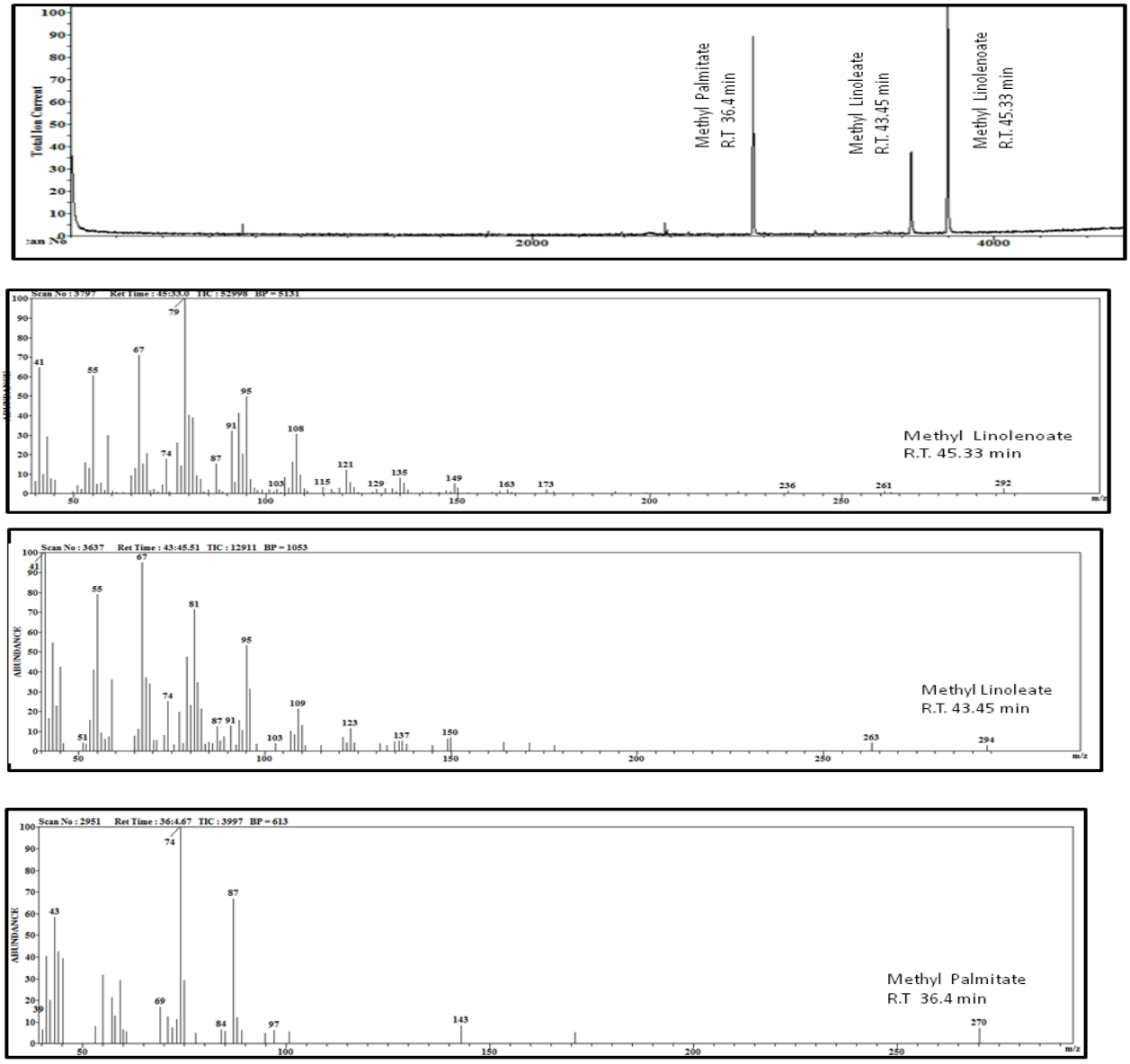

Figure 2-23. GC-MS chromatogram and mass spectrum from the acyl moiety from O-α-D-Gal*p* (1''→ 6')-O-β-D-Glu*p* (1'→ 3)- 2, 1-diacyl-L-glycerol (GGDG) and O-β-D-Gal*p*(1'''-3)-2, 1 diacyl-L-glycerol (MGDG) after the derivatization in fraction 6. The resulting methyl ester derivatives corresponded to methyl linolenoate, methyl linoleate and methyl palmitate. The occurring of the small peak could be linked to the glycerol moiety.

By comparing the NMR spectra with the results in GC-MS analysis between fraction 4 (GGDG) and fraction 6 (GGDG and MGDG), it is possible to deduce that the acyl moieties of each of the fractions are different. Fraction 4 (GGDG) showed a linolenic acid (18:3) as a prominent peak and a low intensity of palmitic acid (16:0), whereas in fraction 6 (GGDG and MGDG) linoleic acid (18:2) is present. Furthermore a medium intensity peak that corresponds to linoleic acid (18:2), and a high intensity peak of palmitic acid is observed. Additionally, a detailed analysis of HMBC, COSY and NOESY was carried out in order to propose that the MGDG in fraction 6 could be linked to the pair of linoleic acids (18:2) and that the GGDG obviously contains the same acyl moiety already elucidated in fraction 4 **(Table 2-10).**

Table 2-10. APCI-MS data of GGDG and MGDG in fraction 6.

ION	**PEAK (A) (R.T.15.2 min) (m/z) GGDG**	**PEAK (B) (R.T.17.1 min) (m/z) MGDG**
$[M+Na]^{\cdot+}$ $[M-Na]^{\cdot+}$	973 950	758 735
diacylglycerol moiety $[CH_2(OCOR^1)CH(OCOR^2)CH_2OH_2]^{\cdot+}$	613	591/573
Monoacylglycerol $[CH_2(OCOR^1)CH(OH)CH_2]^{\cdot+}$,	335	335/313
Acyl moiety (18:3 /18:3) $[R^1]$ $[R^1]$ and $[R^2]$ $-H_2O$	Linolenic acid 278 521	Linoleic acid 261 261

Nevertheless, in contrast with the NMR elucidation of the acyl moiety already proposed above, the LC-APCI-MS data of compounds in fraction 6 exhibited complex fragmentations related to the acyl region compounded of diacylglycerol and monoacylglycerol moieties. It has been very difficult to recognize the fragmentation of MGDG in the spectrum.

In any case, it was possible to identify the fragmentation corresponding to one sugar moiety, in addition to the already recognized daughter ion at *m/z* 423,

identified as the fragment consisting of two sugars and a glycerol moiety in fraction 4 (GGDG).

However, in spite of the abundant signals in the spectrum, two relevant peaks were identified in the total ion chromatogram from fraction 6 (GGDG, MGDG) with retention times of 15.2 and 17.1 min respectively. According to literature data, the ions in fraction 6 (GGDG, MGDG) are identified as follows: a) one prominent ion at *m/z* 613 at the retention time of 15.2 min corresponding to a diacylglycerol moiety $[CH_2(OCOR^1)CH(OCOR^2)CH_2OH_2]^{\cdot+}$; b) the intense fragment at *m/z* 335 of the monoacylglycerol moiety $[CH_2(OCOR^1)CH(OH)CH_2]^{\cdot+}$; c) the fatty acid moiety $[R_1]^{\cdot+}$; d) $[R_2]^{\cdot+}$ at *m/z* 261 and e) *m/z 261* of two linolenic acids represented at *m/z* 521, which suggested that this fragmentation should correspond to the GGDG previously described in fraction 4. Reciprocally, the peak in the total chromatogram with a retention time of 17.1 min yields two prominent daughter ions at *m/z* 591 and *m/z* 573, which could result from the loss of a 2 linoleoyl group, as their corresponding free acid (RCOOH) according to the literature **(Figure 2-24).**

The analysis of the APCI-MS data from fraction 6 is summarized **(Table 2-10)** whereas the pseudomolecular ions at *m/z* 973 and *m/z* 758 do not exist in the spectrum of fraction 6; the prominent daughter ions have been recognized as a product derived from the loss of acyl moieties (Yamauchi et al. 2001; Yamauchi 2005; Klein 1971; Benning et al. 1995).

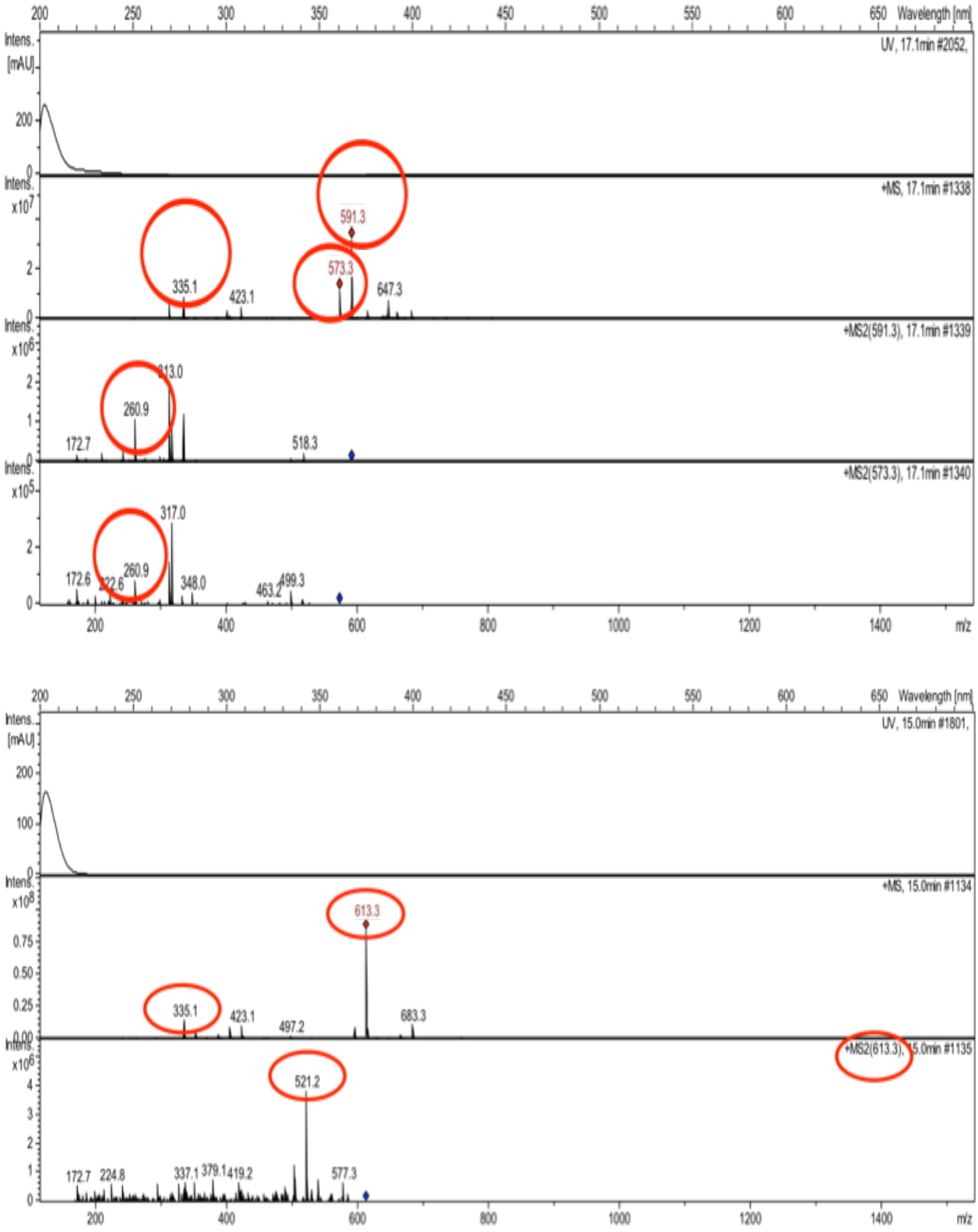

Figure 2-24. APCI-MS spectra for O-α-D-Gal*p* (1''→ 6')- O-β-D-Glu*p* (1'→ 3)- 2, 1-diacyl-L-glycerol (GGDG) (above) and *O*-β-D-Gal*p*(1'''-3)-2, 1 diacyl-L-glycerol (MGDG) in fraction 6 (below).

2.1.2.3 Compositional analysis of the glycolipid GGDG and MGDG

To characterize the fatty acid composition of GGDG a transmethylation reaction was performed and the resulting fatty acid methylesters were analysed by gas chromatography **(cf. 4.3.3.2)**. These results have already been described above. In order to precise the complex fragmentation from the glycolipids by means of the HPLC-APCI-MS method, the sugar moiety residue yield from the transmethylation reaction was analysed by ESI-MS. Thus, fraction 4 and fraction 6, sugar moieties were introduced directly via a syringe at a flow of 200 µL/h according to the literature data (Adden et al. 2006; Tüting et al. 2004; Voiges et al. 2012).

The analysis of the fragmentation pathways of GGDG by means of electrospray ionisation-mass spectrometry/collision induced dissociation (ESI-MS, positive mode) from GGDG showed a precursor ion at *m/z* 439 exhibiting the Na^+ adduct $[M+Na]^+$ which yields one prominent daughter ion at *m/z* 276.9 that results from the loss of a sugar moiety. A second daughter ion at *m/z* 184.9 results from the fragmentation between the glycerol and the sugar in the bottom position. The spectra displayed consistent data which are in line with the elucidation of the structure by NMR experiments. The illustration of the fragmentation pattern and mass spectrum of GGDG is depicted in **Figure 2-25.**

Although HPLC-APCI-MS analysis enables a direct identification of the galactolipid —avoiding both collection of the separated fraction and analysis of the fatty acids by means of GLC — the total ion chromatogram from APCI-MS showed a different pattern of peaks. In comparison with APCI-MS, the ESI-MS results show clearly the fragmentation of the sugar moieties and the glycerol but not the occurrence of fatty acids **(Figure 2-25).**

APCI-MS data cannot define which fatty acid is linked to the sn-position of the glycerol moiety. Without the NMR data and ESI-MS, or the GLC technique, it would have been very difficult to confirm the structure of the glycolipids in fraction 4 and fraction 6.

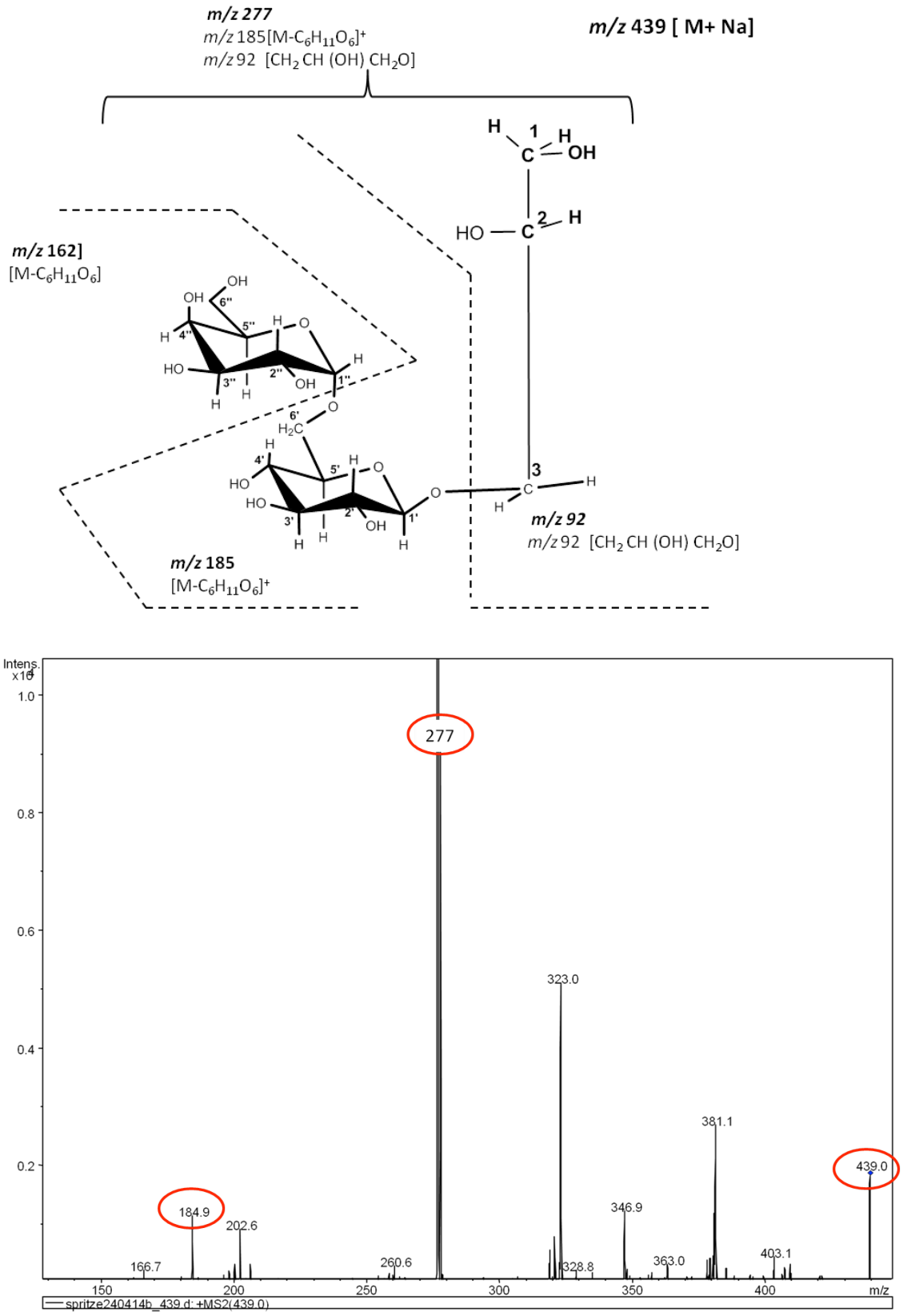

Figure 2-25. Summary of the fragment ions observed for *O*-α-D-Gal*p* (1''→ 6')- *O*-β-D-Glu*p* (1'→ 3)- 2, 1-diacyl-L-glycerol (GGDG) by means ESI-MS and a proposed fragmentation.

In order to identify the glucose and galactose as carbohydrate constituents of GGDG and MGDG the alditol acetate method as a common procedure for sugar analysis was applied. Once the hydrolysis and reduction of the GGDG was performed to obtain glucitol derivatives, a basic acetylation was applied with pyridine and acetic anhydride. Later, the products were extracted with dichloromethane and the alditolacetate derivatives were obtained by means of a liquid-liquid separation. The alditols derivatives were analysed by means of GLC-FID (Voiges et al. 2012; Unterieser and Mischnick 2011).

The occurrence of glucose and galactose was confirmed when their alditol derivatives were evaluated by comparison of the retention time from the gas chromatograms of alditols derivatives, glucose and galactose standards as well as co-injection. The gas chromatogram of glucose standard from a methyl cellulose depicted a retention time of 12.1 min whilst for the galactose standard the retention time was 12.25 min.

When GGDG was analysed the occurrence of two relevant peaks was observed in the gas chromatogram with retention times equivalent to glucose and galactose in comparison with the standards. This was confirmed by co-injection. Taking into account possible sugar-specific or linkage-dependent hydrolysis, or derivation of the head group sugars during the preparation of alditol acetates favouring the formation of galactitol over glucitol, the result is considered in agreement with the glucosylgalactosyl diacylglycerol structure of GGDG **(Figures 2-26, 2-27).**

The partially methylated GGDG glucitol and galactitol acetates were analysed by GC-MS and comparison of the retention times and mass spectra with authentic standards supported the occurrence of glucose and galactose in the GGDG **(Figure 2-28).**

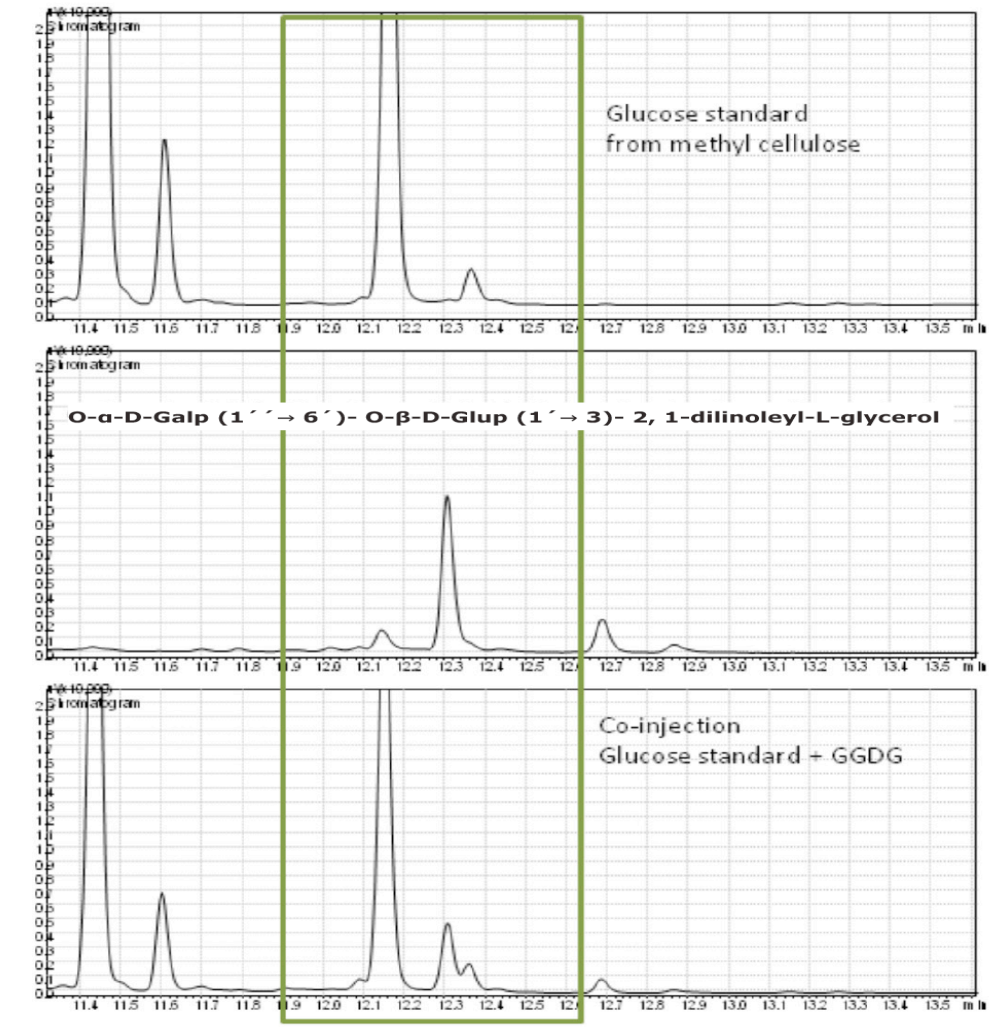

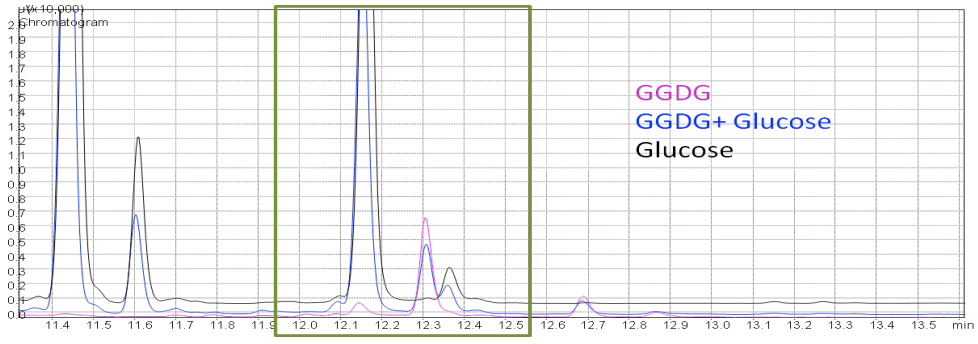

Figure 2-26. Gas chromatogram of alditol acetates of glucose standard from methyl cellulose, GGDG and their co-injection. Comparison in separated chromatograms (above) and comparison between the retention times where the chromatograms are overlapped (below).

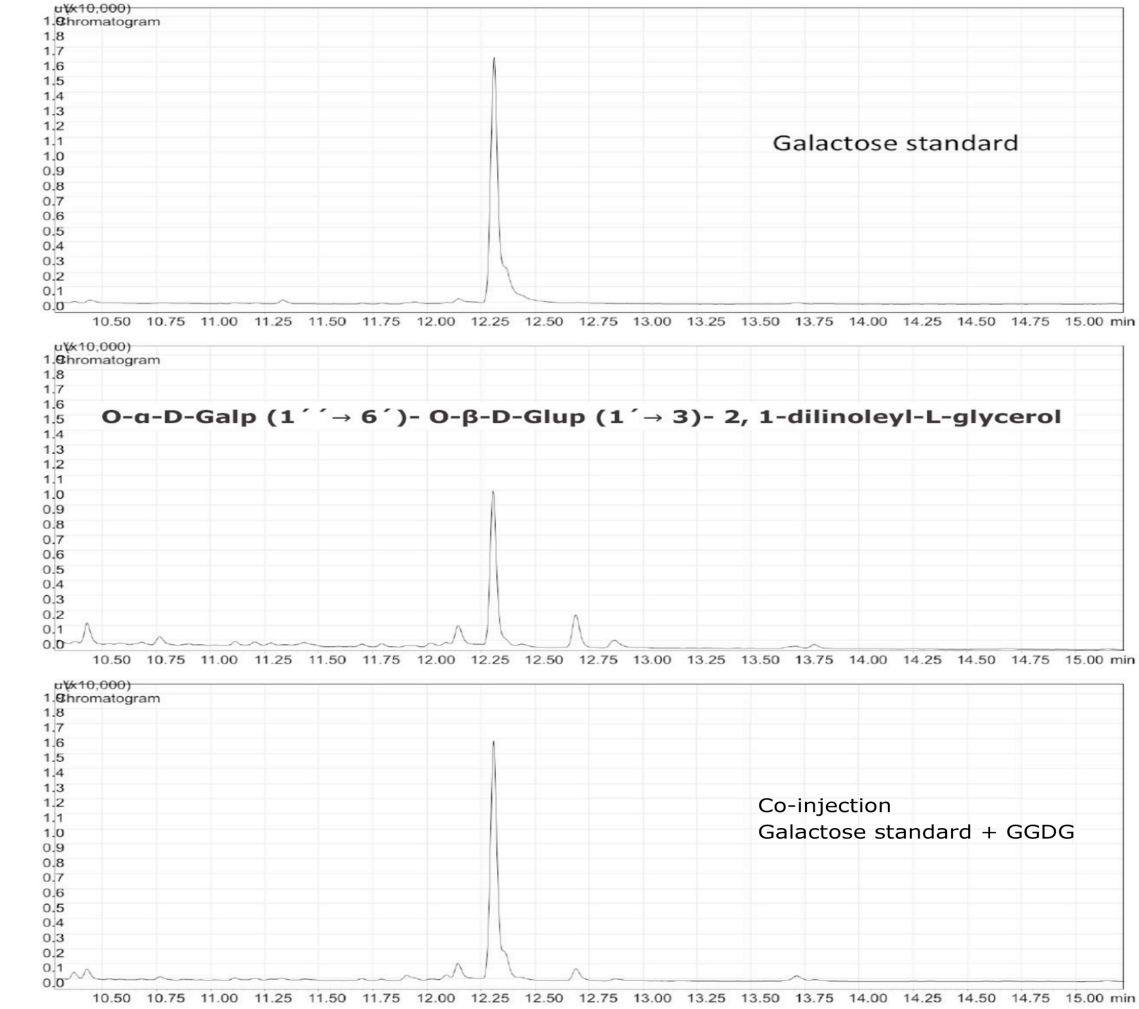

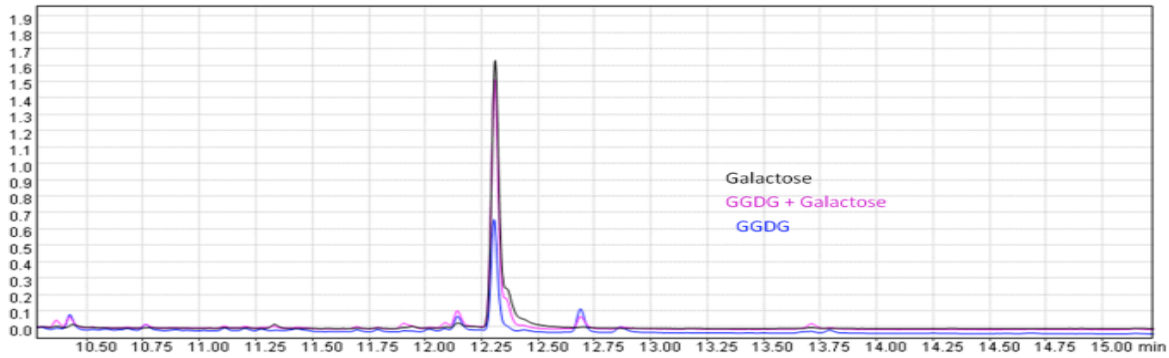

Figure 2-27. Gas chromatogram of alditol acetates of galactose standard, GGDG and their co-injection. Comparison in separated chromatograms (above) and comparison between retention times where the chromatograms are overlapped (below).

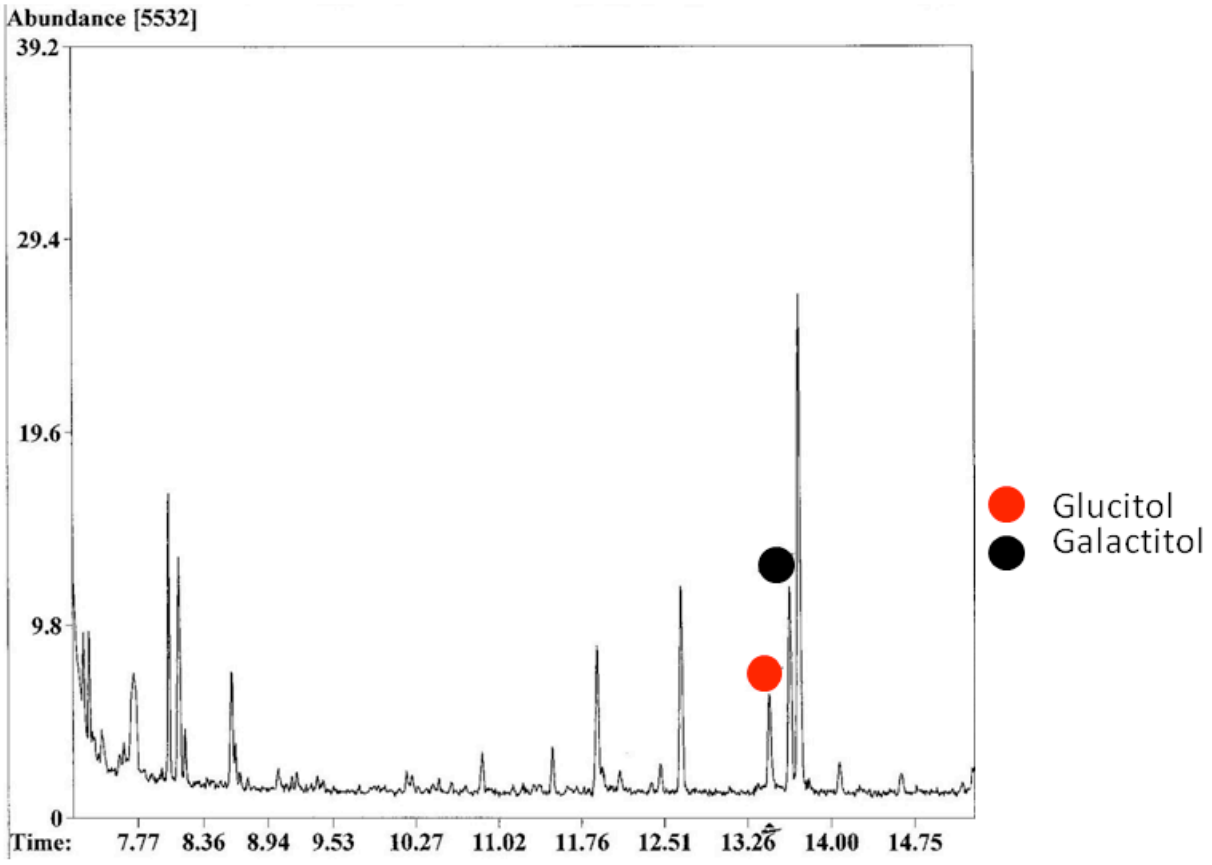

Figure 2-28. Total ion chromatogram from *O*-α-D-Gal*p* (1''→ 6')- *O*-β-D-Glu*p* (1'→ 3)- 2, 1-diacyl-L-glycerol (GGDG) by GCL-MS from alditol acetate GGDG.

2.1.2.4 Summary

Chloroplast membranes contain high amounts of galactolipids, i.e. monogalactosyldiacylglycerol (MGDG) and digalactosyl-diacylglycerol (GGDG). The isolation of the involved genes in the biosynthesis of MGDG and GGDG, and the identification of galactolipids-deficient *Arabidopsis* mutants, greatly facilitated the analysis of both galactolipid biosynthesis and their function (Dörmann et al. 1995). Galactolipids are found in X-ray structures of photosynthesis complex and suggest a direct role in photosynthesis. Furthermore, galactolipids can be substituted for phospholipids, as mentioned, by increases in the galactolipid: phospholipid ratio after phosphate deprivation (Geske et al. 2013). The ratio of MGDG to GGDG is also crucial in the physical phase of thylakoids membranes and may be regulated (Dörmann and Benning 2002; Wieslander et al. 1979, 1980; Wieslander and Rilfors 1977)

Glycolipids are present in all living organism as glycosphingolipids or acylated glycoglycerols. They are present in the cellular membrane, and their concentration is dependent on their biological function. Glycosyldiacylglycerides are the major representatives present in chloroplasts and comprise about 50-80% of the total lipids that constitute the membrane. Galactose is predominant as the sugar component among plant glycerolipids.(Hölz et al. 2006) Monogalactosyldiacylglycerol (MGDG) and digalactosyl-diacylglycerol GGDG are synthesized from UDP-Gal, and diacylglycerol by both MGDG and GDGD synthesis in the chloroplast envelope membranes (Hölzl et al. 2009; Belitz et al. 2009; Nichols 1974; Chapman and Barber 1987; Sassaki et al. 1999).

The encoding genes of galactolipid biosynthesis were isolated from *Arabidopsis* and the structure-function studied in plants, eukaryotic algae and in cyanobacteria. Galactolipids are crucial for growth under normal or phosphate limiting conditions and they are indispensable for maximal efficiency of photosynthesis. A wide variety of glycoglycerolipids is found in different bacteria. These lipids contain glucose or galactose, and in some cases, mannose or other sugars, with different glycosidic linkages in their head groups (Hölzl and Dörmann 2007; Dörmann and Hölzl 2009).

Monoglucosyl diglyceride (MGDG) and diglucosyl diglyceride (GGDG) were reported for the first time as a dominant lipid of the *Acholeplasma laidlawii* membrane which grows statically in a lipid-depleted bovine serum albumin-tryptose medium (Wieslander et al. 1978). GGDG forms a lamellar liquid crystalline phase with water, while MGDG forms a reversed hexagonal phase originated in the *Acholeplasma laidlawii* membrane. Depending on the amount of unsaturated acyl chains of the lipids, a mixture of monoglucosyl diglyceride and diglucosyl diglyceride forms lamellar or reversed cubic phases at physiological temperatures (Wieslander et al. 1981).

Subsequently, a novel glycolipid identified as 1,2-di-*O*-acyl-3-*O*-[β-D-glucopyranosyl-(1→ 4)-*O*-*β*-D-galactopyranosylglycerol (GGD) was found in cells of the photosynthetic bacterium *Rhodobacter sphaeroides* that grows under

phosphate limiting conditions, accumulated non-Phosphorous glycolipids, and lipids carrying head groups derived from amino acids (Benning et al. 1995).

In spite of the extense variety of possible structures, only a small number of different glycogycerolipids have been described as present in nature although the glucosylgalactosyl-diacylglycerol has not been reported yet in plants (Dörmann and Hölzl 2009). However, the introduction of the bacterial glucosylgalactosyl-diacylglycerol (GGD) from *Chloroflexus aurantiacus* into the digalactosyl-diacylglycerol (DGD)-deficient Arabidopsis (*Arabidopsis thaliana) dgd1* mutant, was performed to generate a complementation of growth with the photosynthetic efficiency being partially restored. This experiment confirmed that GGD from bacterial lipid and DGD from authentic plant lipid are subject to the same mechanisms of regulation (Hölzl et al. 2009). Recently, the accumulation of glycolipids such as GGD and DGD, and other non-Phosphorous lipids in *Agrobacterium tumefaciens,* grown under phosphate deprivation, has been studied.

In Banana peels the lipid composition has been studied during the ripening at tropical temperatures and a high proportion of mono and digalactosyl-diacylglycerols containing predominantly polyunsaturated fatty acid, particularly linolenic acid, resembled other photosynthetic tissues. When degreening of Banana peels was complete at 20°C, almost 50% of galactolipids had broken down and the polyunsaturated fatty acids were recovered in the neutral lipid fraction. By comparison, after ripening at 35°C, there was a greater loss of galactolipids and a lower overall recovery of linolenic acid. These findings had correlation with the breakdown of the chlorophyll-protein complexes and with the disappearance of the thylakoid membranes when these Bananas were rippened at 20°C, whereas chlorophyll-bleaching at 35°C was inhibited and consequently the chlorophyll-protein complex and thylakoid membranes were retained. The recovery of linolenic acid is a control parameter to measure both the galactolipids and the chlorophyll-protein complexes breakdown, during the degreening of Banana peels at different temperatures (Blackbourn et al. 1990).

Bean thylakoids membranes treated with various lipolytic enzymes (bean galactolipase, phospholipases A_2, C, D) showed marked changes in their acyl lipid composition. As a consequence of acyl lipids hydrolysis, destruction of some chlorophyll a-protein complex (CP1a, CP1, Cpa) or monomerization of oligomeric light harvesting chlorophyll a/b protein complex (LHCP) was observed. It is concluded that galactolipids and phosphatidylglycerol and to some extent monogalactosyldiacylglycerol are essential for the oligomeric stabilization of the light harvesting chlorophyll a/b protein complex (Krupa 1984; Wada and Murata et al. 2009).

Banana peels from fruit treated with 10^{-3} M benzylaminopurine contained both chlorophyll *a* and chlorophyll *b* at stage 7 of ripening, whereas in the banana control chlorophyll could not be detected. Also an increased accumulation of monoacylglycerol, triacylglycerol and free fatty acid in the peels of banana fruit treated with 10^{-3} M benzylaminopurine was observed. Contrarily to apolar lipids, no remarkable effects of treatments of Bananas with 10^{-3} M benzylaminopurine on polar lipids was observed (Aghofack-Nguemezi and Manka`abiengwa 2012).

Isolation and characterization of glycolipids in Banana peels by NMR 1D/2D experiments have not been reported previously. In spite of this, the occurrence of monogalactosylacylglycerol and digalactosyl-diacylglycerol in Banana peels is known (Blackbourn et al. 1990). On the other hand, steryl glycosides and lipids have been reported in Banana peels (*Musa paradisiaca*) and "Dwarf Cavendish" (*Musa acuminata* Colla var. *Cavendish*) (Oliveira et al. 2006; Ghosal 1985; Wade and Bishop 1978).

The current phytochemical analysis of Baby Banana peels reports the occurrence of two novel glycolipids: *O*-α-D-Gal*p* (1''→ 6')- *O*-β-D-Glu*p* (1'→ 3)-2,1-diacyl-L-glycerol (GGDG) and *O*-β-D-Glu*p* (1'''-3)-2,1 diacyl-L-glycerol -(MGDG). For both of them a proper isolation and characterization has been described in this section.

In view of the literature data about the presence of glycoglycerolipids in chloroplast of plants and eukaryotic algae such as cyanobacteria is not surprising to isolate both GGDG and MGDG in the same fraction of Banana peels. As it has shown before the ratio depends on the configuration of incorporated fatty acids, growth temperature and membrane cholesterol content (Wieslander et al. 1981). The occurrence of GGD and MGDG in Baby Banana peels and the preference of galactose over glucose as head sugar moiety should be studied in order to clarify the role of these glucolipids in the chloroplast membranes and the interaction with the photosynthesis as it has been reported, in the case, when the galactose is part of the head sugar moiety in the digalactosyldiacylglycerol (Dörmann and Benning 2002).

2.1.3 Molecular species of glucocerebroside

The glucocerebroside compound (4*E*, 8*E*)–N-2'–hydroxylinolenoyl-1-O-β–D-glucopyranosyl-4, 8-sphingadienine) **(Fig. 2-29)** was characterized in fraction 8 of the preparative HPLC–reverse phase system. The glucocerebroside (1) structure was elucidated by 1D/2D-NMR spectroscopy (^{1}H, ^{13}C, ^{1}H/^{1}H-COSY, HSQC, HMBC, NOESY) complemented by mass spectroscopy and was in agreement with previously published data (Riaz et al. 2013; Li et al. 2007; de Souza et al. 2007; Yamauchi et al. 2001; Beck et al. 2007; Zhou et al. 2001; Lustosa et al. 2012; Sarmientos et al. 1985; Xu et al. 2001; Moreau et al. 1998)

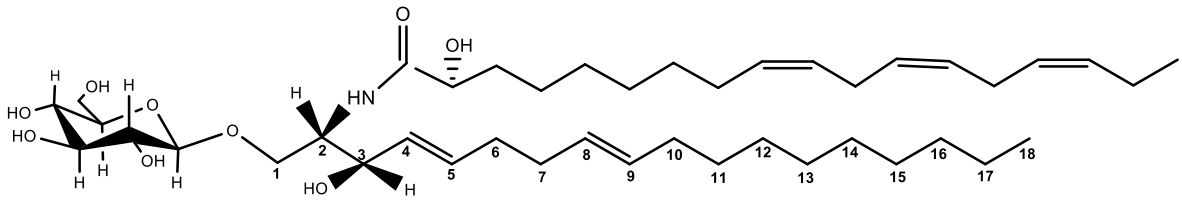

Figure 2-29. Chemical structure of glucocerebroside is characterized as (4*E*, 8*E*) –N-2'–hydroxylinolenoyl-1-O-β–D-glucopyranosyl-4, 8-sphingadienine by 1D/2D-NMR spectroscopy (^{1}H, ^{13}C, ^{1}H/^{1}H-COSY, HSQC, HMBC, NOESY) in fraction 8.

The NMR spectra from fraction 8 showed the characteristic amide ^{1}H proton signal of the ceramide, which resonates in the region between at δ7.52 and δ 7.62; **(Figure 2-30).** These chemical shift resonances contributed to an useful starting point for the assignment of the sphingadienine protons. Thus, the assignments from H-1 to H-5 from the ceramide were confirmed with the support of HMBC, COSY and NOESY experiments to complete the elucidation from glucocerebroside (1). Similar data was found for glucosylceramides compared with literature (de Souza et al. 2007; Sarmientos et al. 1985; Riaz et al. 2013; Toledo et al. 2001; Li et al. 2007) **(Table 2-11).**

The ^{1}H NMR spectrum showed the presence of oxymethines at δ 4.03 (1H, *d*, $J_{3\text{-}5}$ = 1.9 Hz); at δ 3.48 (1H, d, $J_{\text{Ha-Hb}}$ = 2.8 Hz) and δ 3.41 (1H, d, $J_{\text{Hb-Ha}}$ = 2.5 Hz). Also, a methine proton vicinal to the nitrogen atom of the amide group at δ 3.88 (1H *m*); two olefinic regions at δ 5.28 and δ 5.26 such as two aliphatic methylenes at δ 2.02 (1H, *d*, $J_{(6\text{-}5)}$ = 8.5 Hz) and 1.97 (1H, *td*, $J_{(7\text{-}6)}$ = 8.1 Hz $J_{(7\text{-}8)}$ = 16.0 Hz). Sphingoid moiety with two double bonds were found previously in medusa *Phyllorhiza punctata* and in fruit pastes of red bell pepper (*Capsicum annuum L.*): these relevant literature data was in accordance with the glucocerebroside (1) in fraction 8 (de Souza et al. 2007; Yamauchi et al. 2001, Yamauchi 2005; Riaz et al. 2013).

The chemical shifts and coupling constants of the sugar moiety confirmed the assignment of the sugar as glucose in the glucocerebroside (1). The coupling constant of ^{1}H-1 (δ 4.28) anomeric proton $^{3}J_{1\text{-}2}$=7.8 Hz indicated a β-glucopyranosidic linkage to the aglycone moiety, with ^{13}C chemical shift (δ 102.46). Subsequently arrangements of the substituents between C-1 and C-6 in the structure were established by HMBC, COSY and NOESY data (Toledo et al. 2001; Sarmientos et al. 1985; Yamauchi et al. 2001, Yamauchi 2005; Costantino et al. 1996; Ruberto and Tringali 2004; Beck et al. 2007; Lu et al. 1993).

Table 2-11. ^{13}C-NMR and ^{1}H NMR chemical shift data of (4*E*, 8*E*) –N-2' –hydroxylinolenoyl-1-O- β–D-glucopyranosyl-4, 8-sphingadienine (glucocerebroside (1) elucidated from fraction 8) (Levery et al. 1998).

Assignment	**δ ^{1}H (ppm)**	**Multiplicity J/Hz**	**δ^{13}C (ppm)**
C-1	3.48[a]	1H, d, $^{2}J_{(Ha\text{-}Hb)}$ = 2.8 Hz	64.32
	3.41[b]	1H, d, $^{2}J_{(Hb\text{-}Ha)}$ = 2.5 Hz	
C-2	3.88	*m*	54.70
C-3	4.03	1H, *d*, $^{4}J_{(3\text{-}5)}$ = 1.9 Hz	72.84
C-4	5.28	*m*	132.76
C-5	5.26	*m*	129.97
C-6	2.02	1H, *d*, $^{3}J_{(6\text{-}5)}$ = 8.5 Hz	27.89
C-7	1.97	1H, *td*, $^{3}J_{(7\text{-}6)}$ = 8.1 Hz, $^{3}J_{(7\text{-}8)}$ = 16.0 Hz	33.68
C-8	5.19	*m*	128.26
C-9	5.63	1H, *td*, $^{3}J_{(9\text{-}10)}$= 6.3, $^{3}J_{(9\text{-}8)}$= 14.5	134.41
C-10	1.98	*m*	27.86
CH_2(11-14)	2.05	*m*	21.5-28.1
CH_2-15	1.23	*t* [5.9]	24.14
CH_2-16	1.50	*m*	26.81
CH_2-17	1.31	*m*	26.24
CH_3-18	0.93	*s*	19.84
NH	7.53	---	---
NH	7.62	---	---
Glucose	**δ ^{1}H (ppm)**	**Multiplicity J/Hz**	**δ^{13}C (ppm)**
C-1	4.28	*d*, 1H, $^{3}J_{1\text{-}2}$=7.8 Hz	102.46
C-2	3.04	*dd*, 1H, $^{3}J_{1\text{-}2}$=7.8 Hz, $^{3}J_{2\text{-}3}$=9.2 Hz	75.11
C-3	3.24	*dd*, 1H, $^{3}J_{3\text{-}4}$=8.6 Hz, $^{3}J_{3\text{-}2}$=9.4 Hz	78.10
C-4	3.15	*q*, 1H, $^{3}J_{(4\text{-}3),\,(4\text{-}5)}$=9.6 Hz	71.69
C-5	3.25	*t*, 1H, $^{3}J_{(5\text{-}6Hb\text{-}Ha)}$=9.0 Hz	77.90
C-6	3.55-3.74	*m*	62.78

The identification of two methyl signals at δ 0.93 and 0.85 (iso-propyl terminus), whose intensities did not share an integral ratio with respect to those of other signals in the methyl region from fatty acids, showed an occurrence of two sphingoid moieties in the fraction 8, as well as ^{1}H proton chemical shifts at δ 7.52 and δ 7.62 of two amide groups **(Figure 2-30).**

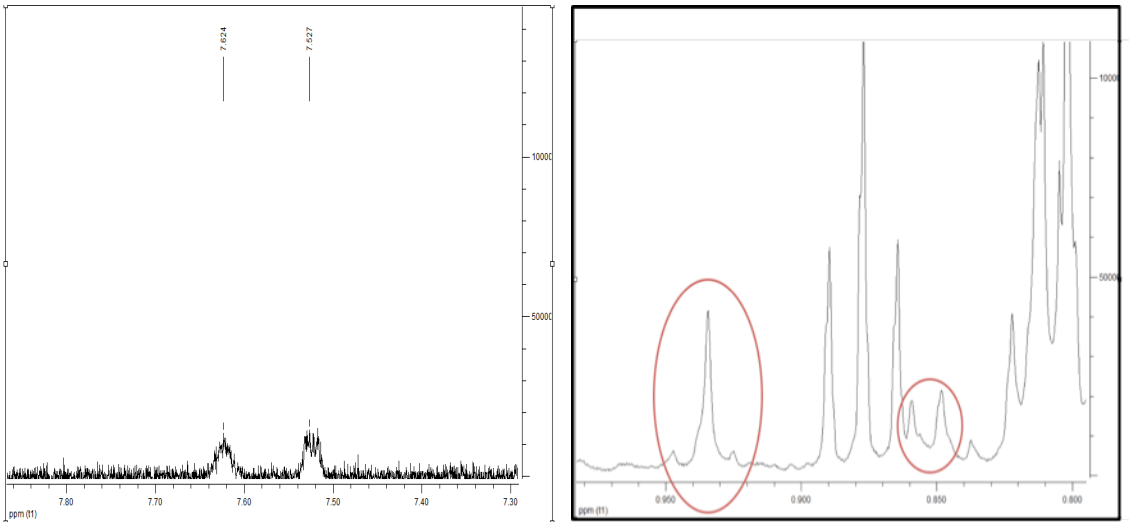

Figure 2-30. Partial ^{1}H NMR spectra (A) Amide characteristic ^{1}H proton signal of the ceramide, which resonances are in the region between at δ 7.52 and δ 7.62 (B) Identification of methyl signals at δ 0.93 and 0.85 (iso-propyl terminus) belonging to ceramides in fraction 8. These relevant enhancements support the presence not only of the glucocerebroside (1) elucidated as (4*E*, 8*E*) –N-2' – hydroxylinolenoyl-1-O-β–D-glucopyranosyl-4, 8-sphingadienine but also a homologous or related compound.

Mixture of sphingolipid homologs were reported previously in the literature and the determination of the structures has been performed on the common part of the homologs and working on the mixture (Costantino et al. 1996; Yamauchi 2005; Zhou et al. 2001; Beck et al. 2007; Riaz et al. 2013; Talbott et al. 2000).

In order to confirm the length of the fatty acid chain and the sphingosine base of the glucocerebroside (1), fraction 8 was submitted to atmospheric pressure chemical ionization mass spectrometry (APCI-MS) in positive mode. The peak $[M+H]^{+}$ 752.4 *m/z* was identified as a molecular ion peak and the fragmentation pattern showed intense fragment ions at *m/z* 572, derived from the loss of the sugar moiety and *m/z* 590, which represents the fragment of both the

sphingoid and the fatty acid chain. The characteristic fragment at *m/z* 262 determines the sphingoid moiety with a loss of water in the structure and also linolenic acid moiety at *m/z* 262. **Figure 2-31** illustrates the schema of the fragmentation and **Figure 2-32** the positive APCI-MS spectra in the glucocerebroside **(1).**

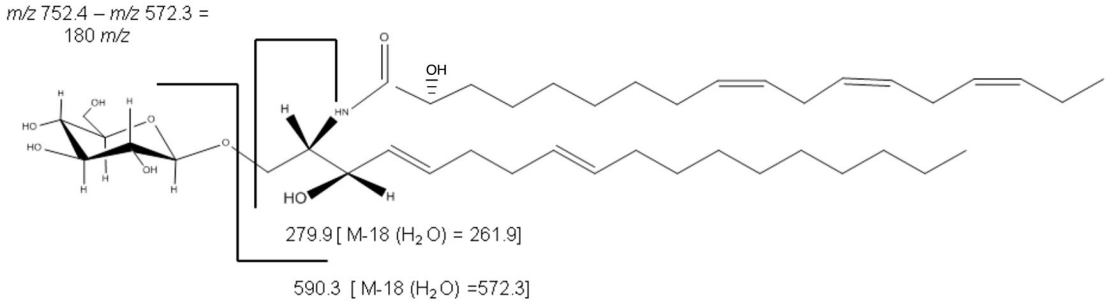

Figure 2-31. APCI-MS mass fragmentation pattern of (4*E*, 8*E*)–N-2′ –hydroxylinolenoyl-1-O-β–D-glucopyranosyl-4, 8-sphingadienine, glucocerebroside (1).

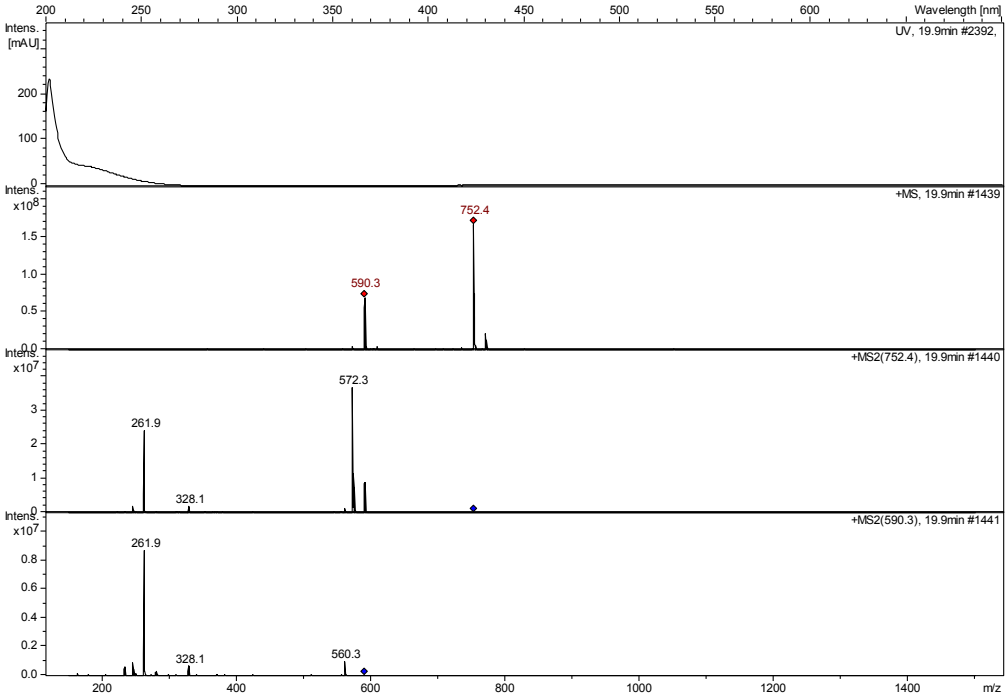

Figure 2-32. Positive-ion APCI mass spectra of (4*E*, 8*E*)–N-2′–hydroxylinolenoyl-1-O-β–D-glucopyranosyl-4, 8-sphingadienine, glucocerebroside (1). Intensity [mAU] depicts the relative percentage abundance plotted against *m/z* values between 150 and 1500. The peak $[M+H]^+$ 752.4 *m/z* was identified as a molecular ion peak; the fragmentation pattern showed the ceramide moiety at *m/z* 572.3 and the sphingoid-(H_2O) moiety at *m/z* 262 from glucocerebroside (Riaz et al. 2013; Yamauchi 2005; Kasumov et al. 2010).

Methanolysis of fraction 8 with methanolic HCl provided the methyl ester of a fatty acid and a sphingosine base. When the methyl ester of fatty acid and sphingosine base on acetylation were analyzed by GC-MS: characteristic fragments at *m/z* 298 were identified as a sphingoid moiety; and at *m/z* 298, including at *m/z* 292*,* 294, 270, were identified as methyl linolenoate, methyl linoleate and methyl palmitate, respectively **(Figures 2-33, 2-34)**

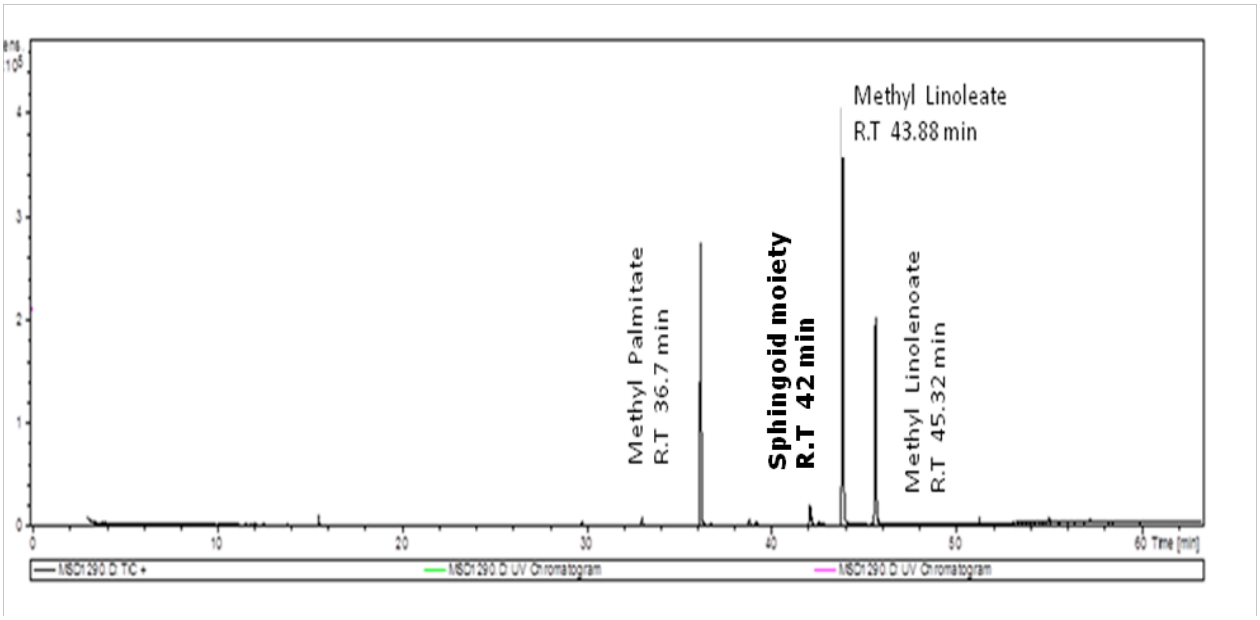

Figure 2-33. GC-MS chromatogram from the acyl moiety in fraction 8 after the derivatization. The resulting methyl ester derivatives corresponding to methyl linolenoate at *m/z* 292 in 45.32 min, methyl linoleate at *m/z* 294 in 43.88 min and methyl palmitate at *m/z* 270 in 36.7 min and the presence of a new peak that represents the sphingoid moiety at *m/z* 298 in 42 min.

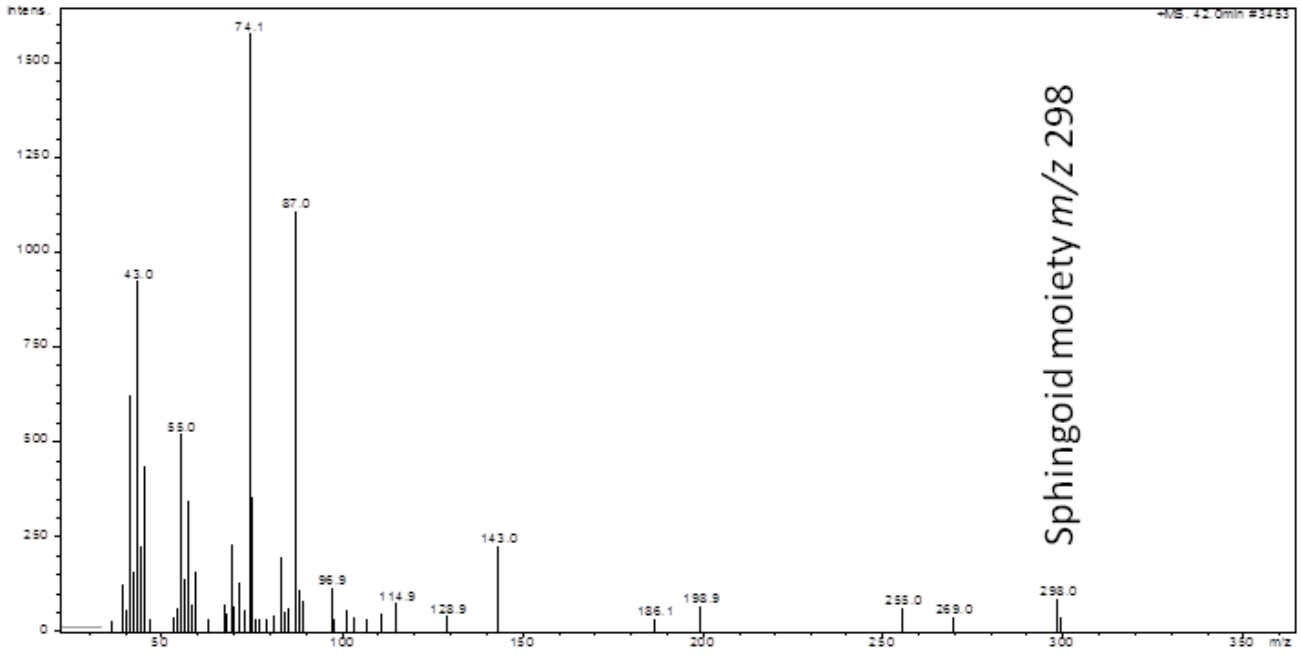

Figure 2-34. Mass spectrum corresponding to the sphingoid moiety [$R^1CH(OH)CH(NH_2)CH_2$] belonging to glucocerebroside (1) (Yamauchi et al. 2001; Riaz et al. 2013).

After characterization of the sphingoid moiety from the glucocerebroside (1) by LC-APCI-MS an additional species was analyzed, which yielded two different forms of fragmentation according to the base peaks shown in the spectrum at *m/z* 766 and 664.4 with retention time of 20.7 min. These new species differ from the glucocerebroside (1) in the chain length of the fatty acid moiety; whereas the glucocerebroside (1) depicted 18h:2, the new one exhibited 22h:0. As a result, the glucocerebroside (2) is tentatively identified as (8*E*)–N-2'–hydroxydocosanoyl-1-O-β–D-glucopyranosyl-4-hydroxy-8-sphingaenine with its mass spectrum being in concordance with literature data (Yamauchi et al. 2001, Yamauchi 2005; Lu et al. 1993) **(Figures 2-35, 2-36).**

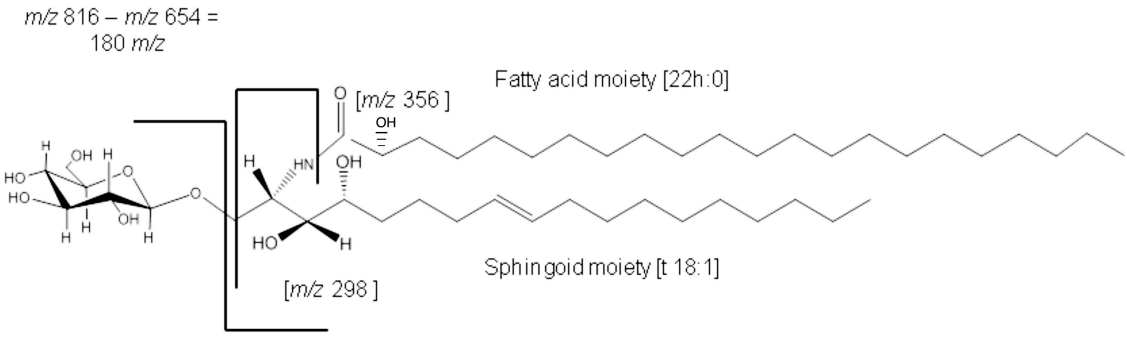

Ion	**Peak *(m/z)***
$[M+H]^{\cdot+}$ $[M\text{-}OH]^{\cdot+}$	816 798
Ceramide moiety $[M\text{-}C_6\ H_9\ O\ _5]^{\cdot+}$	654
Sphingoid moiety $[R^1CH(OH)CH(NH_2)CH_2]^{\cdot+}$,	298
Fatty acid moiety $[R^2\ CH(OH)CONH_3]$ Molecular species Sphingoid/fatty acid	356 t 18:1/22h:0

Figure 2-35. (Above) APCI-MS fragmentation pattern of glucocerebroside **(2)** identified as (8*E*)–N-2'-hydroxydocosanoyl-1-O-β–D-glucopyranosyl-4-hydroxy-8-sphingaenine; (below) APCI-MS data of glucocerebroside (2).

It is remarkable how fraction 8 displayed in RP-18 TLC from the separation by HPLC-reversed phase **(Figure 2-2)** new bands in comparison with the bands in fractions 4 and 5 corresponding to GGDG and MGDG. This result obeys to the occurrence of new compounds in this fraction in addition to the glycolipids previously identified.

After the analysis of fractions 4-5-8 it was possible to distinguish some structures, such as the sphingoid moiety with a soft band in middle of the plate area, the glucose ceramide moiety in the glucocerebroside as a different band with different retention time in comparison with the glycolipids from fractions 4 and 5 and strong gray bands in the bottom of TLC identified as compounds with phosphorous in the structure **(Figure 2-2).**

Although the fraction 8 did not give completely clear ^{1}H and ^{13}C data, it has been possible to elucidate the structure of glucocerebrosides and other compounds.

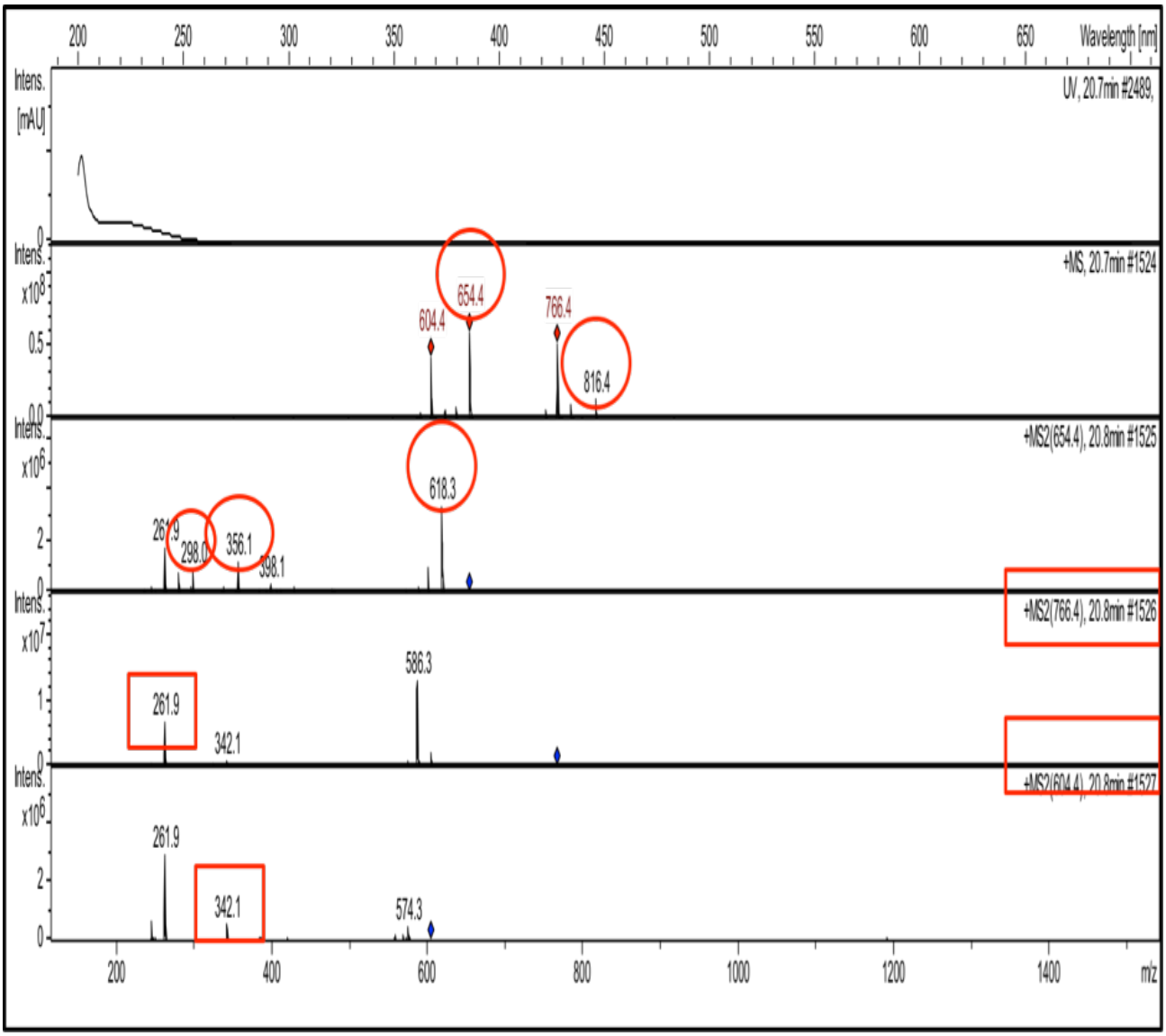

Figure 2-36. Positive-ion APCI mass spectra of (8*E*)–N-2′ –hydroxydocosanoyl-1-O-β–D-glucopyranosyl-4-hydroxy-8-sphingaenine, glucocerebroside (2). Intensity [mAU] depicts the percentage relative abundance plotted against *m/z* values between 150 and 1500. The peak $[M+H]^{+}$ 816.4 *m/z* was identified as the molecular ion peak and the fragmentation pattern showed the ceramide moiety at *m/z* 654 and the sphingoid-(H_2O) moiety at *m/z* 262 from the sphingoid. Two types of fragmentation have been observed and they are indicated in the mass spectra with a circle and a rectangle to differentiate each other (Riaz et al. 2013; Yamauchi 2005; Kasumov et al. 2010).

2.1.4 Sulphoquinovosyl-diacylglycerol (SQDG)

The elucidation of SQDG was carried out using HMBC, COSY, NOESY and the presence of the CH_2-S group in the sulfodeoxyhexosyl unit, due to the presence of an unusually high frequency at δ 54.66 with CH_2 resonances at δ 2.69 and δ 3.05, was confirmed. Furthermore, a distinct resonance at δ 69.7, corresponding to C-5 in the glucose, was identified as part of the SQDG structure (Gage et al. 1992) **Figure 2-37).**

The β configuration of the glucose was confirmed by virtue of the ^{13}C-^{1}H signal at δ 104.75 and the $^{3}J_{1-2}$=7.8 Hz. The HMBC enhancements between C-1 with C-6 and C-5, that belongs to the CH_2-S group, allowed to elucidate the chemical shifts corresponding to the H-2-3-4- in the glucose. The coupling constants gave a relevant information to define the position of the substituents in the molecule, just to conclude that the H-4 is located in an axial position derived from the fact that H-3 showed a typical vicinal coupling constant of ^{3}J=9.6 Hz. The complete NMR assignments are shown in **Table 2-12**.

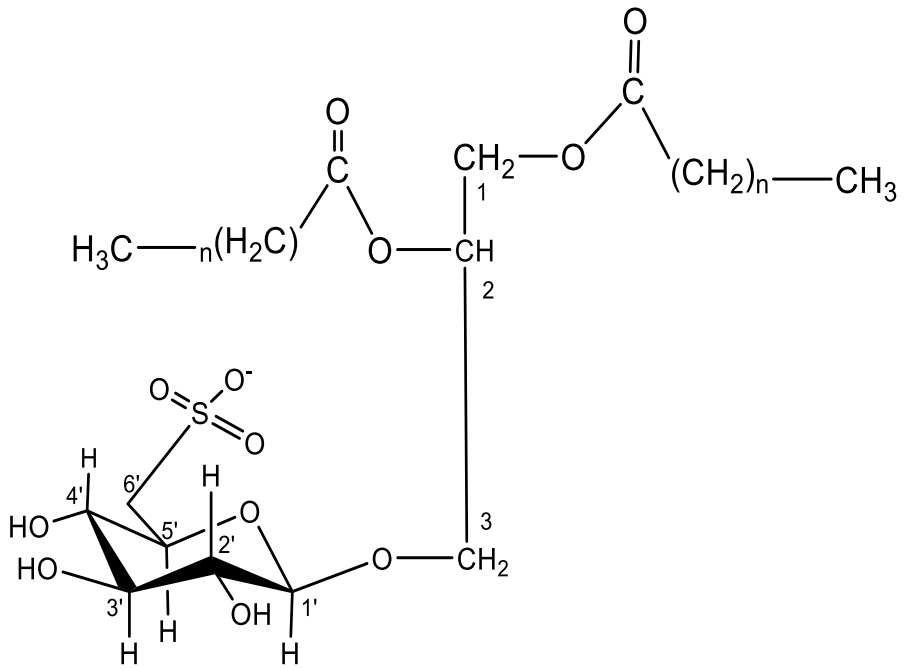

Figure 2-37. Chemical structure of O-β-D-Qui*p*-6-sulphono (1’ ↔ 3)-2, 1—diacyl-L-glycerol, sulphoquinovosyl-diacylglycerol (SQDG) elucidated in fraction 8.

The fatty acids composition in the SQDG was determined by GC-MS analysis which displayed methyl-esters related to linolenic, linoleic and palmitic acid, as part of the acyl region in fraction 8. The high intensity of the methyl linoleyl peak could indicate the linkage with the SQDG, in concordance with the 1D/2D NMR experiments. The total ion chromatogram shows the sphingoid moiety in fraction 8 with a retention time of 42 min **(Figure 2-33)**.

Table 2-12. ^{1}H and ^{13}C NMR spectroscopic data of O-β-D-Qui*p*-6-sulphono(1' ↔ 3)-2, 1—diacyl-L-glycerol, sulphoquinovosyl-diacylglycerol (SQDG) elucidated in fraction 8. The NMR assignments were in agreement with the literature data (de Souza et al. 2007).

Assignment (SQDG)	$\delta^{1}H$ (ppm)	Multiplicity J/Hz	$\delta^{13}C$ (ppm)
C-1	4.16	*d,* 1H, $^{3}J_{1\text{-}2}$=7.8 Hz	104.75
C-2	3.04	*d,* 1H, $^{3}J_{2\text{-}1}$=7.8 Hz, $^{3}J_{2\text{-}3}$=9.2 Hz	75.07
C-3	3.17	q, 1H, $^{3}J_{(3\text{-}4)\ (3\text{-}2)}$=9.6 Hz,	78.00
C-4	3.16	*dd,* 1H, $^{3}J_{(4\text{-}5)}$=4.8 Hz $^{3}J_{(4\text{-}3)}$=6.7 Hz	71.57
C-5	4.0	n. d.	69.74
C-6	3.0-2.68	n. d.	54.66
C-1-Gly	4.07-4.3	n. d.	63.67
C-2-Gly	5.14	n. d.	71.82
C-3-Gly	3.6-3.8	n. d.	64.93

2.1.5 Phosphatidylethanolamine (PE)

The 1D/2D NMR spectra of fraction 9 showed high intensity resonances related to ceramides and also phospholipids. Those chemical shifts in the spectrum supported the fact that the TLC plate - RP-18 separation **(Figure 2-2),** showed in fraction 9 an intensive gray band, in the bottom area, meaningfully stronger than in fraction 8. Hence, fraction 9 was submitted to ^{31}P experiment in order to check the occurrences of Phosphorous in the fractions. This resulted in the elucidation of phospholipids such as ceramide-aminoethylphosphonate (CAEP), phosphatidylethanolamine (PE) and, in lower proportion, phosphatidylcholine (PC).

Two relevants peaks at δ 0.73 and δ 1.49 were found in the ^{31}P spectrum which corroborates the assumption about the presence of phosphorylated compounds in the fraction and could indicate that δ 0.73 belongs to a phosphatidylethanolamine and phosphathidylcholine at δ 1.49 belongs to a ceramide-aminoethylphosphonate (CAEP) **(Figure 2-38).**

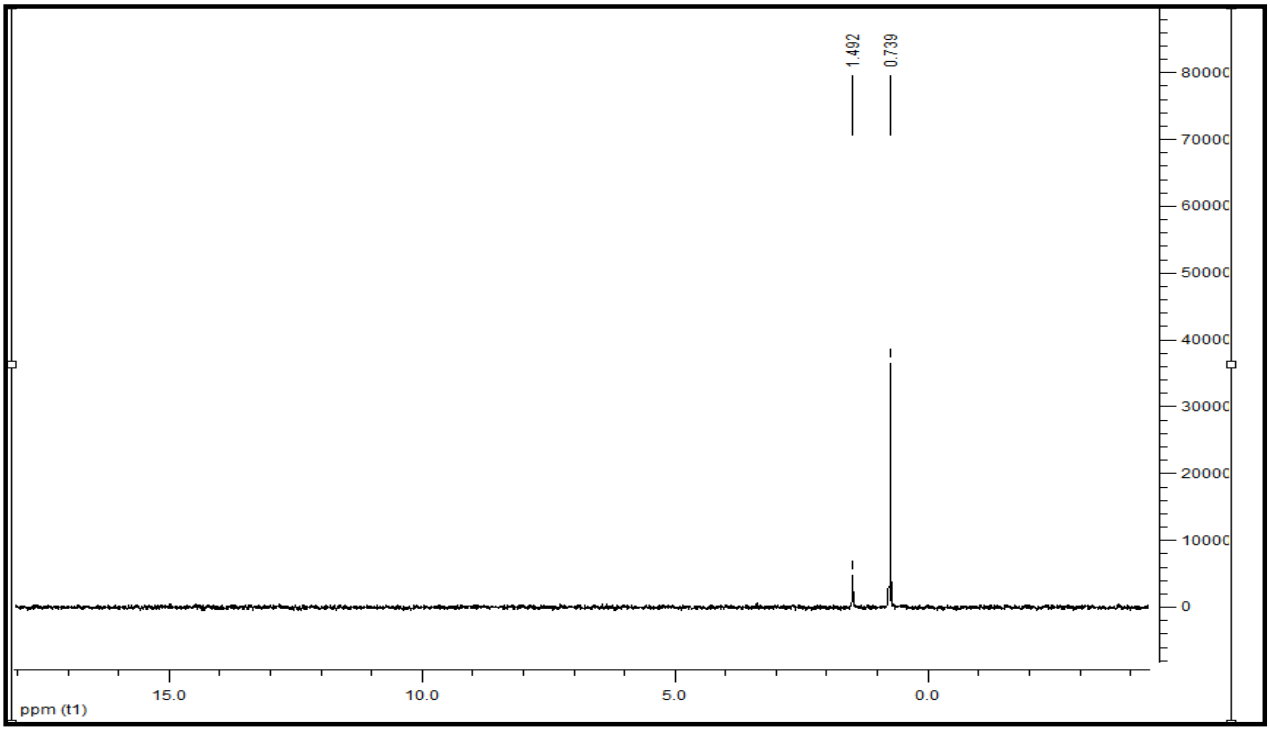

Figure 2-38. ^{31}P spectrum from fraction 9 indicated the occurrence of Phosphorous element at δ 0.73 which corresponds to phophatidylethanolamine (PE) and phosphathidylcholine (PC) in lower proportion, and also at δ 1.49 to the ceramide-aminoethylphosphonate (CAEP).

The elucidation of phosphatidylethanolamine was supported by the comparison of the resonances with those described previously in section 2.1.1 (phosphatidylcholine). The new chemical shift at δ 41.71 gave the key to assure that the new phospholipid in the fraction could be phosphatidylethanolamine. The full assignments of the structures were based on both NMR 1D/2D experiments and literature data (de Souza et al. 2007; Sobolev et al. 2005) **(Figure 2-39, Table 2-13).**

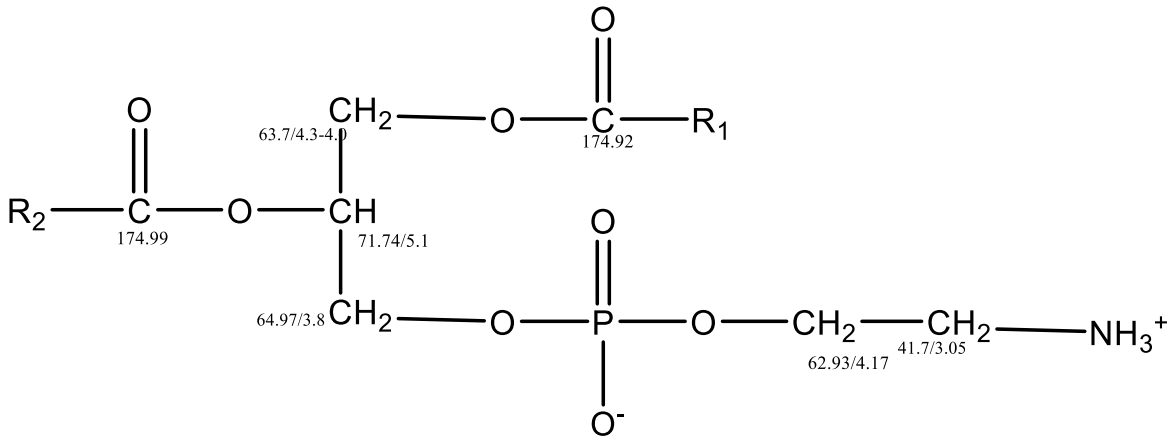

Figure 2-39. Chemical structure of phosphatidylethanolamine (1, 2- dilinoleoylphosphatidyl-ethanolamine) and chemical shift of HSQC correlation with numbering of carbons and protons according to literature data (Sobolev et al. 2005).

Table 2-13. ^{1}H-NMR and ^{13}C-NMR spectroscopic data of phosphatidylethanolamine (PE) elucidated in fraction 9 and assignment of resonances in the 600 MHz ^{1}H-NMR and 150 MHz ^{13}C-NMR in CD_3OD (de Souza et al. 2007; Sobolev et al. 2005).

Assignment	δ ^{1}H (ppm)	Multiplicity J/Hz	δ ^{13}C (ppm)
CH_2*sn*-1	4.30_a 4.00_b	*dd* [12.0;6.9] *dd* [12.0;3.1]	63.70
CH*sn*-2	5.10	m	71.74
CH_2 *sn*-3	3.80	*t* [5.9]	64.97
CH_2OP	4.17	m	62.93
CH_2NH_3	3.05	m	41.71

2.1.6 Ceramide aminoethylphosphonate (CAEP)

The occurrence of the two chemical shifts **(Figure 2-40)** at δ 41.759 and 41.712 in the ^{13}C NMR spectrum corresponding to CH_2NH_3 from PE showed that an additional phospholipid could be present in fraction 9. It was possible to elucidate the structure of a ceramide aminoethylphosphonate (CAEP) with the Phosphorous moiety linked to a glycerol molecule at δ 63.67, which belongs to a C-1 chemical shift of a ceramide moiety **(Figure 2-41)**. The HMBC, COSY and NOESY experiments established significant and relevant information to elucidate the structure of the ceramide aminoethylphosphonate in accordance with the LC-APCI-MS analysis as well as literature data (de Souza et al. 2007).

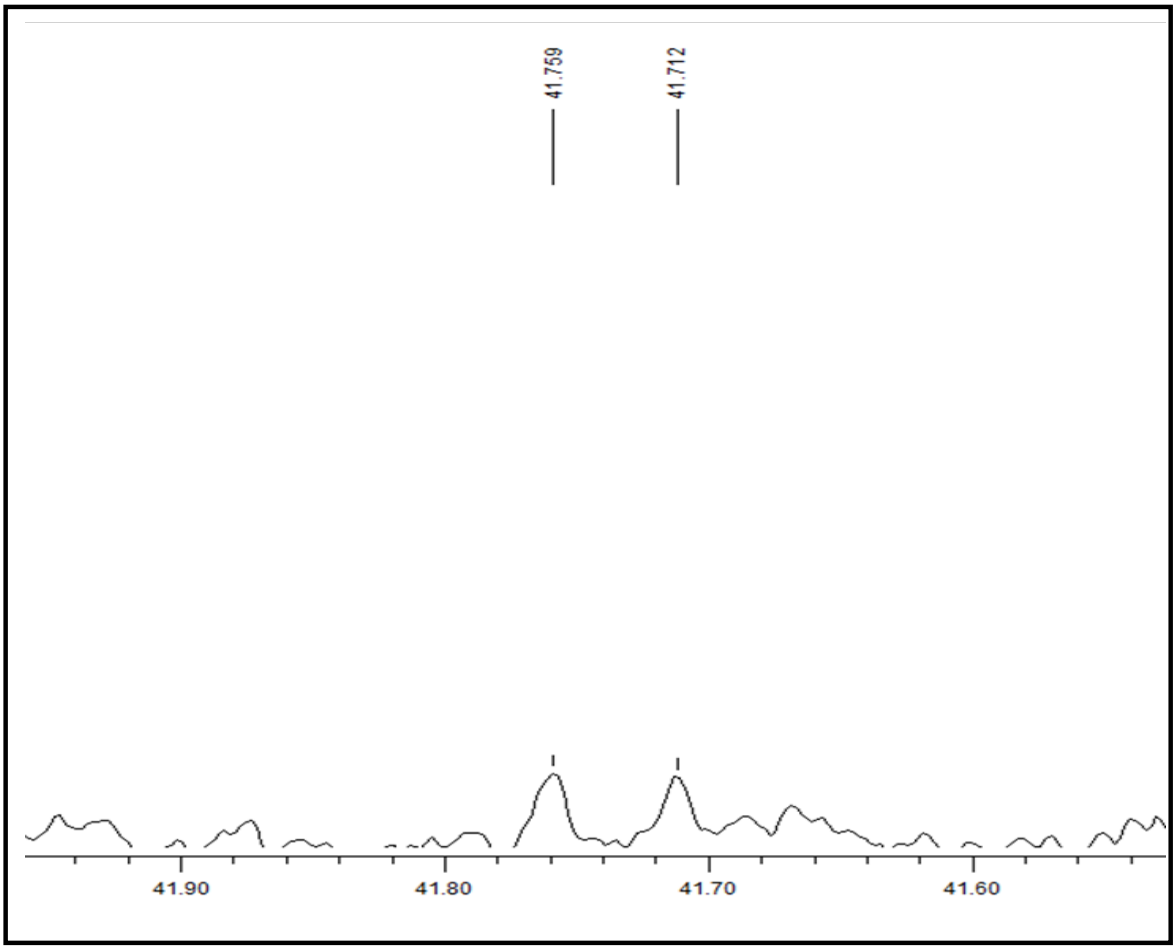

Figure 2-40. ^{13}C spectrum of fraction 9 which showed two resonances at δ 41.759 and 41.712 suggesting the occurrence of two Phosphorous moieties in the fraction belonging to phosphatidylethanolamine (PE).

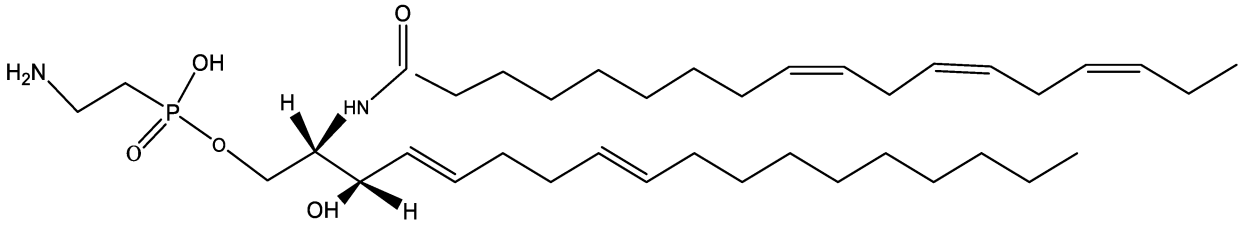

Figure 2-41. Tentative structure of ceramide aminoethylphosphonate (CAEP) elucidated in fraction 9 by HMBC, COSY and NOESY experiments, in concordance with literature data (de Souza et al. 2007).

The identification of CAEP in fraction 9 is the result of assignments from a phosphatidylethanolamide which do not have linkage with glycerol but with an amide-H at δ 7.52, which could be part of the amino group in sphingolipids linked to a fatty acid with a chemical shift at δ 177.25 as it has been observed in COSY and HMBC experiments. Nevertheless, a complete ^{1}H-^{31}P HMBC correlation is required to confirm the structure.

2.1.6.1 Summary

The isolation and characterization by 1/D and 2/D NMR of phosphatidylcholine (PC) and phosphatidylethanolamine (PE) and glucocerebroside in Baby Banana peels has not been reported previously. However, it has been reported that the amount of total lipids in banana fruit pulp tissue remained constant during the climateric rise induced by ethylene. Also the relative proportion of neutral lipid, glycolipid and phospholipid did not change (Wade and Bishop 1978). Furthermore, glycolipids and phospholipids have been analyzed in peels of banana when benzylaminopurine and kinetin were applied during the ripening of banana fruit and by thin-layer chromatography chlorophylls, carotenoids and neutral lipids were identified (Aghofack-Nguemezi and Manka`abiengwa 2012).

The relation between phytosterols, glucosylcerebroside and phospholipids in plant have shown a dynamic of ternary mixtures in the membranes and they play an important role to regulate membrane thermal shocks (Beck et al. 2007).

The scientific interest in the immunological properties of glycosphingolipids (GSLs) from the marine sponge *Agelas dispar* is already reported because they play an important role as therapeutical agents. Likewise, ceramides from Blood

Orange (*Citrus sinensis*) were found to show nutraceutical properties for protection of colon carcinoma (Costantino et al. 1996; Valsecchi et al. 2012) Two lipoxygenase inhibitory sphingolipids from *Chrozophora plicata* were isolated and the ^{1}H and ^{13}C NMR data, HMBC and COSY correlation was reported as well as EI-MS spectrometry (Riaz et al. 2013).

The occurrence of the aminoethylphosphonate derivative (CAEP) and sulfoquinovosyldiacylglycerol (SQDG) in lettuce leaves and in medusa (*Phyllorhiza punctata)* has been reported previously and the data was a relevant support to elucidate these compounds in the current research about the phytochemical profile from Baby Banana peels (Sobolev et al. 2005; de Souza et al. 2007).

The sphingolipids have attracted interest because they are emerging as an important class of messenger molecules linked to many different cellular functions. They are also involved in signal transduction, membrane stability, host-pathogen interactions, and stress responses. They are furthermore serving as intra and intercellular second messengers regulating cell growth, differentiation, apoptosis, and pathogenic defense (Sperling and Heinz 2003).

2.1.7 Linoleic acid

Baby Banana with hyperpigmentation (34.9 kg) was peeled to separate the skin. The stage of ripening was green color that corresponds to a parameter n° 2, according to the established control table of ripening in the market. The peels (3.26 kg) were freeze-dried to produce 401.6 g of sample. Then, the freeze-dried peels were washed three times during 24 h, firstly with hexane and afterward with methanol, to obtain a liquid extract of compounds both in non-polar and polar phases **(cf. 4.3.1.1).**

The unpolar phase which contained the lipid compounds (17.3 g) was fractionated by means of spiral-coil low speed rotary countercurrent chromatography (Spiral-Coil LSRCCC) and 18 fractions were obtained by using a two phase solvent system composed of ACN/Hexane (1:1) at λ 210 nm in elution and extrusion mode **(Figure 2-42).**

A preliminary phytochemical screening was carried out by means of TLC and revealed the presence of a strong band with a grey color in fraction 6 which showed a low intensity of fluorescent compound at UV 366 nm in comparison with the high intensity of the preceding fractions. Subsequently, fraction 6 was submitted to 1/D and 2/D NMR experiments. As result of the elucidation, linoleic acid was identified and additional information from the HPLC-APCI–MS/MS analysis showed that linoleic acid is the major compound in fraction 6 (75.45 mg), corresponding to tubes [82-89] in elution mode of the spiral coil-LSRCCC separation.

The ^{1}H and ^{13}C spectrum of fraction 6 supplied useful information on the signals to deduce that a carbonyl ester at δ 180.2 and a signal of CH_3 at δ 14.3 represent the occurrence of a fatty acid. The allylic region with 12 lipid signals from δ 23.0 to δ 34.2 with predominant signal of CH_2 at δ 27.5 depicted clearly that only one fatty acid is represented in the spectrum. The olefinic region showed two double bonds, with signals at δ 128.8, δ 128.5, δ 130.3 and 130.4 and comparison of resonances in ^{13}C and DEPT NMR spectra confirmed that a 18:2 (Δ9, 12) unsaturated linoleic acid has been elucidated in fraction 6 **(Figures 2-43, 2-44).**

The HSQC spectrum showed correlations to the ^{13}C at δ 14.3 with ^{1}H signals at δ 0.9 and the olefinic carbons at δ 128.8 and 128.5 with a region of ^{1}H spectrum at δ 5.35 together with δ 130.4 and 130.3 enhancements correlations at δ5.38. The characteristic ^{13}C signal at δ 26.6 showed resonance with ^{1}H signal at δ 2.81 which confirm the CH_2-11 in the middle of the double bonds. In spite of the region of the ^{1}H spectrum at δ 1.3 could display overlapped, CH_2-3-4-5-15-17 were elucidated clearly. **Table 2-14** summarizes the HSQC resonances in the linoleic acid (Gunstone 1990; Vlahov 2009).

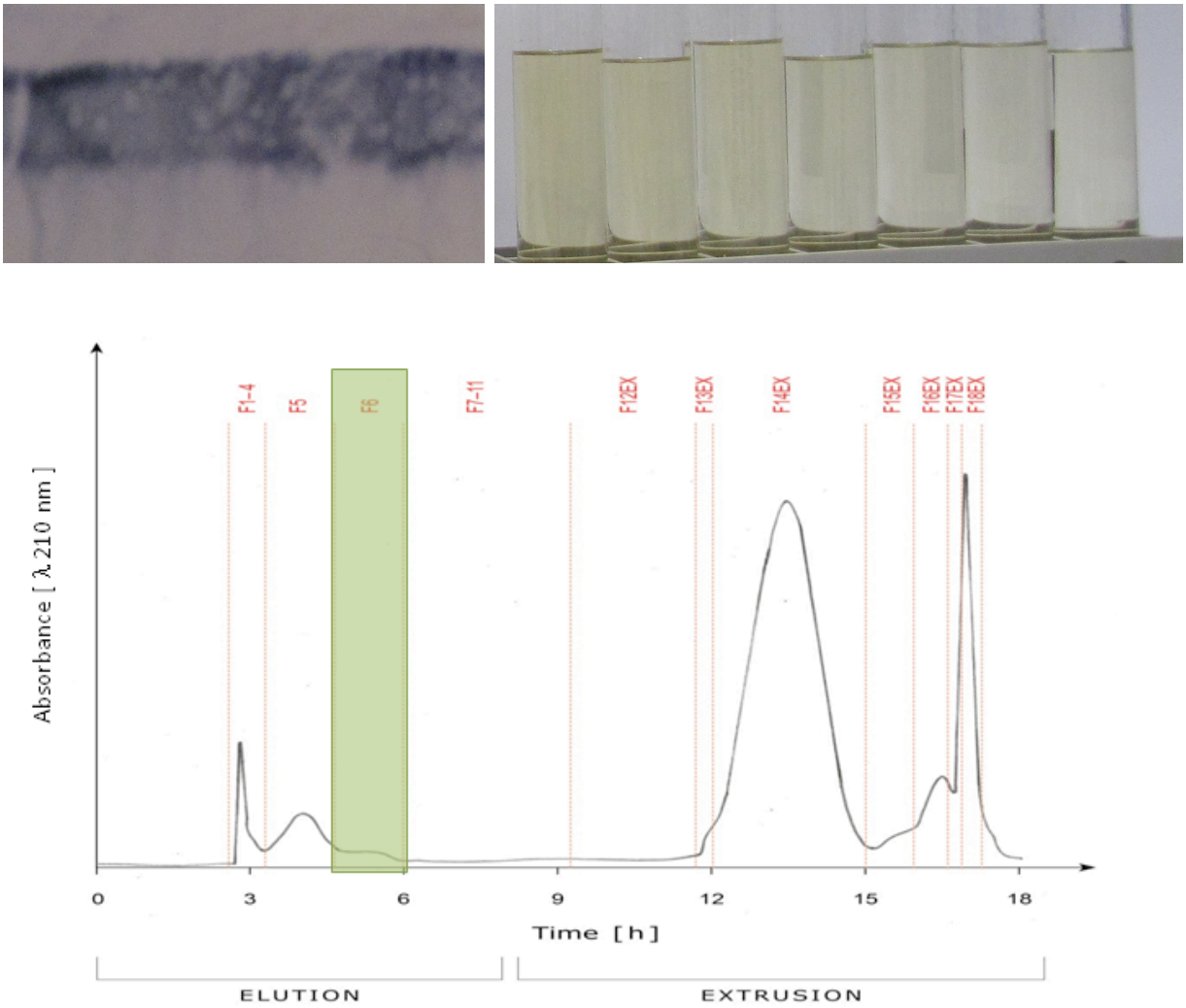

Figure 2-42. (Above) RP-18 TLC (Thin Layer Chromatography) in MeOH (100%) of linoleic acid in fraction 6 that corresponds to the tubes [82-89] in elution mode. (Below) Spiral coil LSRCCC chromatogram of Baby Banana peels with hyperpigmentation (HP). Fraction 6 in elution mode contains linoleic acid which was isolated and identified by 1/D and 2/D NMR experiments.

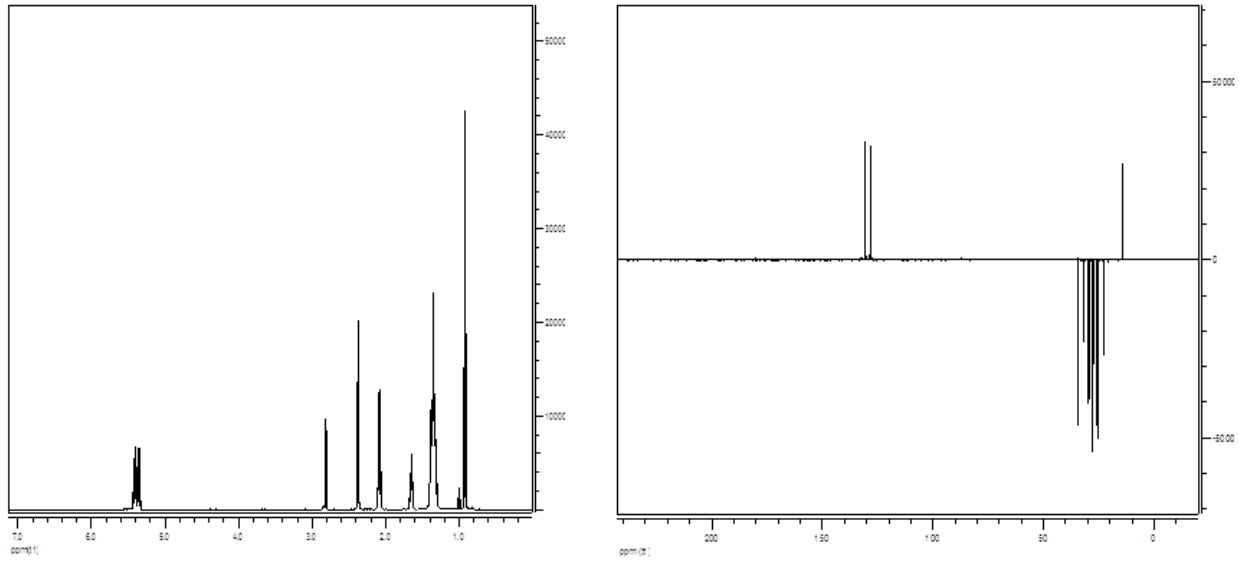

Figure 2-43. 600 MHz ^{1}H-NMR spectrum of linoleic acid in CD_2Cl_2 (Left); 150 Hz DEPT spectrum of linoleic acid in CD_2Cl_2 (Right).

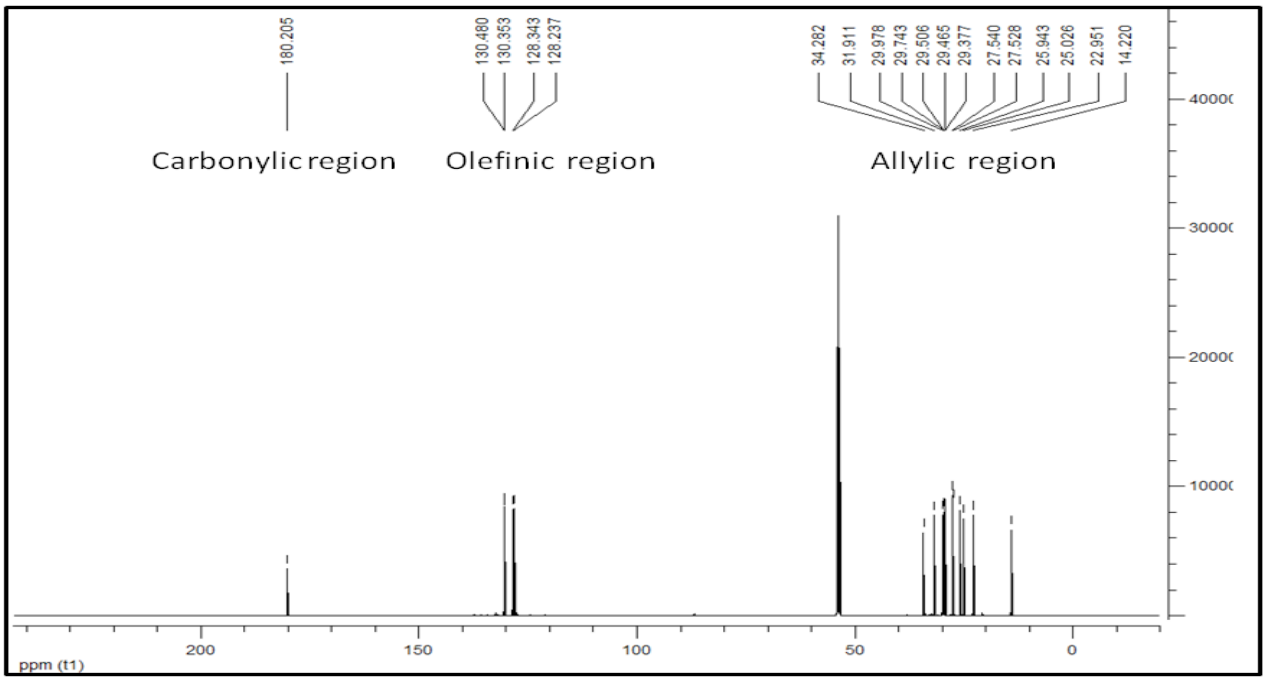

Figure 2-44. 600 MHz ^{13}C-NMR spectrum of linoleic acid in CD_2Cl_2. The olefinic, allylic and carbonylic regions are precisely identified in the spectrum such as the 18 carbons which conform the chemical structure of the linoleic acid (Hatzakis et al. 2011; Zamora et al. 2002).

Table 2-14. ^{1}H-NMR and ^{13}C-NMR spectroscopic data of linoleic acid in fraction 6 and assignments of resonances in the 600 MHz ^{1}H-NMR and 150 MHz ^{13}C-NMR spectra in CD_2Cl_2 (Gunstone 1990).

Assignment	Δ^1 H (ppm)	Multiplicity J/ Hz	δ^{13}C (ppm)
CH_2-1	----	---	180.2
CH_2-2	2.33	*m*	34.2
CH_2-3	1.65	*m*	25.5
CH_2-4, 7	1.34	*m*	29.3-29.9
CH_2-8	2.06	*q* [7.2]	27.5
CH-9	5.38	*td* [1.5,3.4]	130.3
CH-10	5.35	*td* [1.3,2.8]	128.5
CH_2-11	2.81	*t* [7.1]	26.6
CH-12	5.35	*td* [1.3,2.8]	128.8
CH-13	5.38	*td* [1.5,3.4]	130.4
CH_2-14	2.06	*q*[7.2]	27.5
CH_2-15	1.30	*m*	29.4
CH_2-16	1.30	*m*	31.9
CH_2-17	1.31	*m*	23.0
CH_3-18	0.90	*t*[7.1]	14.3

The ^{1}H- ^{13}C-NMR HMBC spectrum gave relevant information to confirm the correlation between the carbonylic C-1 with C-2-3, and besides it, the connectivity between C-7-8-14-15 resonances with the olefinic region is confirmed. The significant HMBC enhancements between the CH_3 –18 with C-17-16-14 support the chemical structure of the linoleic acid, 18:2 (Δ9Z, 12Z) **(Figure 2-45).** The ^{1}H- ^{13}C-NMR HMBC spectrum supported the fact that linoleic acid is the major compound in fraction 6 **(Figure 2-46).**

The results of the 2D experiments COSY and NOESY provided assignments to confirm the proximity between the ^{1}H-^{1}H signal and also through-space, respectively. The COSY spectrum showed the connectivities between protons in the structure of linoleic acid according to the HMBC and HSQC results described above and also brought overriding support in order to confirm that it is a polyunsaturated omega-6 fatty acid **(Figure 2-47).**

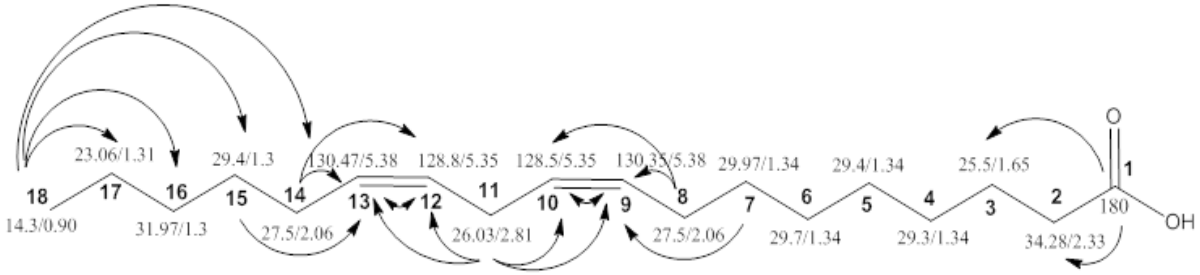

Figure 2-45. Structure relevant HC-correlation in the HSQC (Heteronuclear single-quantum correlation) and the HMBC (Heteronuclear multiple bond correlation) from linoleic acid 18:2 (Δ9Z, 12 Z) in fraction 6**.** HSQC and HMBC analysis were in agreement with literature data (Vlahov 2009; Hatzakis et al. 2011; Zamora et al. 2002; Gunstone 1990; Gunstone 1993).

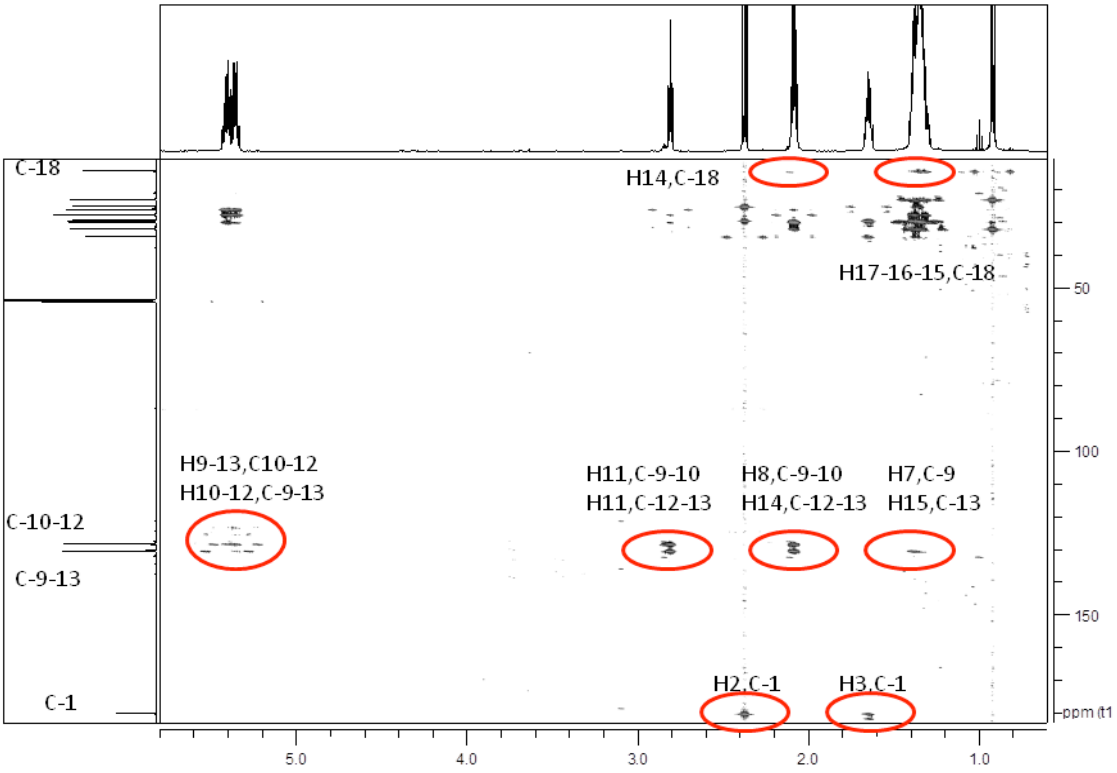

Figure 2-46. The 600 MHz 2D HMBC spectrum of linoleic acid 18:2 (Δ9Z, 12Z) shows the enhancements between olefinic and allylic regions which support the chemical structure of an unsaturated fatty acid in fraction 6.

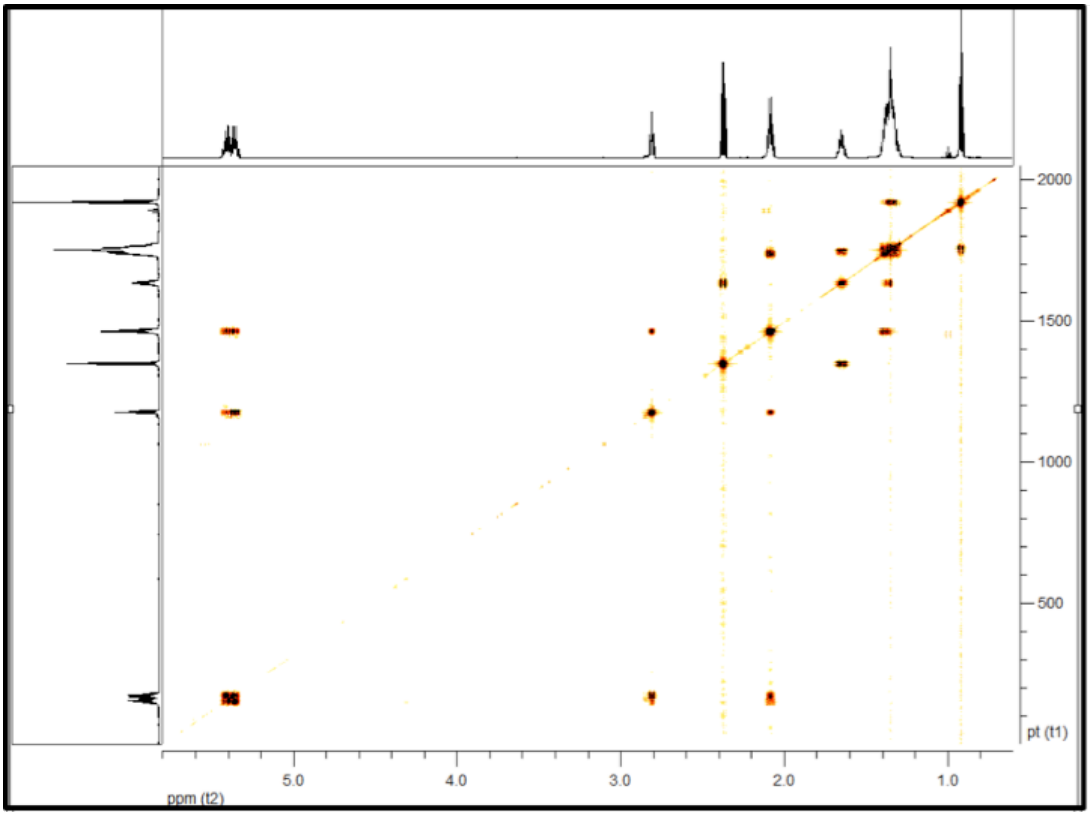

Figure 2-47. The 600 MHz COSY spectrum of ω-6 linoleic acid in fraction 6 from spiral coil–LSRCCC separation of Baby Banana peels with hyperpigmentation (CD_2Cl_2).

Furthermore, NOE assignments confirmed the olefinic side chain with two double bonds in cis-configuration which are supported by the triplet of doublets at 5.35 ppm *td* (*t*, $^3J_{(10\text{-}11)(12\text{-}11)}$= 1.3; *d*, $^3J_{(10\text{-}9)(12\text{-}13)}$= 2.8) and 5.38 ppm *td* (*t*,$^3J_{(9\text{-}8)(13\text{-}14)}$=1.5;*d*, $^3J_{(9\text{-}10)(13\text{-}12)}$= 3.4), corresponding to H-9 and H-10 as well as H-12 and H-13. Thus, the equatorial conformation shows the proximity between the protons in the olefinic region. Moreover, the coupling constants for H-11 at δ 2.81 and H-8-14 at δ 2.06 exhibit a value of 7.1 and 7.2 Hz, respectively **(Table 2-14).**

Additionally, the stereochemistry of the linoleic acid could be elucidated by NOE enhancements which showed three relevant resonances between H-18 at δ 0.9 with H-3 at δ 1.65, between H-2 at δ 2.33 with H-14 at δ 2.06 and between H-11 at δ 2.81 with H-4, 7 at δ 1.3 which illustrate that the molecule could be twisted **(Figures 2-48, 2-49).**

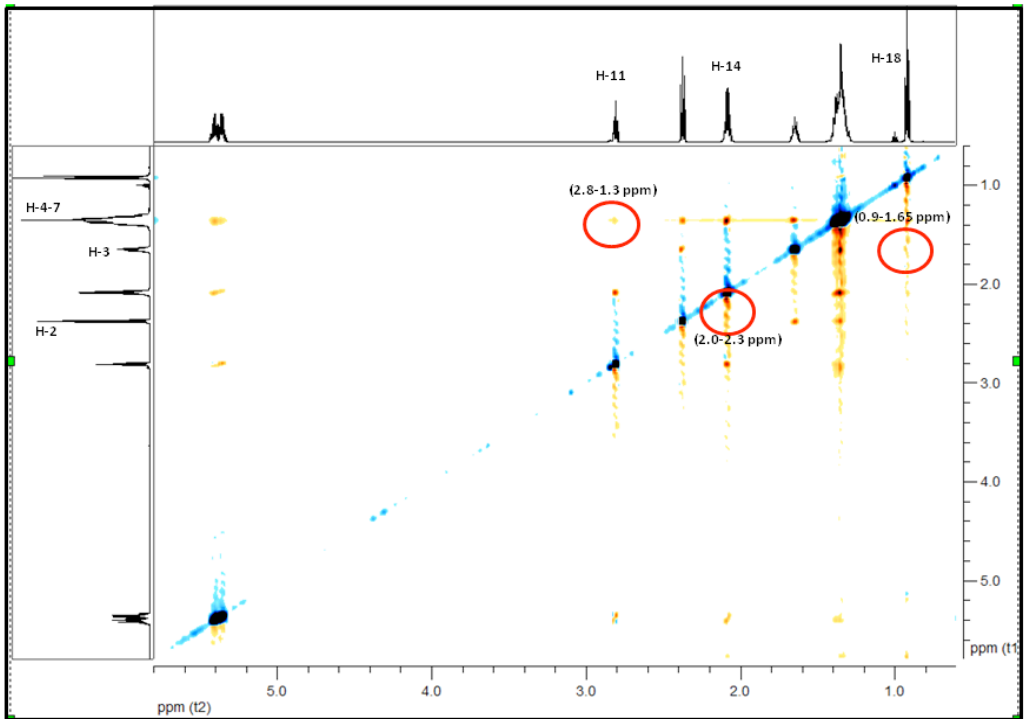

Figure 2-48. Relevant NOE enhancements used to define the stereochemistry of ω-6 linoleic acid in fraction 6 from spiral coil–LSRCCC separation of Baby Banana peels with hyperpigmentation. The red circles indicate the correlation between three relevant resonances between H-18 at δ 0.9 with H-3 at δ 1.65, between H-2 at δ 2.33 with H-14 at δ 2.06 and between H-11 at δ 2.81 with H-4,7 at δ 1.34 which illustrate that the molecule could be twisted (600 MHz, CD_2Cl_2).

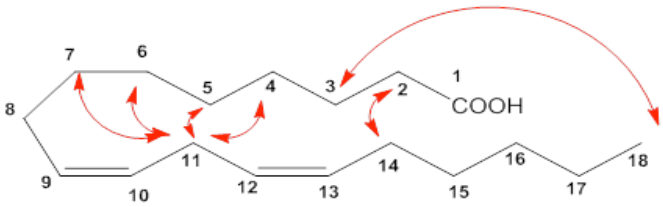

Figure 2-49. Final stereochemistry proposal of the ω-6 linoleic acid (18:2, Δ9*Z*, 12Z) according to NOESY and COSY experiments in fraction 6 from spiral coil–LSRCCC separation of Baby Banana peels with hyperpigmentation (CD_2Cl_2).

The analysis of HPLC-APCI-MS-MS (positive ion mode) data showed at the retention time of 2.9 min the occurence of linoleic acid (*m/z* 278.6) as a major compound in fraction 6. However, the chromatogram revealed traces of arachidic acid (20:0) with *m/z* 295 at 3.0 min, hydroxypheophytin *a* with *m/z* 887 and pheophytin b with *m/z* 885 at a retention time of 22.4 min. The DAD-contour-plot displays at UV 423 and 677 nm traces of hydroxypheophytin *a* in fraction 6 (Jakab et al. 2002; Holčapek et al. 2003) **(Figure 2-50).**

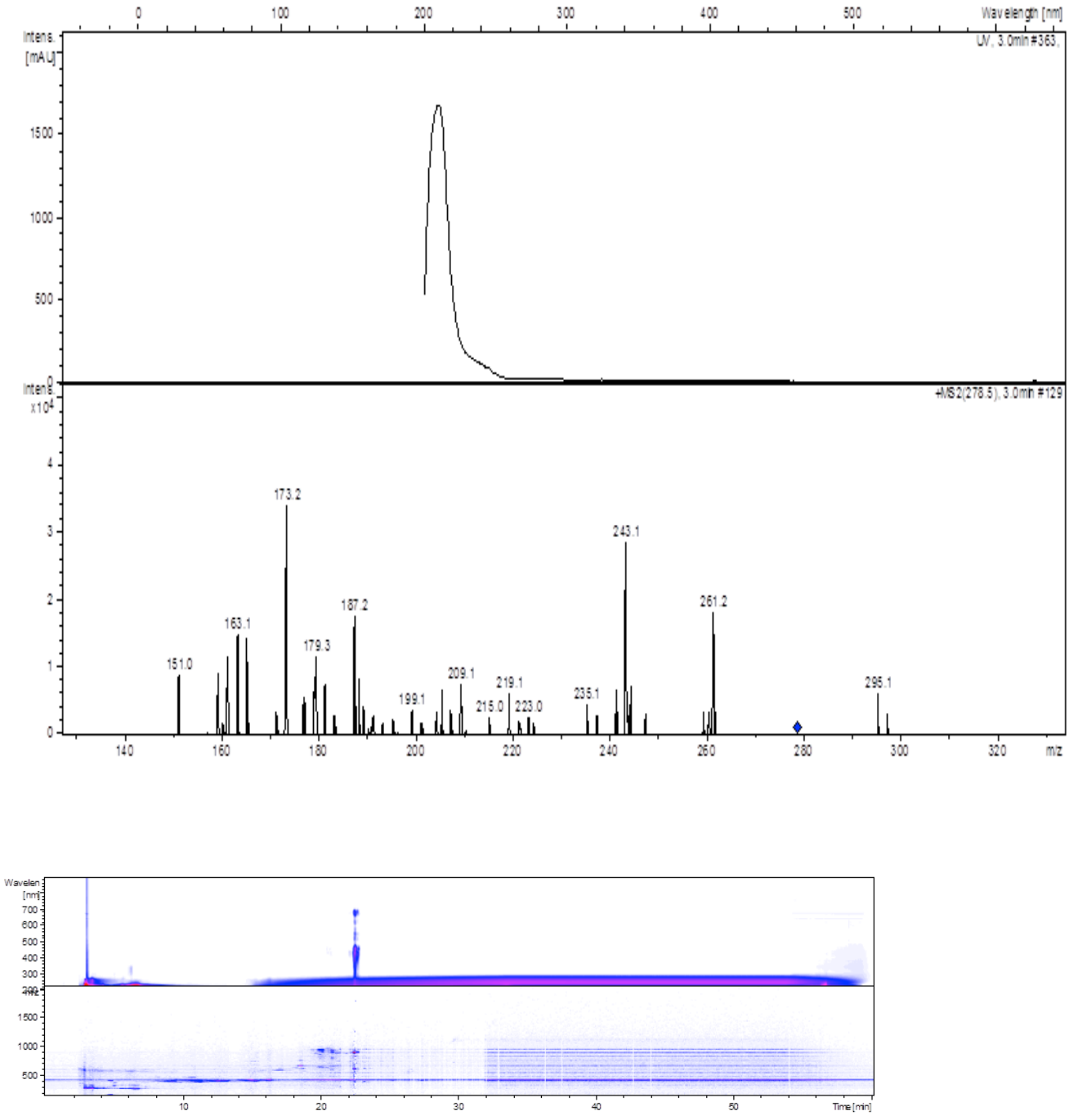

Figure 2-50. HPLC-APCI-MS-MS analysis (positive ion mode) of fraction 6 from spiral coil-LSRCCC of Baby Banana peels. (Above) Linoleic acid is the major fatty acid with *m/z* 278 and traces of arachidic acid (20:0) with *m/z* 295, in 3.0 min (Below). Traces of pheophytin *b* and hydroxypheophytin *a* with *m/z* 885 and 887, respectively at 22.4 min (displays fluorescence at UV 423 and 677 nm) in DAD-contour-plot (Jakab et al. 2002; Holčapek et al. 2003).

2.1.7.1 Summary

The elucidation of linoleic acid in fraction 6 from the spiral coil-LSRCCC separation of Baby Banana peels with hyperpigmentation was achieved on the basis of 1/D and 2/D NMR spectra and consequently they were useful in order to do comparisons with other spectra which contained fatty acids as part of the chemical structure e.g mono/di-galactosyldiacylglycerols, phosphatidylcholine and phosphatidylethanolamine.

High resolution 1/D and 2/D NMR data of linoleic acid was obtained in the frame of studies of mono-, di- and triacylglycerols (MAG; DAG; TAG) in vegetable oils and they were confirming the linoleic acid which was isolated and identified in Baby Banana peels (Vlahov 2009; Hatzakis et al. 2011; Zamora et al. 2002; Gunstone 1990, Gunstone 1993).

Different dichloromethane extracts of different morphological parts of banana plant *Dwarf Cavendish*, cultivated in Madeira Island (Portugal), were studied by gas chromatography-mass spectrometry and phytosterols and fatty acids such as palmitic, stearic, linoleic, linolenic, 22-hydroxydocosanoic, 24-hydroxytetracosanoic and 26-hydroxyhexacosanoic acids, were the major components found in all morphological zones (Oliveira et al. 2006). Besides, six varieties of banana peels from Cameroon, Africa, were studied at three stages of ripeness to explore their potential applications. The content of lipids was analyzed by GLC and varied from 2.2% to 10.9%. It was rich in polyunsaturated fatty acids, 42.1-52.2% of the total fatty acids in all varieties and particularly linoleic acid (ω-6) and **β**-linolenic acid (ω-3). Among the saturated acids, the main representatives were palmitic and stearic acid with small amounts of arachidic and myristic acid (Happi Emega et al. 2007).

The important interaction between fatty acid and glycolipids during the degreening of bananas ripened at tropical temperatures and the relation with the photosynthetic capacity has been reported in section 2.1.2.3 (Blackbourn et al. 1990; Wada et al. 2009).

Additionally, the studies in bean thylakoids membranes treated with various lipolytic enzymes showed marked changes in their acyl lipid composition and also that galactolipids, phosphatidylglycerol and to some extent monogalactosyldiacylglycerol are essential for the oligomeric stabilization of the light harvesting chlorophyll a/b protein complex (Krupa 1984; Luzzati and Spegt 1967). It is known that there is a strict light dependency of fatty acids synthesis in leaf chloroplasts but the relevance to TAG accumulation in oilseeds was revealed only recently at the metabolic level. Even low levels of light penetrating to developing embryos provide sufficient reductants and ATP for fatty acid biosynthesis (Goffman et al. 2005).

A recent study reported by the American Society for Biochemistry and Molecular Biology described that triacylglycerols (TAG) from plants supply 25% of dietary calories to the developed world. They are increasingly used as a source for renewable biomaterials and fuels. Demand for vegetable oils will double by the year 2030, which can only be met by increase oil production. TAG synthesis is accomplished through the coordinate action of multiple pathways in multiple subcellular compartments and recent information has revealed an underappreciated complexity in pathways for synthesis and accumulation of this important, energy-rich class of molecules (Chapmann and Ohlrogge 2012).

2.1.8 Lutein

The extraction of 401.6g from freeze dried peels of Baby Banana with hyperpigmentation **(cf. 4.3.1.1)** yielded 17.17 g of hexane phase and 3.65 g of methanol phase. From the total amount of methanol phase 1.03 g was fractionated by means of High Speed Countercurrent Chromatography and a total of 12 fractions was obtained in elution mode (6 fractions) and extrusion mode (6 fractions). The conditions for the separation were as follows: solvent system hexane/MeOH/water/EtOAc (10/10/1/1) at a flow rate of 3.5 mL/min in elution and extrusion mode" head to tail" with detection at λ 440 nm **(Figure 2-51).**

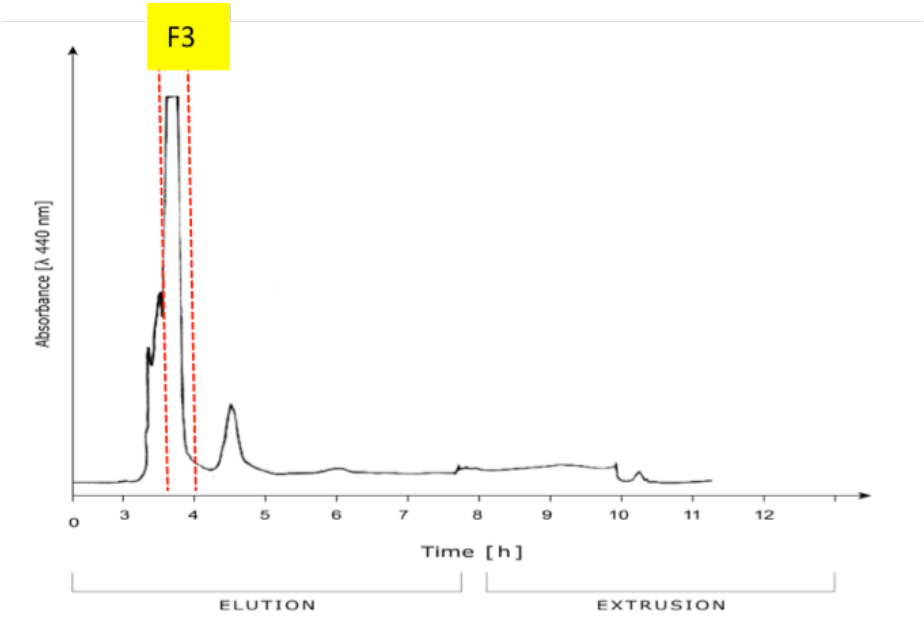

Figure 2-51. HSCCC chromatogram of Baby Banana peels with hyperpigmentation (HP) from the methanol extract. Fraction 3 in elution mode contained 12.4 mg of lutein which was identified by 1/D and 2/D NMR experiments in CD_2Cl_2.

On the TLC-RP-18 from elution and extrusion mode a yellow band was observed corresponding to the tubes of fraction 3 in elution mode **(Figure 2-52).** Subsequently, when the plate was developed with anisaldehyde, one gray band was noticed which showed that a carotenoid had been isolated. Therefore, the fraction was submitted to 1/D and 2/D NMR experiments.

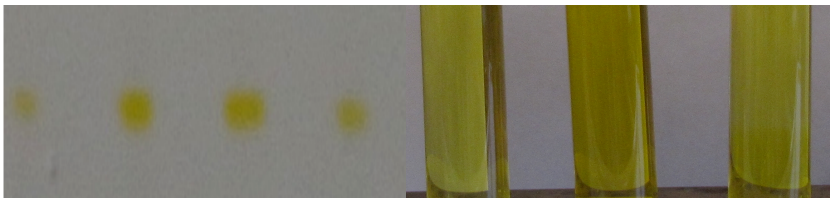

Figure 2-52. RP-18 TLC screening, under white light, of tubes corresponding to fraction 3 from HSCCC elution.

The chemical structure of lutein (3*R*, 3'*R*, 6'*R*)-*β*, *ε*-carotene-3, 3'-diol was elucidated by means of 1/D and 2/D NMR experiments and the assignments of ^{1}H and ^{13}C-NMR signals were supported by ^{1}H-^{1}H–COSY and NOESY as well as the calculation of the coupling constants (*J*) **(Figures 2-53, 2-54, 2-55).** The ^{1}H and ^{13}C data were in agreement with literature data, with the exception of the

coupling constants (*J)* from C-4 which showed at δ 2.26, *dd,* $^{2}J_{(a\text{-}b)}$= 1.9 Hz, $^{3}J_{(4\text{-}3)}$ = 5.9 Hz instead at δ 2.04 *dd,* $^{2}J_{(a\text{-}b)}$= 16.8, $^{3}J_{(4\text{-}3)}$= 9.5 Hz. The large coupling constant of the doublet at δ 2.04 (16.8 Hz) which would show a diaxial position between $H_{a\text{-}b}$ is not present in the data elucidated and in contrast the coupling constant shows an equatorial arrangement at δ 2.26, *dd;* $^{2}J_{(a\text{-}b)}$= 1.9 Hz. In the same way, the coupling constant between H-4 and H-3 differs with the data; whereas the literature reports $^{3}J_{(4\text{-}3)}$= 9.5 Hz, the lutein isolated yielded $^{3}J_{(4\text{-}3)}$= 5.9 Hz (Molnár et al. 2004; Molnár et al. 2006; Aman et al. 2005a) **(Table 2-15).**

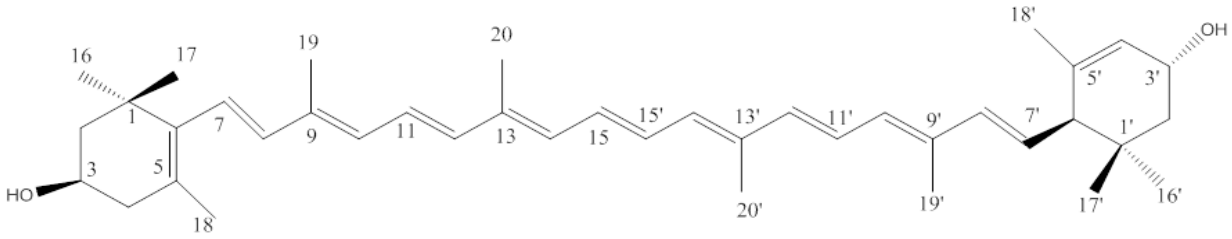

Figure 2-53. Structure of (all-E)-lutein (3R, 3'R, 6'R)-*β*, *ε*-carotene-3, 3'-diol isolated from Baby Banana peels with hyperpigmentation by means of High Speed Countercurrent Chromatography (HSCCC).

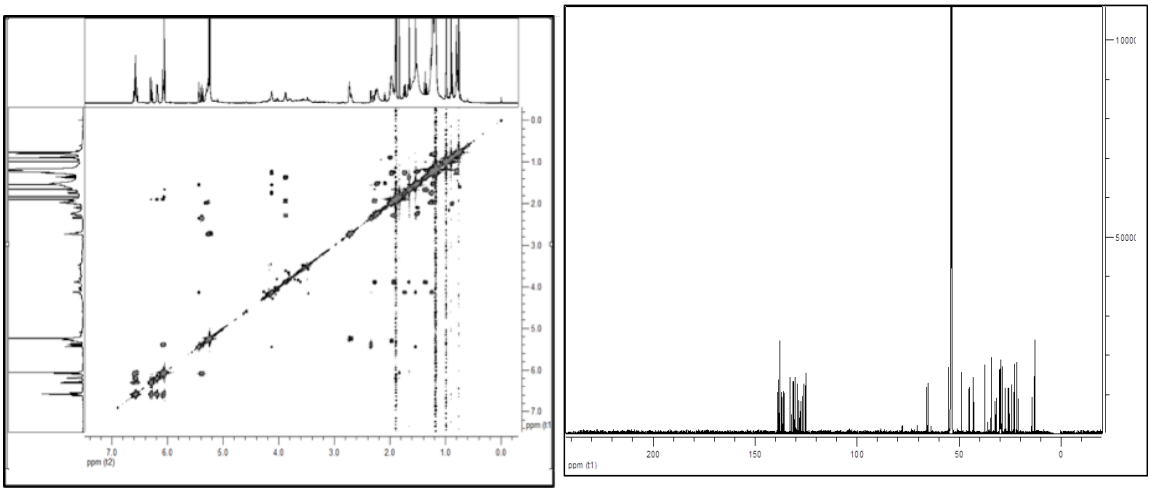

Figure 2-54. The 600 Hz COSY spectrum (left) and ^{13}C spectrum (right) of lutein isolated from Baby Banana with hyperpigmentation by HSCCC in CD_2Cl_2.

In **Table 2-15,** complete ^{1}H and ^{13}C-NMR assignments are given for the lutein with a characteristic ε-type according to literature data (Molnár et al. 2004).

Table 2-15. ^{1}H and ^{13}C–NMR data of lutein (3R, 3'R, 6'R)-β, ε-carotene-3, 3'-diol at 600 MHz and 150 MHz, respectively, in CD_2Cl_2 isolated from Baby Banana peels by means of High Speed Countercurrent Chromatography (Molnár et al. 2004; Liaaen-Jensen 1973).

Assignment	**δ^{1}H (ppm)**	**Multiplicity J/ Hz**	**δ^{13}C (ppm)**
C-1	----	----	37.40
C-2	1.35	*t,* $^{2}J_{(a\text{-}b)}$= 11.9 Hz, $^{3}J_{(2\text{-}3)}$ = 11.9 Hz	48.85
	1.65	*dd*, $^{4}J_{(2\text{-}4)}$= 5.9, $^{3}J_{(2\text{-}3)}$= 12.9 Hz	
C-3	3.87	*m*	65.10
C-4	2.26	*dd,* $^{2}J_{(a\text{-}b)}$ = 1.9 Hz, $^{3}J_{(4\text{-}3)}$= 5.9 Hz	42.97
	1.92	*d*, $^{3}J_{(4\text{-}3)}$= 6.7 Hz	
C-5	----	----	126.20
C-6	----	----	138.0
C-7	5.42	*m*	125.13
C-8	6.0	*m*	138.68
C-9	----	----	135.62
C-10	6.09	*m*	131.48
C-11	6.55	*q*, $^{3}J_{(11\text{-}10;\ 11\text{-}12)}$= 7.2 Hz	125.47
	6.28	*dd*, $^{3}J_{(12\text{-}11)}$= 2.3 Hz, $^{4}J_{(12\text{-}14)}$ = 15.0 Hz	137.67
C-12	----	----	136.99
C-13	6.16	*m*	132.8
C-14	6.58	*m*	130.4
C-15			
C-16	0.98	*s*	28.78
C-17	0.98	s	30.42
C-18	1.65	s	21.73
C-19	1.88	s	12.80
C-20	1.87	s	12.82
C-1'	----	----	34.30
C-2'	1.25	*dd*, $^{2}J_{(a\text{`-}b\text{`})}$= 7.1 Hz, $^{3}J_{(2\text{`-}3\text{`})}$= 13.2 Hz	45.09
	1.73	*dd*, $^{4}J_{(2\text{`-}4\text{`})}$= 5.8 Hz, $^{3}J_{(2\text{`-}3\text{`})}$= 13.1 Hz	
C-3'	3.87	*m*	65.09
C-4'	5.47	br.*s*	125.13
C-5'	----	----	137.99
C-6'	2.32	*d,* $^{2}J_{(6\text{`-}7\text{'})}$= 10.0 Hz	55.32
C-7'	5.2	*m*	128.57
C-8'	6.08	*m*	137.92
C-9'	----	----	135.19
C-10'	6.07	*m*	130.97
C-11'	6.59	*q*, $^{3}J_{(11\text{`-}10\text{`};\ 11\text{`-}12\text{`})}$=7.2 Hz	125.38
C-12'	6.29	*dd*, $^{3}J_{(12'\text{-}11')}$= 2.3 Hz, $^{4}J_{(12\text{-}14)}$= 15.0 Hz	137.67
C-13'	----	----	136.91
C-14'	6.45	*m*	132.80
C-15'	6.58	*m*	130.43
C-16'	0.9	*s*	29.60
C-17'	0.76	*s*	24.29
C-18'	1.53	*s*	22.93
C-19'	1.83	*s*	13.20
C-20'	1.88	*s*	12.89

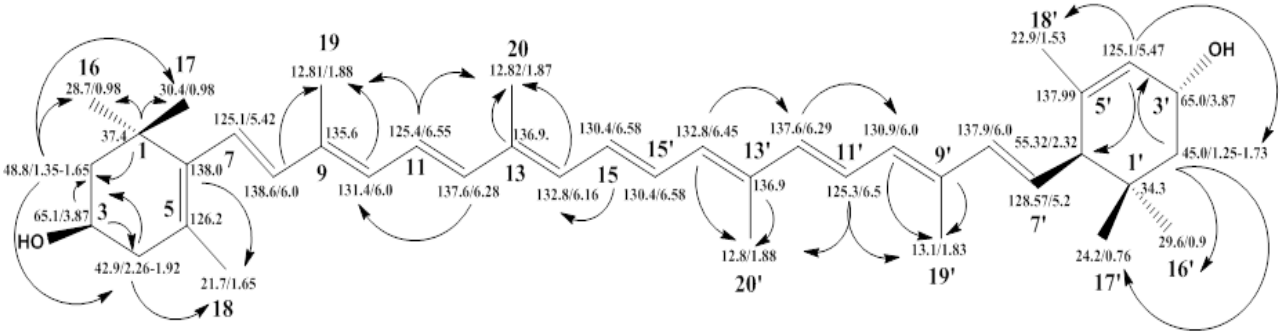

Figure 2-55. Structure relevant long-range HC-correlation in the HMBC and HSQC of lutein (3R, 3'R, 6'R)-β, ε-carotene-3, 3'-diol from Baby Banana peels in CD_2Cl_2

The confirmation of the structure was performed by HPLC-APCI-MS-MS. Fraction 3 showed a single peak with quasimolecular ion at *m/z* 551 [M+H-H_2O] at 16.2 min with the characteristic spectrum of lutein with absorption maxima of 420, 444 and 472 nm which is in agreement with literature data **(Figure 2-56)** (de Rosso and Mercadante et al. 2007; Britton et al. 1995; Gross et al. 1973a; Subagio et al. 1996).

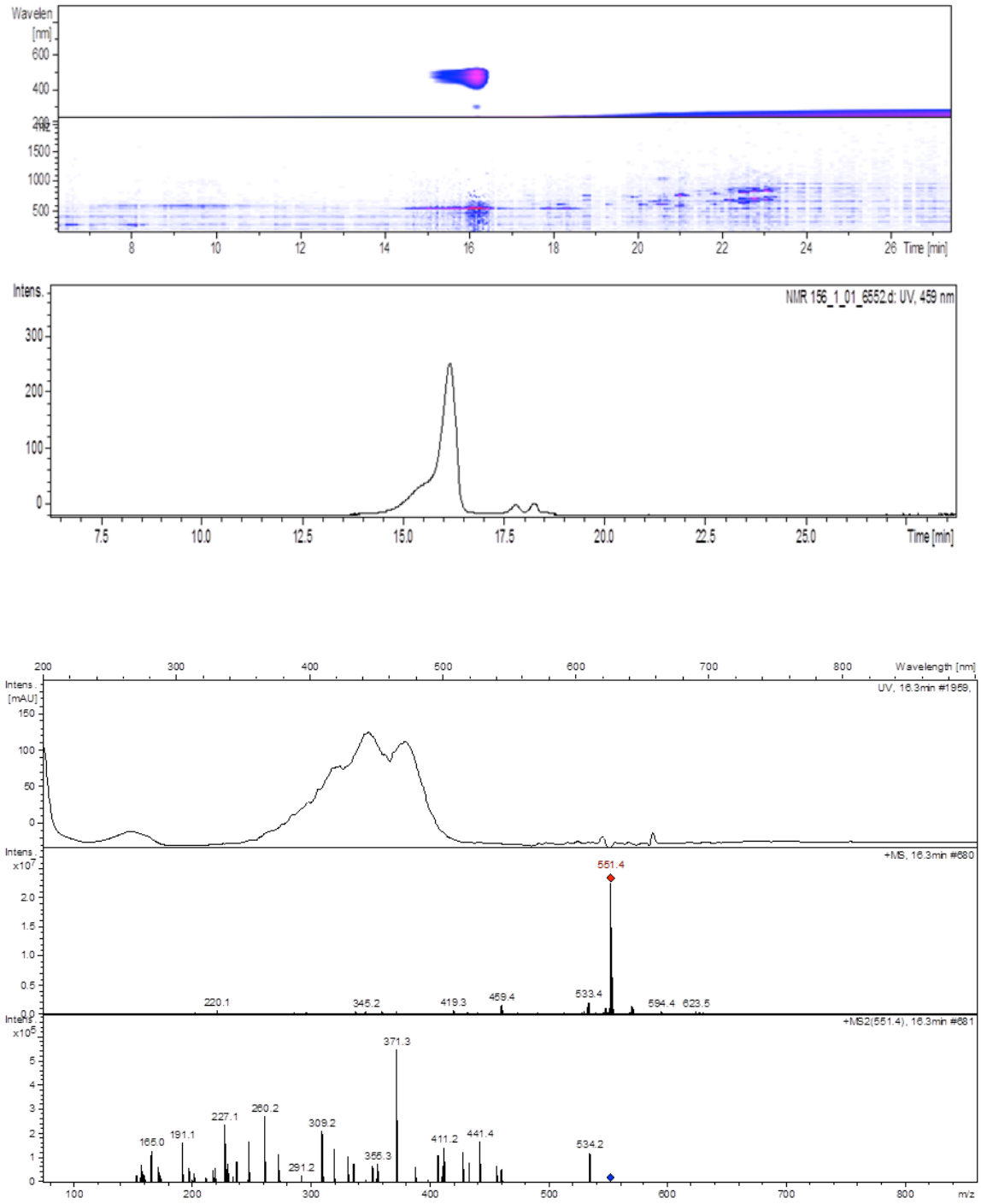

Figure 2-56. HPLC-APCI-MS-MS spectra (positive ion mode) of a quasimolar ion at *m/z* 551 [M+H-H_2O] corresponding to lutein isolated in fraction 3 from Baby Banana peels with hyperpigmentation (below), at 16.2 min according to the chromatogram (middle), at 420, 444 and 472 nm as the UV absorption maxima (above), in concordance with literature data (de Rosso and Mercadante 2007; Mercadante et al. 1997; Britton et al. 1995; Gross et al. 1973a; Subagio et al. 1996).

2.1.9 Violaxanthin-di-laurate and β-Carotene isomers

The extraction of 401.6 g freeze dried peels of baby banana with hyperpigmentation yielded 17.17 g of hexane phase and 3.65 g of methanol phase **(cf. 4.3.1.1).** The total amount of hexane phase (17.17 g) was not fractionated by means of spiral coil low-speed rotary countercurrent chromatography (LSRCCC), but only 26.6% because not all the compounds in the extract were dissolved in the solvent system (ACN/Hexane [1:1]) **(Section 2.2 Optimization of Solvent System).**

The rest of the hexane phase extract was retained in the filter paper during the preparation of the sample while the injection was performed in the spiral coil - LSRCCC experiment. Subsequently, the retained rest (8.02 g) was dissolved in acetone and denominated as "acetone extract" for further experiments.

For this purpose, 1.0 g of the acetone extract was fractionated by means of HSCCC and a total of 14 fractions was obtained; in elution mode (6 fractions) and in extrusion mode (8 fractions). The conditions for the separation were the following: solvent system hexane/EtOH/Water/(6/5/2), flow rate 3.5 mL/min in elution mode, and 6.0 mL/min in extrusion mode, elution mode ”head to tail”, detection at λ 220 nm **(Figure 2-57).**

The HSCCC chromatogram and the screening of TLC plates showed that fraction 12 in extrusion mode represented the major peak in the chromatogram and also contained several compounds. Hence, an additional purification by a normal phase chromatography was performed, and various solvent systems were tested.

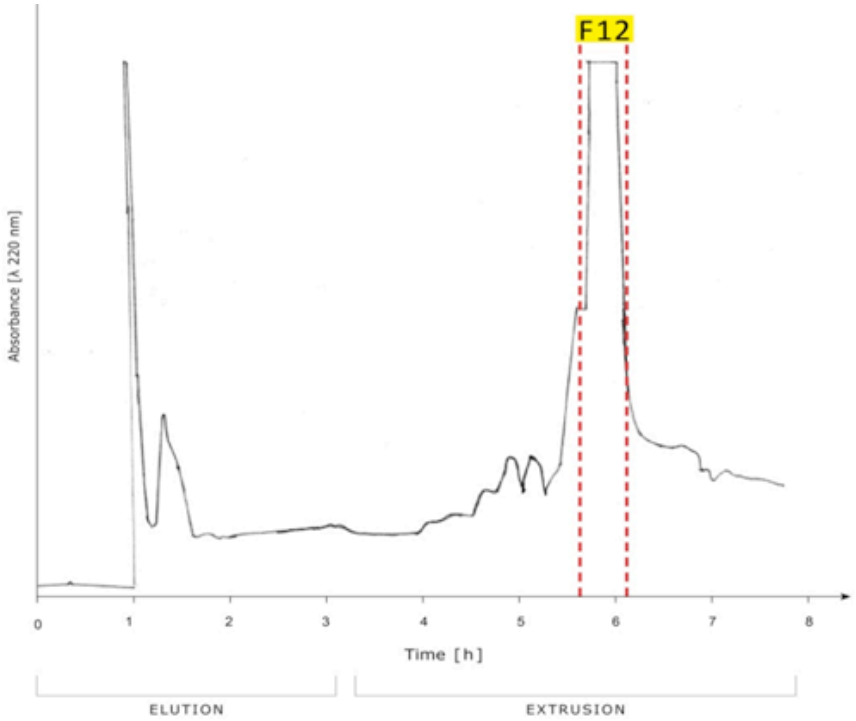

Figure 2-57. HSCCC separation of the "acetone extract", solvent system: hexane/EtOH/Water/ (6/5/2), flow rate 3.5 mL/min in elution and 6.0 mL/min in extrusion mode, elution mode ” head to tail”, detection at λ 220 nm.

The assay was conducted by analytical thin layer chromatography, using aluminum sheets of silica gel F_{251} [Merck©]. The mobile phase CH_2Cl_2/MeOH (9.9/0.1) showed the best separation for HSCCC fraction 12.**(cf. 4.3.2.1)** Accordingly, a normal phase chromatography with CH_2Cl_2/MeOH (9.9/0.1) as mobile phase in a column of 60 mL was performed.

100 mg of fraction 12 was dissolved in 200 mL of CH_2Cl_2/MeOH (9.9/0.1). The separated compounds were collected in 15 fractions and monitored by TLC in order to observe the purity of the separation.

Fraction 1 (27.8 mg) showed a single band of yellow color under white light, after spraying with anisaldehyde a grey color replaced the yellow band in the silica gel TLC plate **(Figure 2-58).** The presence of only one band indicated that carotenes have been isolated. Therefore, fraction 1 was submitted to 1/D and 2/D NMR experiments.

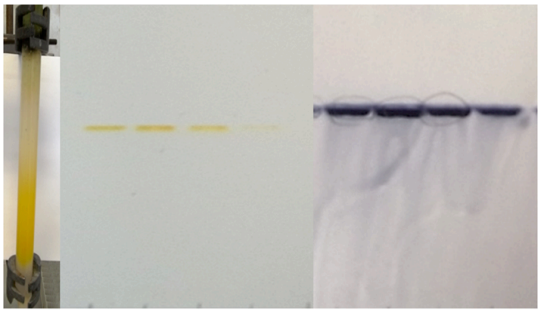

(A) (B) (C)

Figure 2-58. (A) Normal phase chromatography of 100 mg of HSCCC fraction 12; (B) TLC plate of silica gel of fraction 1 corresponding to tubes [9-12] in the normal phase separation; (C) TLC plate of silica gel of fraction 1 corresponding to tubes [9-12] in the normal phase separation, after been developed with anisaldehyde as chromogenic agent.

The ^{1}H-NMR spectrum of fraction 1 depicted resonances at δ 6.02, 6.4, 6.5, 6.9 for the olefinic region of the carotenoids, as well as the characteristic methyl groups H-16-16’ and 17-17’- at δ 1.17, in addition to the chemical shift of H-19-19’, and H-20-20’ methyl groups at δ 1.89 and 1.87, respectively. The ^{13}C spectrum confirmed that chemical shifts corresponded to both β-carotene as well as a fatty acid ester at δ 173.70; 173.67; 173.65; 173.61. A wide range of resonances between δ 20-35 ppm, which represents methylene, methine and methyl groups, indicated that there are more than one compound in the fraction.

The high intensity of several chemical shifts in the ^{1}H-NMR and ^{13}C-NMR spectra, which correspond to triterpenoid and fatty acids, contrasted with the low intensity of ^{1}H-chemical shift and ^{13}C chemical shift of carotenoids. For this reason, it was extremely difficult to elucidate the complete structure of the carotenoid without the relevant support of HPLC-APCI-MS-MS mass spectrometry. The appropriate interpretation of the UV spectra defines the type of carotenoids in the fraction, either *cis/trans* isomers of ß-carotene or carotenoid esters in agreement with the literature data. Nevertheless, the elucidation of the 1/D and 2/D NMR experiments enabled to gather the resonances of each one of the carotenoids, fatty acid and triterpenoids in fraction 1 **(Figure 2-59).**

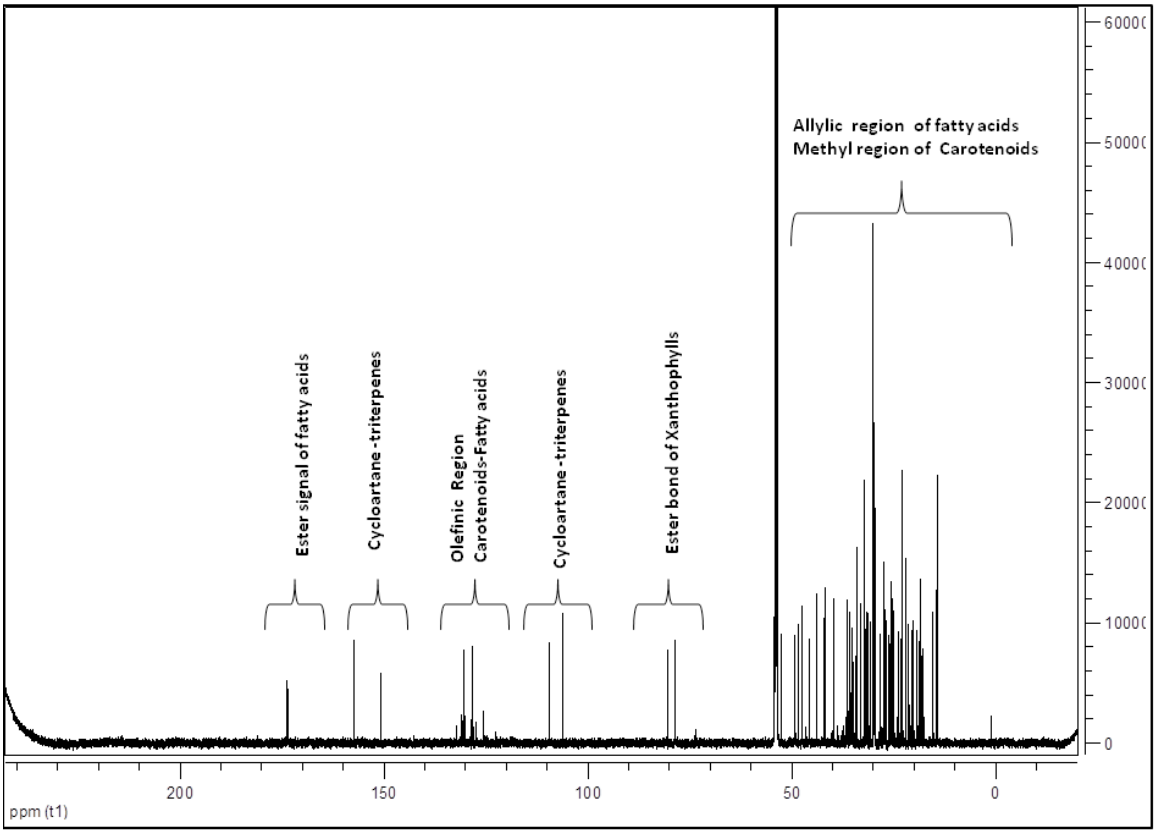

Figure 2-59. ^{13}C NMR spectrum of fraction 1 obtained by means of normal phase chromatography from the "acetone extract" of Baby Banana peels with hyperpigmentation. The ^{13}C chemical shifts in the spectrum represent the resonances of carotenoids, carotenoid ester, fatty acid and triterpenoids which were gathered according to ^{1}H, HSQC, HMBC, COSY and NOESY experiments.

The HMBC spectrum detected heteronuclear correlations between the ester signal of fatty acid (δ173.61-173.69) and two unexpected ^{1}H resonances at δ 4.39 and 4.45 which showed the clue to define the presence of carotenoid esters. Besides, the HSQC spectrum confirmed the single correlation at δ 78.42 /4.39 and δ 80.54/4.38 which support the ester bond of C-1 from the fatty acids with an oxygen in form of alcohol, epoxy or oxo group, which are the main characteristics of xanthophylls **(Figures 2-60, 2-61).**

The identification of the xanthophyll was performed through the analysis of the UV spectrum and the absorption maxima in the spectrum of HPLC-APCI-MS-MS, in agreement with literature data. The contour-plot of fraction 1 showed two broad bands between 400 and 500 nm and two peaks between 25.4 and 25.5 min in the chromatogram **(Figure 2-62).**

The UV spectrum of the first peak in 25.4 min showed a three-maxima spectrum of a xanthophyll at 422, 446, 472 nm, which was in agreement with literature data about carotenoids. The analysis of the mass spectrum **(Figure 2-63),** obtained by HPLC- APCI-MS-MS, showed a relevant information for the identification of the structure (Gross et al. 1973b; Weller and Breithaupt 2003; Breithaupt and Schwack 2000; Subagio et al. 1996; Mercadante et al. 1997).

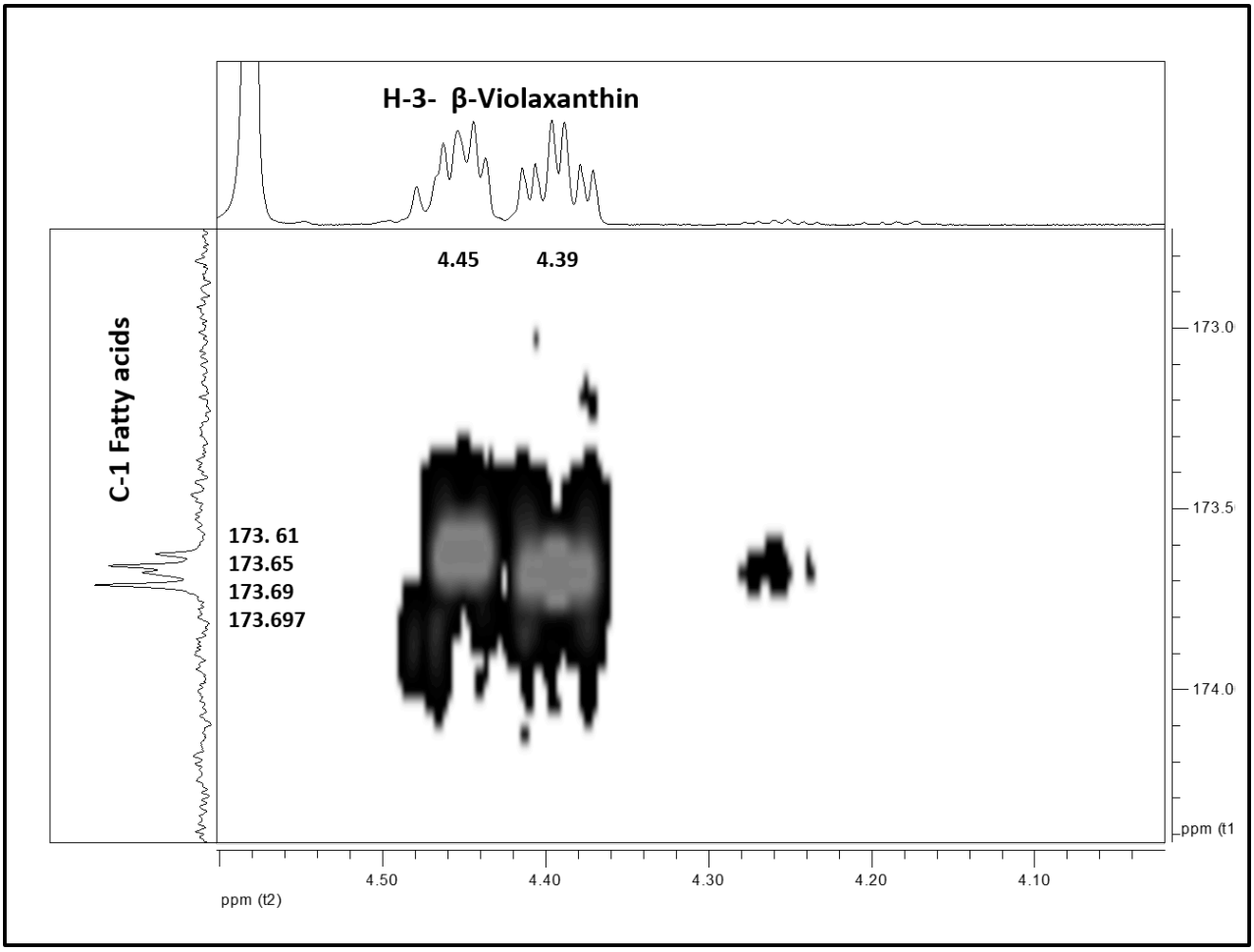

Figure 2-60. HMBC spectrum at 600 MHz confirms the multiple-bond correlation between C-1 from fatty acid at (δ 173.61-173.69) with H-3 (δ 4.45-4.39) of ß-violaxanthin identified by means of 1/D, 2/D NMR experiments and HPLC-APCI-MS-MS mass spectrometry, in fraction 1 from an acetone extract of Baby Banana peels with hyperpigmentation (HP).

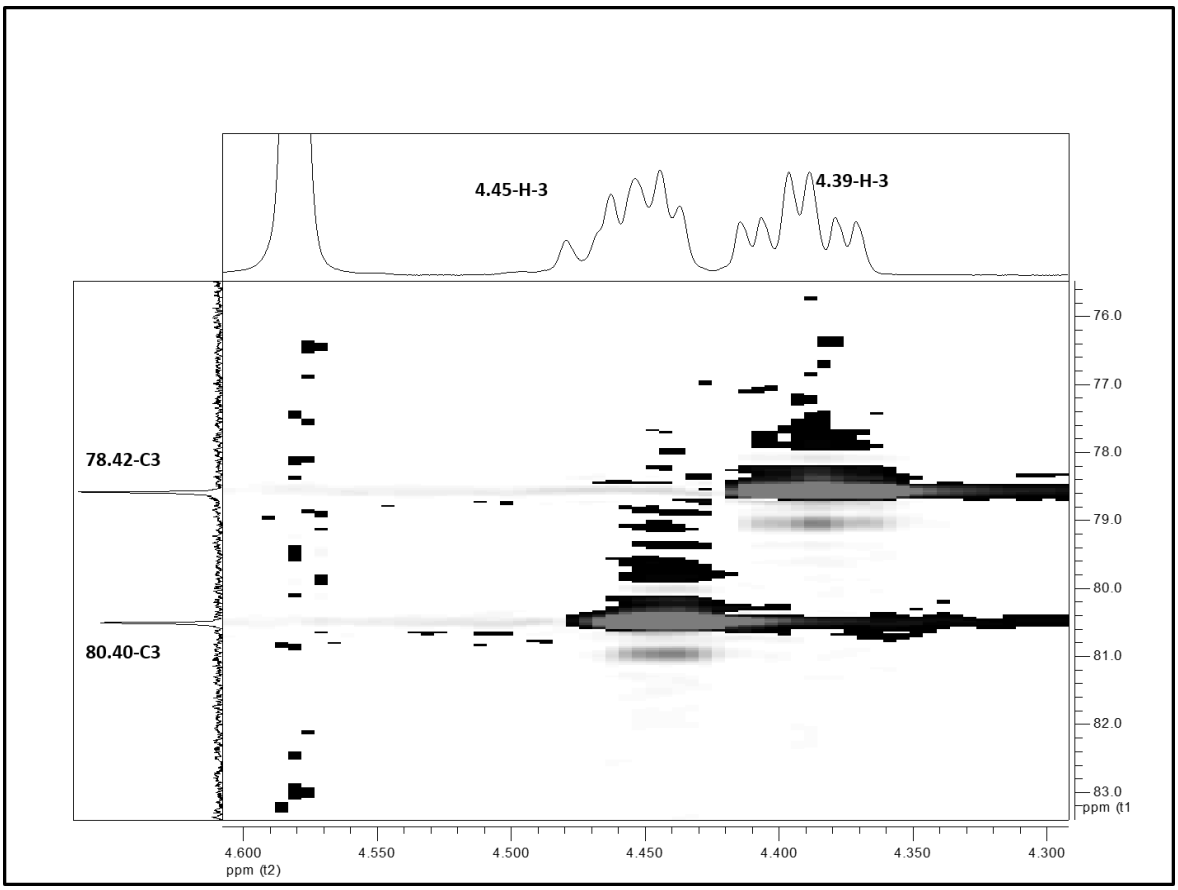

Figure 2-61. HSQC spectrum at 600 MHz confirms the single quantum correlation of two ester bonds at δ 78.42-80.40 with protons at δ 4.39-4.45, whose resonances could correspond to ester bonds between C-3 of ß-violaxanthin and C-1 of fatty acids.

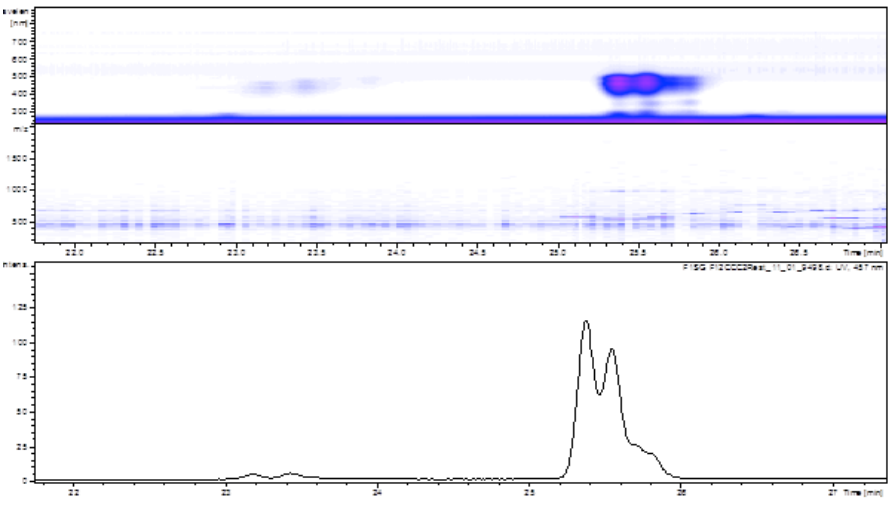

Figure 2-62. HPLC–APCI–MS-MS chromatogram (below) and contour-plot of fraction 1 obtained in a normal phase chromatography separation from the "acetone extract" of Baby Banana peels. Two peaks at 25.4 and 25.5 min in the chromatogram represent two carotenoids in fraction 1 with absorptions between λ 400- 500 nm.

The mass spectrum in **Figure 2-63** exhibited a quasimolecular ion ($[M+H]^+$) at *m/z* 964 with two daughter peaks at *m/z* 655 and 347 as well as a low intensity peak at *m/z* 645.6 $[M-H_2O]^+$. The fragmentation yielded a base peak at *m/z* 347.1 which represents two lauric acids (12:0) at *m/z* 182.5 $[M-H_2O]$. The second most abundant fragment ion at *m/z* 655.3 $[M+ H_2O]^+$ depicted the cleavage of the 15, 15' carbon-carbon bond with a loss of a water molecule at *m/z* 290 $[M-H_2O]$. Also, the peak at *m/z* 291 showed the second moiety of the violaxanthin. As a confirmation, the low region of the spectrum showed the molecular mass of violaxanthin at *m/z* 581.3 $[MH-18]^+$ that also could support the linkage of both fragmentation moieties at *m/z* 290. Therefore, the mass spectrum of HPLC-APCI-MS in positive mode indicated the presence of ß-violaxanthin-di-laurate in fraction 1 derived from hyperpigmented Baby Banana peels (van Breemen et al. 2012) **(Figure 2-64).**

In addition, the COSY and NOESY experiments supported the assignments illustrated in **Figure 2-65**.

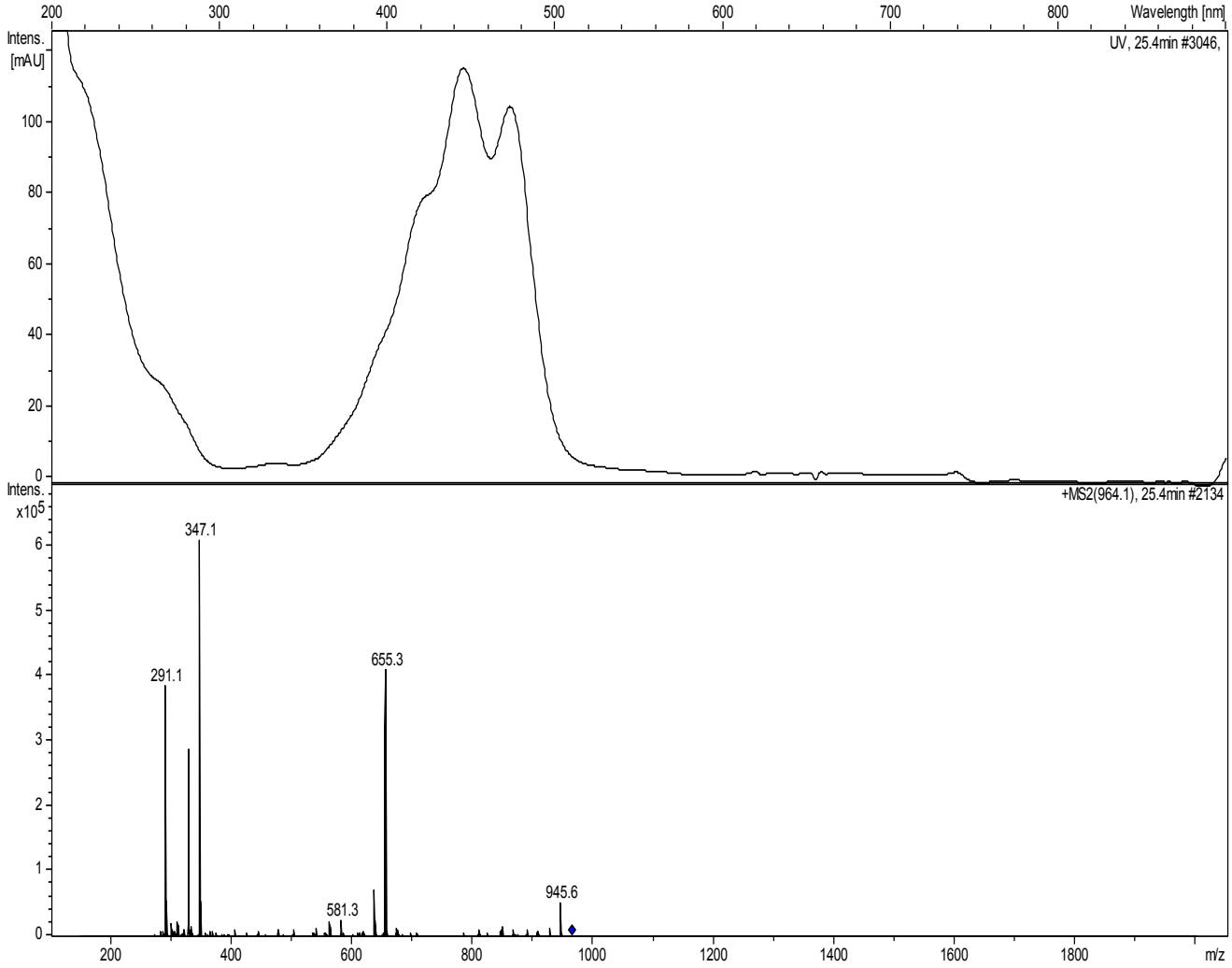

Figure 2-63. UV-spectrum of a violaxanthin-di-laurate recorded on line during the HPLC-APCI analysis by using a photodiode-array detector with three absorption maxima at 422, 446, 472 nm (above) and the mass spectrum with a quasimolecular ion at *m/z* 964 $[M+H]^+$ (below), in fraction 1, from acetone extract of Baby Banana peels with hyperpigmentation (van Breemen et al. 2012; Kohler 1995).

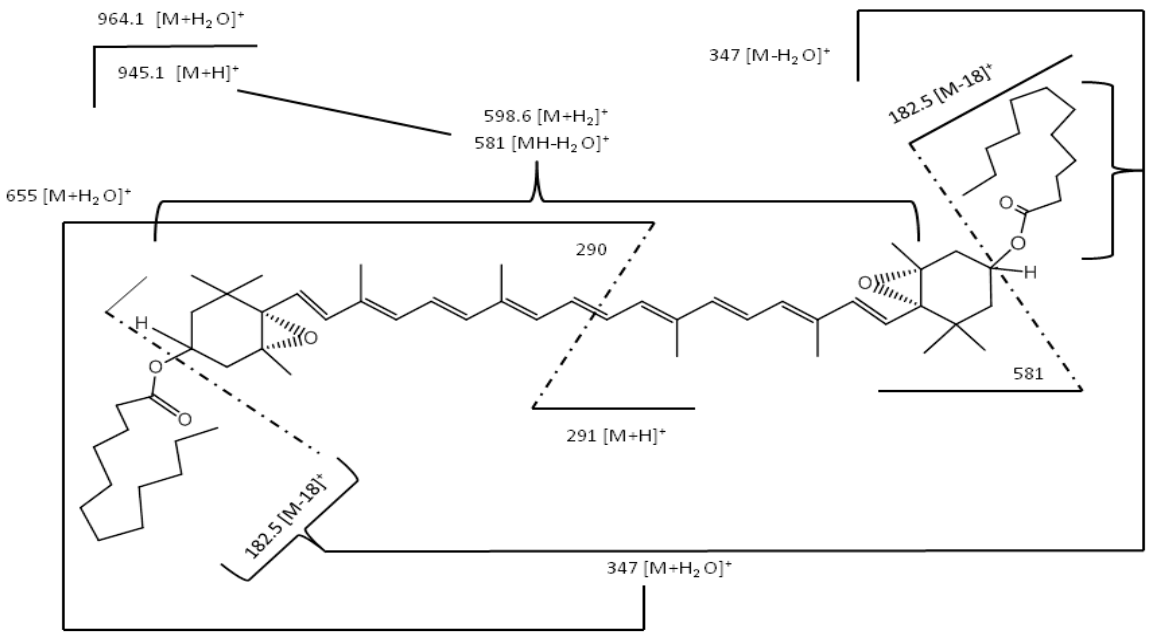

Figure 2-64. Positive ion APCI mass spectra of violaxanthin-di-laurate (C 12:0, C 12:0) and the pattern of fragmentation. The data was in concordance with the literature (van Breemen et al. 2012; Breithaupt 2004; Schweiggert et al. 2005).

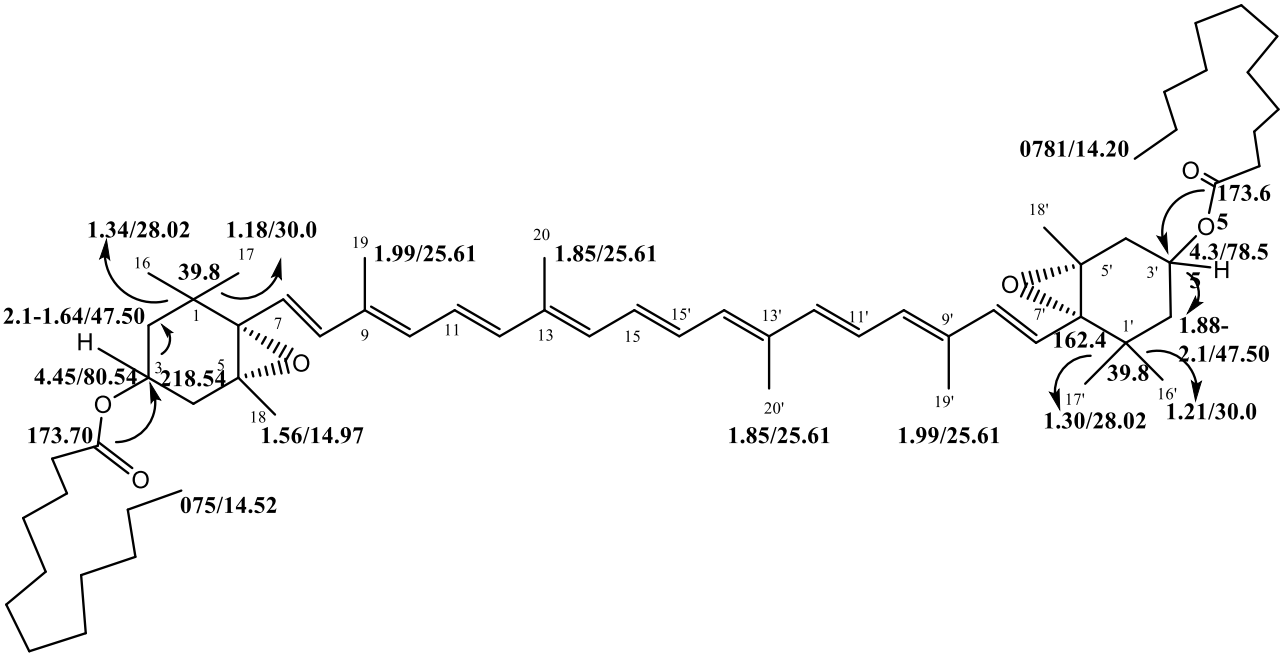

Figure 2-65. Relevant long-range HC-correlation in the HMBC, HSQC and COSY of (3*S*, 3 *S')*-violaxanthin-di-laurate (C 12:0;C 12:0) elucidated in fraction 1 and obtained by means of a normal phase chromatography from acetone extract of Baby Banana peels with hyperpigmentation. The data was in agreement with the literature (Englert et al. 1977).

The assignment of the isoprenoid chain between C-8 and C-8’ was not defined because of the overlap and low intensity of the olefinic carbons which belong to both of the carotenoids in fraction 1. Likewise, the occurrence of high intensity signals in ^{1}H and ^{13}C NMR spectra which correspond to one triterpenoid compound hindered the complete elucidation of the carotenoids. The APCI-MS shows at *m/z* 423 the occurrence of a triterpenoid without UV absorption in the contour-plot of HPLC-photodiode-array. Nevertheless, it was clearly detected in the 1/D ^{1}H NMR spectra (600 MHz) **(Figure 2-66).**

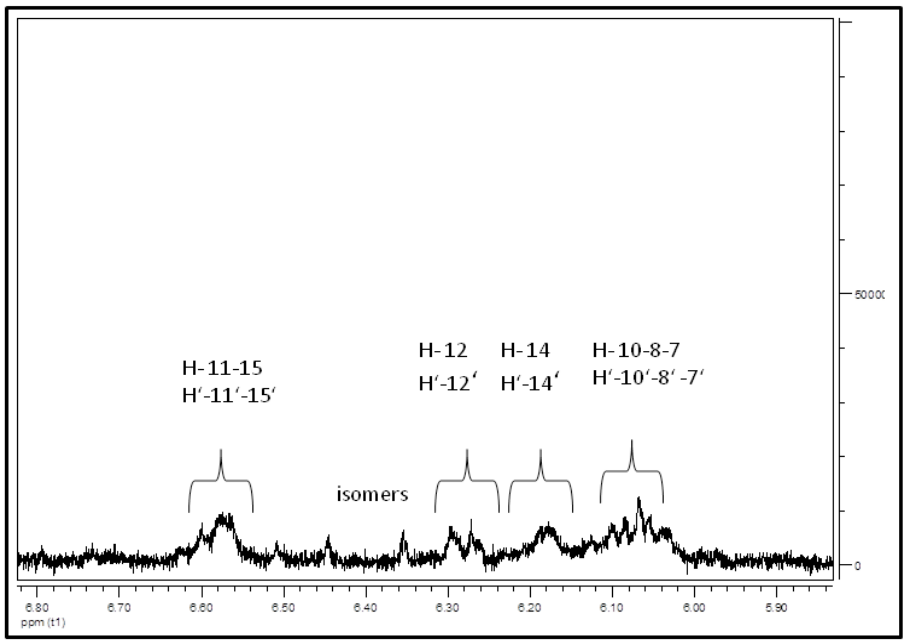

Figure 2-66. ^{1}H spectra at 600 MHz of the olefinic region of the carotenoids in fraction 1. The brakets gather the ^{1}H resonances of each group of protons in the carotenoids according to the position in the isoprenoid chain between H-8 and 8’. The data was in agreement with literature (Molnár et al. 1997; Maoka and Akimoto 2011; Putzbach et al. 2005a; Putzbach et al. 2005b; Strohschein et al. 1997).

Likewise, the isomer cis-neo-ß-carotene was identified by the UV spectra on the basis of four absorption maxima at 335, 420, 443, 473 nm at a retention time of 25.3 min. In addition, the mass spectrum exhibited a quasimolecular ion *m/z* 537 which represents an isomer of ß-carotene, with a fragmentation pathway that showed the most abundant fragment peak at *m/z* 453.2 and represents the loss of methyl-cyclopentadiene [M-85] for cis-neo-ß-carotene. The fragment of *m/z* 413 in the positive mode APCI mass spectrum was formed by a loss of a ß-ionone moiety from the protonated molecule. In the low mass region of the mass spectrum, the fragment ion at *m/z* 256 results from the cleavage 15', 14'-carbon-carbon double bonds. The results were in agreement with the literature data (van Breemen et al. 2012; Gross et al. 1973a; Lacker et al. 1999; Maoka et al. 2002; de Rosso and Mercadante 2007; Lutnaes et al. 2003; Shaw and Apperley 1996) **(Figures 2-67, 2-68).**

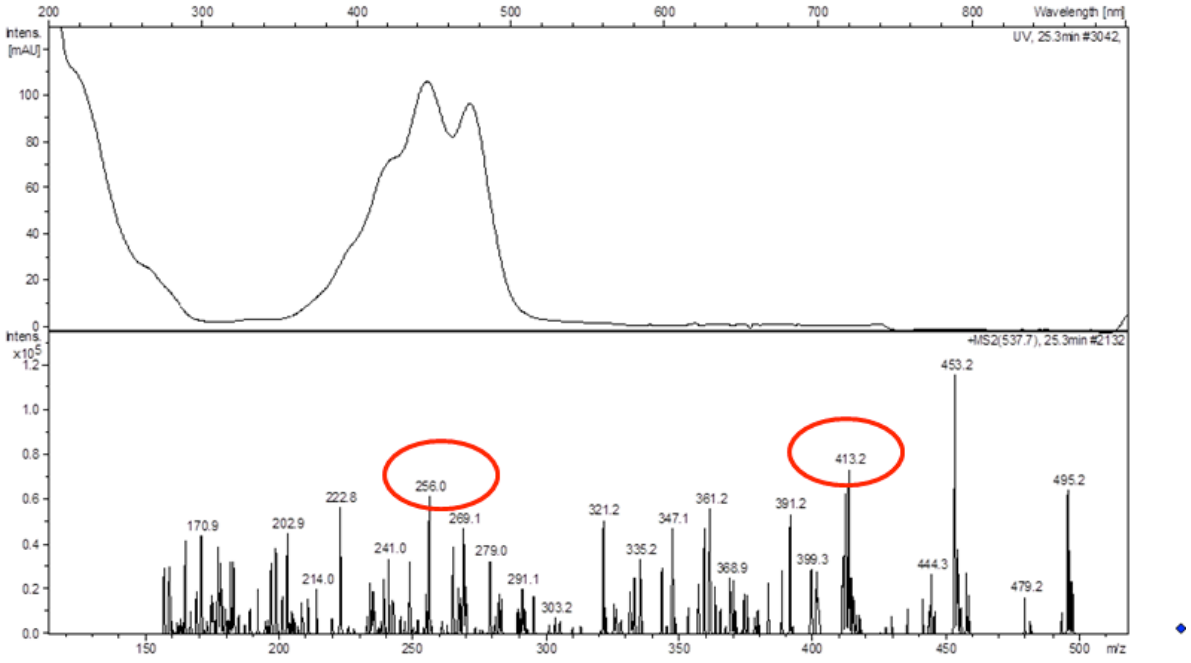

Figure 2-67. UV-spectra of cis-neo-β-carotene recorded on line during the HPLC-APCI analysis by using a photodiode-array detector at 25.3 min with four absorption maxima at 335, 420, 443, 473 nm (above) and mass spectrum with a base peak of *m/z* 537 $[M+H]^+$ (below) in fraction 1 from the acetone extract of Baby Banana peels with hyperpigmentation (Gross et al. 1973a; Lacker et al. 1999; Maoka et al. 2002; de Rosso and Mercadante 2007).

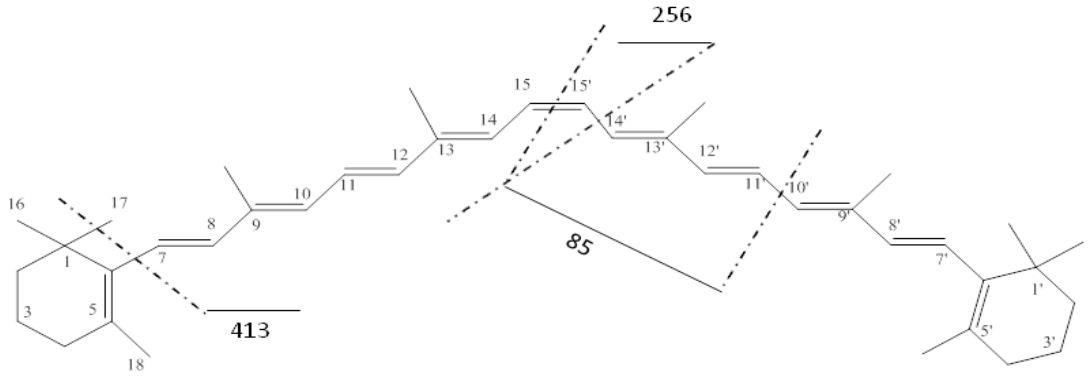

Figure 2-68. Schema of positive ion APCI mass spectral fragmentation of cis-neo–ß-carotene (15-cis) and the pattern of fragments according to literature data (van Breemen et al. 2012; Weller and Breithaupt. 2003; Breithaupt and Schwack 2000; Subagio et al. 1996; Mercadante et al. 1997; Hu et al. 1997; Lacker et al. 1999; Tsukida and Saiki 1982).

In the second peak with a retention time of 25.5 min, corresponding to the second violet board band in the contour-plot, an isomer 15-*cis*-*ß*-carotene was identified by HPLC-APCI-MS analysis **(Figure 2-62).** The photodiode array-UV-visible absorbance depicted a spectrum with three absorption maxima at 335, 448, 475 nm that revealed the characteristic spectrum of the isomer 15-*cis*-*ß*-carotene in concordance with literature data. As additional confirmation, the mass spectrum exhibited a major ion of *m/z* 537 with a fragmentation usual for the ß-carotene (van Breemen et al. 2012; Hu et al. 1997; Lacker et al. 1999) **(Figure 2-69).**

The fragment ion of *m/z* 411.1 in positive APCI mode spectrum of 15-cis ß-carotene was formed by loss of a ß-ionone moiety from the protonated molecule and the fragmentation at the 9, 10 bond produced the ion of *m/z* 176.9. The cleavage of the 15, 15’ bond is represented as the ion *m/z* 251.0 which is a characteristic fragment of carotenoids. The data is in agreement with the literature (van Breemen et al. 2012; Gross et al. 1973a; Lacker et al. 1999; Maoka et al. 2002; de Rosso and Mercadante 2007; Tsukida and Saiki 1982) **(Figure 2-70).**

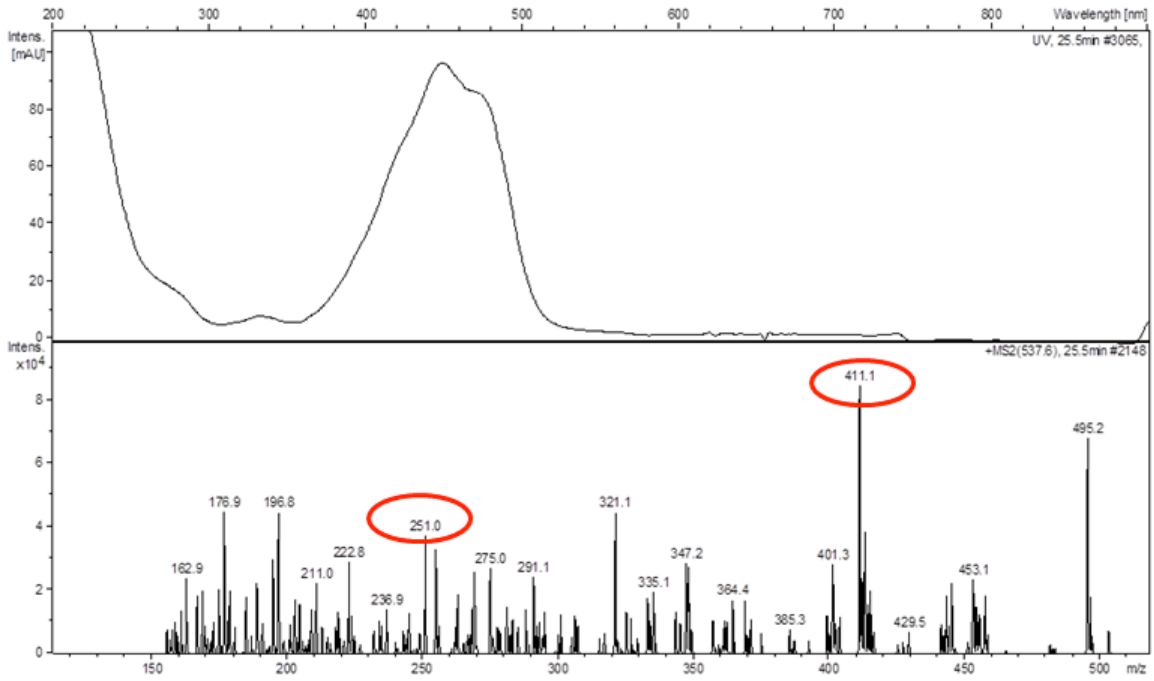

Figure 2-69. UV spectrum of 15-cis ß-carotene recorded on-line during the HPLC-APCI –MS analysis at 25.5 min by using a photodiode-array detector with three maxima at 335, 448, 475 nm (above) and mass spectrum with a base peak of *m/z* 537 [M+H]+ (below) in fraction 1 from the acetone extract of Baby Banana peels with hyperpigmentation (Hu et al. 1997; Lacker et al. 1999).

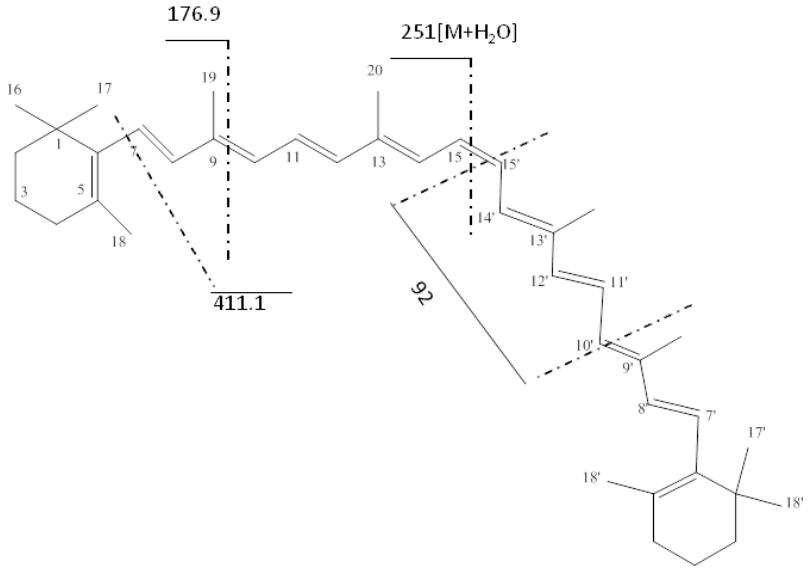

Figure 2-70. Schema of positive ion APCI mass spectral fragmentation of 15-cis ß-carotene and the pattern of fragments according to literature data (van Breemen et al. 2012; Weller and Breithaupt 2003; Breithaupt and Schwack 2000; Subagio et al. 1996; Mercadante et al. 1997; Hu et al. 1997; Lacker et al. 1999; Kohler 1995).

2.1.9.1 Summary

The photosynthetic tissue contain both chlorophylls and carotenoids which are confined to the photosynthetic organelles and they are present in the chloroplasts of higher plant and algae, where they play an important role in relation with the photosynthesis. Although there are minor quantitative and qualitative variations, the major pigment components are always ß-carotene, lutein, violaxanthin and neoxanthin. Quantitative results show that while ß-carotene is always the major carotene, β-carotene occurs sporadically in small amounts. Lutein is always the major xanthophyll present. In essence, the carotenoids in the photosynthetic tissue of higher plants resemble the chlorophylls which exist together as chlorophylls *a* and *b* with no variants. Taxonomically this can mean only that all higher plants are derived from the same common ancestor (Swain 1966; Goodwin 1964).

In flowers and fruit a variability of carotenoids is found which have been studied broadly. Carotenoids in fruits were divided into seven main groups (Goodwin et al. 1964) according to:

- Those which produce insignificant amounts of carotenoids,
- Those which produce the usual chloroplast carotenoids,
- Those in which there is a marked synthesis of the acyclic carotene lycopene,
- Those which produce large amounts of ß-carotene and/or its derivatives such as cryptoxanthin and zeaxanthin,
- Those that synthesize large amounts of epoxides,
- Those that synthesize large amounts of unique pigments such as capsanthin, rubixanthin, rhodoxanthin,
- Those which synthesize mainly poly *cis*-carotenes, such as pro-γ-carotene and prolycopene.

According to the review above, the Baby Banana peels distribution of the carotenoids identified in the current research obey the classification of those

which produce large amounts of ß-carotene and/or its derivatives, such as cryptoxanthin and zeaxanthin.

The carotenoids of the banana (*Musa Cavendish*) pulp and peels were investigated separately without saponification (Gross et al. 1976), and the identification was based on chromatographic and spectrophotometrical properties, chemical test and co-chromatography with pure, authentic pigments. The major pattern of pulp carotenoids is α-carotene (31%), β-carotene (28%) and lutein (33%), which appeared in equal parts of diester, monoester and the free form. In banana pulp it seems that a massive synthesis of β-carotene takes place which may subsequently be transformed into lutein undergoing further esterification. β-Carotene is partially isomerized and oxidized to a much lesser extent. It is noteworthy that a third of the total amount of lutein is still free in the mature fruit and no epoxides of lutein are found. The peel carotenoid concentration was low (5-6µg/g fr.wt). The main discernible pattern in the peel was the following: α-carotene (7%), β-carotene (14%), 3-Hydroxy-α-carotene ester (2%), cryptoxanthin ester (5%), total lutein (56% diester, monoester and free 1:2:1), isolutein, chrysanthemaxanthin, violaxanthin and neoxanthin (2-4%) appearing both free and esterified. The concentration of β-carotene was much lower than in the pulp.

The quantitative changes of carotenoids pattern in the peel of banana during ripening reported that the level of total carotenoids decreased to its half at color break and subsequently again increased in the ripe fruit reaching virtually the initial level of the green fruit. The carotenoids pattern was that of the chloroplast in both unripe and ripe fruit. In the ripe fruit an additional monol fraction in small amounts was detected. During ripening, the main pigments underwent the same concentration changes as those shown in the ripening curve, a mechanism not encountered in other fruit. The xanthophylls underwent gradual esterification. The occurrence of the minimum in the ripening curve as well as the gradual esterification of the xanthophylls may be correlated with ultrastructural changes from chloroplasts into chromoplasts (Gross and Fluegel 1982).

A second study of carotenoids and their fatty-acid esters in Banana peels was reported (Subagio et al. 1996; Subagio et al. 1997). The carotenoids were first separated on an alumina column into five fractions, of which each was further subfractionated by HPLC with different kind of solvents. Only one fraction of the five obtained was analyzed by LC-MS due to the low concentration of carotenoids collected in the fractions. Additionally, the fatty acids from the carotenoids esters were identified by GLC. The carotenoid content of the banana peel was in the range of 3-4 µg per gram as lutein equivalent, and lutein, ß-carotene, β-carotene, violaxanthin, auroxanthin, neoxanthin, isolutein, b-cryptoxanthin and β-cryptoxanthin were identified. The characterization of carotenoids and their fatty-acid esters in banana peels showed that the patterns are quite different from those of carrots and tomatoes in which carotenoids of the β-carotene category are dominant. This suggests that the carotenoid plastid in banana peel is a gerontoplast, which is a kind of chromoplast developed from a chloroplast, whereas those of tomatoes and carrots are real chromoplast. As the chlorophyll is degraded during ripening, the structure of aged chloroplasts resembles chromoplasts.

The amount of oxygenated carotenoids esterified by fatty acid was 38% of the total carotenoids, or more than 51% of total oxygenated carotenoids. The major fatty acids as esterified forms were myristate, laurate, palmitate and caprate. In addition, lutein, as the major oxygenated carotenoid, was presumed to be in the 4:2:1 ration of free lutein, lutein monoester and lutein diester, differing from the 1:2:1 ratio described previously (Gross and Fluegel 1982). The degree of ripening influenced the amount of carotenoid fatty acid esters and the free/ monoester/ diester ratio of lutein. In green bananas, the OH groups of carotenoids were not esterified; in greenish-yellow bananas, half of them were esterified; and in fully yellow bananas almost all OH groups were esterified. During ripening, chloroplast thylakoids membranes were degraded gradually, and released fatty acids. It then seems likely that the oxygenated carotenoids would be gradually esterified by the released fatty acids (Gross et al. 1973ab; Gross et al. 1976; Gross and Fluegel 1982).

Carotenoids in fruits have been extensively studied due to the functional properties and diversity of application in the food industry. Hence, their isolation, identification and quantification will be always a current topic of research nowadays. Certainly, a combination of liquid chromatography/UV-visible absorption spectroscopy by photodiode-array detector (PAD) and atmospheric pressure chemical ionization mass spectrometry (LC-PDA-APCI-MS) is a relevant support when the identification and quantification of carotenoids are performed in fruits and other sources of carotenoids (van Breemen et al. 1996; van Breemen et al. 2012; Maoka et al. 2002; Lacker et al. 1999).

Additionally, a summary of carotenoids in amazonian fruit and carotenoids books have been issued during the last years and this information is an important database for the researcher of carotenoids (Britton et al. 2004; Rodríguez-Amaya 2001; Mercadante et al. 1997, Mercadante et al. 1998, de Rosso and Mercadante 2007).

Carotenoids ester in vegetable and fruits have been reported by Breithaupt and co-workers during the last years and their identification and quantification by LC-APCI-MS are an essential database for analysis of carotenoids ester (Breithaupt and Schwack 2000; Breithaupt and Bamedi 2001; Weller and Breithaupt 2003).

Isolation of carotenoids from spinach and sweet corn by high-speed countercurrent chromatography (HSCCC) were reported by Aman and co-workers reported (*all-E*)-lutein and (*all-E)*-zeaxanthin were characterized by ^{1}H NMR spectroscopy, by LC-APCI-MS in positive ionization mode, and by UV-vis spectroscopy. In addition, neoxanthin, violaxanthin and ß-carotene as well as chlorophylls *a* and *b* were also considered (Aman et al. 2005b).

2.1.10 4-Epi-cycloeucalenone and 4-Epi-cyclomusalenone

Lyophilized banana peel (17.7 g) was extracted 3 times on 3 successive days with *n*-hexane at room temperature to give an extract (4 g). Then preparative High Speed Counter-current chromatography was applied. Hence, 1 g from the total n-hexane phase extract was injected by using a solvent system (*n*-hexane/ MeOH) in a 2:1 mixture of upper and lower phase, in order to yield 13 fractions **(Figure 2-71).**

Preparative HPLC was performed to F7 (15.4 mg) and F10 (32.2 mg) with an isocratic system of 100% MeOH as a result of studying the HPLC-DAD analysis **(cf. 4.2.1.6.3).** Preparative HPLC of fraction F10 yielded three fractions and F3 (3.9 mg) contained two positional isomers 4-epicyloeucalenole and 4-epicyclomusalenone which were identified by NMR spectroscopy **(see Table 2-16).**

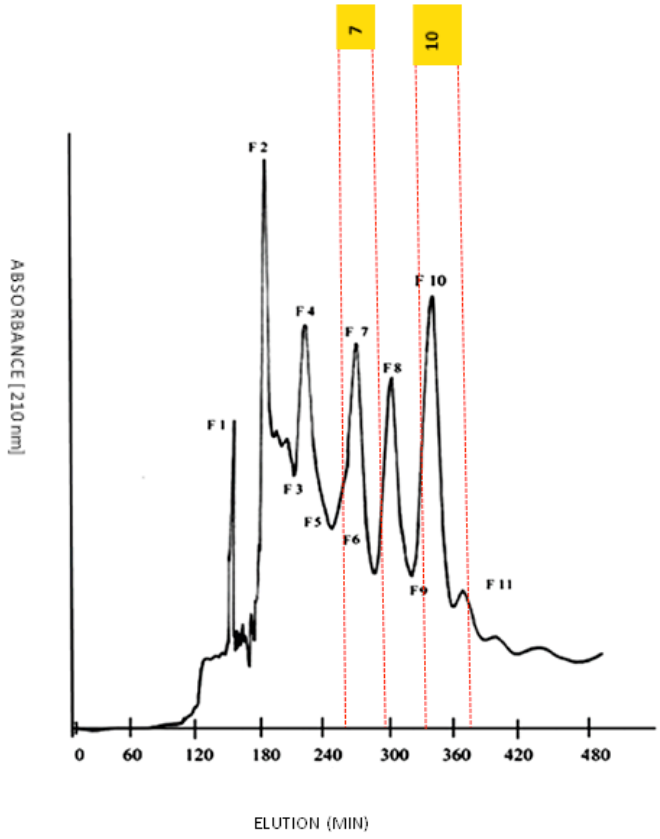

Figure 2-71. HSCCC chromatogram of Baby Banana n-hexane phase extract (1.0 g) in elution mode with a solvent system (n-hexane/MeOH), (2:1). Two positional isomers, 4-epicycloeucalenole and 4-epicyclomusalenone were isolated from fraction 10.

After the separation of fraction 10 by using reversed phase HPLC three fractions were obtained which were monitored and duplicated on TLC silica gel and RP-18. Two violet bands were observed after using anisaldehyde corresponding to silica gel; and two blue color bands were detected corresponding to RP-18 in fraction 3 **(Figure 2-72).**

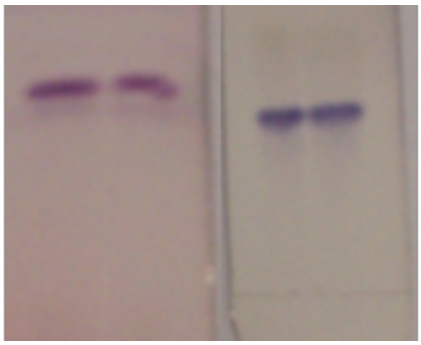

Figure 2-72. TLC plate of silica gel (left) and RP-18 (right) of fraction 3. The bands show the characteristic violet color 10of a triterpenoid on silica gel and blue color on RP-18. The peak contained 3.9 mg of 4-epicyloeucalenole and 4-epicyclomusalenone isomers elucidated by NMR spectroscopy **(cf. 4.3.2).**

The elucidation of a structure with two 3-oxo-28-norcycloartanes in fraction 10 was based on the identification of a quaternary carbon with a ^{13}C chemical shift of δ 213.5 that corresponds to C-3, with additional ^{13}C-DEPT resonances of methyl groups at δ 19.3-10.8-18.1 linked to C-30-29-18, respectively, in the cycloartenol-backbone. The combined use of homonuclear and heteronuclear two dimensional NMR provided support to establish the arrangements of the cycloartenol-backbone, which was elucidated at the same time, with the side-chain relevant fragments of the structure and identified as a cycloartane-type triterpenes **(Figures 2-73, 2-74).** The data was in agreement with those published in the literature (Akihisa et al. 1997).

The occurrence of two ^{1}H signal(s) at δ 4.67 and 4.72, associated with the presence of a double bond in C-24 (1A) and C-25 (1B) as well as the side chain ^{1}H signals (H-21, H-22, H-25 H-26, H-27, H-24) in the ^{1}H, HMBC, HSQC, COSY spectra, confirm the difference between the stereoisomers, whereas those related to the skeleton are agreeing well in both structures **(Figure 2-74; Table 2-16).**

The ^{13}C NMR spectrum **(Table 2-16)** indicated that the structure has thirty carbon atoms in the molecule, including a carbonyl group at δ 213.5 (C-3); four olefinic carbons at δ 156.8 (C-24; CH); δ 150 (C-25; CH); δ 106 (C-28)-(CH_2); δ 109.4 (C-27; CH_2) and complementary, seven methyl groups (Lago et al. 2000). The predominant components in the fraction 10 were elucidated as 4-epicycloeucalenole (1A) and 4-epicyclomusalenone (1B) **(Figures 2-74, 2-73)** (Akihisa et al. 1997).

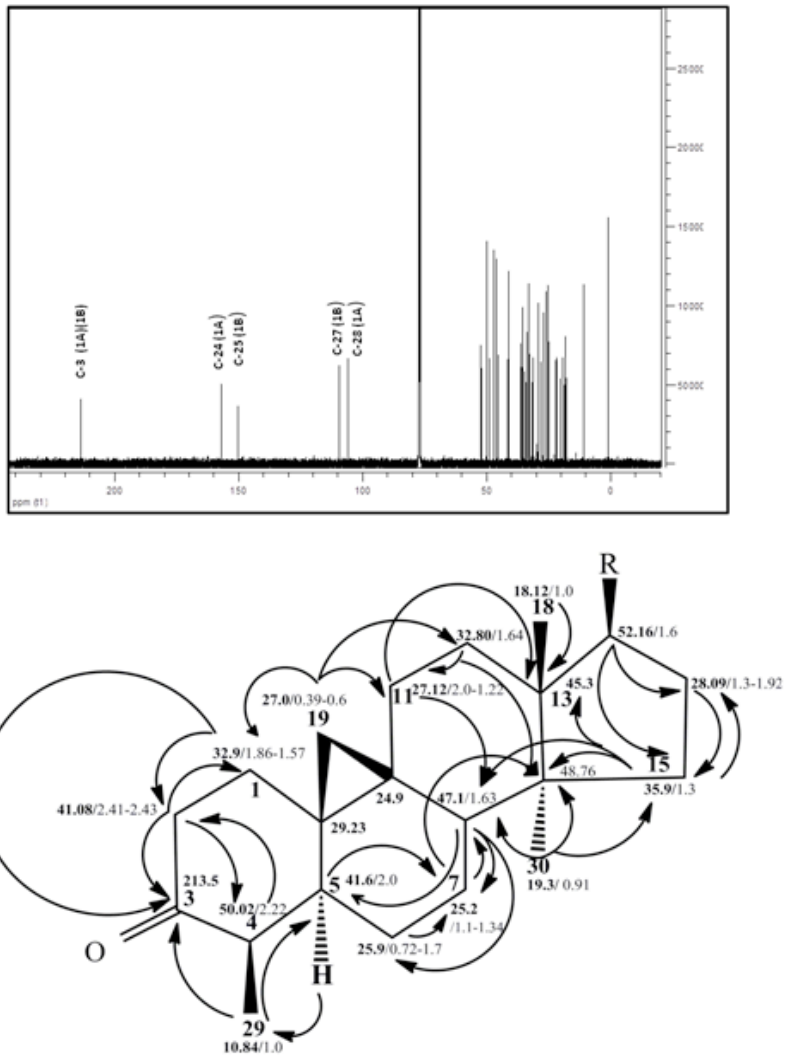

Figure 2-73. ^{13}C NMR spectrum of the isomers 4-epicycloeucalenone and 4-epicyclomusalenone and the identification of side chain relevant double bonds and keto-functions (Above); HSQC and HMBC correlation in the cycloartenol-backbone of isomers 4-epicycloeucalenone and 4-epicyclomusalenone in fraction 10 from Baby Banana peel n-hexane extract fractionated by HSCCC (Below) (Oliveira et al. 2006; Akihisa et al. 1986; Knapp and Nicholas 1969a).

Table 2-16 ^{1}H and ^{13}C NMR data and correlations observed in HSQC for 4-epicycloeucalenole (1A) and 4-epicyclomusalenone (1B) isolated from fraction 10 applying HSCCC separation on Baby Banana peel hexane extract (Akihisa et al. 1997).

Assignment	$\delta^{1}H$ (ppm)		$\delta^{13}C$ (ppm)	
	(1A)	(1B)	(1A)	(1B)
C-1	1.57/1.86		32.9	32.9
C-2	12.41/2.43		41.0	41.0
C-3	---		213.5	213.5
C-4	2.22		50.0	50.0
C-5	2.0		41.9	41.9
C-6	0.72/1.17		25.9	25.9
C-7	1.1/1.34		25.2	25.2
C-8	1.63		47.0	47.0
C-9	---		24.9	24.9
C-10	---		29.3	29.3
C-11	2.0/1.22		27.1	27.1
C-12	1.64 (2H)		32.8	32.8
C-13	---		45.3	45.3
C-14	---		48.7	48.7
C-15	1.3 (H)		35.9	35.9
C-16	1.3/1.92		28.0	28.0
C-17	1.6		52.1	52.1
C-18	1.0		18.1	18.1
C-19	0.39/0.6		27.0	27.0
C-20	1.4 *J*= 6.5		36.0	36.0
C-21	**0.9**	**0.87**	18.3	18.3
C-22	**1.56/1.13**	**1.3/0.94**	35.3	33.9
C-23	**1.9/2.17**	**1.15/1.43**	31.2	31.2
C-24	**---**	**2.1**	**156.8**	**41.6**
C-25	**0.9**	**---**	**33.9**	**150.0**
C-26	**2.23**	**1.64**	**21.9**	**18.5**
C-27	**1.03**	**4.65/4.7**	**22.0**	**109. 4**
C-28	**4.67/4.72**	**1.0**	**106.0**	**20.2**
C-29	**1.0**	**1.0**	**10.8**	**10.8**
C-30	**0.91 (*s*)**	**0.91 (*s*)**	**19.3**	**19.3**

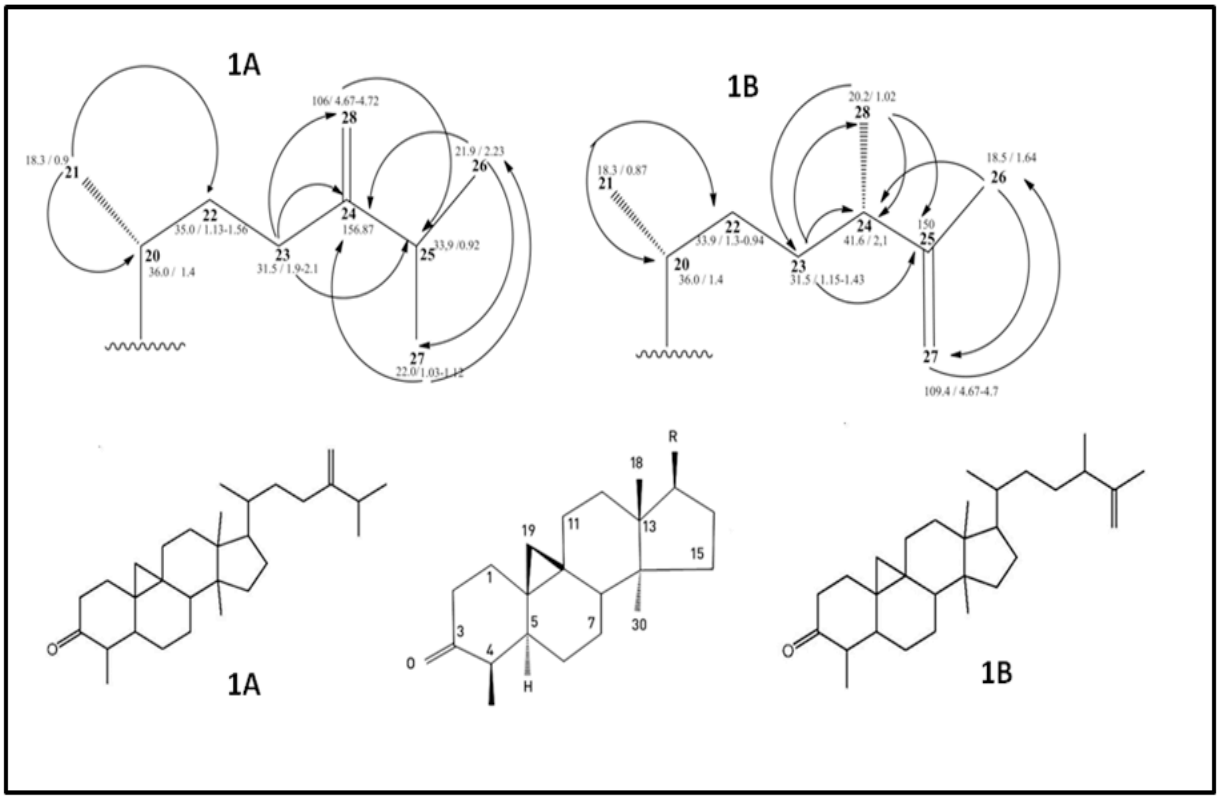

Figure 2-74. Relevant structure $^{2\text{-}3}J$-CH long–range correlation (HMBC) and (HSQC) in the side chains of 4-epi-cycloeucalenole (1A) and 4-epicyclomusalenone (1B, above). Cycloartenol-backbone (below, middle) and isomers of the 4-epi-cycloeucalenole (1A) and 4-epicyclomusalenone (1B, below) isolated from fraction 10 of a hexane extract from Baby Banana peels (Oliveira et al. 2006; Akihisa et al. 1986; Knapp and Nicholas 1969b).

The resulting purified fraction showed under LC-APCI-MS conditions **(cf. 4.2.2)** a single peak in the chromatogram at 20.7 min which corresponds to a quasimolecular ion at $[M+H]^+$ *m/z* 425, accompanied by two fragments at *m/z* 341.3 $[M^+\text{-}C_6H_{13}]$ and 219.3 $[M^+\text{-}C_9H_{14}]$ **(Figure 2-75)**. As additional information, the pattern of fragmentation is depicted in the schema of positive APCI-MS-MS spectrum in order to support the identification of 3-oxo-28-norcycloartane-type triterpenes (Akihisa et al. 1997) **(Figure 2-76).**

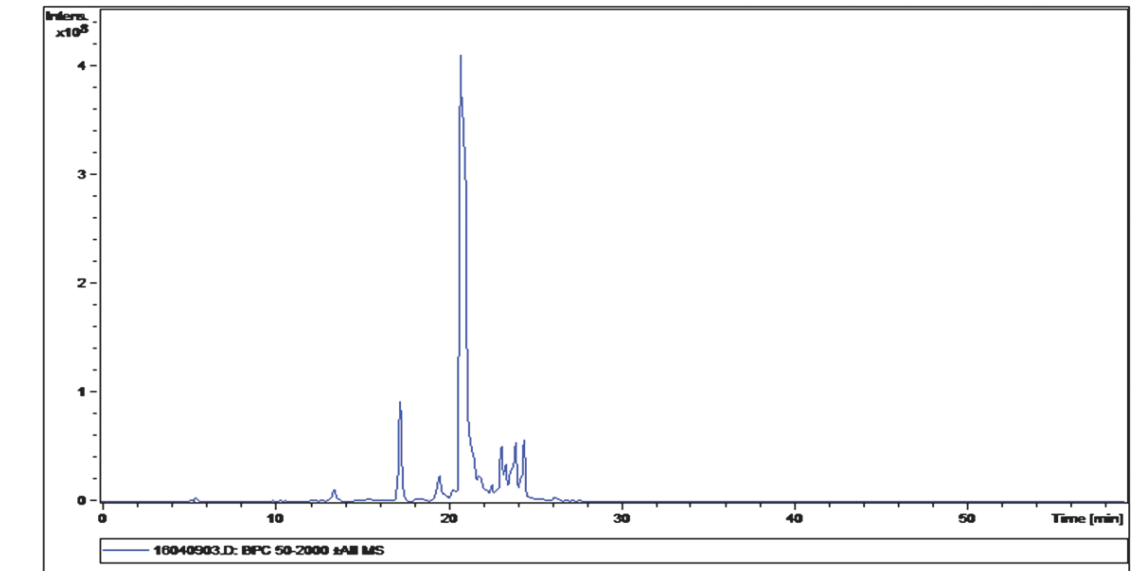

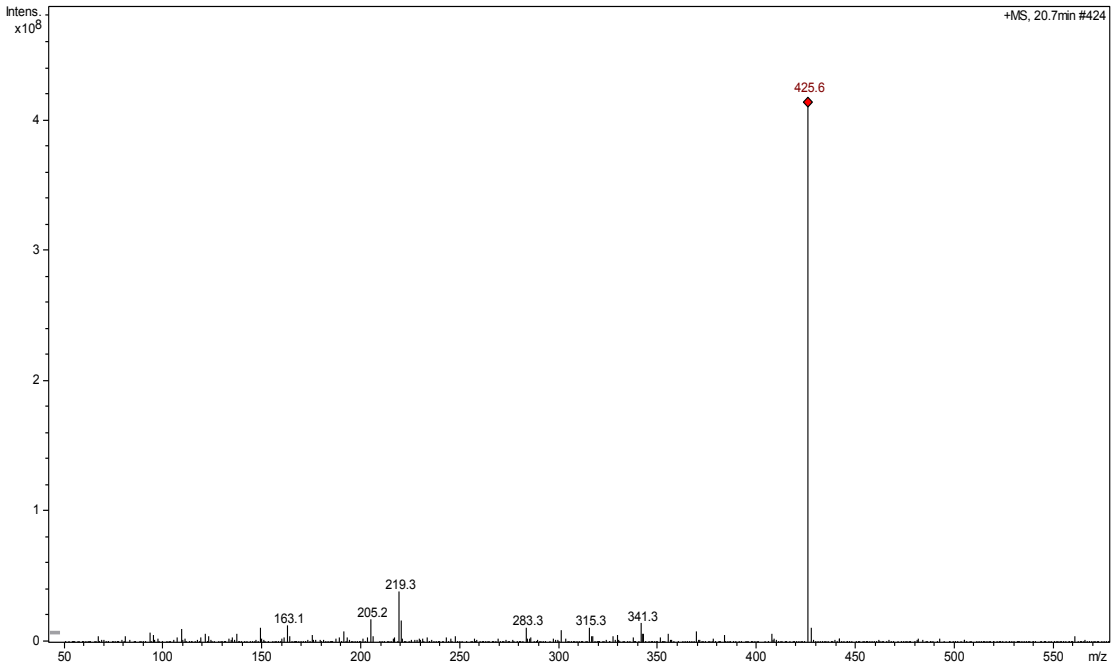

Figure 2-75. APCI-MS spectra of 3-oxo-28-norcycloartane-type triterpenes with their 4-β-methyl-epimers which confirm the structure of 4-epi-cycloeucalenole and 4-epicyclomusalenone isolated in fraction 10 from a hexane extract of Baby Banana peels.

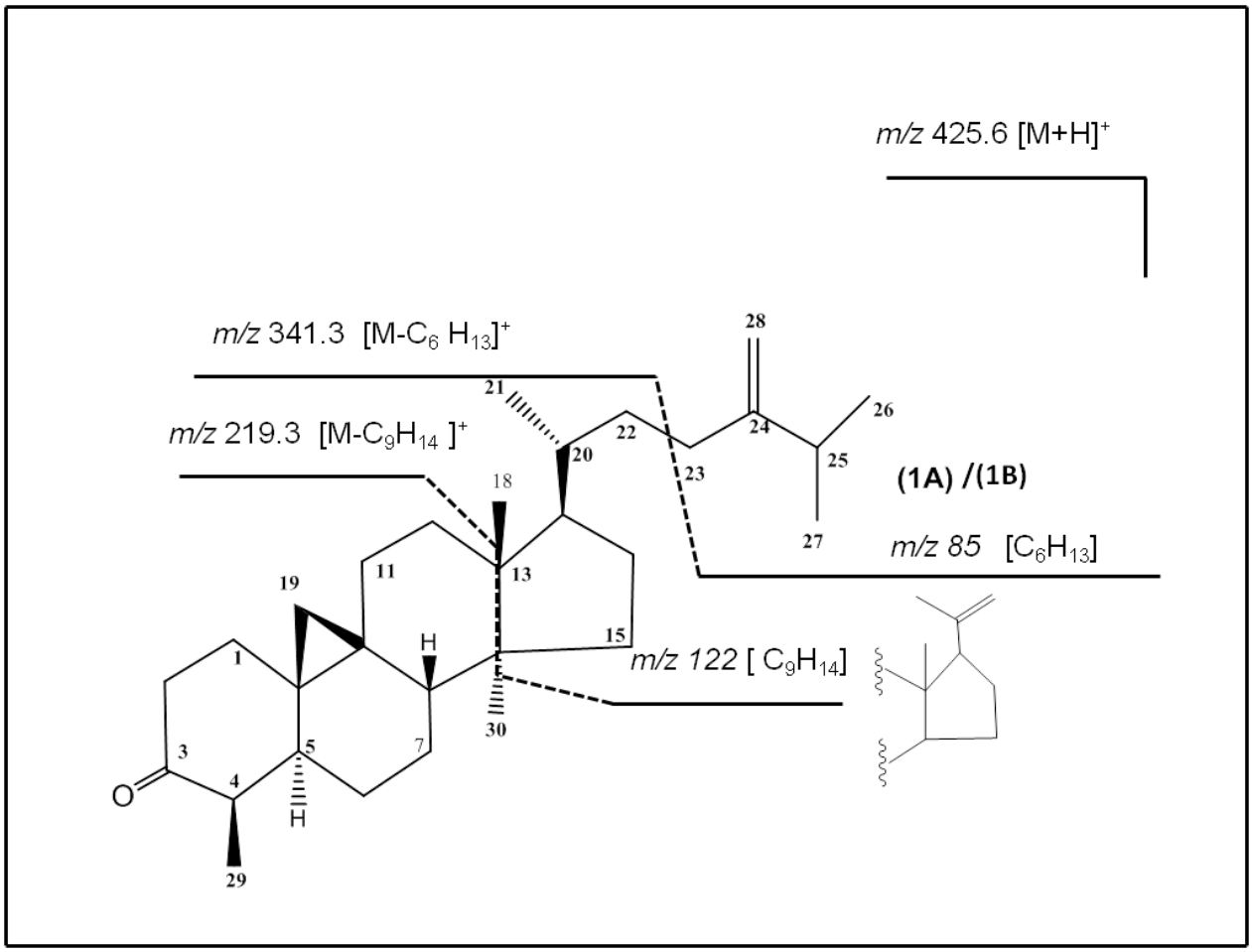

Figure 2-76. Schema of positive ion APCI-MS fragmentation of 3-oxo-28-norcycloartane-type triterpenes with their 4-β-methyl-epimers which confirm the structure of the 4-epi-cycloeucalenole and 4-epicyclomusalenone (Akihisa et al. 1997).

2.1.11 ß-Sitosterol

Fraction 7 (15.4 g) was obtained from the HSCCC separation of a *n*-hexane extract from Baby Banana peels. 1 g was purified with preparative reversed phase HPLC by using an isocratic system (MeOH 100%, flow rate 6 mL/min, Phenomemex Luna column (5µ, 250 x 10 cm). The separation yielded 13 fractions which were monitored by RP-18 with 100% MeOH **(cf. 4.2.1.7.2).** Two fractions (5 and 6) showed a blue band when the plate was developed with anisaldehyde reagent. Consequently, the 2.0 mg recollected from the fractions 5 and 6 were submitted to 1/D and 2/D NMR experiments **(Figure 2-77).**

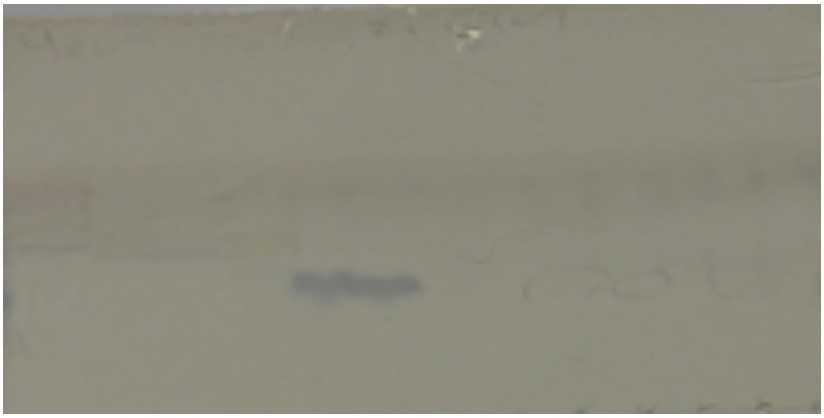

Figure 2-77. RP-18 TLC screening under white light and developed with anisaldehyde from the fractionation of HSCCC fraction 7 (15.4 g). The blue band in TLC showed that fraction 5 and 6 contained 2 mg of a pure compound which was submitted to 1/D and 2/D NMR experiments.

According to 1/D and 2/D NMR experiments, ß-sitosterol was detected in fraction 7 and the assignments were summarized in **Table 2-17.** The application of HSQC and HMBC experiments supported the presence of six methyl groups (C-29, 27-26-21-19-18) together with ^{13}C resonance at δ 71.7, that depicted the hydroxyl group with the characteristic ^{1}H signal at δ 3.53. The presence of both an olefinic chemical shift at δ 121.6/5.34 and a quaternary carbon at δ 140.7 enabled to conclude that the steroid in the fraction corresponded to Δ^5-3 hydroxyandrosterone. The COSY experiment established significant and relevant information in order to elucidate the side chain of the structure between the methyl, methines and methylenes groups which confirmed the structure **(Figure 2-78).**

Table 2-17. ^{1}H and ^{13}C spectroscopic data of ß-sitosterol elucidated in fraction 7 (Sohn et al. 2009; Seo et al. 1986; Kovganko et al. 1999).

Assignment	$\delta^{13}C$ (ppm)	$\delta^{1}H$ (ppm)
C-1	37.2	1.84-1.0
C-2	31.6	1.85-1.5
C-3	71.7	3.53(*m*)
C-4	42.2	2.22- 2.29
C-5	140.7	---
C-6	121.6	5.34(*m*)
C-7	31.8	1.98-1.53
C-8	31.9	1.24
C-9	50.0	0.92
C-10	36.5	---
C-11	21.0	1.48-1.44
C-12	39.74	1.14-2.0
C-13	42.2	---
C-14	56.6	0.98 (*dd*) *J*=2.1 *J*=6.3
C-15	24.3	1.56-1.05
C-16	28.2	1.24-1.83
C-17	55.9	1.08 (*m*)
C-18	**Met(18)–11.7**	**0.67(*s*)3H**
C-19	**Met(19)–19.4**	**1.01(*s*)3H**
C-20	36.1	1.34
C-21	**Met(21)–18.7**	**0.92(*d*) J=6.6**
C-22	33.8	1.0 /1.3
C-23	26.0	1.14 (*m*)
C-24	45.7	0.9 (*d*) J= 6.5 Hz
C-25	29.0	1.21
C-26	**Met(26)19.8**	**0.83(*dd)* (5H)** **J = 2.2, J=7.2**
C-27	**Met(27)–19.0**	**0.80(*d*) J= 6.8 (3H)**
C-28	22.9	1.24-1.19
C-29	**Met(29)-**11.8	**0.84(*m*)**

The analysis of the mass spectrum was done by atmospheric pressure chemical ionization coupled with HPLC.**(cf. 4.2.2.2)** A base peak at *m/z* 397.6 $[M\text{-}CH_3]^+$ at 21.3 min was observed that corresponds to the *m/z* 414 of the ß-sitosterol, with a pattern of fragmentation consistent with steroids. Once it was confirmed in the spectrum that the base peak at *m/z* 397.6 $[M\text{-}CH_3]^+$ could correspond to a steroid, the fraction was monitored by TLC chromatography and reversed phase HPLC was performed **(Figure 2-79) (cf. 4.3.2.2; 4.2.1.7.2).**

The mass spectrum showed a fragmentation typical for Δ^5-androstene with fragment ions at *m/z* 306.6; 146.3 and 85.4 **(Figure 2-80).** The loss of ring D, when the unsaturation at C-22 of the side chain occurred, yields the fragment ion at *m/z* 306.6 and, consequently, two additional fragments at *m/z* 146.3 and 85 were observed in the spectrum. A second pattern of fragmentation has been suggested in concordance with the spectrum in its upper part in agreement with the characteristic profile of fragmentation for Δ^5-sterol **(Figure 2-81).**

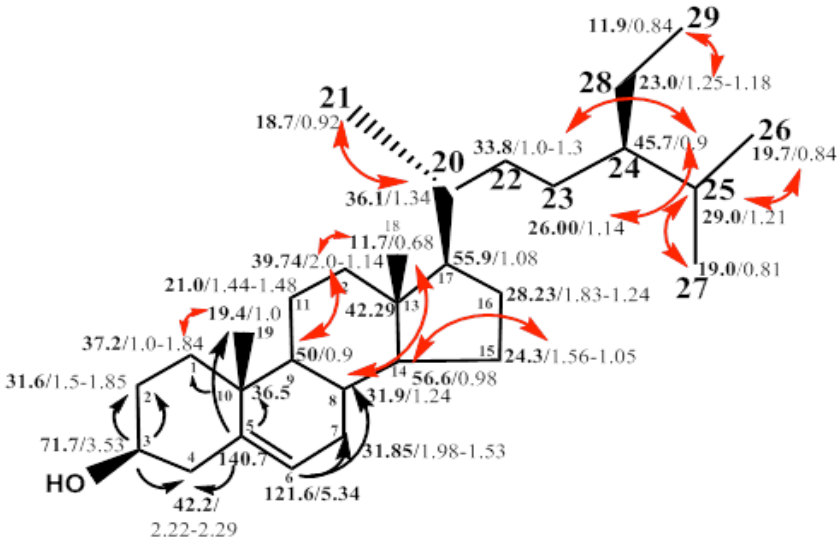

Figure 2-78. Chemical structure of ß-sitosterol according to HSQC, HMBC experiments (black arrows) and relevant COSY correlation both in the side chain and in the steroid skeleton of the structure (red arrows).

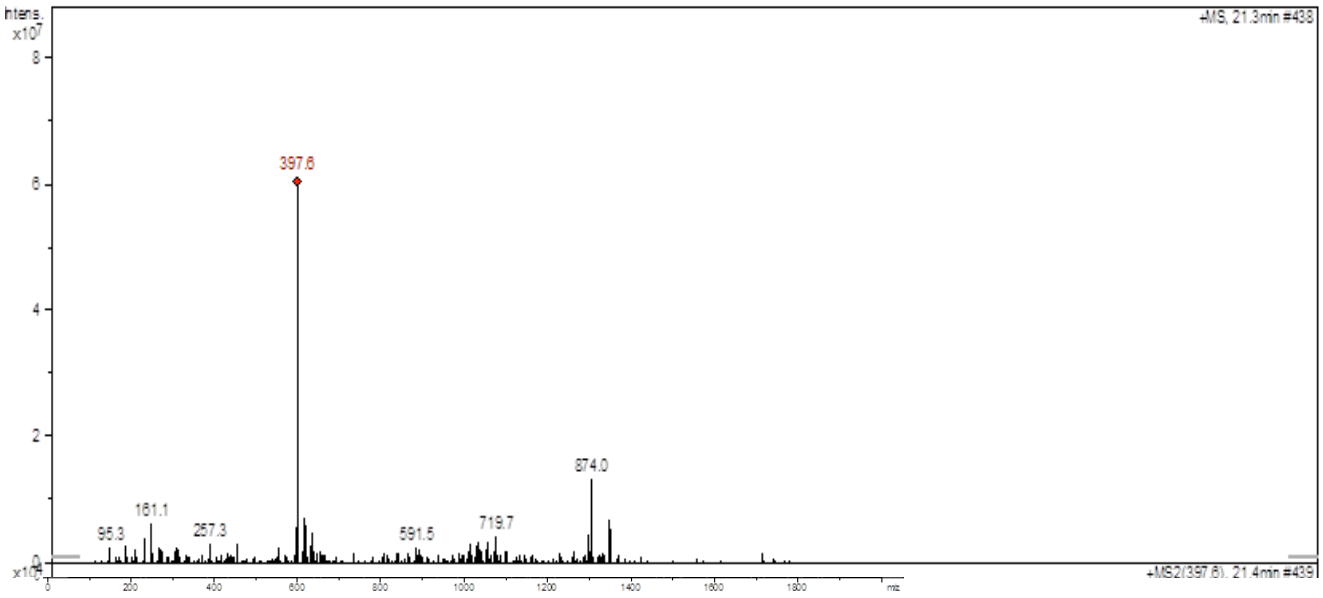

Figure 2-79. APCI spectrum (positive mode) of fraction 7 from HSCCC with ß-sitosterol at *m/z* 397.6 $[M\text{-}CH_3]^+$ together with an impurity of chlorophyll derivatives at *m/z* 874 at 21.4 min.

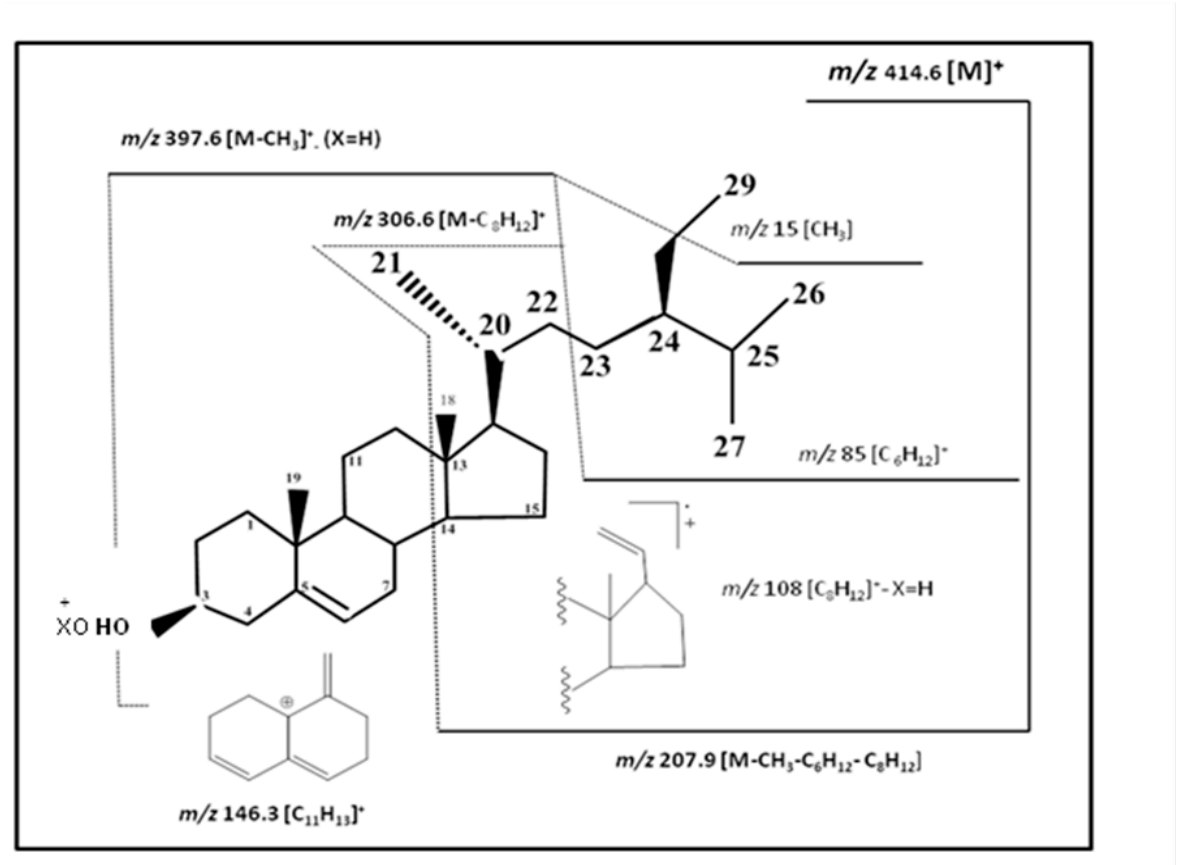

Figure 2-80. Schema of the characteristic fragmentation for Δ^5-sterols according to the APCI mass spectrum shown in Figure 2-79 (Kobayashi et al. 1993; Martinez 2002; Williams et al. 1963)

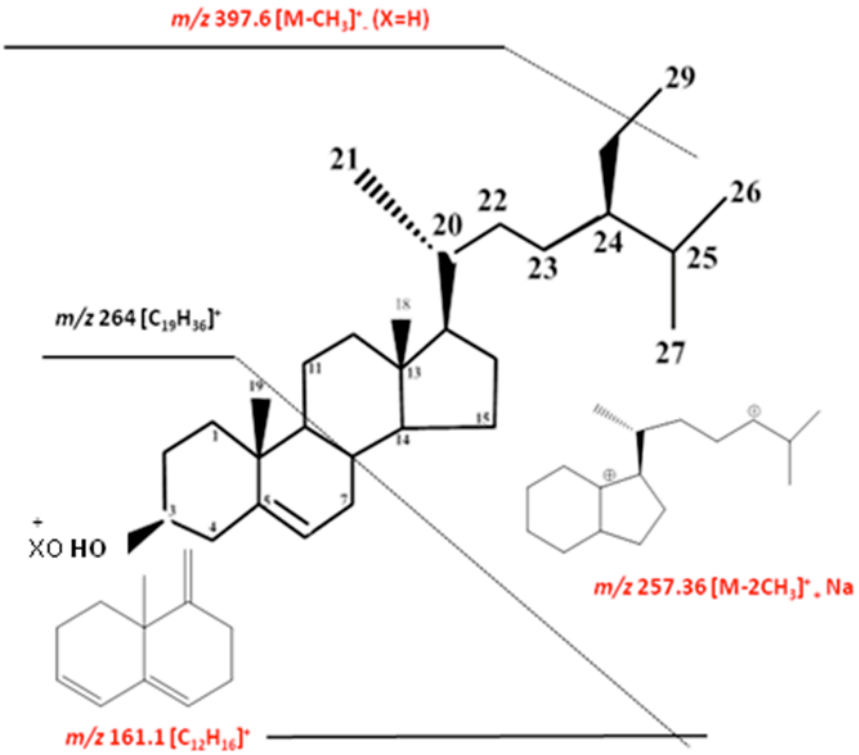

Figure 2-81. Schema of the characteristic pattern of fragments for Δ^5-sterols according to the mass spectrum shown in Figure 2-79 (Kobayashi et al. 1993 and Williams et al. 1963; Martinez 2002;Oliveira et al. 2006*).*

2.1.11.1 Summary

The first studies of sterols and triterpenes in banana peel have been reported by Knapp and Nicholas during the years 1969 and 1971. Sterols and triterpenes were identified as ß-sitosterol, stigmasterol, campesterol, cycloeucalenol, cycloartenol, and 24-methylene cycloartenol. In addition, 24-methylene cycloartenoyl palmitate was identified by gas chromatography (GC) and combined gas chromatography-mass spectrometry (GC-MS).

During the research the biosynthesis of phytosterols in *Musa sapientum* was investigated. Banana peel is a rich source of triterpenes and it was postulated that triterpenes are biosynthetic intermediates of the phytosterols. As experimental procedure, the incubation of banana peel slices with 2-^{14}C-mevalonic acid for varying time intervals represented a means to study the turnover of

squalene, triterpenes, triterpene esters and phytosterols. As conclusion of the studies, the conversion of ß-sitosterol to stigmasterol was reported.

In addition the conversion of cycloeucalenol to the phytosterols was observed after removal of the 4α-methyl group by four steps. These are the opening of cyclopropane ring, isomerization of the double bond, removal of the C-14 methyl group and alkylation at C-24. Therefore, obtusifoliol, 24-methylenelophenol and 24-ethyldienelophenol or similar triterpenes undoubtedly are formed during this series of transformations. Neither mass peaks nor radioactive metabolites with retention times similar to these triterpenes had been detected in banana peels. They do not accumulate in this tissue or if formed during phytosterol biosynthesis in banana peels, they must represent short-lived, enzyme-bound intermediates.

The cycloeucalenyl and 24-methylenecycloartenyl palmitic acid esters were identified and complementary the distribution of radioactivity between the individual esterified triterpenes and free triterpene alcohols was analyzed. As a conclusion, it was demonstrated that the labeling in esterified triterpenes labeled with 2-^{14}C-mevalonic acid was different than the distribution in the free triterpene alcohols. Besides, the triterpene ketone 31-norcyclolaudenone (cyclomusalenone) was isolated from banana peels and it was the first report that supported the occurrence of two isomers together with the cycloeucalenone in banana peels. Thus, the concomitant formation of the alcohol of one isomer and the ketone of the other may reflect some type of biochemical control (Knapp and Nicholas 1969a; Knapp and Nicholas 1970a, 1970b; Knapp and Nicholas 1971a, 1971b).

Two new acyl steryl glycosides, sitoindoside-III and sitoindoside-IV and two new steryl glycosides, sitosterol gentiobioside and sitosterol *myo*-inosityl-ß-D-glucoside were isolated by gradient solvent extraction and extensive chromatography (Column Chromatography (CC), preparative TLC, GC and HPLC) from peeled fruits of *Musa paradisiaca.* The compounds were characterized by IR, ^{1}H NMR and GC mass spectra. Additionally, seasonal variations of the total ster-

ols, free sterols, steryl esters, steryl glycosides and acyl steryl glycosides in the active samples of banana have been analyzed. Anti-ulcerogenic activity of the extracts has been observed (Ghosal, 1985).

Fatty acids and sterols are the major products present in the dichloromethane lipophilic extract of " Dwarf Cavendish" cultivated in Portugal, representing ca. 33-66% and 12-43 %, of the total amount of lipophilic components. By gas chromatography-mass spectrometry the lipophilic extracts from different morphological parts of banana plant, (petioles/ midrib, leaf blades, floral stalk, leaf sheaths and rachis) were analyzed. The five different morphological fractions in study have a similar qualitative chemical composition. Among all the identified compounds, campesterol, stigmasterol, sitosterol, and fatty acids, such as palmitic, stearic, linoleic, linolenic, 22-hydroxydocosanoic, 24-hydroxytetracosanoic and 26-hydroxyhexacosanoic acids, were the major components in all morphological zones. Other compounds, such as aromatic compounds, fatty alcohols and alkanes were also identified. It is remarkable that the fatty alcohols were reported for the first time in the study which represents only a small fraction of the total lipophilic extract (Oliveira et al. 2006).

A triterpene elucidated as 31-norcyclolaudenone from the corm of a wild banana from Philippines (*Musa errans*) was reported and squalene as well as a mixture of stigmasterol and sitosterol were identified by means of HPLC analysis. Also antimicrobial tests were performed and low antimicrobial activity was reported for the triterpenes (Ragasa et al. 2007).

The cycloartane-type triterpene elucidated as 4-epi-cycloeucalenole and 4-epi-cyclomusalenone as well as the ß-sitosterol isolated from the baby banana peels by HSCCC could be used as standards to enable the identification of additional phytosterols in the fractions. According to 1/D NMR spectrum and the HPLC-APCI-MS data more triterpenes and phytosterols occur in the fractions. Moreover, the methanol extract from baby banana peels with hyperpigmentation depicted a major amount of triterpenes than the control.

2.1.12 Pheophytin-*a*

In the search of chlorophylls and derivatives from Baby Banana peels using HSCCC a pheophytin could be identified as a first derivative by means of HPLC-APCI-MS-MS at *m/z* 872. The turquoise color of the pheophytin was observed in those fractions corresponding to elution mode in the first separation of HSCCC from the hexane phase extract of Baby Banana peels using a solvent system Hexane/MeOH [2:1]. The occurrence of derivatives of chlorophylls were confirmed when the fractions were monitored by RP-18-TLC with 100% ACN as mobile phase and the characteristic red fluorescence at 366nm was depicted on the plate. However, the APCI mass spectrum showed that the chlorophylls derivatives were not isolated and, consequently, additional experiments were performed as described below **(Figure 2-82).**

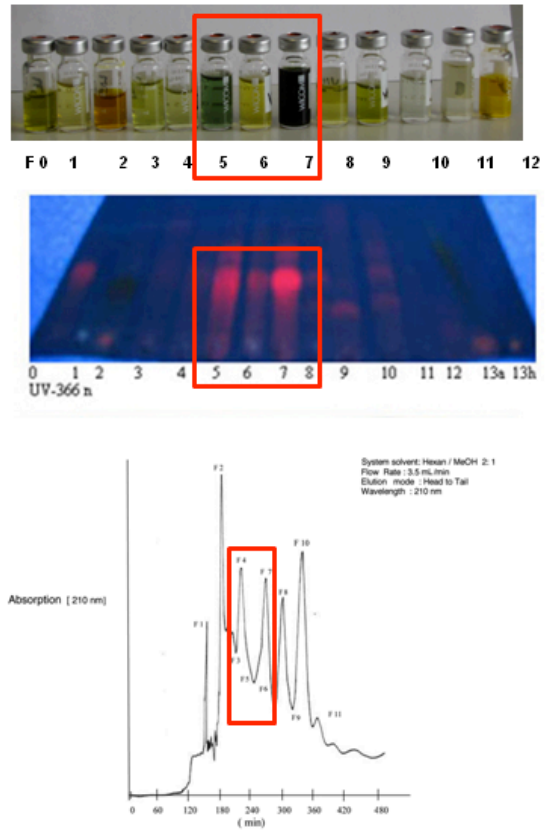

Figure 2-82. First separation from Baby Banana peels by means of HSCCC with a solvent system Hexane/MeOH [2:1] in elution mode. Fractions 5 and 7 showed in elution mode the occurrence of chlorophyll derivatives. Pheophytin a was identified in fraction 7 by means of HPLC-APCI-MS-MS.

A second separation of 1.65 g of the Baby Banana peel extract was performed by changing two parameters, in order to optimize the separation condition. The first condition has relation with the mobile phase which was switched from methanol to acetonitrile (ACN) to accelerate the elution of compounds. The ACN elution coefficient was 0.65 instead of 0.95 in MeOH. Consequently, the elution is faster and the first peak elutes after 40 min instead of 150 min in the case of MeOH.

The second parameter is the application of the extrusion mode after performing the elution mode. This new parameter allowed to fractionate the coil after the elution mode. Thus, elution with hexane forces the separation of the non-polar compounds **(cf. 4.2.3).** The fractions of elution and extrusion modes were recollected and the number of peaks and fractions demonstrated that the extrusion procedure was successful, as the coil volume got fractionated. Subsequently, six fractions in elution and seven fractions in extrusion mode were analyzed by means of HPLC-APCI-MS-MS and monitored by TLC technique. Fraction 1, eluted in extrusion mode, depicted chlorophylls derivatives **(cf. 4.2.2.4; 4.3.2).**

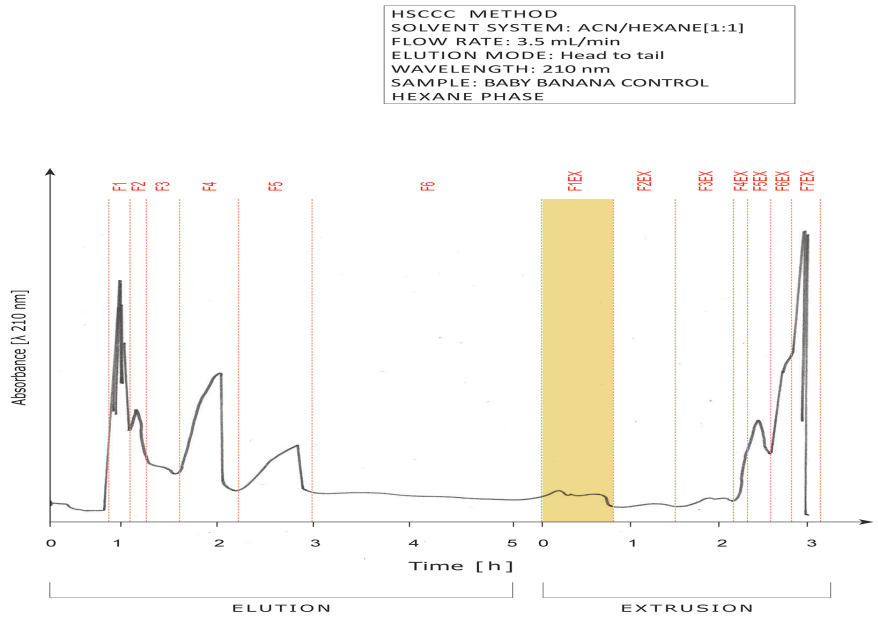

Figure 2-83. Second separation from Baby Banana peels by means of HSCCC with a solvent system ACN/MeOH [1:1] in elution and extrusion mode. Chlorophylls derivatives were identified by HPLC-APCI-MS-MS and TLC technique in fraction 1 of the extrusion mode.

The semipreparative HPLC separation on a RP 18-column was carried out to fractionate 8.8 mg of fraction 1.**(cf. 4.2.1.7.2)** 1.5 mg of purified pheophytin *a* were obtained and the result confirmed by HPLC- APCI-MS-MS at *m/z* 872 $[M+H]^+$ **(Figure 2-84) (cf. 4.2.2.1).**

This amount (1.5 mg) was suitable for the analysis of NMR proton spectra of pheopythin *a* at 600 MHz in CD_2Cl_2 but not enough for ^{13}C NMR and 2/D NMR experiments. The chemical shift and assignments **(Table 18)** and the confirmation of the structure was performed by comparison with previous reports (Smith et al. 1984; Islam et al. 2008; Abraham et al. 1982) **(Figure 2-85)**.

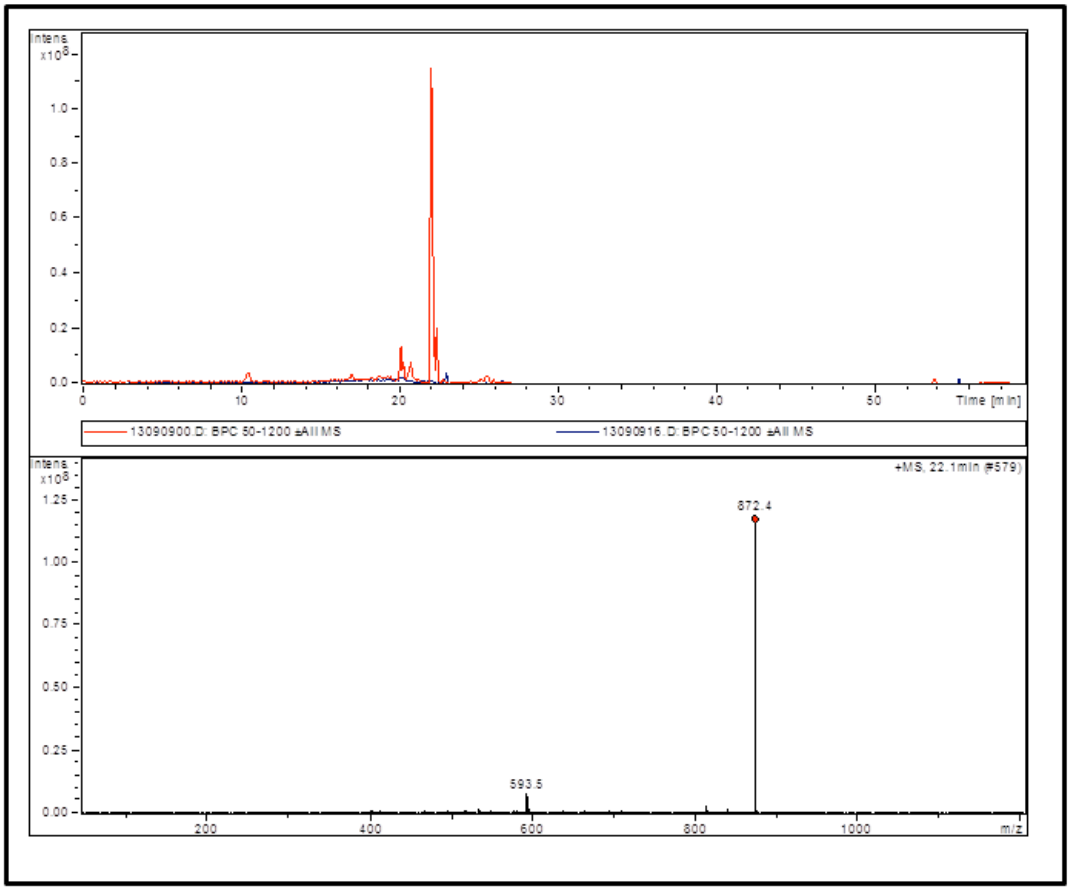

Figure 2-84. APCI mass spectra of 1.5 mg of pheophytin *a* isolated by a preparative RP-18 –HPLC from fraction 1 (extrusion mode of HSCCC). The peak with a retention time of 22.1 min at *m/z* 872 $[M+H]^+$ corresponds to pheophytin *a* in concordance with literature data (Van Breemen et al. 1991a, 1991b; Hyvärinen and Hynninen 1999).

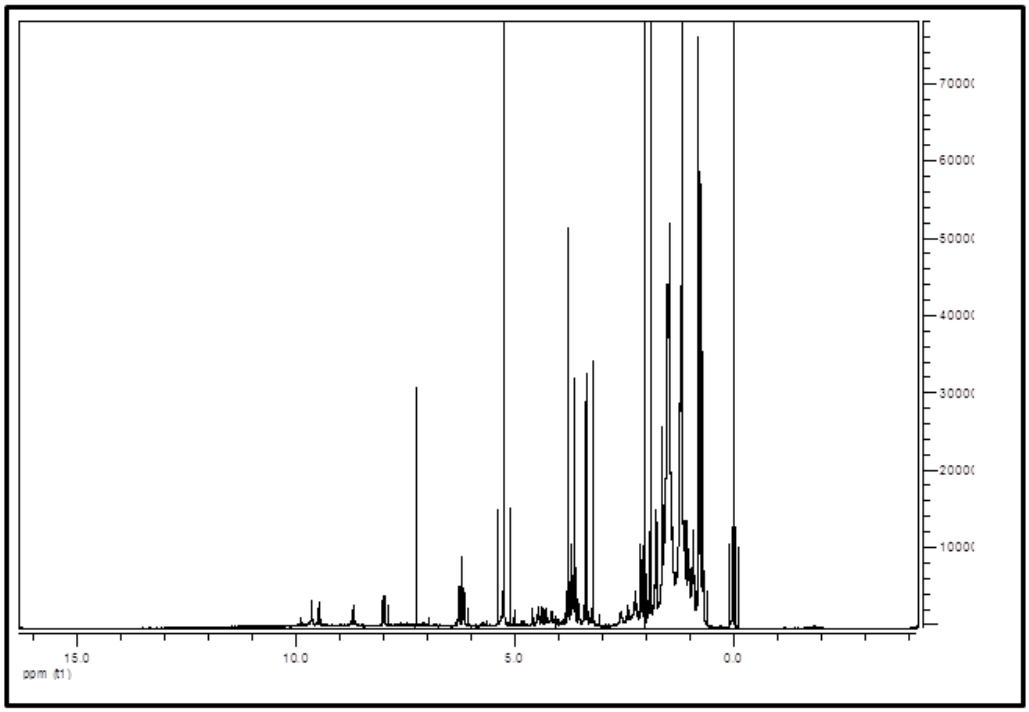

Figure 2-85. 600 MHz proton NMR spectrum of pheophytin *a,* 1.5 mg in CD_2Cl_2 purified from fraction 1 (extrusion mode of HSCCC separation) by means of preparative RP-18-HPLC (Smith et al. 1984).

Table 2-18. Proton chemical shift (δ) of pheophytin a isolated from Baby Banana peels by HSCCC and preparative RP-18 HPLC in concordance with the literature data (Smith et al. 1984).

Proton	**δ ^{1}H (ppm)**
Meso ß	9.71
Meso α	9.39
Meso δ	8.55
Vinyl=CH	8.12
Vinyl H- *t*	6.23
Vinyl H- *c*	6.01
H-10	6.19
H-8	4.56
H-7	4.18
4-CH_2	3.81
10-CO_2Me	3.82
ß 5-Me	3.60
ß 1-Me	3.34
ß 3-Me	3.29
CH_2 H-7_a	2.60
CH_2 H-$7_{a'}$	2.43
CH_2 H-7_b	2.43
CH_2 H-$7_{b'}$	2.04
8- Me	1.77
4b- Me	1.70/4.36
P-1(CH_2)	4.27
P-2(=CH)	5.01
P-3_a(=CM_e)	1.53
P-4(=CCH2)	1.84
P-5/P-15 (CH_2,CH_2)	1.0-1.2
P-7_a, P-11_a	0.85
P-15_a, P-16 (M_e)	0.81/0.79

P: Phytyl

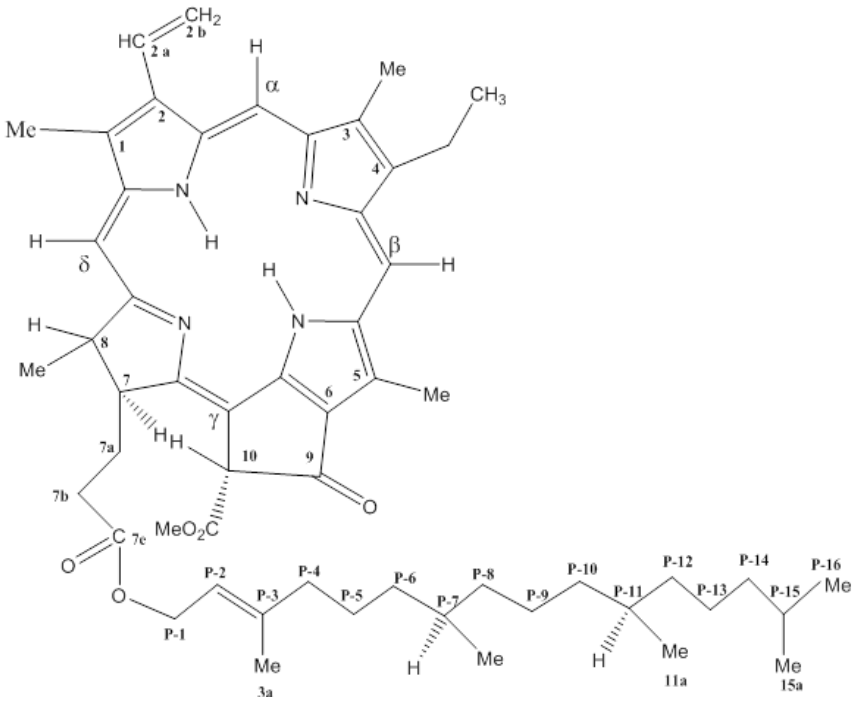

Figure 2-86. Chemical structure of pheophytin *a* according to ^{1}H chemical shift reported in the literature (Smith et al. 1984).

For acquiring a sufficient amount of pheophytin *a* to elaborate the ^{13}C NMR spectra, the methanol extract of Baby Banana peels was studied **(cf. 4.3.1.1; 4.3.4).** It was expected to identify more quantities of chlorophyll and chlorophylls derivatives in this extract. Hence, two HSCCC separations from Baby Banana peels corresponding to a methanol extract, using 1.19 g for the first separation and 604 mg for the second one, were performed. Two chromatograms were obtained with a high level of accuracy and reproducibility. It was possible to recollect from both separations 8 fractions in elution mode and 7 fractions in extrusion mode **(Figure 2-87).**

TLC chromatography and HPLC-APCI–MS-MS identified pheophytin *a* in fraction 6 of extrusion mode, in both of the HSCCC separations. Thus, the quantification of the fractions 6 in extrusion mode yielded 4 mg of pheophytin *a* corresponding to the first HSCCC separation, and 12.34 mg of pheophytin *a* from the second HSCCC separation.

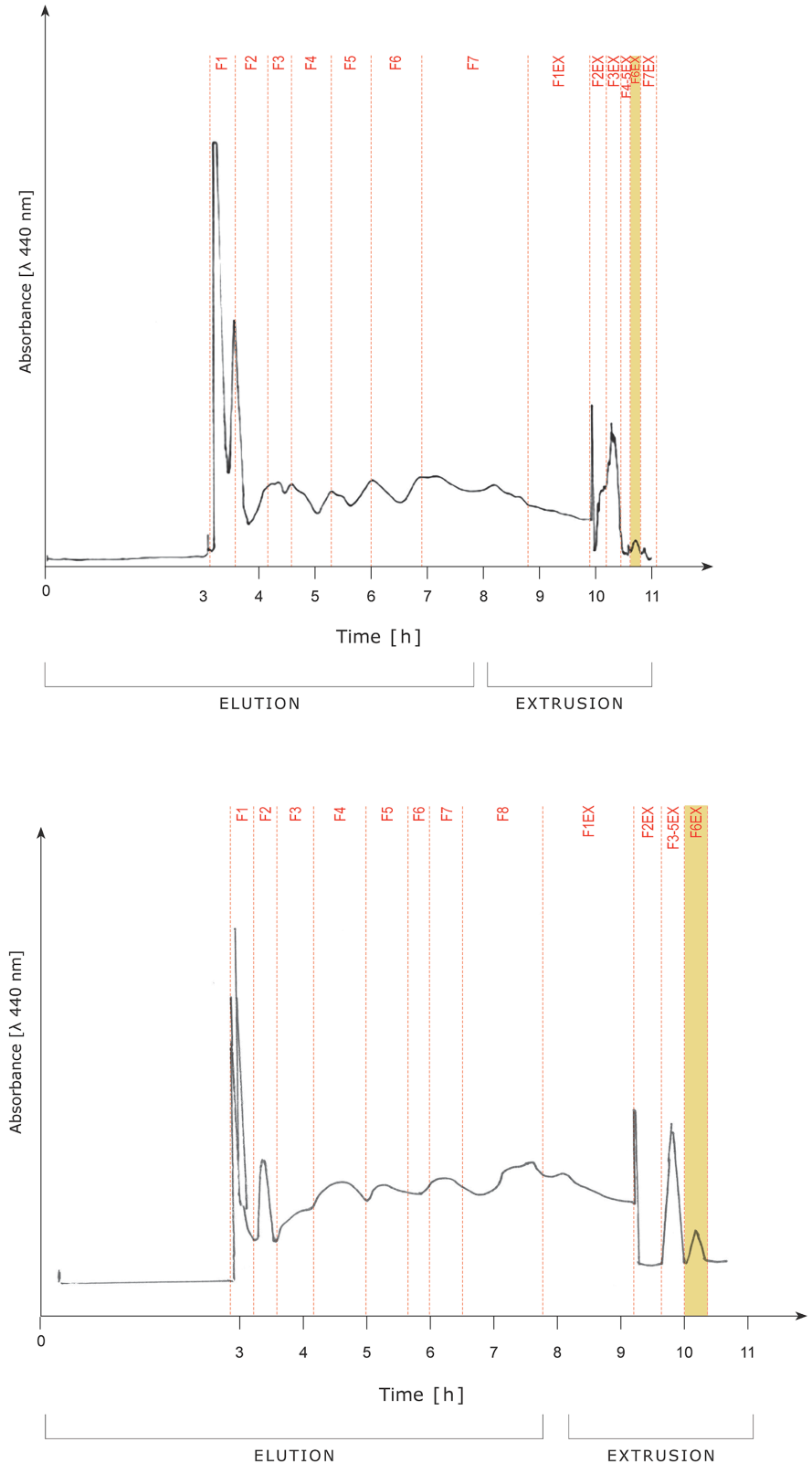

Figure 2-87. HSCCC chromatograms of two separations of a methanol extract of Baby Banana peels using a solvent system of hexane/MeOH/water/EtOAc (10:10:1:1). Fractions 6 in the extrusion mode from both chromatograms were collected to isolate 3.3 mg of pheophytin *a*.

However, pheophytin *a* was detected together with triterpenoids in the 16.34 mg sample recollected from both fractions 6 of extrusion mode by means of TLC chromatography which showed the characteristic band of triterpenoids together with the bands of pheophytins. For this reason, additional separations by normal phase chromatography with silica gel and subsequent HPLC RP-18 preparative separation were necessary **(cf. 4.3.4).**

In this way, it was possible to obtain 3.3 mg of purified pheophytin *a* and 1/D and 2/D NMR experiments were recorded in $CDCl_3$ successfully in order to establish the complete assignment of ^{13}C chemical shifts of pheophytin *a* of Baby Banana peels (Lötjönen and Hynninen 1983) **(Figure 2-88).**

Table 2-19 depicts the ^{13}C chemical shifts of pheophytin *a* purified from Baby Banana peels according to the chemical structure reported in the literature by Lötjönen and Hynninen (1983) **(Figure 2-88).** The HSQC, HMBC and COSY experiments were used as support when assignments showed relevant differences in contrast with the literature data **(Figure 2-89).**

The variation of the ^{1}H NMR data of chlorophyll *a* and pheophytin *a* by differents solvents, e.g. acetone-d_6, methanol-d_4, tetrahydrofuran-d_8 and $CDCl_3$ (Smith et al. 1984) has been reported in the literature. **Figure 2-89** shows the ^{13}C and COSY spectra of the NMR experiment of 3.3 mg of purified pheophytin obtained from a methanol extract of Baby Banana peels.

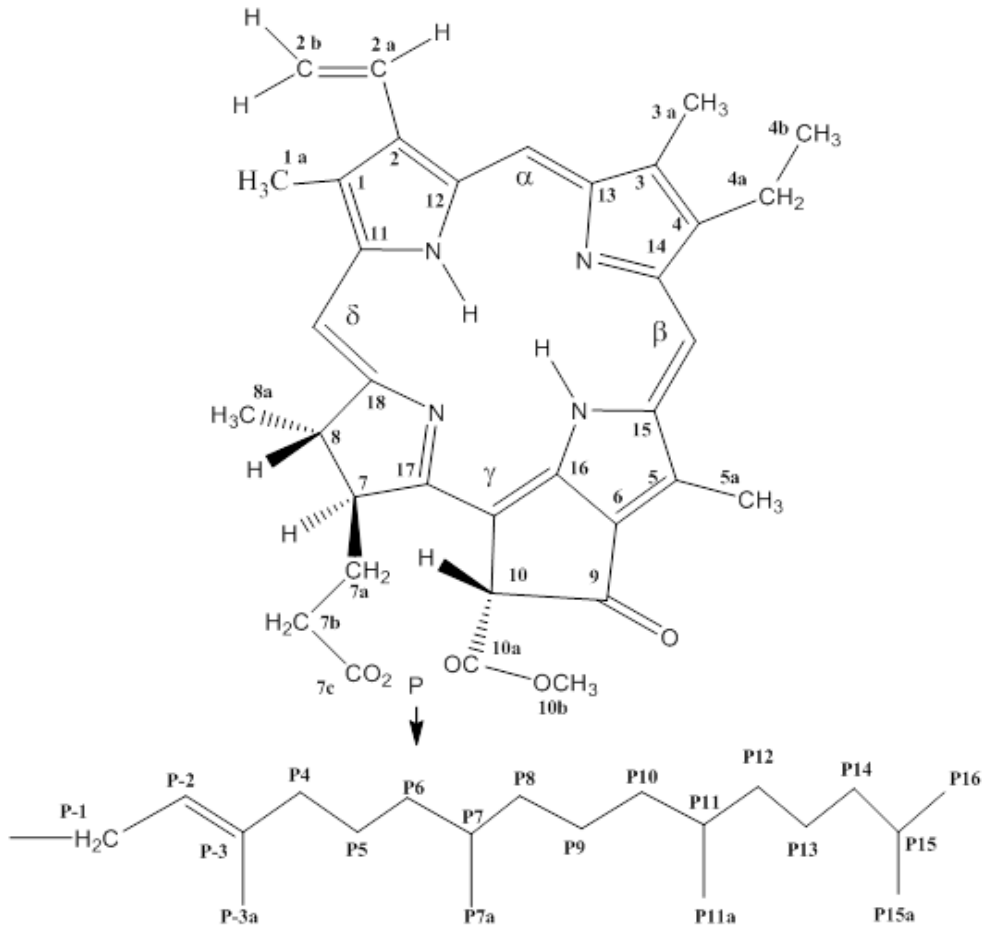

Figure 2-88. Chemical structure of pheophytin *a* isolated from Baby Banana peels (Lötjönen and Hynninen 1983).

Table 2-19. ^{13}C chemical shifts of pheophytin *a* (3.3 mg in $CDCl_3$) from a Baby Banana peels methanol extract (cf. Fig. 2-88).

Carbon	^{13}C chemical shift (ppm)
1	131.8
2	136.2
3	136.1
4	145.2
5	128.9
6	129.0
7	52.86
8	50.08
9	189.6
10	64.6
11	142.0
12	136.5
13	155.6
14	150.9
15	137.9
16	149.9
17	161.2
18	172.2
α	97.5
ß	104.4
γ	105.2
δ	93.9
1a	11.2
2a	129.0
2b	122.8
3a	11.2
4a	19.4
4b	17.4
5a	12.1
7a	31.9
7b	31.1
7c	172.9
8a	23.06
10a	169.6
10b	51.09

Carbon	^{13}C chemical shift (ppm)
P-1	61.4
P-2	177.6
P-3	142.8
P-3a	16.2
P-4	49.9
P-5	24.9
P-6	37.2
P-7	32.7
P-7a	19.7
P-8	37.3
P-9	25.2
P-10	37.3
P-11	33.6
P-11a	19.6
P-12	25.6
P-13	39.33
P-14	39.77
P-15	27.95
P-15a	22.6
P-16	24.4

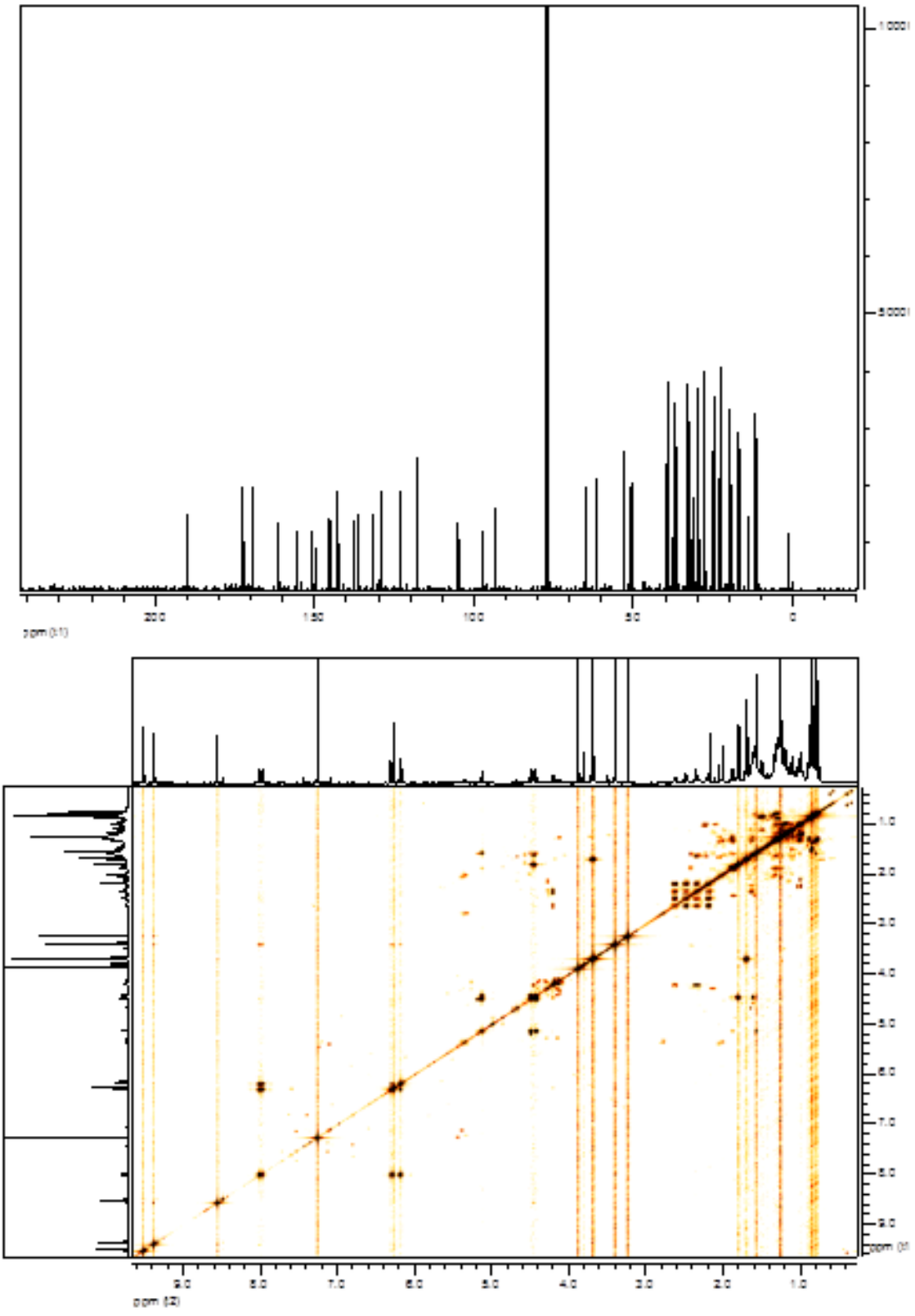

Figure 2-89. ^{13}C NMR (above) and COSY spectra (below) of 3.3 mg of purified pheophytin *a* from Baby Banana peels in $CDCl_3$. The 2/D NMR spectra supported the ^{13}C chemical shift assignments depicted in **Table 2-19.**

2.1.13 Summary

The attempts to isolate chlorophylls by the application of HSCCC with the recurrent result of finding pheophytin as the major derivative of chlorophylls draws some questions: Where are the chlorophylls? Why it is so recurrent to find pheophytin *a* in the extraction samples, when a HSCCC preparative technique was applied? In fact, the finding of pheophytin as major chlorophyll derivative prompted us to closer check the isolation and separation conditions:

- How does the pheophytinization occur and how can it be delayed?

- Can the extraction method play a relevant role in the pheophytinization?

- Is it appropriate to recycle the solvent system already used in the previous HSCCC separation?

- With a sample amount of 1000 mg being injected in the first HSCCC separation and 427.4 mg being recovered in the mobile phase during the elution mode, where is the rest 572.6 mg?

A review of data from the literature on chlorophyll isolation by HSCCC was relevant to test other solvent systems to find answers for these questions. A method for the isolation of chlorophylls from spinach by countercurrent chromatography was developed by Jubert and Bailey (2007) at Oregon State University. Here, chlorophyll *a* and *b* were separated by the application of a solvent system consisting of heptane/ethanol/acetonitrile/water [10:8:1:1]. The confirmation of the chlorophyll purity was carried out by reversed-phase HPLC in comparison with authentic standards monitored with FAB-MS in positive mode.

13^2-hydroxy-(13^2-S)-pheophytin-*a* from leaves and steams of *Amaranthus tricolor* was isolated by HSCCC using a solvent system n-hexane/methanol [2:1]. The structural characterization of pheophytin *a* was performed by 1/D and 2/D experiments and a supplementary ESI-LC-MS mass-spectrometric analysis was applied to confirm the chemical structure (Jerz et al. 2007).

Indeed, not more reported literature in relation with the isolation and characterization of chlorophylls and their derivatives by High Speed Countercurrent Chromatography was found. Moreover, there exist no reports in relation with the characterization of chlorophylls in Baby Banana peels. For these reasons, the circumstances mentioned above forced the huge compromise, in this stage, to find answers by means of new paths. A new chapter was opened in order to establish an experimental design where a variety of factors could indicate the lack of occurring chlorophylls in the Baby Banana peels separation by HSCCC.

This new chapter was defined as the optimization of a solvent system for the separation of chlorophylls and derivatives by means of High Speed Countercurrent Chromatography in Baby Banana peels, spinach and grass.

2.2 Optimization of the solvent system for the separation of chlorophylls and derivatives by means of High-Speed Countercurrent Chromatography in Baby Banana peels, spinach and grass

2.2.1 Experimental Design

In order to study the phenomenon of hyperpigmentation in Baby Banana peels it was assumed that this could be related to the degradation of chlorophylls in the peels during the first stages of ripening. For this reason, it was essential to isolate the chlorophylls and their derivatives by means of HSCCC and thus to analyze the behaviour of the chlorophyll degradation during the postharvest of the fruits in the green stage of ripening.

During the first separations of Baby Banana peel extracts by HSCCC, pheophytin *a* was isolated instead of chlorophyll *a*, which demonstrated that the chlorophylls underwent the loss of magnesium to produce the respective pheo-derivative.

Methodological difficulties had obviously hampered the isolation of chlorophylls and consequently it was necessary to propose an experimental design, which allowed the evaluation of different methodological factors that could cause the pheophytinization of the extracts, such as:

1. Extraction method (EM).
2. Type of sample (TS).
3. HSCCC solvent system (SS).

The response and the effects of the interactions between the three relevant factors mentioned above could evaluate the HSCCC separation in relation with target compounds, in the current research, the isolation of chlorophylls *a, b*

and their derivatives as well as the estimation of the HSCCC separation according to the amount of sample load recovered in the elution and extrusion mode.

To estimate the HSCCC separation the yield of recovered sample was calculated in relation with the amount of sample load. It means that the yield could be quantified as the milligrams recovered in the stationary phase in relation with the total sample load (expressed in percentage).

Subsequently, the first factor to examine consisted in the design of an extraction method which delayed the pheophytinization. According to literature data this is possible by handling of the sample with *N,N*-dimethylformamide saturated with $MgCO_3$, and besides obtaining the elimination of the occurring lipids in the green phase with hexane. The elimination of phenols was performed by washing the green phase with an additional hexane and diethyl ether step in the presence of Na_2SO_4 **(cf. 4.3.1.2)** (Minguez-Mosquera and Garrido-Fernandez 1989; Jubert and Bailey 2007).

Once tested with spinach, the extraction method proposed by Minquez-Mosquera and Garrido-Fernández clearly enabled the separation of the chlorophylls. Chlorophyll *a* and chlorophyll *b* were detected by thin layer chromatography TLC (silica gel, solvent system: petroleum ether /acetone/ dietylamine [10/4/1]) **(Figure 2-90) (cf. 4.3.2).**

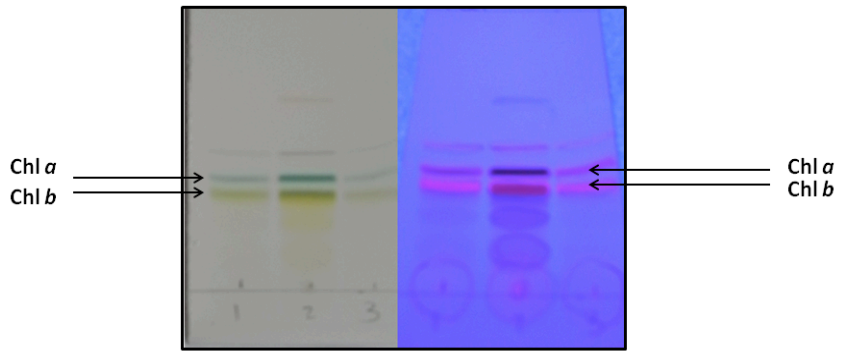

Figure 2-90. Chlorophyll *a* and *b* bands identified by thin layer chromatography (silica gel) at white light and 366 UV from ethyl ether/hexane phase from spinach (solvent system: petroleum ether/ acetone/ dietylamine [10/4/1]) according to literature data (Minguez-Mosquera and Garrido-Fernández 1989).

HPLC-APCI-MS-MS data confirmed the separation of the chlorophylls obtained from spinach. The chromatograms showed the retention time for chlorophyll *a* (21.1 min), chlorophyll *b* (18.8 min) and pheophytin *a* (23.7 min) as well as the mass spectrum of each one of the compounds identified **(Figures 2-91, 2-92, 2-93, 2-94).**

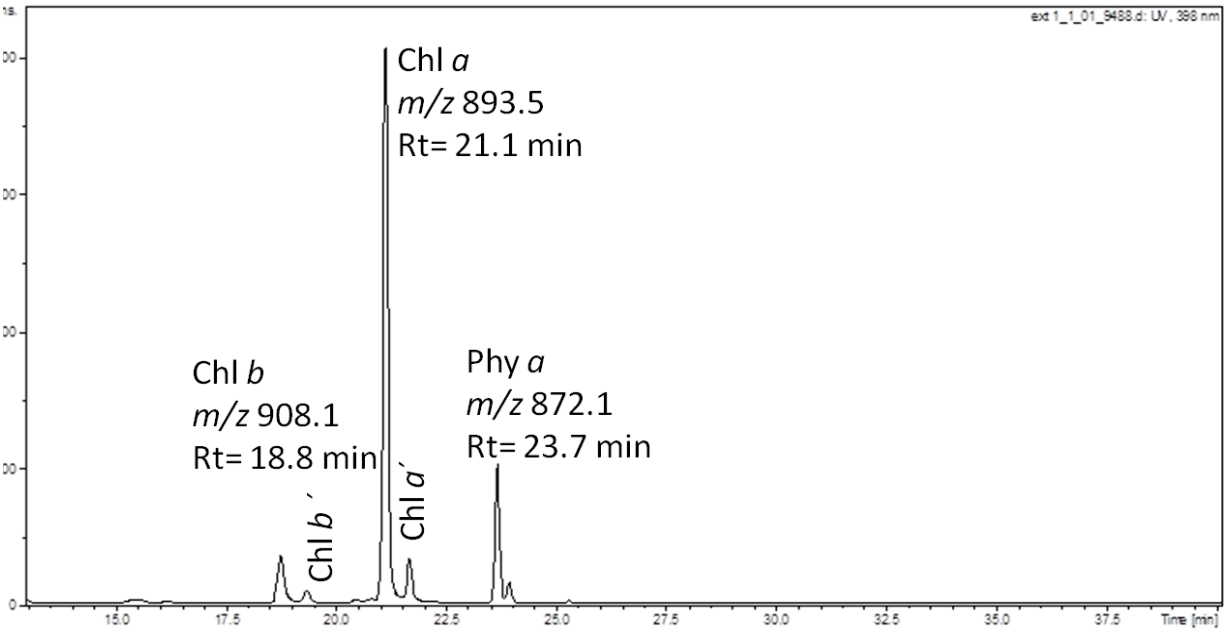

Figure 2-91. Chromatogram of the HPLC-APCI-MS-MS of the ethyl ether/ hexane extract of spinach. Chlorophyll *a*, *b*, and pheophytin *a* eluted at 18.8 min, 21.1 min, and 23.7 min, respectively (Huang et al. 2008).

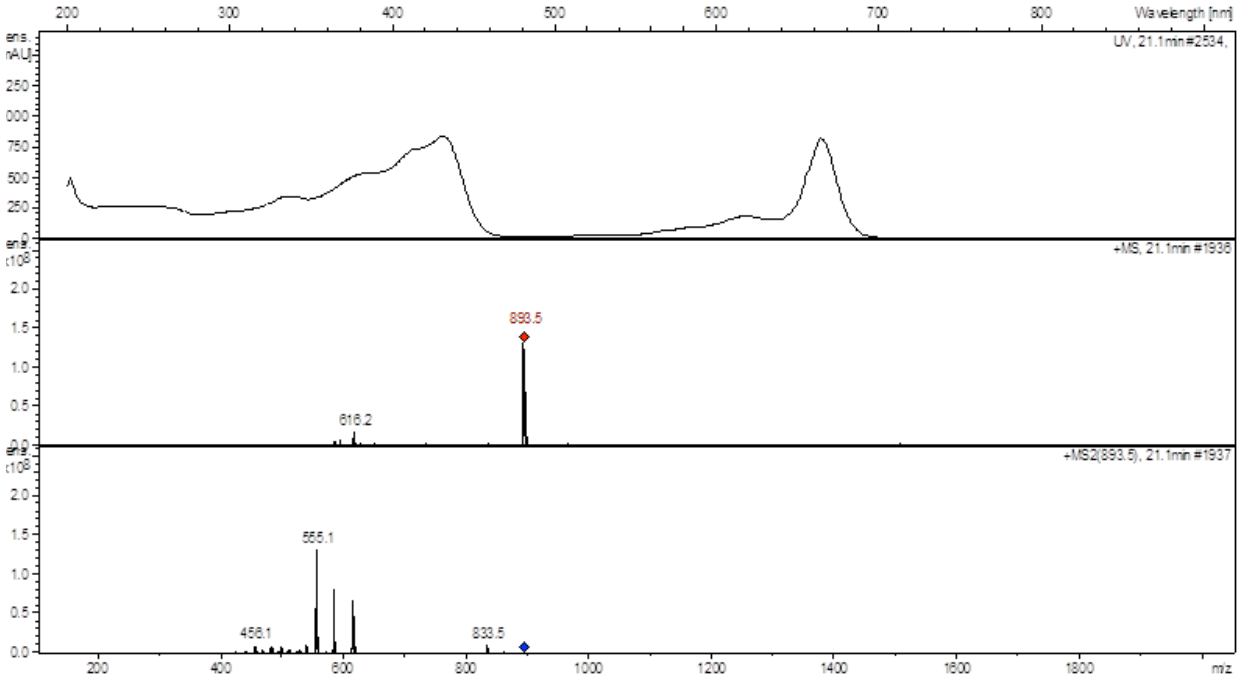

Figure 2-92. APCI-HPLC-MS-MS data of chlorophyll *a* from spinach ethyl ether/ hexane extract with *m/z* 893.5. Chl-*a* is the major peak in the extract (Huang et al. 2008).

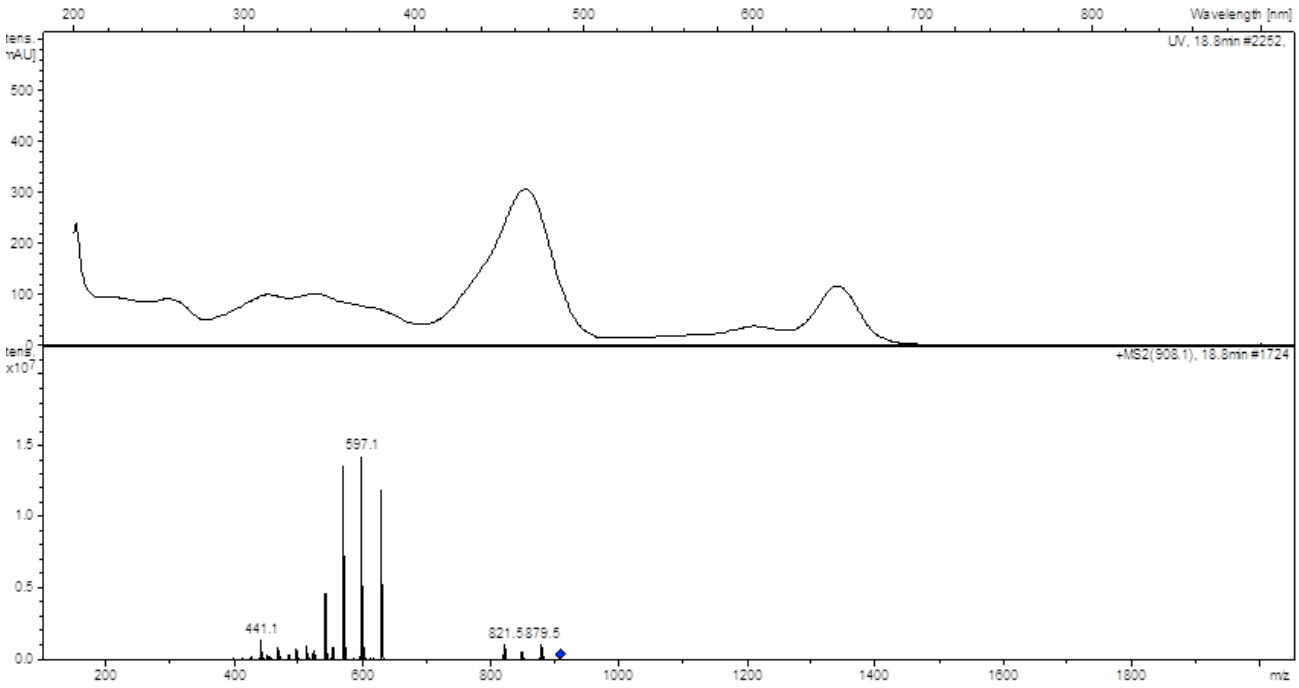

Figure 2-93. APCI-HPLC-MS-MS data of chlorophyll *b* from spinach ethyl ether/ hexane extract with *m/z* 908.1. Chl-*b* is the minor peak in the extract (Huang et al. 2008).

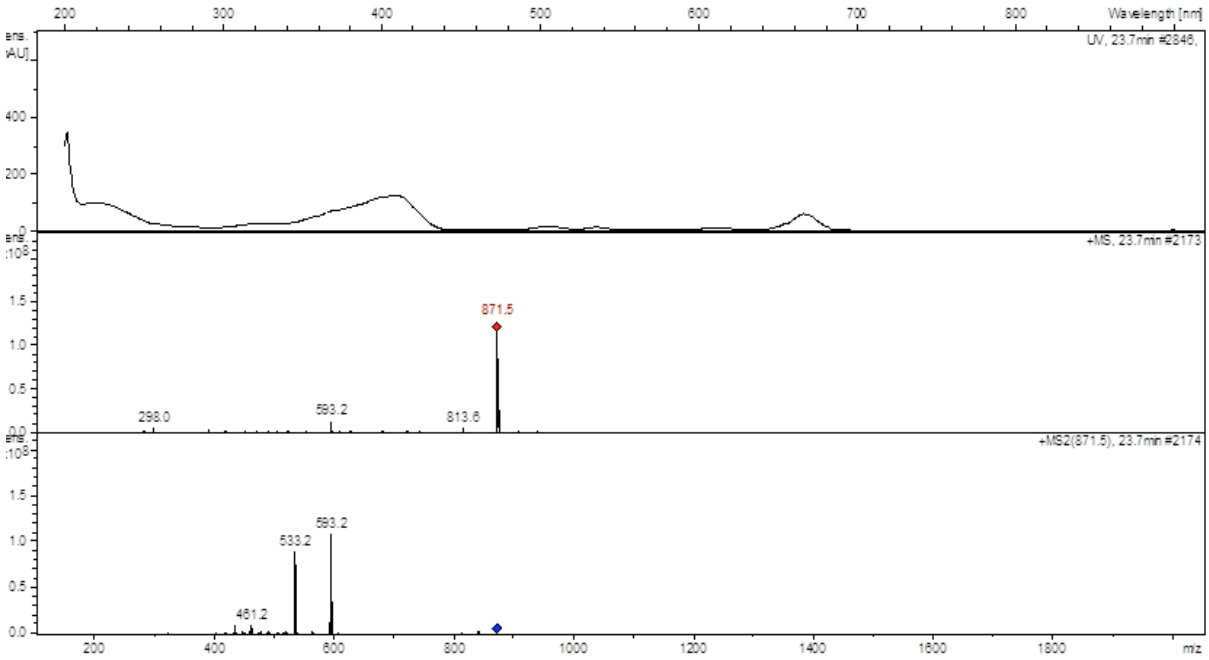

Figure 2-94. APCI-HPLC-MS-MS data of pheophytin *a* from spinach ethyl ether/ hexane extract with *m/z* 872.1 (Huang et al. 2008).

The second relevant analysis played an important role to define the effect of the extraction method on the samples together with the choice of the solvent system for the HSCCC separation. The factor denominated "yield of HSCCC-separations" was calculated for four HSCCC separations and the results are summarized in **Tables 2-20, 2-21.**

Tables 2-20, 2-21 show yields before the optimization of the solvent system. These yields are ranged between 16 and 44.9%, which means that a large amount of the sample load was not recovered in the stationary phase either in elution or extrusion mode.

Where is the remainder part found? The answer was found by the examination of the procedure executed before the injection of the sample into the loop of the HSCCC. When the filtration of the sample is carried out (before the injection of the sample into the loop), the remainder part of the extract is retained in the filter paper. Indeed, those solvent systems based on ACN/hexane, MeOH/hexane and hexane/MeOH/water/EtOAc do not dissolve completely the

compounds occurring in the Baby Banana extract. This was confirmed later when the filter paper was washed with acetone, and the green remainder was readily dissolved in acetone. This extract was denominated “acetone extract” and stored in the freezer at -20°C for further experiments.

Consequently, 3 extraction methods were performed and 4 extract phases were obtained:

1. Extraction method based on methanol and hexane solvents yields two extract phases labeling:

- Methanol phase extract (1).
- Hexane phase extract (2).

2. Extraction method based on the recovery of the sample for HSCCC separation yields one phase labeling:

- Acetone extract phase (3)

3. Extraction method based on the delayed pheophytinization yields one phase labeling:

- Diethyl ether/ Hexane phase (4)

Table 2-20. Evaluation of the yield (%) of the HSCCC separations before the optimization of the solvent system to isolate chlorophylls in Baby Banana peels. Three solvent systems were assessed in extracts of Baby Banana control and with hyperpigmentation (HP) by using the first extraction method.

HSCCC FIRST SEPARATIONS **BEFORE OPTIMIZATION** **SOLVENT SYSTEM (SS)** **[V:V:V:V]**	**LABELING OF SOLVENT SYSTEM TESTED**	**BEFORE OPTIMIZATION**	**EXTRACT PHASES (EP) LABELING (Nº)** **TYPE OF SAMPLE (TS)**	**SAMPLE LOAD (mg)**	**RECOVERY (mg)**	**YIELD (%)**
MeOH/Hexane [2:1]	1		Hexane phase (2) Baby Control	1000	283.3	28.3
ACN/Hexane [1:2]	2		Hexane phase (2) Baby Control	1650	264.6	16.0
Hexane/MeOH/Water/EtOAc [10:10:1:1]	3		MeOH phase (1) Baby Control	1190	427.4	35.0
Hexane/MeOH/Water/EtOAc [10:10:1:1]	3		MeOH phase (1) Baby HP	728	159.5	21.8

Table 2-21. Evaluation of the yield (%) corresponding to the spiral coil-scale up separations before the optimization of the solvent system to isolate chlorophylls from Baby Banana peels. The solvent system ACN/Hexane [1:2] was applied to fractionate 10 g of Baby Banana extract by using the first method of extraction **(cf. 4.3.1.1; 4.2.5).**

SPIRAL-COIL-LSRCCCC **BEFORE OPTIMIZATION** **SOLVENT SYSTEM (SS)** **[V:V]**	**LABELING OF SOLVENT SYSTEM TESTED**	**BEFORE OPTIMIZATION**	**EXTRACT PHASES (EP) LABELING (No)** **TYPE OF SAMPLE (TS)**	**SAMPLE LOAD (g)**	**RECOVERY (mg)**	**YIELD (%)**
ACN/Hexane[1:2]	2		Hexane Phase (2) Baby HP	10.0	4.4	44.9

With the information given above, the priority was to find a suitable solvent system based upon the difference in the equilibrium distribution of the target compounds between the mobile and the stationary phase. In CCC, the partition coefficient ($K_{U/L}$) is expressed as the amount of solute in the upper phase divided by the amount of the solute in the lower phase. According to literature data the recommended $K_{U/L}$ values for CCC are in the range of $0.5 \leq K_{U/L} \leq 1.0$ (Ito 1991, Ito 2005).

For determination of the partition coefficient, frequently HPLC (quantitatively) and TLC (qualitatively) are used. The procedure consists of dissolving the sample into a test tube which contains the two solvent systems in order to check how the distribution of the compound in the two phases is accomplished. In the current research, the qualitative evaluation by using TLC technique was used which permitted to observe the bands and their retention factors (R_f) in both of the phases. The bands represent the components of the extract and their distribution in the lower and upper phase of the solvent system **(Figure 2-95).**

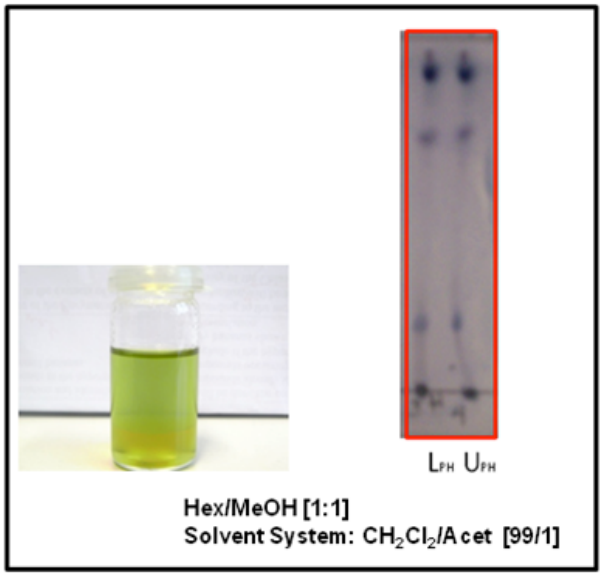

Figure 2-95. Analysis of the solvent system Hex/MeOH [1:1] by thin layer chromatography (TLC) to evaluate the partition coefficient qualitatively through the distribution in the lower and upper phase. The plate shows if the solvent system is suitable to separate triterpenoids present in the mixture which are represented as bands in the lower phase (L_{ph}) and upper phase (U_{ph}).

Additionally, the evaluation of the partition coefficient of a grass extract by TLC was important to find a suitable solvent system for the isolation of chlorophylls in Baby Banana peels. The TLC technique applied for grass (extract phase of diethylether) depicted clearly the distribution both in the lower and in the upper phase for chlorophyll *a*, chlorophyll *b,* pheophytin *a*, chlorophyllide *a/b* and xanthophylls. The silica gel TLC plate was analyzed at natural light and UV 366 nm with a solvent system petroleum ether/ acetone/ diethylamine [10/4/1] according to literature data **(Figure 2-96)** (Minguez-Mosquera and Garrido-Fernandez 1989) **(cf. 4.3.2).**

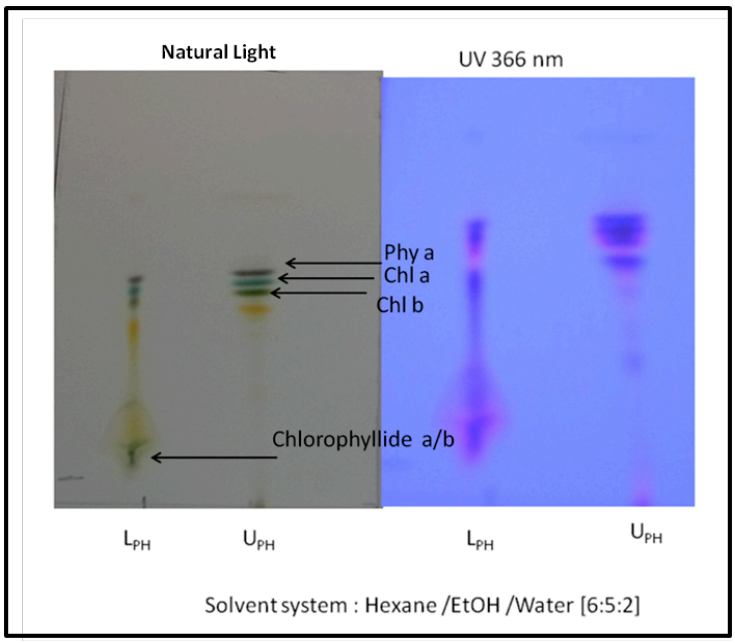

Figure 2-96. The analysis of a hexane /EtOH/ water [6:5:2] solvent system to optimize the isolation of chlorophylls and their derivatives in grass by HSCCC by application of thin layer chromatography for qualitative evaluation of the partition coefficient in lower (L ph) and upper phases (U ph).

In total, seven solvent systems were tested for the optimization of the solvent system for the isolation of chlorophylls, in which three (3) were applied before the optimization **(Tables 20, 21)** and four ones (4) were assayed thereafter **(Table 23) (cf. 4.2.3.1)**

Table 2-22 summarizes the experimental design for the optimization of the solvent systems to isolate chlorophylls according to the total assays of solvent system, type of samples and extraction phase used during the optimization.

Table 2-22. Summary of the experimental design for the optimization of the solvent systems to isolate chlorophylls and their derivatives in Baby Banana peels and plants based on the application of 7 solvent systems, 4 assessed samples and 4 extraction phases.

HSCCC SEPARATIONS **SUMMARY** **SOLVENT SYSTEM (SS)**	**TOTAL LABELING OF SOLVENT SYSTEM TESTED**	**TYPE OF SAMPLE (TS)**	**EXTRACTION PHASES (EP)**
HSCCC-solvent system	**7**	Baby Banana control **(1)** Baby Banana with Hyperpigmentation **(2)** Spinach **(3)** Grass **(4)**	Hexane phase **(1)** Methanol phase **(2)** Acetone phase* **(3)** Diethyl ether/ Hexane phase **(4)**

***Acetone phase**: remainder of extracts retained in the filter paper when the filtration of the methanol and hexane phases extracts was performed before the injection of the sample into the loop of the HSCCC.

Table 2-23. Evaluation of the yield (%) corresponding to HSCCC separations during the optimization of the solvent system to isolate chlorophylls from Baby Banana peels (control and with hyperpigmentation) as well as in spinach and grass. Four additional solvent systems were assessed during the optimization for the isolation of chlorophylls and their derivatives in plants.

HSCCC SEPARATION SOLVENT SYSTEM (SS) [V:V:V:V]	**LABELING OF SOLVENT SYSTEM TESTED**	**EXTRACTION PHASE (EP)** **TYPE OF SAMPLE (TS)**	**SAMPLE LOAD (mg)**	**RECOVERY (mg)**	**YIELD (%)**
Hexane/EtOH/water [6:5:2]	4	Acetone phase-Baby hyper	1000.0	699.1	69.9
Hexane/ACN/$CHCl_3$ [4:6:1]	5	Acetone phase-Grass	621.6	425.1	68.4
Hexane/CH_2Cl_2/EtOH/water [4:2:6:2]	6	Diethyl ether/hexane-Baby control	405.5	185.7	45.8
Hexane/$CHCl_3$/EtOH/water [4:2:6:2]	7	Diethyl ether/hexane-Spinach	486.1	300.2	61.7
Hexane/$CHCl_3$/EtOH/water [4:2:6:2]	7	Diethyl ether/hexane-Grass	559.4	321.0	57.4
Hexane/CH_2Cl_2/EtOH/water [4:2:6:2]	6	Diethyl ether/hexane-Grass	205.3	175.2	85.4
Hexane/CH_2Cl_2/EtOH/water [4:2:6:2]	6	Diethyl ether/hexane-Baby hyper	813.0	812.7	99.9

As it is shown in **Table 23** the yield of the HSCCC separation increased from 69.9 to 99.9% during the trials when hexane/EtOH/water [6:5:2] and hexane/CH_2Cl_2/EtOH/water [4:2:6:2] were used, respectively, with Baby Banana Hyper extract as sample.

Ethanol gave adequate separation during CCC purification while methanol revealed several chlorophyll degradation products (isomers and allomers) in the initial trials. Moreover, an added advantage is that ethanol forms an azeotrope with water enabling easier solvent removal post isolation (Jubert and Bailey 2007).

The effect of chloroform and dichloromethane as part of the solvent systems is also remarkable. This issue explains the result of HSCCC separation's yield of 85.4 and 99.9% when dichloromethane is used in comparison to 61.7 and 57.4%, when the solvent system contains chloroform.

The main challenge in CCC is the choice of a suitable solvent system for an optimal separation and the results shown in the current sections could demonstrate it. The objective was accomplished since chlorophyll *a*, chlorophyll *b* and derivatives were purified and characterized by 1/D and 2/D NMR experiments when the solvent systems hexane/$CHCl_3$/EtOH/water [4:2:6:2] and hexane/CH_2Cl_2/EtOH/water [4:2:6:2] were assessed in HSCCC separations from Baby Banana peels and plants. The following section describes the HSCCC separation and the effect on the behaviour of the chlorophylls and derivatives in Baby Banana peels with hyperpigmentation, spinach and grass.

In summary, the solvent system hexane/CH_2Cl_2/EtOH/water [4:2:6:2] could be denominated as novel solvent system for the separation of chlorophylls in fruits and plants.

2.2.2 Isolation of chlorophylls and derivatives from spinach by HSCCC

The preparation of the plant extract (20 g) was performed with N,N-dimethylformamide and the filtrates were treated with hexane in a separation funnel in order to extract and separate the carotenoids occurring in the samples. The phase of N,N-dimethylformamide retained chlorophylls and chlorophyll derivatives. Eight extractions with diethyl ether/hexane were carried out in order to collect a chlorophyll extract (1 g) for a subsequent HSCCC separation **(Figure 2-97) (cf. 4.3.1.2).**

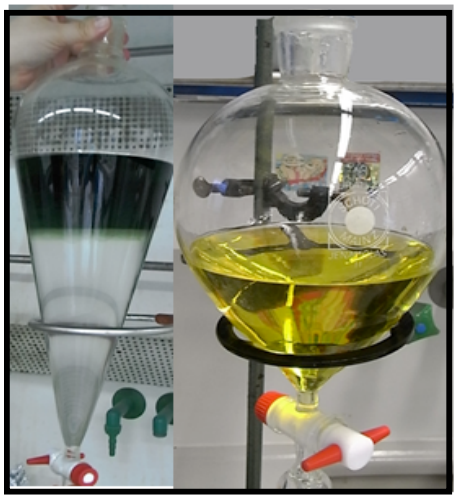

Figure 2-97 Spinach extracts of diethyl ether/hexane with chlorophylls and xanthophylls (left) and of the hexane phase with carotenoids (right).

The elution mode used in the separation was "*head-to-tail*" and the solvent system was n-hexane/chloroform/EtOH/H_2O (4/2/6/2). From the N,N-dimethylformamide extract an amount of 486 mg was injected. The flow rate of the mobile phase (EtOH/H_2O) was set at 3.5 mL/min and the detector at λ 440 nm **(Figure 2-98).**

In the elution mode polar carotenoids, such as neoxanthin (F4), canthaxanthin (F5), neochrome/luteoxanthin (F6) and lutein (F8) were separated and their identification supported by an APCI-HPLC-MS-MS coupled to a photodiode array detector, which enabled the analysis of the spectra **(Figure 2-99) (cf. 4.2.2).**

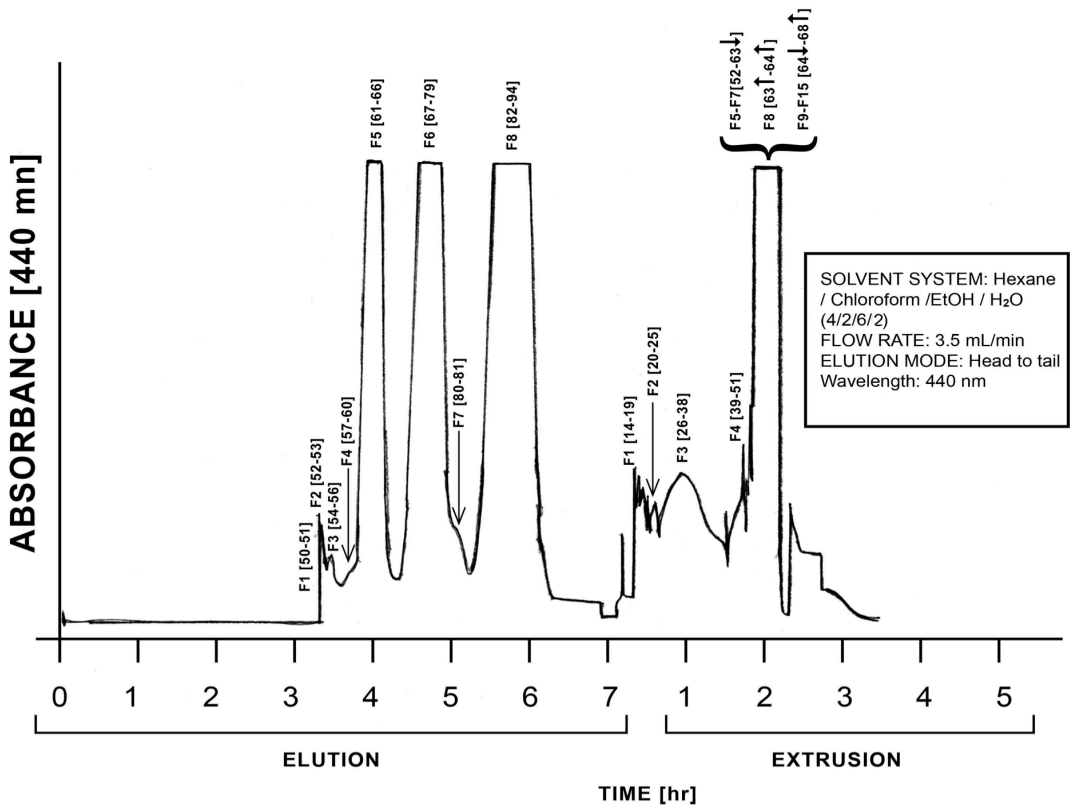

Figure 2-98. HSCCC chromatogram of a separation of 486 mg of ethyl/hexane extract from spinach. Eight fractions in elution mode and fifteen in extrusion mode were obtained. Xanthophylls and chlorophylls were identified by APCI-HPLC-MS-MS and isolated by HSCCC.

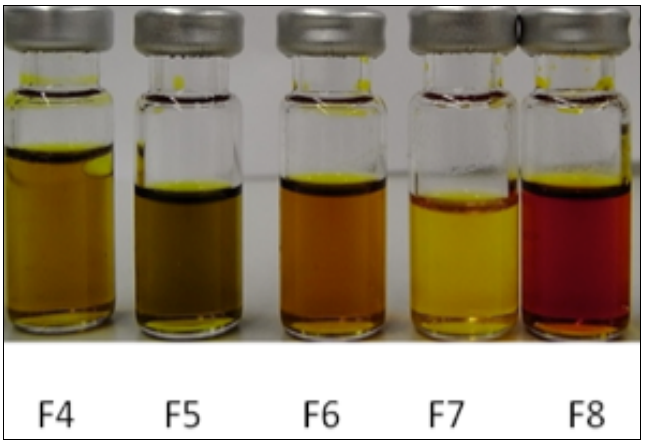

Figure 2-99. Elution fractions of xanthophylls in spinach identified by APCI-HPLC-MS-MS. Fraction 7 was not clearly identified. Neoxanthin (F4), canthaxanthin (F5), neochrome/ luteoxanthin (F6) and lutein (F8).

Table 2-24 summarizes the major fragments (m/z) and the absorption maxima (nm) for the fractions 4, 5, 6 and 8 in elution mode. The data is in agreement with the literature (Putzbach et al. 2005a; Lacker et al. 1999; Mendes-Pinto et al. 2005; Britton et al. 1995; Britton et al. 2004; de Rosso and Mercadante 2007; Rodríguez-Amaya 2001).

Table 2-24. Xanthophylls separated from a spinach extract by HSCCC and identified by APCI-HPLC-MS-MS. The absorption maxima (nm) and the major fragments (*m/z*) could correspond to neoxanthin, canthaxanthin, neochrome/luteoxanthin and lutein, according to literature data.

Fraction elution mode (Tubes)	**Xanthophylls**	**Major fragments *(m/z)***	**Identity**	**Absorption maxima (nm)**
F4 [57-60]	Neoxanthin	601 583	$[M+H]^+$ $[M+H-H_20]^+$	456
F5 [51-66]	Canthaxanthin	565	$[M+H-H_20]^+$	492
F6 [67-79]	Neochrome/ luteoxanthin	601 583	$[M+H]^+$ $[M+H-H_20]^+$	422
F8 [82-94]	Lutein	551	$[M+H-H_20]^+$	478

During the extrusion mode the fractions were monitored by TLC and APCI-HPLC-MS-MS according to the methodology described previously in section 2.1.12.**(cf. 4.2.2.4; 4.3.1)** A total of 22.88 mg of chlorophyll *b* and 19.70 mg of chlorophyll *a* were recollected during the extrusion. The characteristic color of the isolated chlorophyll *a* and *b* was observed for the first time in the tubes during the HSCCC separation **(Figures 2-100, 2-102).**

The fractions 13 and 6 (in extrusion mode) showed under LC-APCI-MS single peaks with the quasimolecular ion at $[M+H]^+$ 894 *m/z* for chlorophyll *a* and for chlorophyll *b* at 907 *m/z* which correspond to 12.4 mg of chlorophyll *a* and 12.6 mg of chlorophyll *b*. Furthermore, the fractions were submitted to 1/D and 2/D NMR experiments for analysis of its purity **(Figure 2-101, 2-103).**

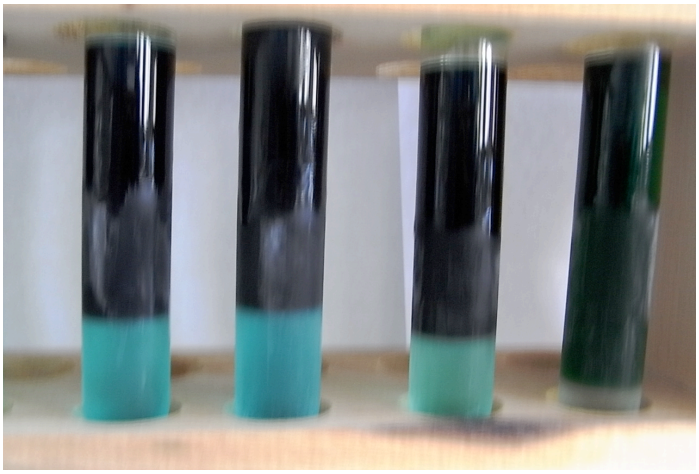

Figure 2-100. The characteristic color of chlorophyll *a* was observed during the extrusion mode for first time in the spinach HSCCC separation and recorded during the recollection of the fractions.

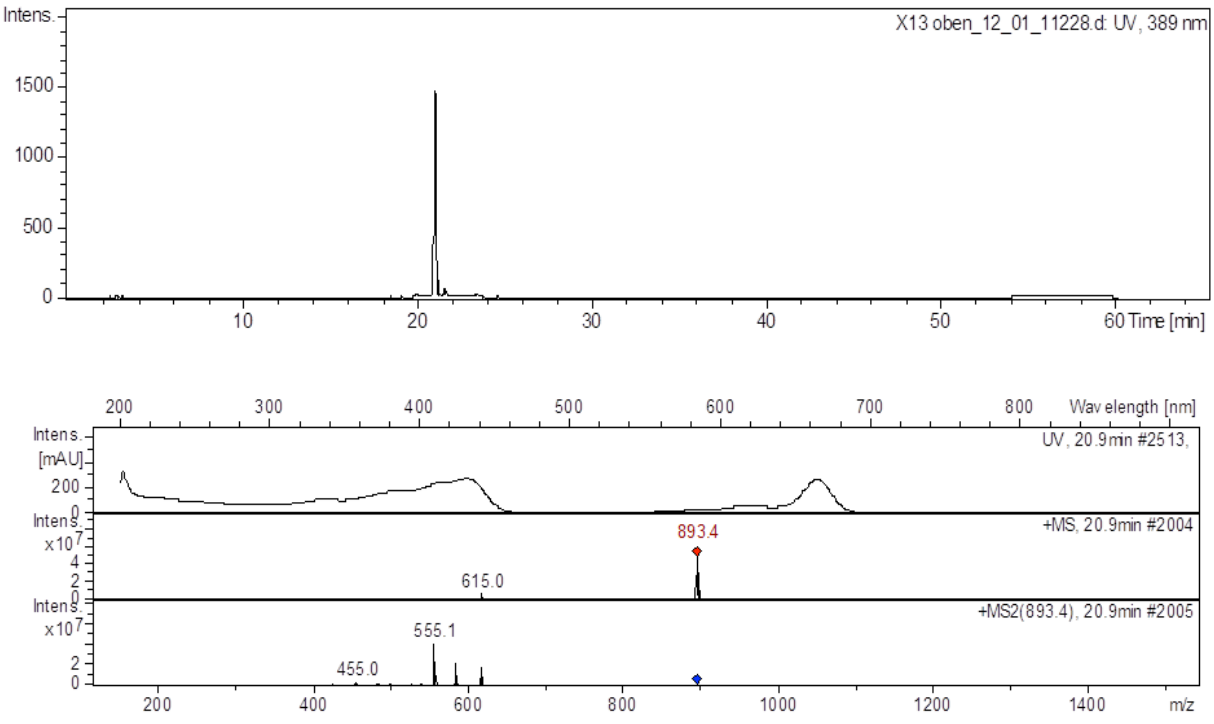

Figure 2-101. APCI-HPLC-MS-MS spectrum of chlorophyll *a* in fraction 13 with a quasimolecular ion of *m/z* 894 $[M+H]^+$ at 20.9 min (Huang et al. 2008; Van Breemen et al. 1991b).

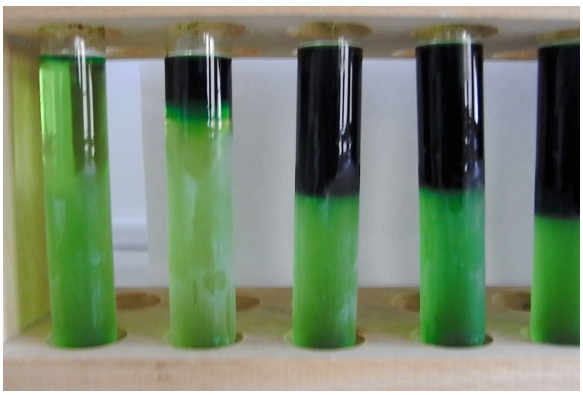

Figure 2-102. The characteristic color of chlorophyll *b* was observed during the extrusion mode for first time in the spinach HSCCC separation and was recorded during the recollection of the fractions.

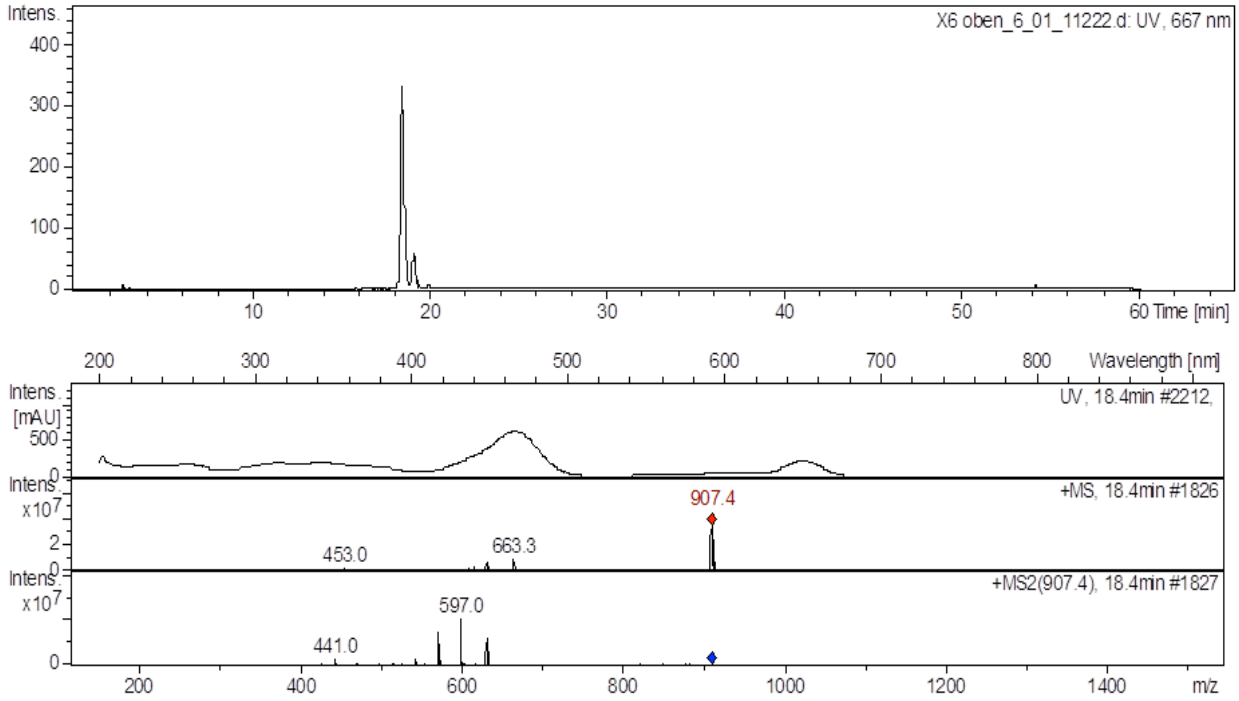

Figure 2-103. APCI-HPLC-MS-MS spectrum of chlorophyll *b* in fraction 6 with a the quasimolecular ion of *m/z* 907 $[M+H]^+$ at 18.4 min (Huang et al. 2008; van Breemen et al. 1991b).

Chlorophyll *b* (12.6 mg) was obtained in a high purity. ^{1}H and ^{13}C NMR spectra of chlorophyll *b* were recorded at 600 MHz and 150 MHz respectively and supported the structure (**Figures 2-104, 2-105, 2-106).** Data for chlorophyll *b* is in agreement with the literature **(Table 2-25)** (Risch and Brockmann 1983; Abraham and Rowan 1991; Lötjönen and Hynninen 1981).

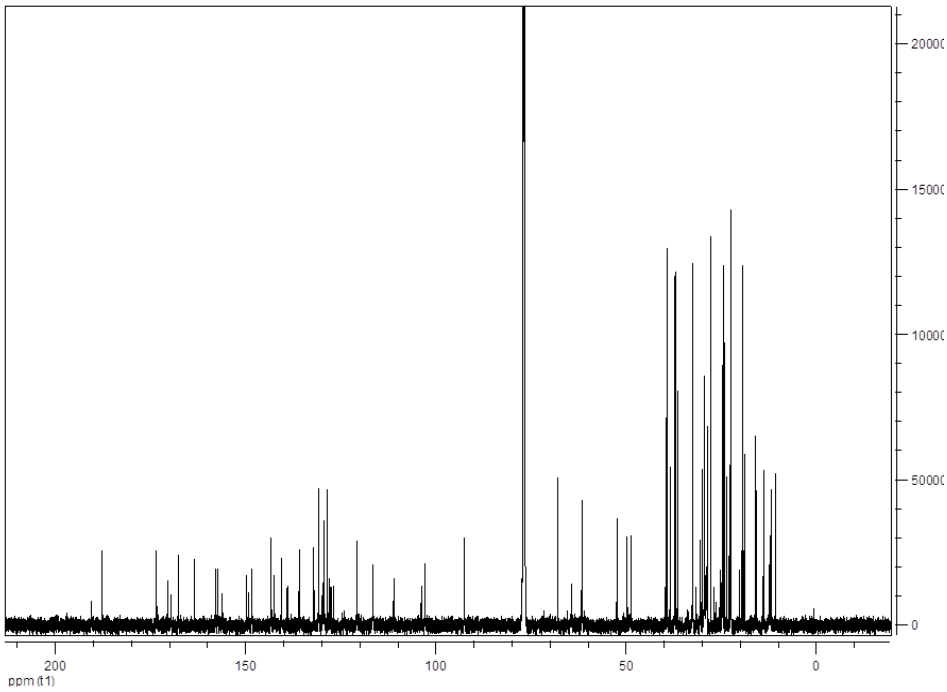

Figure 2-104. ^{13}C NMR in spectra of chlorophyll *b* isolated from spinach by HSCCC recorded at 150 MHz in $CDCl_3$.

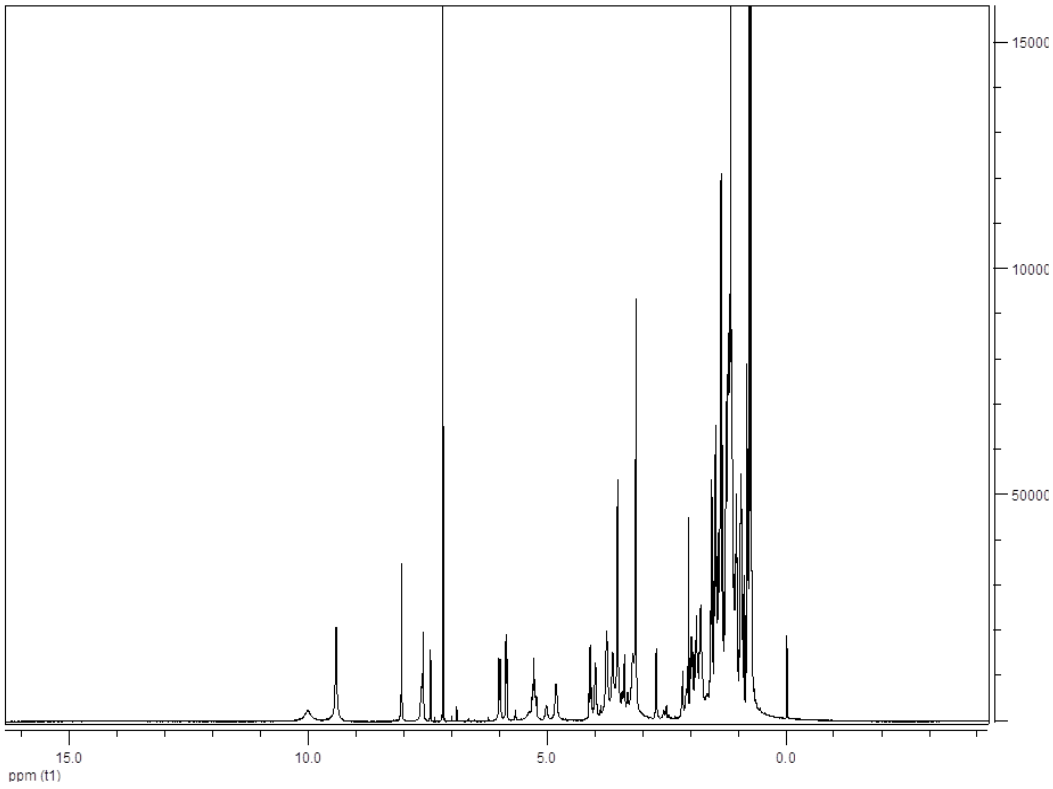

Figure 2-105. ^{1}H NMR spectra of chlorophyll *b* isolated from spinach by HSCCC recorded at 600 MHz in $CDCl_3$.

Table 2-25 ^{13}C NMR data recorded at 150 MHz in $CDCl_3$ of 12.6 mg of chlorophyll *b* isolated from spinach by HSCCC. The data was in agreement with literature (Risch and Brockmann 1983).

Carbon	^{13}C chemical shift (ppm)
9	190.6
3_a	187.8
7_c	173.5
10_a	170.5
18	169.7
16	163.1
17	158.0
11	157.4
4	155.8
12	149.9
13	149.3
15	148.4
14	142.5
2	140.6
5	139.1
1	136.1
6	131.9
3	129.4
2_a	129.8
2_b	120.9
β	111.2
γ	104.1
α	103.0
δ	92.6
10	64.5
10_b	52.6
7	49.9
8	48.8
7_a	31.9
7_b	29.7
8_a	23.7
4_a	19.2
4_b	19.0
1_a∫	12.5
5_a∫	12.2

Carbon	^{13}C chemical shift (ppm)
P1	61.8
P2	119.4
P3	142.2
P3a	16.1
P4	39.8
P5	25.0
P6	37.4
P7	32.7
P7a	20.5
P8	38.6
P9	25.5
P10	38.6
P11	32.6
P11a	20.5
P12	38.6
P13	25.6
P14	39.8
P15	22.7
P15a	22.9
P16	23.0

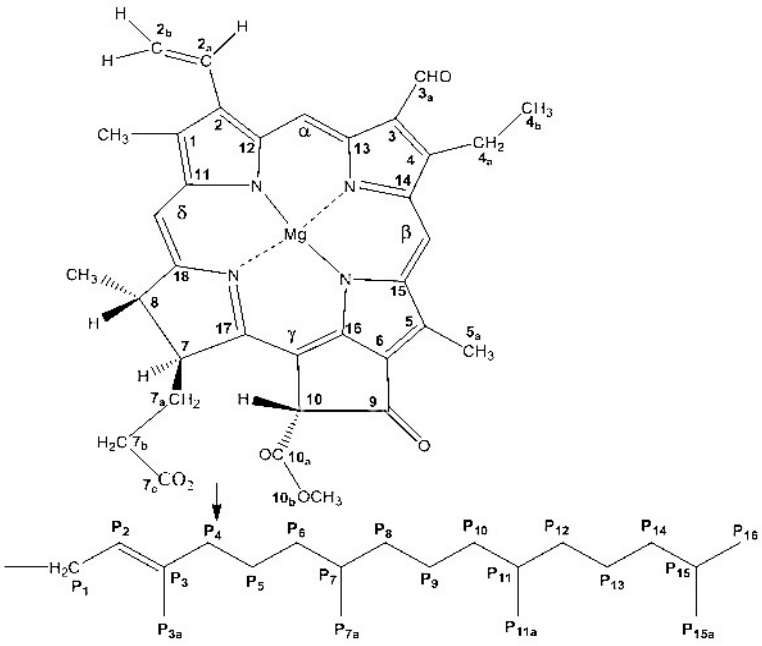

Figure 2-106. Structure and numbering of chlorophyll *a* (C-3_a = $CH_{3)}$ and *b* used throughout this section (Abraham and Rowan 1991).

Compared with the relevant spectrum of chlorophyll *b*, the ^{13}C NMR spectrum of chlorophyll *a* showed a difference in the region between 190-180 ppm (keto group) **(Table 2-26).** The intensity of the chemical shift at 190.1 ppm was meaningfully lower in comparison with the resonance of the keto function at C-9 from the chlorophyll *b* spectrum. This feature of the Chl *a* spectrum was reproduced at C-10; and C-10a where the carbomethoxy group is attached, as well as at C-13, C-18 and at the *meso* region (α, β, γ, δ). The low resolution in this region contrasted with the high intensity of the peaks corresponding to the methyl/methylene groups bonded to the large phytyl moiety and to several conjugated bonds which confirm the porphyrin structure **(Figures 2-107, 2-108, Table 2-26)**.

This result could be explained as:

a) Chlorophyll *a* was dissolved in CD_2Cl_2 and not in $ClCD_3$ as it was the case for chlorophyll *b*. The ^{13}C chemical shifts signals from dichloromethane-d2 at 53.8 ppm and chloroform-d at 77.0 ppm are depicted in the Chl-*a* and Chl-*b* spectra respectively **(Figures 2-107, 2-104)**.

b) The chemical shift of chlorophylls is not only related to a concentration that is solvent-dependent of their magnesium-free counterparts. Chlorophylls are in a high grade solvent-dependent, and this effect is associated with the coordination state of the central Mg atom. Electronic absorption spectra measured for Chl *a* indicated that the Mg atom is predominantly hexacoordinated in tetrahydrofuran and pentacoordinated in acetone (Smith et al. 1984; Abraham and Rowan 1991; Scheer 1991; Katz et al. 1966).

During the current research and when the experiment described here was carried out, it was not expected that a meaningful difference between chloroform and dichloromethane as solvents existed. For this reason deuterated dichloromethane has been used for chlorophyll *a* in 1/D and 2/D NMR experiments.

However, this issue has been reported as one of the main reasons for the developing of NMR studies of chlorophylls during the 80’s and 90’s, as it is described by Abraham and Rowan (1991). In addition, these facts have had a meaningful effect in the results of the current research as it is described in **section 2.2.3**, especially towards the role of dichloromethane and chloroform in the isolation of xanthophylls and chlorophylls by HSCCC.

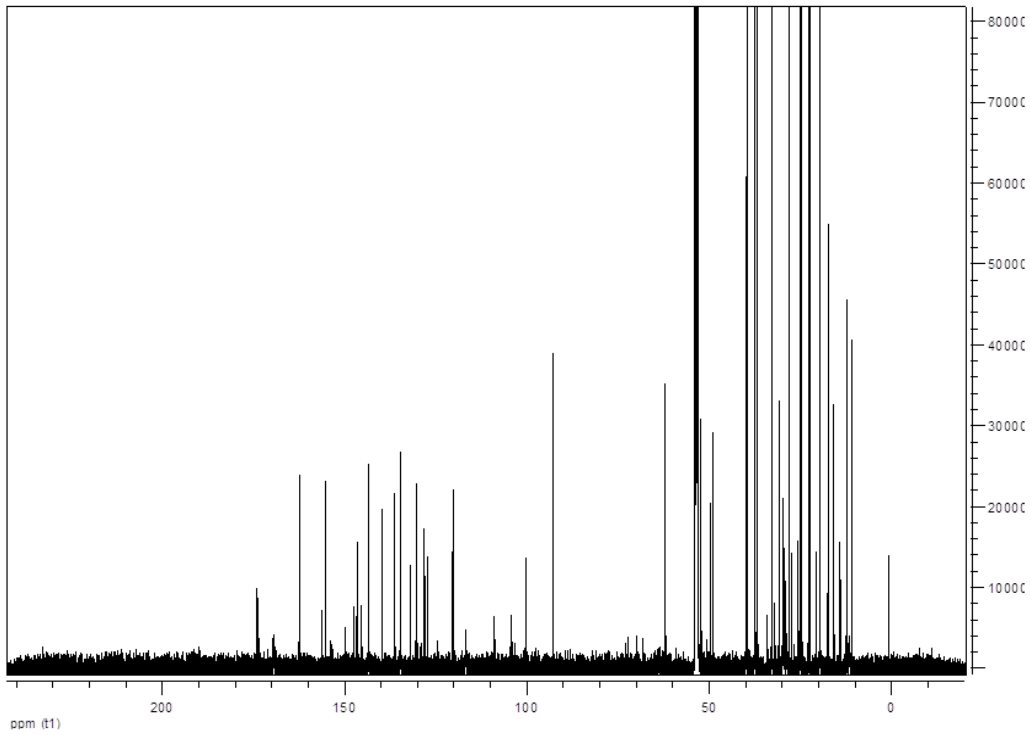

Figure 2-107. ^{13}C NMR spectra of chlorophyll *a* isolated from spinach by HSCCC recorded at 150 MHz in CD_2Cl_2

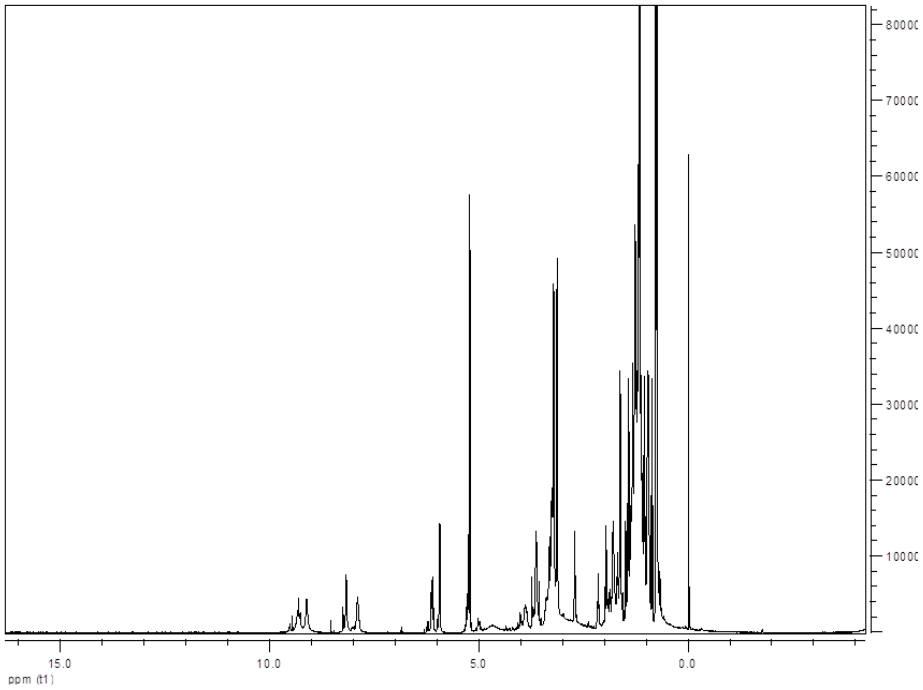

Figure 2-108. ^{1}H NMR spectra of chlorophyll *a* isolated from spinach by HSCCC recorded at 600 MHz in CD_2Cl_2.

Table 2-26. ^{13}C chemical shifts recorded at 150 MHz of chlorophyll *a* (12.4 mg) in CD_2Cl_2 isolated from spinach by HSCCC. The data is in agreement with the literature (Lötjönen and Hynninen 1981,1983).

Carbon	^{13}C chemical shift (ppm)
9	190.1
3_a	11.2
7_c	174.1
10_a	169.6
18	171.6
16	162.4
17	156.5
11	155.3
4	143.7
12	149.8
13	153.9
15	147.7
14	146.7
2	139.9
5	134.7
1	134.9
6	130.7
3	136.6
2_a	130.4
2_b	117.0
β	109.1
γ	104.3
α	100.3
δ	92.9
10	64.1
10_b	52.4
7	49.9
8	48.1
7_a	30.9
7_b	30.0
8_a	23.0
4_a	20.8
4_b	17.5
1_a∫	12.6
5_a∫	12.4

Carbon	^{13}C chemical shift (ppm)
P1	61.2
P2	120.5
P3	143.7
P3a	16.2
P4	40.1
P5	25.4
P6	37.6
P7	33.4
P7a	20.8
P8	37.7
P9	25.5
P10	37.7
P11	33.0
P11a	19.8
P12	37.7
P13	25.9
P14	39.7
P15	28.3
P15a	22.8
P16	23.0

2.2.3 Role of dichloromethane and chloroform as stationary phase in the solvent system for the isolating of chlorophylls and xanthophylls from plant extracts by HSCCC

In order to isolate chlorophyll from plant extracts by means of High Speed Countercurrent Chromatography (HSCCC) excluding the use of acetone as part of the stationary phase, a novel solvent system composed of hexane–dichloromethane-ethanol-water 4:2:6:2 (v/v/v/v/) was applied. The isolation of chlorophylls *a, b* and pheophytins *a*, *b* was successfully performed in the case of grass when the dichloromethane was part of the solvent system **(Figure 2-109).** Comparatively, when chloroform was applied as part of the stationary phase, the xanthophyll separation depicted better resolution compared to chlorophylls **(Figure 2-110).**

In an initial step, 559.5 mg and 205 mg of N,N dimethylformamide extract of grass treated with hexane were introduced into the HSCCC system in a mixture of 20 mL, consisting of upper and lower phase (1:1, v/v) through an injection loop. The elution mode used in the separation was *head-to-tail* and the flow rate of the mobile phase ethanol/water was set to 3.5 mL/min. Detection was at λ 440 nm for chlorophylls and xanthophylls.

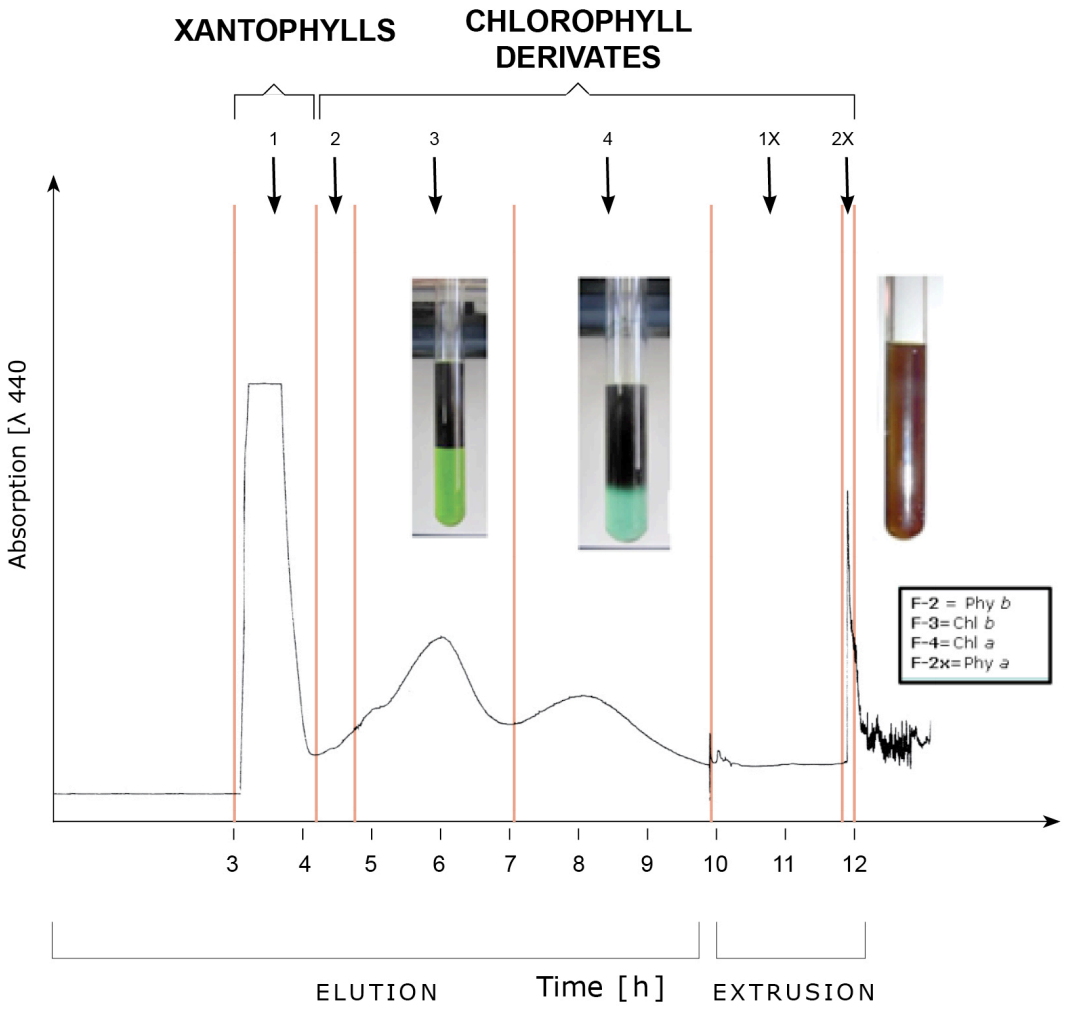

Figure 2-109. HSCCC chromatogram (grass extract) with elution and extrusion mode. Solvent system: hexane-dichloromethane-ethanol-water (4/2/6/2). Chlorophyll separation showed a higher resolution in comparison to xanthophylls in elution and extrusion mode.

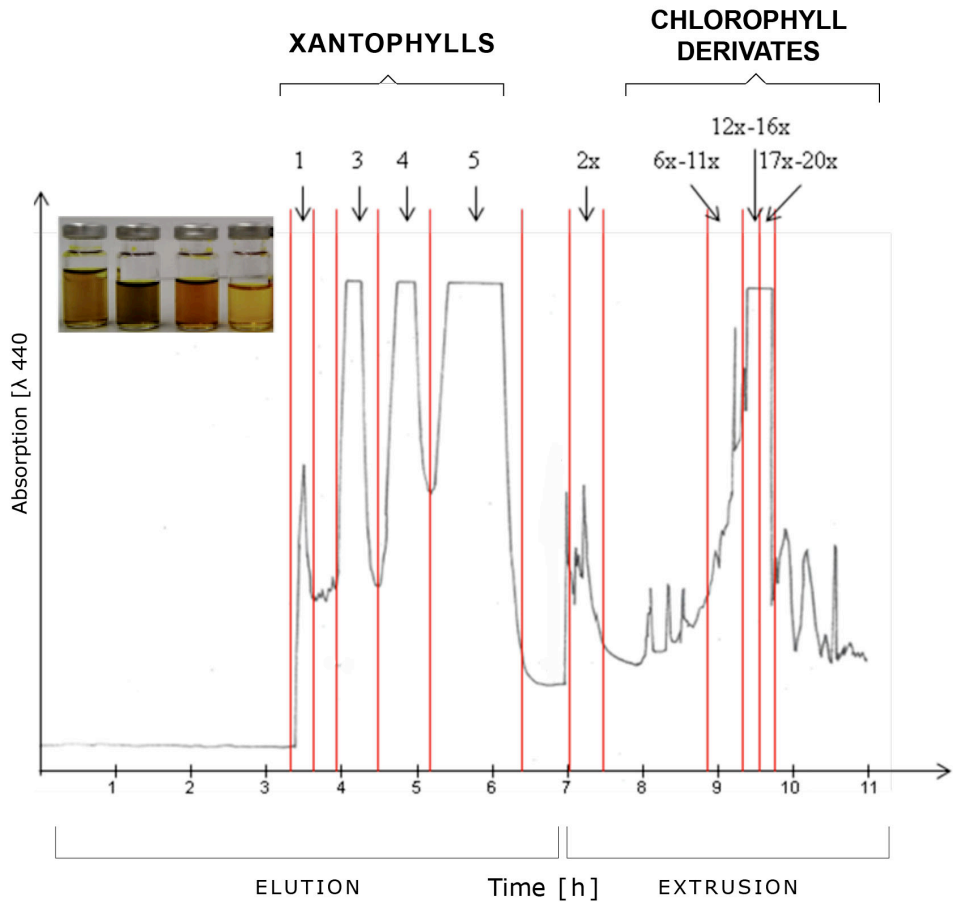

Figure 2-110. HSCCC chromatogram (grass extract) with elution and extrusion mode. Solvent system: hexane-chloroform-ethanol-water (4/2/6/2). Xanthophyll separation showed a higher resolution in elution mode in comparison to the chlorophyll separation in extrusion mode.

On-line high performance liquid chromatography/atmospheric pressure chemical ionization mass spectrometry (HPLC/APCI-MS) was applied in positive mode to identify xanthophylls and chlorophyll in the HSCCC fractions.

Lutein, auroxanthin and luteoxanthin-neochrome were identified in fraction 5, 4, 3, respectively, in elution mode from the HSCCC separation that used chloroform as part of the solvent system. In addition, the identification of the xanthophylls was defined by comparison of the mass spectra in positive mode with the literature data **(Figure 2-110, Table 2-27)** (Putzbach et al. 2005ab; Lacker et al. 1999; Mendes-Pinto et al. 2005; Britton et al. 1995, 2004; de Rosso and Mercadante 2007; Rodríguez-Amaya 2001). Structure elucidation of lutein, chlorophylls and pheophytins were done by 1D/2D-NMR experiments (^{1}H,^{13}C, ^{1}H -^{1}H COSY, HSQC, HMBC) **(cf. 4.2.6).**

Table 2-27. Xanthophylls identified in the HSCCC separation from grass by APCI-HPLC-MS-MS when chloroform is used as part of the solvent system. The mass spectra in positive mode were compared with literature data (Putzbach et al. 2005ab; Lacker et al. 1999; Mendes-Pinto et al. 2005; Britton et al. 1995; Britton et al. 2004; de Rosso and Mercadante 2007; Rodríguez-Amaya 2001).

FRACTION	TUBES	*m/z*	UV-MAXIMA [nm]	ANALYTES
1	53-55	593	408, 665	Pheophorbide *a*
3	60-67	601 601	395, 419, 443	Luteoxanthin Neochrome
4	68-78	601	379, 400, 425	Auroxanthin
5	79-93	569	419, 447, 469	Lutein

J.J. Katz, a pioneer of chlorophyll research, studied the chlorophyll-ligand co-ordination interaction that revealed NMR spectra as he was observing a "ring-current effect" at the proton chemical shift of ligands bound to chlorophyll (Katz et al. 1966).

In order to understand the chlorophyll-ligand coordination it is important to recognize that chlorophylls interact with nucleophilic ligands and for this reason coordinate water, alcohols, amines, ketones and ethers in a very strong way. Thus, chlorophylls are highly fluorescent when solvated and nonfluorescent in the unsolvated state. Nuclear magnetic resonance explained this behaviour and confirmed the role of the magnesium in these phenomena (Katz et al. 1968, Katz et al. 1978).

Hence, the unsaturation coordination of the magnesium leads to chlorophyll-nucelophile interactions, and in the absence of other nucleophiles, chlorophylls do self-interactions to form dimers. In nonpolar solvents the coordination un-saturation of the magnesium is relieved by a coordination of the ketone oxygen function of one chlorophyll molecule with the magnesium function of another chlorophyll molecule to form a dimer. Additionally, chlorophyll monomer-dimer equilibria has been achieved by changing electronic absorption and fluores-

cence spectra as an index of aggregations (Katz et al. 1968). Subsequently, NMR techniques were used successfully to elucidate the mode of aggregation of the chlorophylls dimers (Storm et al. 1966).

In the absence of an external ligand, the vacant coordination sites on the central magnesium are satisfied by a second chlorophyll molecule which coordinates directly, using a carbonyl function, or indirectly via water with hydrogen bond to the carbonyl. This aggregation is determined by the solvent, concentration and temperature (Lötjönen and Hynninen 1981, 1983).

On the other hand, the ring current effect was initially recognized (Abraham and Rowan 1991) as an effect in the chlorophyll molecule due to the large π system of the macrocycle in the structure. Despite the structural complexity of chlorophylls, the chemical shift assignment for ^{1}H proton is relatively easy. The protons of the macrocycle are well separated and only four protons of the vinyl group (2a and 2b), ethyl group (C-4), and the protons of side chain of ring IV show spin-spin interactions. The most important feature of the chlorophylls in this context is the large π -system of the macrocycle, which produces an "induced ring current". This effect causes that peripheral protons in the plane of the macrocycle are deshielding, whereas protons situated above or below the plane of the macrocycle are significantly shielding. In the case of magnesium-free derivatives, the central NH protons are strongly deshielded and appear upfield of TMS. This ring current effect accounts for the large range of chemical shift values seen for chlorophylls. In Chl *a*, the range of ^{1}H chemical shift is about 10 ppm and in the magnesium-free derivative it is still larger, about 12 ppm, due to the deshielding (Abraham and Rowan 1991).

Dichloromethane and chloroform are non-polar solvents. Although, they have the similar density (1.49 and 1.32 g/mL), the dielectric constant is higher for dichloromethane in comparison with chloroform. That means that the polarity of dichloromethane is higher than chloroform **(Table 2-28).**

Additionally, the Hansen solubility parameters values show that δ P (Polar bonds) and δ H (Polar hydrogen bonding) are meaningfully different. The δ P

and δ H values for dichloromethane are 7.3 and 7.1, respectively, and for chloroform 3.1 and 5.7. That means that dichloromethane is more polar than chloroform. Therefore, the type of solvent classification changes considerably because dichloromethane is a polar aprotic solvent and chloroform a non-polar solvent **(Table 2-29).**

Table 2-28. Classification of the solvent according to polarity values (Kosower et al. 1969; Kosower 1968; Mohammad and Kosower 1970).

Solvent	**Density** **g/mL**	**Dielectric constant**	**Dipole moment**	**Type of solvent**
Dichloromethane CH_2Cl_2	1.326	9.1	1.04	Non-polar solvent
Chloroform $CHCl_3$	1.498	4.81	1.60	Non-polar solvent

Table 2-29. Classification of the solvent according to Hansen solubility parameter values (Hansen 2007).

Solvent	**δ d** **Dispersion bonds**	**δ p** **Polar bonds**	**δ H** **Hydrogen bonding**	**Type of solvent**
Dichloromethane CH_2Cl_2	17	7.3	7.1	Polar aprotic solvent
Chloroform $CHCl_3$	17.8	3.1	5.7	Non-polar solvent

In consequence, the solvent system hexane/dichloromethane/ethanol/ water [6:2:4: 2] is adequate for chlorophyll separation since that will change the system to yield more polarity due to the features described above. This hypothesis is supported also by the fact that the elution mode length was 10 hours and the extrusion mode 2 hours, whereas the elution mode length with chloroform was 7 hours and the extrusion mode 4 hours.

Dichloromethane increases the elution mode and chloroform increases the extrusion mode. These conditions enable the separation of xanthophylls with higher resolution than the chlorophylls due to the decreased elution mode time in comparison with the extrusion mode in the HSCCC separation with hexane/chloroform/ethanol/water [6:2:4:2]. Solubility plays an important role in the solvent system and increase or decrease the separation depending on the affinity with the solute (chlorophylls or xanthophylls) in concordance with the polarity as well.

The novel system for HSCCC separation of chlorophylls (hexane /dichloromethane/ethanol/water [6:2:4:2]) enables the isolating of chlorophylls and their derivatives in order to accomplish the objective of this study, i.e. the degradation of chlorophylls in Baby Banana peels with hyperpigmentation.

2.2.4 Chlorophylls *a*/*b* ratio and derivatives in Baby Banana peels and other plants by HSCCC

The isolation and quantification of chlorophylls *a*/*b* and derivatives by HSCCC was successfully accomplished in different plants like spinach, grass and in fruits as Baby banana peels. Baby Banana peels were used as control and also other hyperpigmented ones with the peels displaying *stay-green* lesion. The chlorophyll *a*/*b* ratio of the different plants and fruits changed meaningfully and it was clearly reflected in the chromatograms obtained with preparative HSCCC **(cf. 4.2.3).** The elution mode used in the separation of compounds was "head to tail", the flow rate of the mobile phase was 3.5 mL/min and the wavelength 445 nm. The solvent system was hexane/EtOH/$CHCl_3$/H_2O [6:2:4:2] for

spinach and hexane/EtOH/CH_2Cl_2/H_2O [6:2:4:2] for grass and also for both Baby Banana peels (control and hyperpigmented).

On-line high performance liquid chromatography/atmospheric pressure chemical ionization mass spectrometry (APCI/positive mode) was applied to the identification of the fractions **(cf. 4.2.2) (Table 2-30)** (Huang et al. 2008).

HSCCC chromatograms revealed that grass in comparison with spinach produced degradation of chlorophylls derivatives like pheophytin *a* and *b*, whereas spinach only reflects the occurrence of chlorophyll *a* and *b* in similar proportion.

The Chl *a*/*b* ratio for spinach of 0.86 was higher than 0.58 for grass due to the higher biosynthesis of Chl-*b* in grass. Nonetheless, the Phy *a*/*b* ratio in grass of 0.63 in contrast with any yield of derivatives in spinach demonstrates that chlorophylls in spinach have a meaningful protection in their morphological and physiological structure which does not permit their degradations **(Figures 2-111, 2-112).**

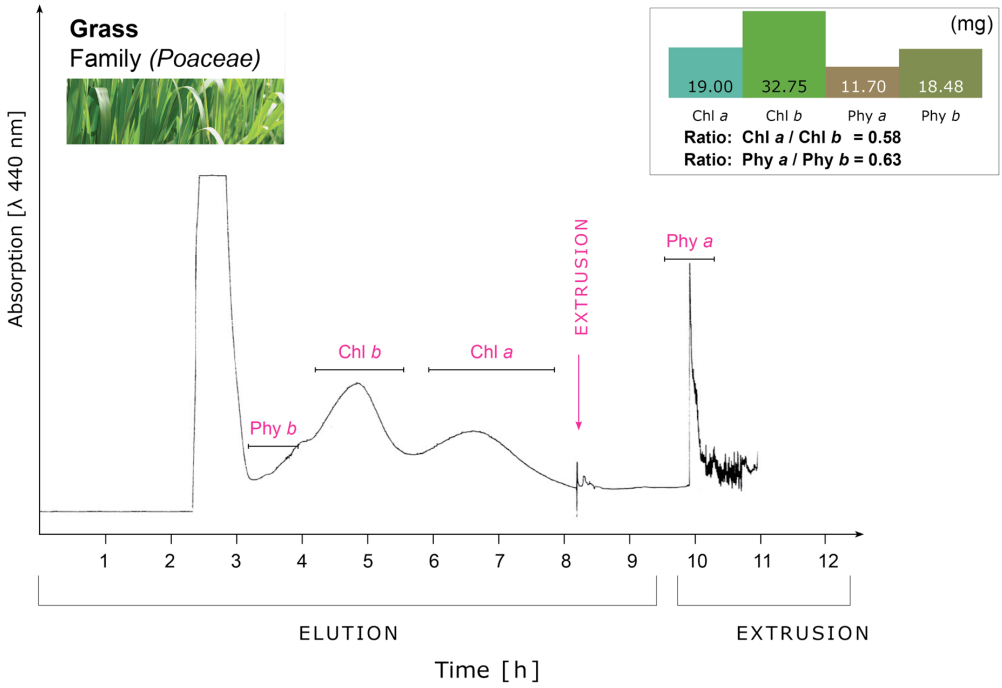

Figure 2-111. HSCCC chromatogram of chlorophylls and derivatives from grass extract using hexane/EtOH/CH_2Cl_2/H_2O [6:2:4:2] as solvent system.

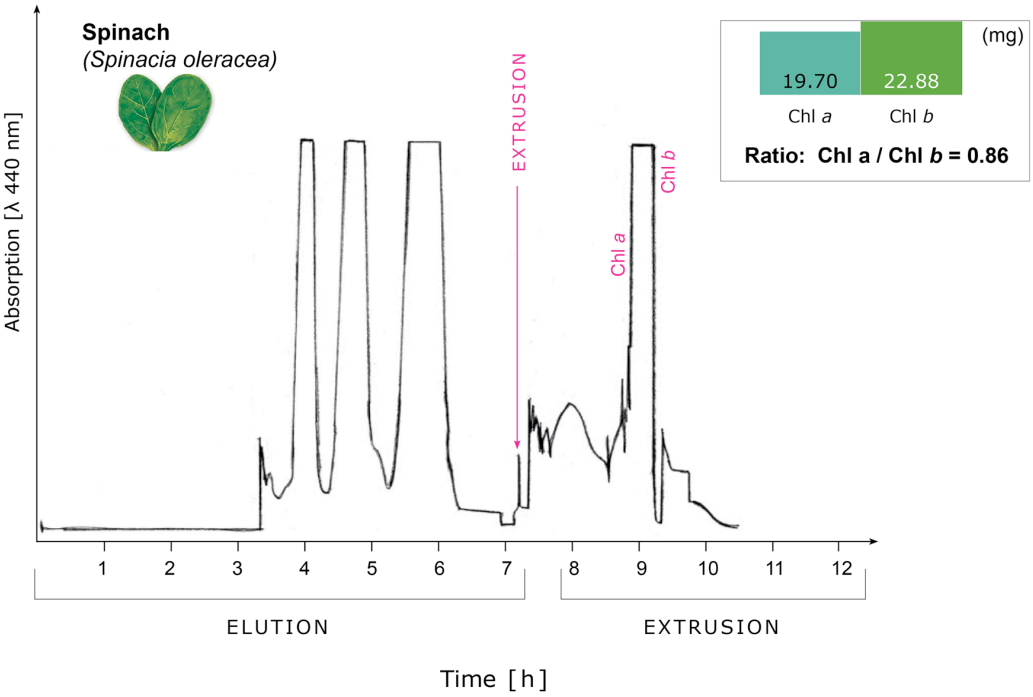

Figure 2-112. HSCCC chromatogram of chlorophylls from spinach extract by using hexane/EtOH/$CHCl_3$/H_2O [6:2:4:2] as solvent system.

Figure 2-113 depicts the separation of Chl *a*, Phy *a* and Phy *b* in Baby Banana control in extrusion mode and in elution mode chlorophyllide whereas **(Figure 2-114)** in Baby Bananas with hyperpigmentation Chl *b*, Hydroxy-Phy *b,* Phy *a* are identified in extrusion mode.

The results elicit the physiological and biochemical behaviour of chlorophylls in plants and fruits during the degradation of the pigments and consequently detected the problems during the senescence stage. According to the chlorophyll cycle of higher plants, Chl *a* and Chl *b* interconverted via 7-hydroxy Chl *a* and there are good reasons to believe that a reversal of Chl *b* biosynthesis to Chl *a* takes place (Hörtensteiner 1999).

Likewise, the disappearance of chlorophylls is a visual sign of fruit ripening and recently a variety of new fluorescent chlorophyll catabolites (FCCs) and nonfluorescent chlorophylls catabolites (NCCs) in banana peels have been detected. All NCCs of higher plant identified up to now are derived from chlorophyll *a* (Moser et al. 2012).

The difference between the Chl a/*b* and the Phy a/*b* ratios in the control and hyperpigmented banana peels could indicate that Baby Banana control used the reversal Chl-*b* biosynthesis during the degradation pathway to produce just Chl-*a* while banana with hyperpigmentation did not produce more Chl-*a* and accumulate Chl-*b* **(Figures 2-113, 2-114, 2-115).**

Table 2-30. LC-APCI-MS mass spectrum of chlorophylls, pheophytins and hydroxy-phy with $[M+H]^+$, in positive mode (Huang et al. 2008).

Analytes	**Major ions $[M+H]^+$ (*m/z*)**	**UV- maxima (nm)**
Chlorophyll *b*	907,4	465,6
Chlorophyll *a*	893,4	431,6
Pheophytin *a*	871,4	408,6
Pheophytin *b*	885,4	432,6
Hydroxy-Phy *b*	901,0	436,6

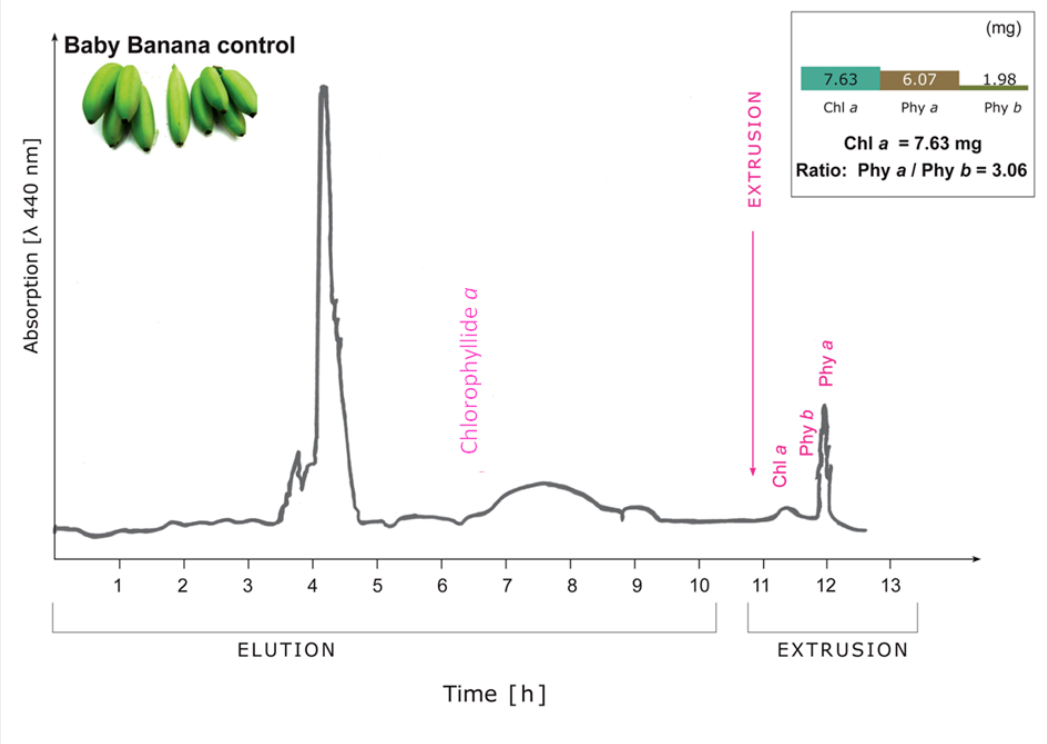

Figure 2-113. HSCCC chromatogram of chlorophylls and their derivatives from Baby Banana control peel extract using the solvent system hexane/EtOH/CH_2Cl_2/H_2O [6:2:4:2].

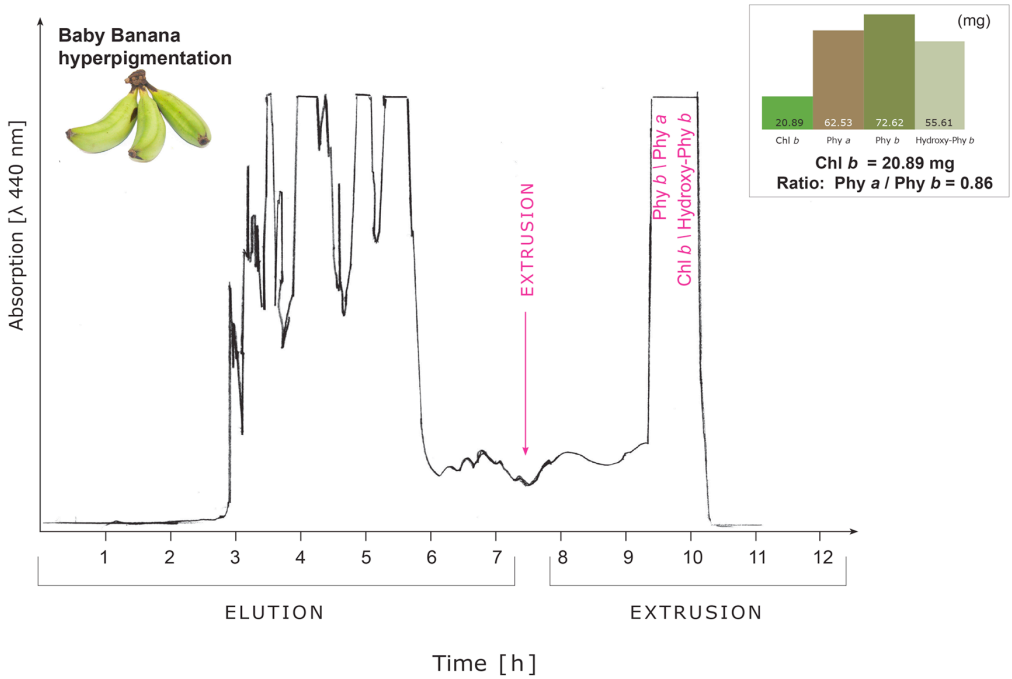

Figure 2-114. HSCCC chromatogram of chlorophylls and their derivatives from Baby Banana peel extract with hyperpigmentation using the solvent system hexane/EtOH/CH_2Cl_2/H_2O [6:2:4:2].

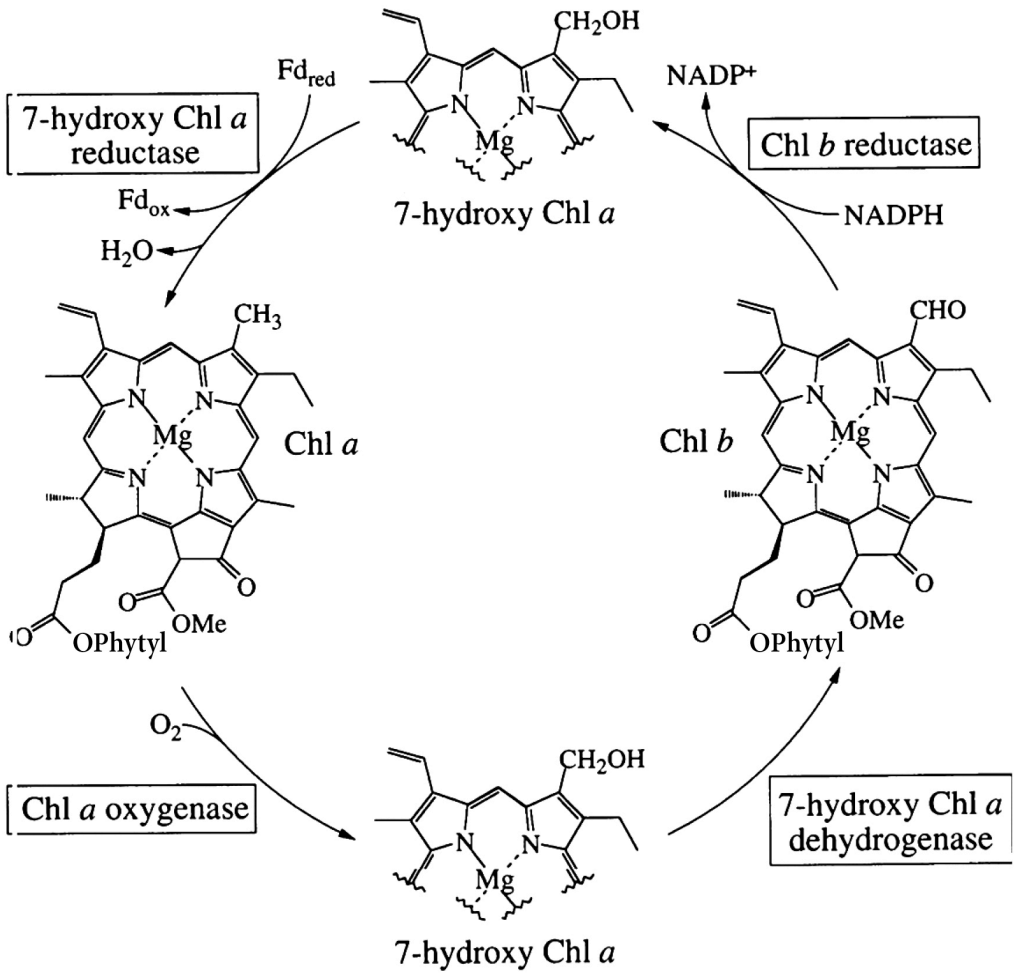

Figure 2-115. The chlorophyll cycle of higher plants, whereby Chl *a* and *b* are interconverted via 7-hydroxy Chl-*a* (Hörtensteiner 1999; Vicentini et al. 1995).

2.3 Preparative Spiral-Coil Low Speed Rotary Countercurrent chromatography of Baby Banana peels (*Musa acuminata*) with hyperpigmentation

Countercurrent chromatography is one of the few liquid chromatographic techniques that can be predictably managed from analytical to semi-industrial scale (kg range). High-Speed Countercurrent Chromatography (HSCCC) was applied to the phytochemical analysis of both Baby Banana peel control and hyperpigmented Baby Banana peel extracts.

Hyperpigmented Baby Banana (*Musa acuminata)* was harvested in Colombia, (Cundinamarca) on October 2010 through the export company Cidella localized in Bogotá. 34.92 kg of hyperpigmented Baby Banana corresponding to 771 fingers were peeled to separate the skin; the stage of ripening was green color and corresponds to a parameter nº 2, according to the established control table of ripening in the market. 3.26 kg of peels were subjected to lyophilization and 401.6 g freeze dried peels were transported to Germany **(Figure 2-116).**

Figure 2-116. 34.92 kg of hyperpigmented Baby Banana produced 401.6 g freeze-dried peels that were analyzed by Spiral-Coil-LSRCCC.

The freeze-dried peels were washed three times, first with hexane, and afterward with methanol, to obtain a liquid extract of compounds in non-polar and

polar phases **(cf. 4.3.1).** After the extraction 17 g of hexane phase and 4.5 g of methanol phase were recollected to be used in further experiments.

The spiral-coil low speed rotary countercurrent chromatography is a versatile and gentle all-liquid-partition chromatographic method used for several applications in natural product isolation. The prototype has become a powerful tool for enrichment and isolation of target compounds in large quantities and consists of three spiral layers connected in series with a total volume of 500 mL. The column is composed of a convoluted PTFE tubing (8.5 mm I. D) of 9.7 m length. The assembly is mounted onto a seal-less flow-through centrifuge, which is operated by a speed control unit. The pitch of the spiral is ca. 3.7 cm. The spiral starts at 6.7 cm and ends at 22 cm from the center of rotation, forming nearly four spiral turns. A pair of flow tubes (standard–wall 0.85 mm ID Teflon tubing) from each terminal of the spiral column is led through the central axis of the apparatus, supported by a hollow plastic guide pipe, and then rigidly held at the stationary exit spot. The rotary speed of the column was regulated with a speed control unit. The solvents were delivered by a HPLC pump/Waters, model 515, Milford, MA. (Köhler et al. 2004) **(Figure 2-117).**

Figure 2-117. Spiral-Coil Assembly of the CCC prototype that combines two advantages in comparison with the Low Speed Rotary Countercurrent chromatography such as short separation time and large sample load. It is a preparative model for semi-industrial scale separations.

To fractionate 17 g of the hexane phase extract from Baby Banana freeze-dried peels the solvent system acetonitrile/methanol (1:1, v/v) prepared by saturating each phase in a separatory funnel at room temperature was used. The solvents were degassed directly before use. Elution and extrusion modes were performed during the scale-up separation.

On-line high performance liquid chromatography/atmospheric pressure chemical ionization mass spectrometry was applied to the analysis of the fractions by means of the mass spectra in positive (+) mode **(cf. 4.2.2).** The method can be applied to analyze natural chlorophyll degradation products and other metalloporphyrines (Gauthier-Jaques et al. 2001, Verzegnassi et al. 2000).

The solvents for HPLC were **(cf. 4.2.2.4)**:
A: MTBE/MeOH/H_2O 4/92/4 (v/v/v)
B: MTBE/MeOH/H_2O 90/6/4/ (v/v/v)

A RP-18 column (ProntoSIL $C_{18}A_9$ 250 x 2 mm) was used at a flow rate of 0.8 mL/min. Gas was nitrogen with a flow rate of 7.0 mL/min. Temperature of APCI: 400 °C. ESI-MS parameters: capillary, 4500 V; cap, 2800 V. The solvent elution changed to 100% A, 0%B in 0 min, 100% A, 0%B in 10 min, 50% A, 50% B in 20 min, 0% A, 100%B in 30 min, 0% A, 100%B in 50 min, 100% A, 0%B in 55 min **(cf. 4.2.2.4).**

Spiral-Coil LSRCCC separated 17g of hexane extract from Baby Banana peel with hyperpigmentation and 18 fractions were collected during the separation, in which 11 fractions are corresponding to elution mode and 7 to extrusion mode.**(cf. 4.2.5)** The chromatogram is shown in **Figure 2-118.**

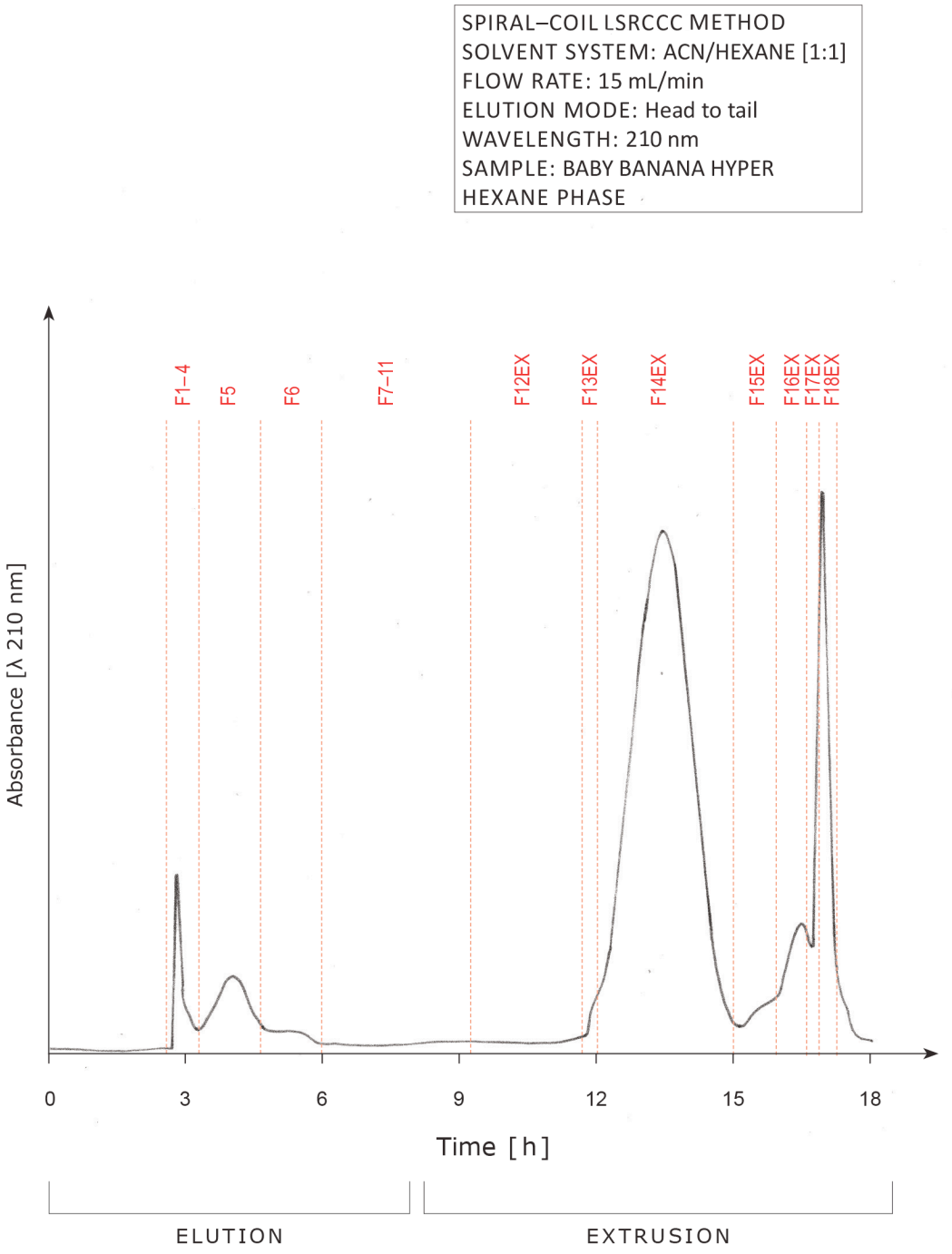

Figure 2-118. Spiral-Coil LSRCCC chromatogram of 10 g of a hexane extract from Baby Banana peels with hyperpigmentation (HP) in elution and extrusion mode.

In spite that the chromatogram does not depict peaks which could represent an optimal separation, chlorophyll derivatives were identified by APCI-HPLC - MS-MS. Additional compounds were identified subsequently in comparison with authentic standards separated by HSCCC.

It should be mentioned that the experiment above was carried out before the optimization of the solvent system to isolate the chlorophylls, described in section 2.2. Therefore, the parameters of the separation corresponded to the initial trials of experiments.

Nevertheless, the results are relevant in relation with the identification of chlorophyll derivatives in Baby Banana peels with hyperpigmentation by means of Spiral-Coil (LSRCCC) **(Figure 2-119).**

2.3.1 APCI-HPLC-MS-MS analysis of Spiral-Coil-LSRCCC fractions from Baby Banana peels with hyperpigmentation

Spiral-Coil-LSRCCC separated 17g of hexane extract of Baby Banana peel with hyperpigmentation and 18 fractions were obtained. Chlorophyll derivatives were fractionated according the polarity. In elution mode, hydroxypheophytin *b,* pheophytin *b*, hydroxypheophytin *a*, pyropheophorbide *a* ester $C_{(27\text{-}30)}$ sterols (*m* or *l)* and pheophytin *a.* Additionally, in extrusion mode pyropheophytin *a*, pyropheophorbide *a* ester C_{29} sterol *l,* Zn pheophytin *a* were identified by APCI-HPLC-MS-MS **(Tables 2-31, 2-32, Figure 2-119).**

Furthermore, lutein, linoleic acid and several chlorophyll derivatives (hydroxypheophytin *a* and *b,* pheophytin *a* and *b)* were elucidated by 1D/2D-NMR experiments (^{1}H, ^{13}C, $^{1}H/^{1}H$-COSY, HSQC, HMBC) **(cf. 4.2.6).**

Phosphatidylcholine, O-α-D-galactosyl-glucosyl-diacy-L-glycerol (GGGD), lutein and arachidic acid (20:0) were identified according to the results described in section 2.1, in which the isolation and elucidation of phospholipids and glycolipids from Baby Banana peels (control) has been described.

The chemical structure of the chlorophyll derivatives are depicted in concordance with the literature **(Figure 2-120)**. The understanding of the changes in the chemical structure of the chlorophyll gives clues for the analysis of the hyperpigmentation phenomenon in Baby Banana peels. The summary of the compounds fractionated in scale-up Spiral-Coil-LSRCCC from Baby Banana peels with hyperpigmentation (HP) is given in **Tables 2-31, 2-32.**

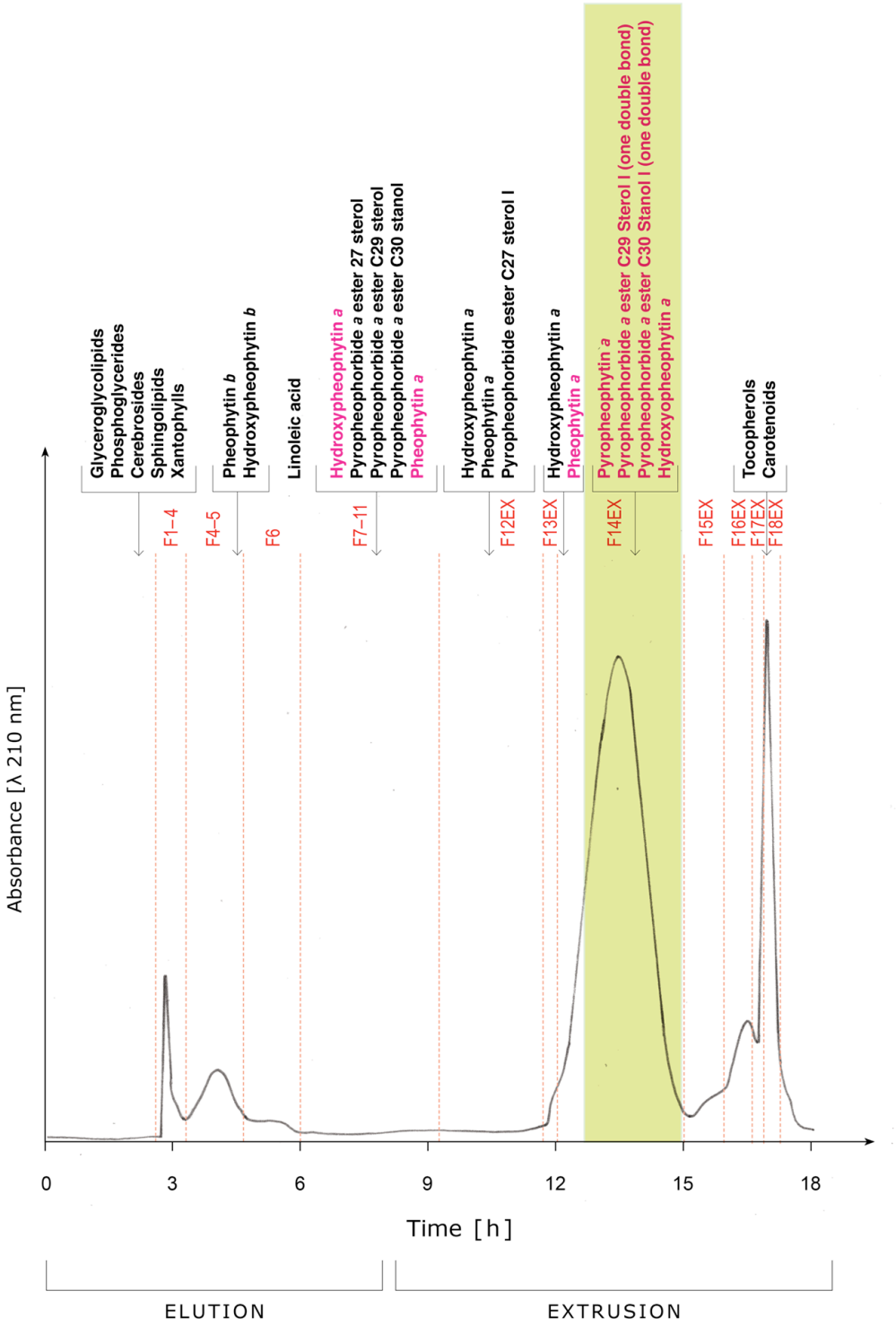

Figure 2-119. Spiral-Coil LSRCCC chromatogram of 17 g from Baby Banana peels with hyperpigmentation (HP). The fractions were identified by means of APCI-HPLC-MS-MS as chlorophylls derivatives (red color). The green bands depict the chlorophyll derivatives linked to sterols. The mass spectra of the fractions were compared with literature data (Huang et al. 2008; Eckardt et al. 1991; van Breemen 1991ab).

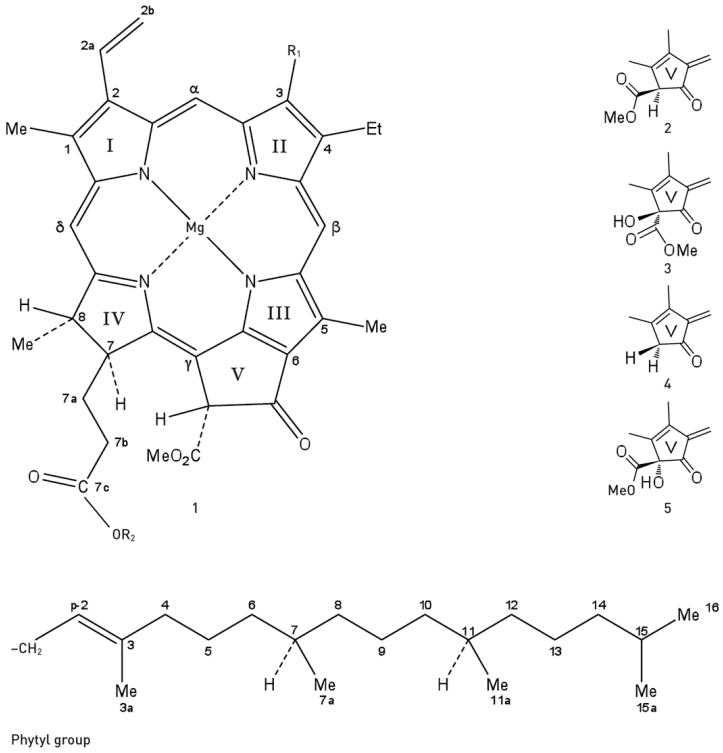

Compound	**Mg***	**R_I**	**R_2**	**Isocycling Ring (V)**
Chlorophyll *a*	+	CH3	Phytyl	1
Chlorophyll *b*	+	CHO	Phytyl	1
Chlorophyll *a'*	+	CH3	Phytyl	2
Chlorophyll *b'*	+	CHO	Phytyl	2
Hydroxypheophytin a	–	CH3	Phytyl	3
Hydroxypheophytin *a'*	–	CH3	Phytyl	5
Pheophytin *a*	–	CH3	Phytyl	1
Pheophytin *a'*	–	CH3	Phytyl	2
Hydroxypheophytin *b*	–	CHO	Phytyl	3
Hydroxypheophytin *b'*	–	CHO	Phytyl	5
Pheophytin *b*	–	CHO	Phytyl	1
Pheophytin *b'*	–	CHO	Phytyl	2
Hydroxychlorophyll *a*	+	CH3	Phytyl	3
Hydroxychlorophyll *b*	+	CHO	Phytyl	3
Pyropheophytin a	–	CH3	Phytyl	4

*Mg is represented by 2H in pheophytins.

Figure 2-120. Nomenclature of chlorophylls and their derivatives (Huang et al. 2008; Katz et al. 1968).

Table 2-31. Molecular ions and mass fragments (*m/z*) in (+) mode of the compounds identified in Baby Bananas peels (HP) in elution mode fractions from Spiral-Coil-LSRCCC separation by APCI-HPLC-MS-MS.

ELUTION MODE			**REFERENCES**
SPIRAL-COIL-LSRCCC **HEXANE PHASE** **BABY BANANA WITH HYPERPIGMENTATION (HP)** **Fractions (mg)**	**Compound**	**APCI$^{[+]}$ molecular ion peak $[M+H]^+$** /Main fragment ions/ **(*m/z*)**	**APCI$^{[+]}$ molecular ion peak $[M+H]^+$reported** **(*m/z*)**
1 (19.9)	Phosphati–dylcholine*****	**[751.5]$^+$** /663 / 495.3	[780]$^+$ Klein 1971 Ismaiel et al. 2008 Subagio and Morita 1997 Yang et al. 2009
2 (8.32)	All-E lutein***** GGDG* Arachidic acid*****	**[551]$^+$** /533.4 [**976]$^+$** 419 / 250 **[295]$^+$** 277/ 195	[551]$^+$ Molnár et al. 2006 Putzbach et al. 2005ab Aman et al. 2005a Yamauchi 2005 Jakab et al. 2002 Holčapek et al. 2003 Happi Emaga et al. 2007
3 (154.71)	All-E lutein	**[551]$^+$** /533.5	[551]$^+$ Molnár et al. 2006 Putzbach et al. 2005ab Aman et al. 2005a
4 (27.5)	Hydroxy-pheophytin *b*	**[902.1]$^+$** /623.2	[901]$^+$ Huang et al. 2008
5_1 (83.95)	Hydroxy-pheophytin *b* Pheophytin *b* fatty acid Linoleic acid*****	**[902]$^+$** /623.2 **[885.6]$^+$** /607.2 **[279.2]$^+$** /243	[901]$^+$ Huang et al. 2008 [884.7]$^+$ van Breemen et al. 1991ab [278.43]$^+$ Happi Emaga et al. 2007

*Compounds isolated and elucidated (section 2.1 Phytochemical profile of Baby Banana Peels).

Table 2-31. Cont.

ELUTION MODE			**REFERENCES**
SPIRAL-COIL-LSRCCC **HEXANE PHASE** **BABY BANANA WITH HYPERPIGMENTATION (HP)** **Fractions (mg)**	**Compound**	**APCI$^{[+]}$ molecular ion peak $[M+H]^+$** /Main fragment ions/ **(*m/z*)**	**APCI$^{[+]}$ molecular ion peak $[M+H]^+$reported** **(*m/z*)**
5_2 (106.53)	Hydroxy-pheophytin *b* Pheophytin *b* Linoleic acid*****	**[902]$^+$** /623.2 **[885.6]$^+$** /607.2 **[279.2]$^+$** /243.2	[901]$^+$ Huang et al. 2008 [884.7]$^+$ van Breemen et al. 1991ab [278.43]$^+$ Happi Emaga et al. 2007
5_3 (1525.18)	Pheophytin *b* Glycosyldiacyl-glycerolipids	**[885.6]$^+$** /607.2 /[419]$^+$	[884.7]$^+$ van Breemen et al. 1991ab Benning et al. 1995 Yamauchi et al. 2001
6 (75.45)	Linoleic acid*****	**[279.2]$^+$** /243.1	[278.43]$^+$ Jakab et al. 2002 Holčapek et al. 2003 Happi Emaga et al. 2007
7 (69.75)	Hydroxy-pheophytin *a*	**[887.9]$^+$** /609.2	[887]$^+$ Huang et al. 2008
8 (40.32)	Hydroxy-pheophytin *a*	**[887.9]$^+$** /609.2	[887]$^+$ Huang et al. 2008

*Compounds isolated and elucidated (section 2.1 Phytochemical profile of Baby Banana Peels).

Table 2-31. Cont.

ELUTION MODE	**REFERENCES**	**ELUTION MODE**	**REFERENCES**
SPIRAL-COIL- LSRCCC **HEXANE PHASE** **BABY BANANA WITH HYPERPIGMENTATION (HP)** **Fractions (mg)**	**Compound**	**APCI$^{[+]}$ molecular ion peak $[M+H]^+$** /Main fragment ions/ **(*m/z*)**	**APCI$^{[+]}$ molecular ion peak $[M+H]^+$reported** **(*m/z*)**
9 (36.19)	Hydroxy-pheophytin *a*	**[887.9]$^+$** /609.2	[887]$^+$ Huang et al. 2008
	Pyropheo-phorbide *a* ester C_{29} sterol *m*	**[929.7]$^+$**	[928]$^+$ Eckardt et al. 1991
	Pyropheo-phorbide a ester C_{27} sterol *l*	**[903.6]$^+$**	[902]$^+$ Eckardt et al. 1991
	Pyropheo-phorbide *a* ester C_{30} stanol	**[945.7]$^+$**	[946]$^+$ Eckardt et al. 1991
10 (23.86)	Hydroxy-pheophytin *a*	**[887.9]$^+$** /609.2	[887]$^+$ Huang et al. 2008
	Tocopherols	**[419]$^+$**	[431]$^+$ [417]$^+$ [403]$^+$ Lampi et al. 2008, Ryynänen et al. 2004
	Pyropheo-phorbide *a* ester C_{30} stanol	**[945.7]$^+$**	[946]$^+$ Eckardt et al. 1991

*Compounds isolated and elucidated (section 2.1 Phytochemical profile of Baby Banana Peels).

Table 2-31. Cont.

ELUTION MODE	**REFERENCES**	**ELUTION MODE**	**REFERENCES**
SPIRAL-COIL-LSRCCC **HEXANE PHASE** **BABY BANANA WITH HYPERPIGMENTATION (HP)** **Fractions (mg)**	**Compound**	**APCI$^{[+]}$ molecular ion peak $[M+H]^+$** /Main fragment ions/ **(*m/z*)**	**APCI$^{[+]}$ molecular ion peak $[M+H]^+$reported** **(*m/z*)**
11 (100.96)	Pheophytin *a** Hydroxy–pheophytin *a* Pyropheo–phorbide *a* ester C_{27} sterol *I* Tocopherols	**[871.5]$^+$** /594 **[887.9]$^+$** /609.2 **[903.6]$^+$** **[419]$^+$**	[870.5/592.5]$^+$ van Breemen et al. 1991ab [871.5 /594]$^+$ Gauthier-Jaques et al. 2001 [887]$^+$ Huang et al. 2008. [902]$^+$ Eckardt et al. 1991 (Actually in NMR analysis) [425]$^+$ [411]$^+$ [397]$^+$ Lampi et al. 2008, Ryynänen et al. 2004

*Compounds isolated and elucidated (section 2.1 Phytochemical profile of Baby Banana Peels).

Table 2-32. Molecular ions and mass fragments (*m/z*) in (+) mode of the compounds identified in Baby Bananas peels (HP) in extrusion mode from Spiral-Coil- LSRCCC separation by APCI-HPLC-MS-MS.

EXTRUSION MODE			**REFERENCES**
SPIRAL-COIL-LSRCCC **HEXANE PHASE** **BABY BANANA WITH HYPERPIGMENTATION (HP)** **Fractions (mg)**	**Compound**	**APCI$^{[+]}$ molecular ion peak $[M+H]^+$** /Main fragment ions/ **(*m/z*)**	**APCI$^{[+]}$ molecular ion peak $[M+H]^+$reported** **(*m/z*)**
12 EX (12.80)	Hydroxy–pheophytin *a*	**$[887.9]^+$** /609.2	$[887]^+$ Huang et al. 2008
	Pheophytin *a**	**$[871.5]^+$** /594	$[870.5/592.5]^+$ van Breemen et al. 1991ab $[871.5/594]^+$ Gauthier-Jaques et al. 2001 (Actually in NMR analysis)
	Pyropheophor-bide a ester C_{27} sterol *I*	**$[903.6]^+$**	$[902]^+$ Eckardt et al. 1991
	Tocopherols and Tocotrienols	**$[419]^+$**	$[431]^+$ $[417]^+$ $[403]^+$ $[425]^+$ $[411]^+$ $[397]^+$ Lampi et al. 2008, Ryynänen et al. 2004 Ohnmacht et al. 2008
	Triterpene alcohol and sterols ferulates	**$[615]^+$** **$[597]^+$**	Fang et al. 2003. Liu et al. 2013 Angelis et al. 2011
13 EX (7.24)	Hydroxypheo–phytin *a*	**$[887.9]^+$** /609.2	$[887]^+$ Huang et al. 2008
	Pheophytin *a**	**$[871.5]^+$** /594	$[870.5/592.5]^+$ van Breemen et al. 1991ab $[871.5/594]^+$ Gauthier-Jaques et al. 2001

Table 2-32. Cont.

	Pyropheophorbide a ester C_{27} sterol *I*	**[903.6]$^+$**	[902]$^+$ Eckardt et al. 1991
	Tocopherols and Tocotrienols	**[419]$^+$**	[431]$^+$ [417]$^+$ [403]$^+$ [425]$^+$ [411]$^+$ [397]$^+$ Lampi et al. 2008 Ryynänen et al. 2004 Ohnmacht et al. 2008
14 EX (697.74)	Tocopherols Tocotrienols	**[419]$^+$**	[431]$^+$ [417]$^+$ [403]$^+$ [425]$^+$ [411]$^+$ [397]$^+$ Lampi et al. 2008 Ryynänen et al. 2004 Ohnmacht et al. 2008
	Cycloartenol ferulate	**[599.5]$^+$**	Fang et al. 2003 Lui et al. 2013 Angelis et al. 2011
	24-hydroxy-24-methylcylcoartenol transferulate	**[617]$^+$**	Fang et al. 2003 Liu et al. 2013 Angelis et al. 2011
15 EX (366.96)	Pyropheophytin *a*	**[814.2]$^+$**	[813.8]$^+$ Gauthier-Jaques et al. 2001
	Zn pheophytin *a*	**[934.3]$^+$**/ 635.5	[933]$^+$ Gauthier-Jaques et al. 2001
	Tocotrienols and tocopherols	**[419]$^+$**	[431]$^+$ [417]$^+$ [403]$^+$ [425]$^+$ [411]$^+$ [397]$^+$ Lampi et al. 2008 Ryynänen et al. 2004 Ohnmacht et al. 2008
16 EX (172.45)	4-epicyclo-eucalenone* 4-epicyclo-musalenone*	**[425]$^+$**	[425]+ Oliveira et al. 2006 Akihisa et al. 1986 Knapp and Nicholas, 1969ab, 1970ab, 1971ab
17 EX (97.45)	Zn pyropheophytin *a*	**[875.7]$^+$**	[875.5]$^+$ Gauthier-Jaques et al. 2001
18 EX (865.47)	Unidentified carotenoids		

*Compounds isolated and elucidated (section 2.1 Phytochemical profile of Baby Banana Peels).

The results summarized in the **Tables 2-31 and 2-32** describe how the Spiral-Coil-LSRCCC separates complex mixtures into fractions containing compounds with decreasing polar character. At the beginning of the elution polar compounds such as phospholipids, glycolipids and xanthophylls and also polar chlorophyll derivatives were identified. After three hours pheophytin *b* and hydroxypheophytin *b* were eluted. Other compounds (less polar) were identified between the elution and extrusion mode and were identified as linoleic acid, hydroxypheophytin *a*, pheophytin *a* and pheophorbide *a* esterified with sterols. The extrusion mode shows unpolar compounds, like 4-epicyclo-eucalenone and 4-epicyclo-musalenone. The sterols bound to pheophorbide *a* were eluted together with the carotenoids.

Chlorophyll derivatives are clearly separated in the fractions of elution and extrusion mode. Pheophytin *b* with an aldehyde group at C-3_a accounts for the polar effects in the molecule. Contrary, the unpolar pheophytin *a*, with a methyl group at C-3_a is separated between elution and extrusion mode. In addition, the hydroxypheophytin *a* and *b* eluted before of pheophytins due to the hydroxyl group linked to β-keto esters system **(Figure 2-119).**

2.3.2 Identification of polar compounds in Spiral-Coil-LSRCCC

The first fraction of 19.9 mg corresponded to 1,2 diacyl-phosphorylcholine in elution mode **(Figure 2-121).** The mass spectra showed a single peak at 18.4 min with a strong fluorescence at 200 nm corresponding at *m/z* 751 and identified as a molecular peak with a daughter peak at *m/z* 663. The thin layer chromatography and the mass spectra were compared with the standard isolated by HSCCC in section 2.1 **(Figure 2-122).**

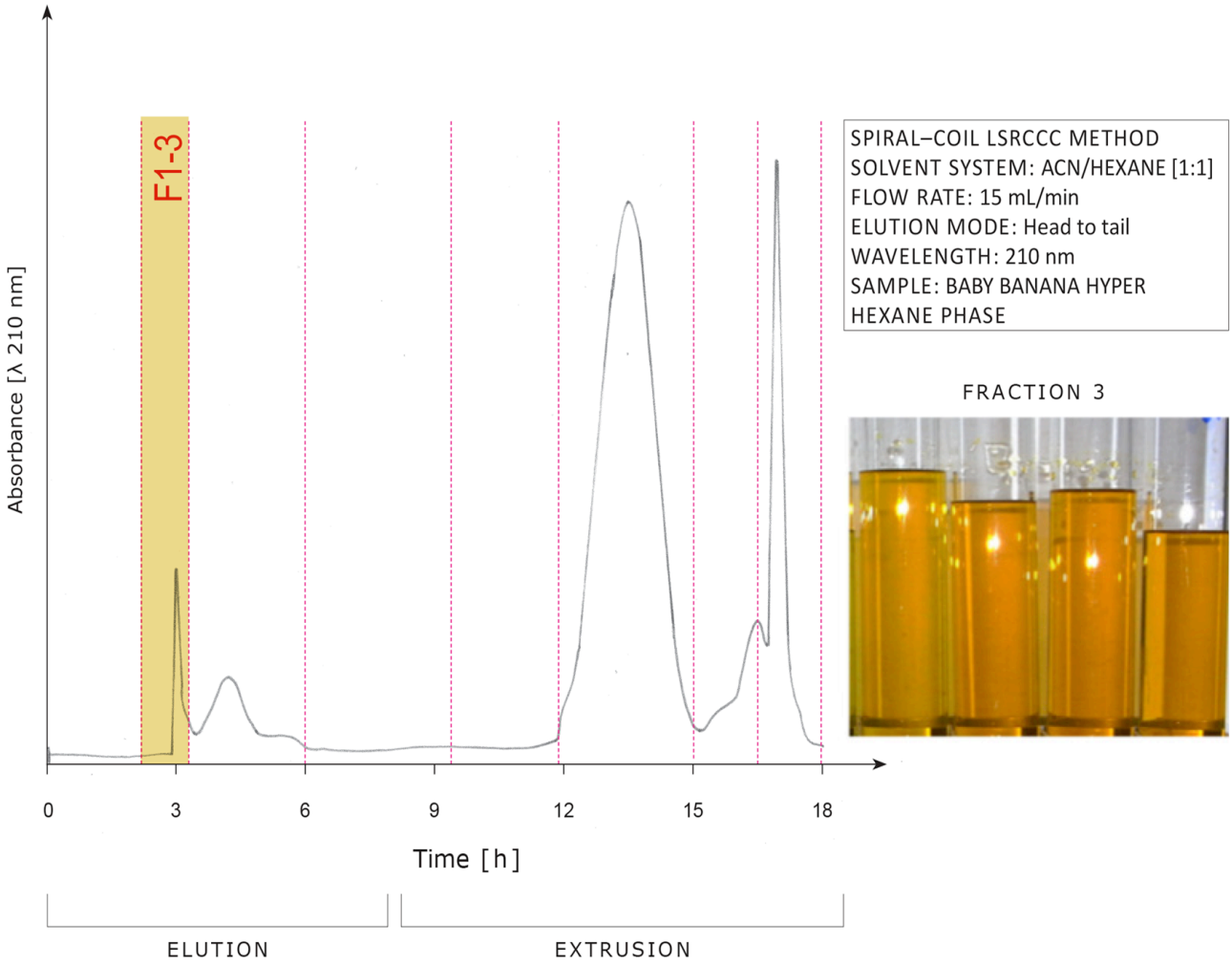

Figure 2-121. Fraction 1 of elution mode corresponds to 19.9 mg of 1,2 diacyl-phosphorylcholine and fraction 3 to 154.7 mg of lutein in Spiral-Coil-LSRCCC chromatogram (Left), which were identified by comparison with authentic standards isolated by HSCCC. Tubes of Spiral-Coil-LSRCCC of 154.7 mg of lutein in elution mode identified by APCI -HPLC-MS-MS (Right).

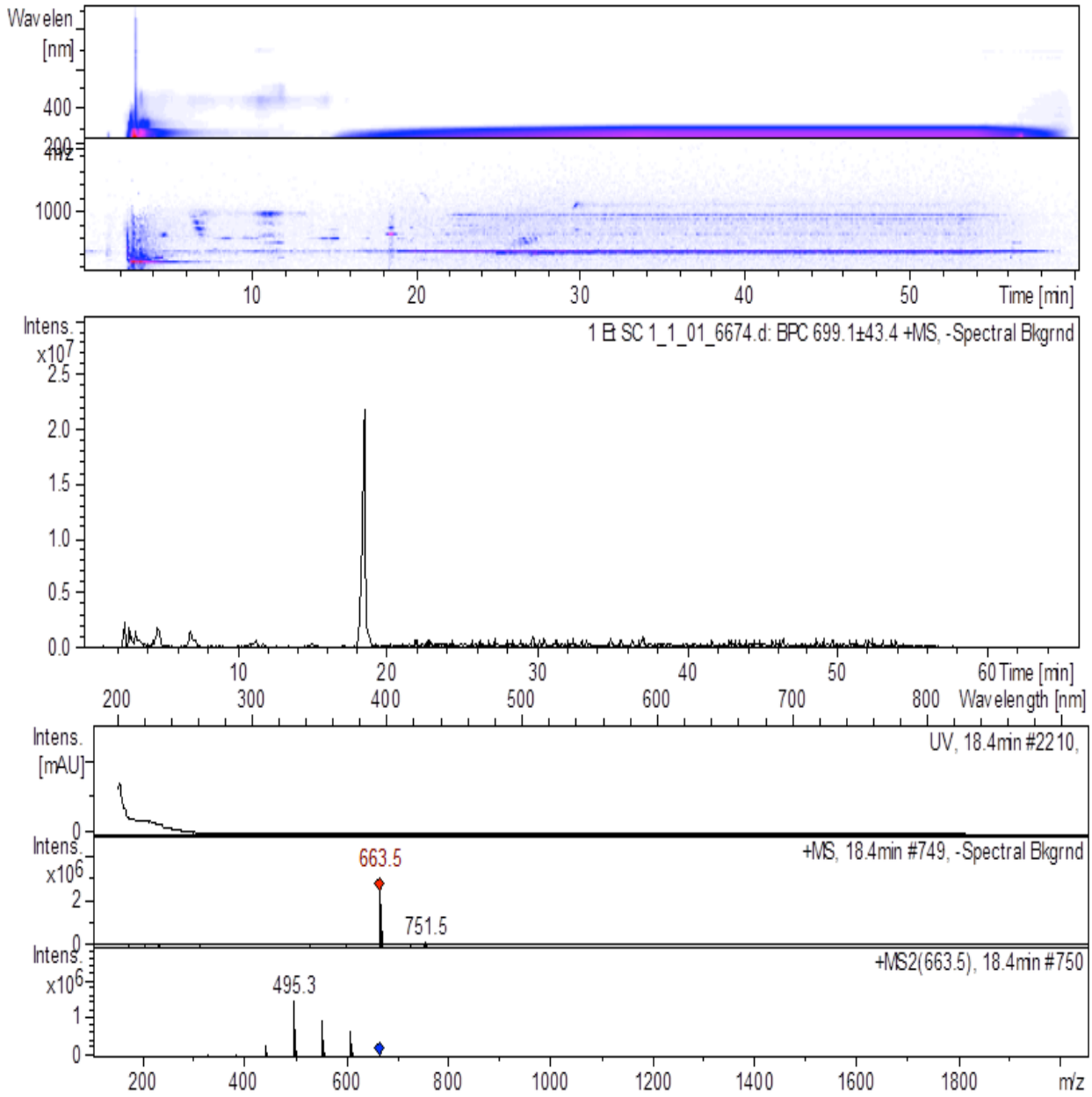

Figure 2-122. Positive-ion APCI HPLC-MS-MS spectrum of 1,2 diacyl-phosphorylcholine in fraction 1 from elution mode obtained by Spiral-Coil-LSRCCC from Baby Banana peels with hyperpigmentation.

.

Furthermore, fraction 3 in elution mode corresponded to 154.7 mg of lutein, and was identified by APCI-HPLC-MS-MS at *m/z* 551.4 as a molecular peak. The fragmentation is in concordance with the isolated standard of lutein by HSCCC, which is described in section 2.1 **(Figure 2-123).**

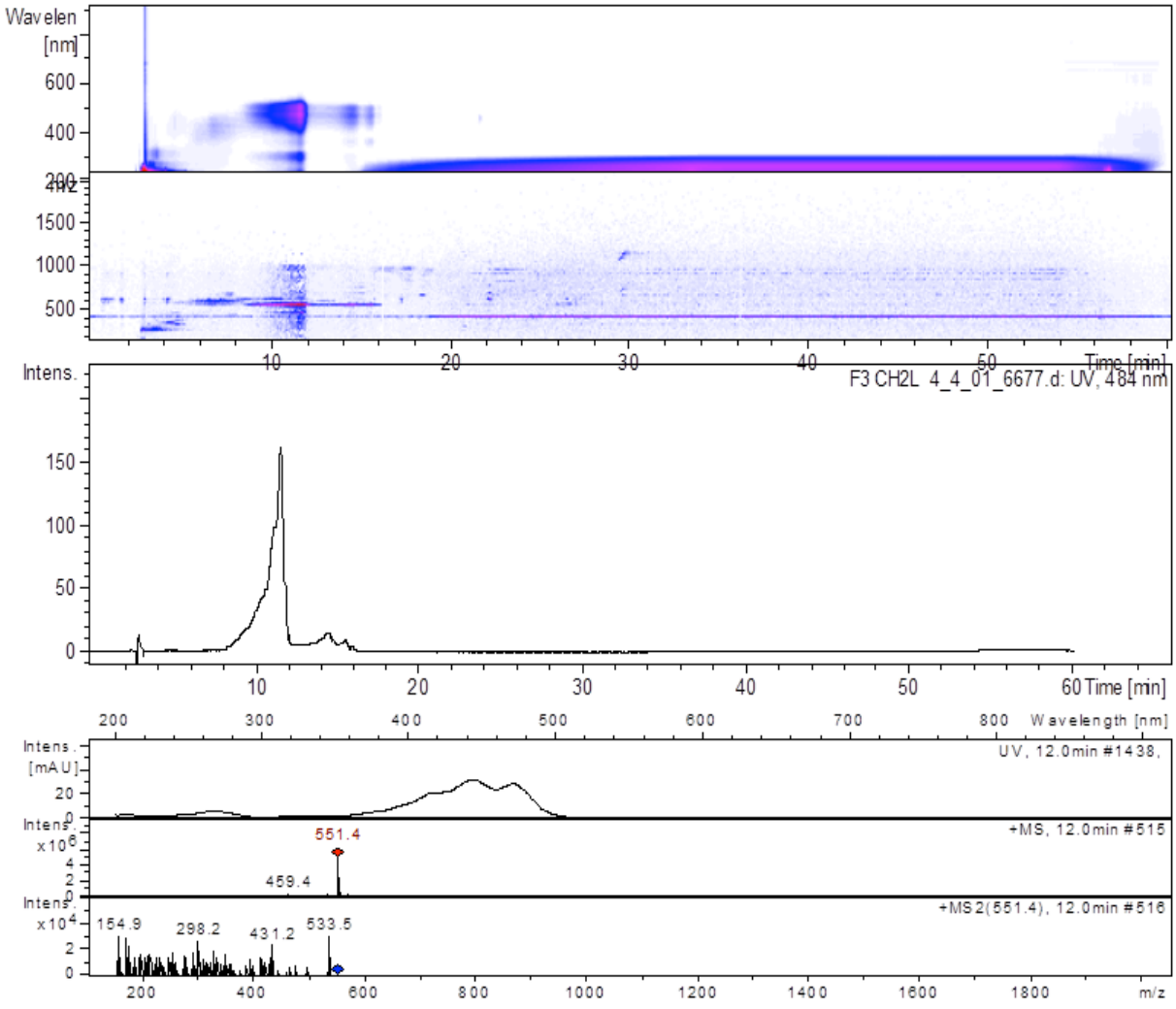

Figure 2-123. Positive-ion APCI HPLC-MS-MS spectrum of lutein (*m/z* 551.4) in fraction 3 of elution mode from Spiral-Coil-LSRCCC (Yuan et al. 1997).

2.3.3 Identification of chlorophyll derivatives esterified with sterols in Spiral-Coil-LSRCCC

During the elution mode the polar compounds eluted whereas during the extrusion mode mainly the nonpolar compounds are separated. Nevertheless, there is an intermediate zone in the chromatogram that shows how some compounds with a polar and unpolar component in the chemical structure are fractionated by application of the system ACN/Hexane [1:1] **(Figure 2-127).** The most relevant identification of components in this zone has relation with derivates of chlorophyll esterified with sterols as well as hydroxypheophytin *a* and pheophytin *a.* The APCI-HPLC-MS-MS spectrum confirmed pyropheoborbide *a* ester 27 sterol *l,* 29 sterol *m* and 30 stanol between fraction 9-11 (of elution) **(Table 2-31; Figures 2-124, 2-125, 2-126, 2-127).**

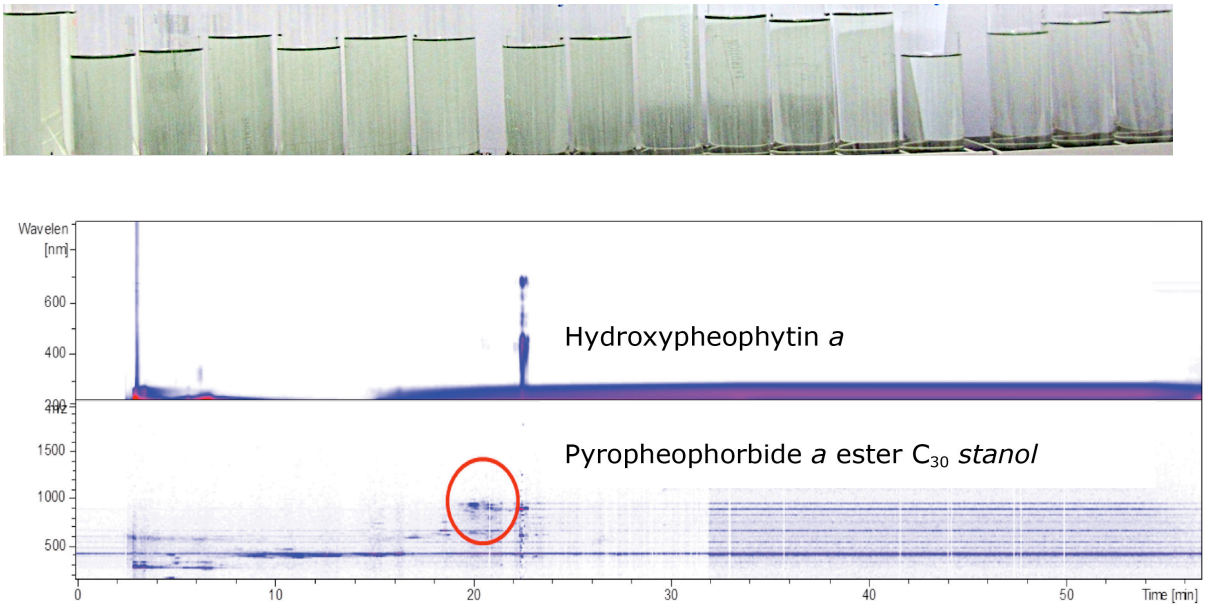

Figure 2-124. UV-Contour plot of APCI-HPLC- MS-MS of fraction 9. Hydroxypheophytin *a* is identified as a fluorescent compound in contrast to pyropheophorbide *a* ester C_{30} stanol pointed out with a red circle without fluorescence (below). Tubes of Spiral Coil-LSRCCC separation corresponding to fraction 9 (above).

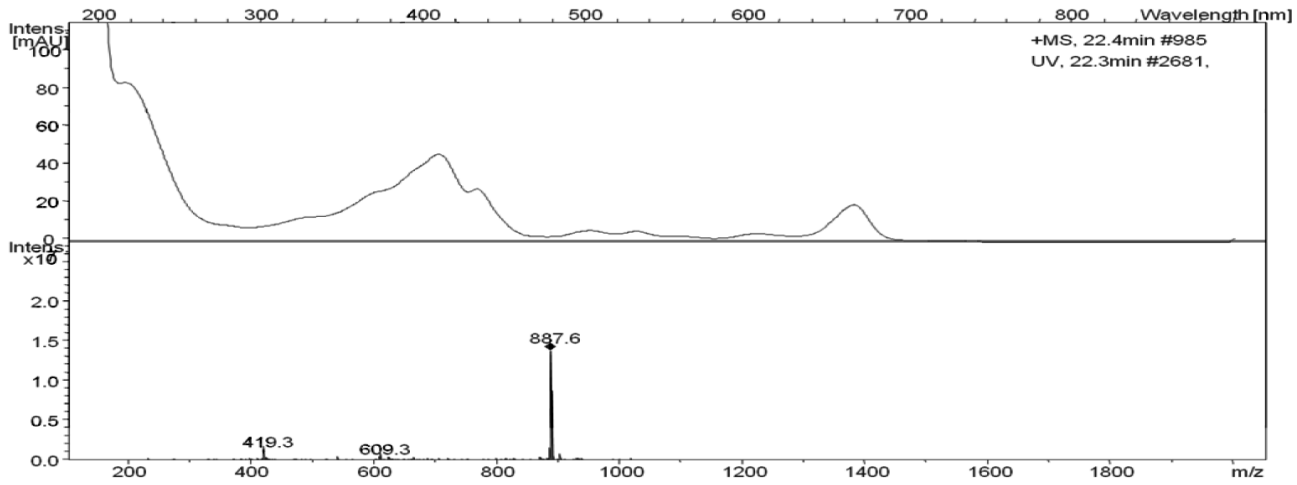

Figure 2-125. Positive-ion APCI mass spectrum of hydroxypheophytin *a* at m/z 887.6 in fraction 9 of elution mode in Spiral-Coil- LSRCCC (Huang et al. 2008).

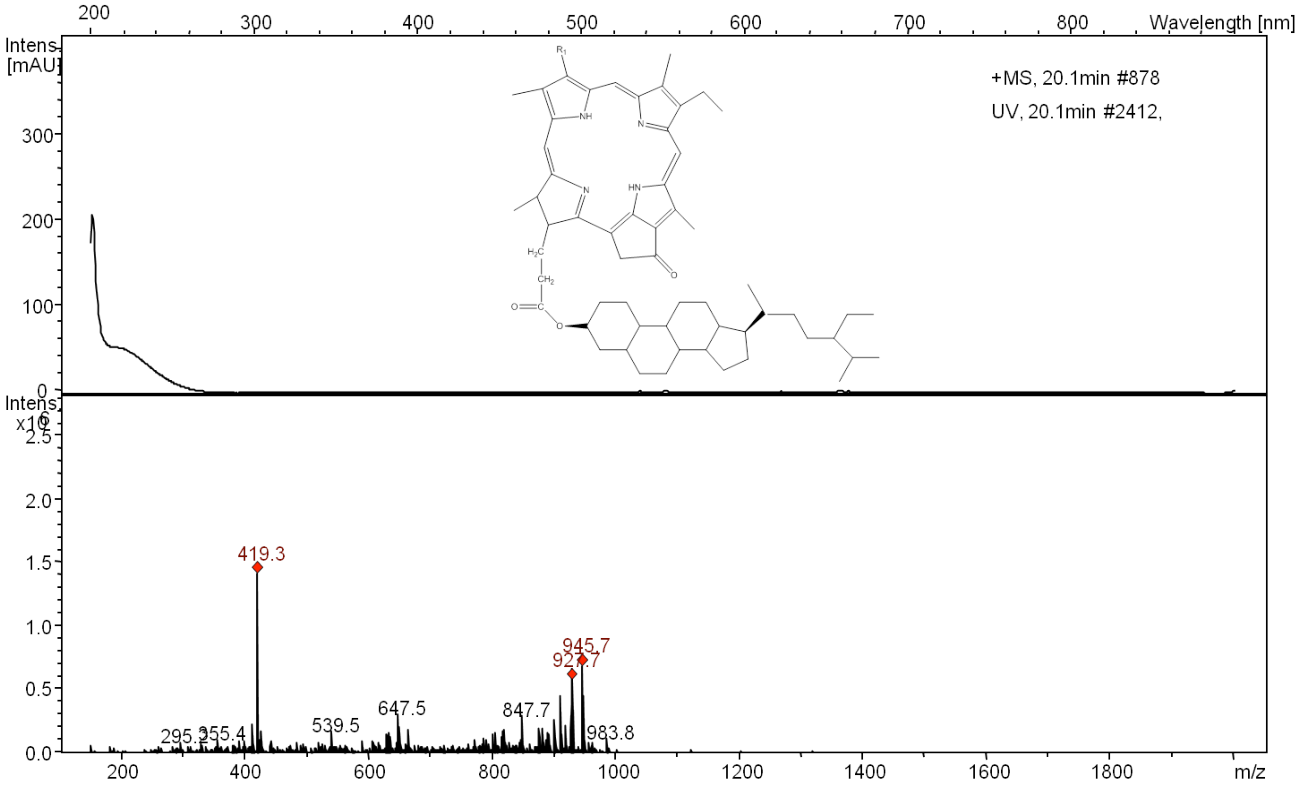

Figure 2-126. Positive-ion APCI mass spectrum of pyropheophorbide *a* ester C $_{30}$ stanol *a* at *m/z* 945.7 in fraction 9 of elution mode in Spiral-Coil-LSRCCC (Eckardt et al. 1991).

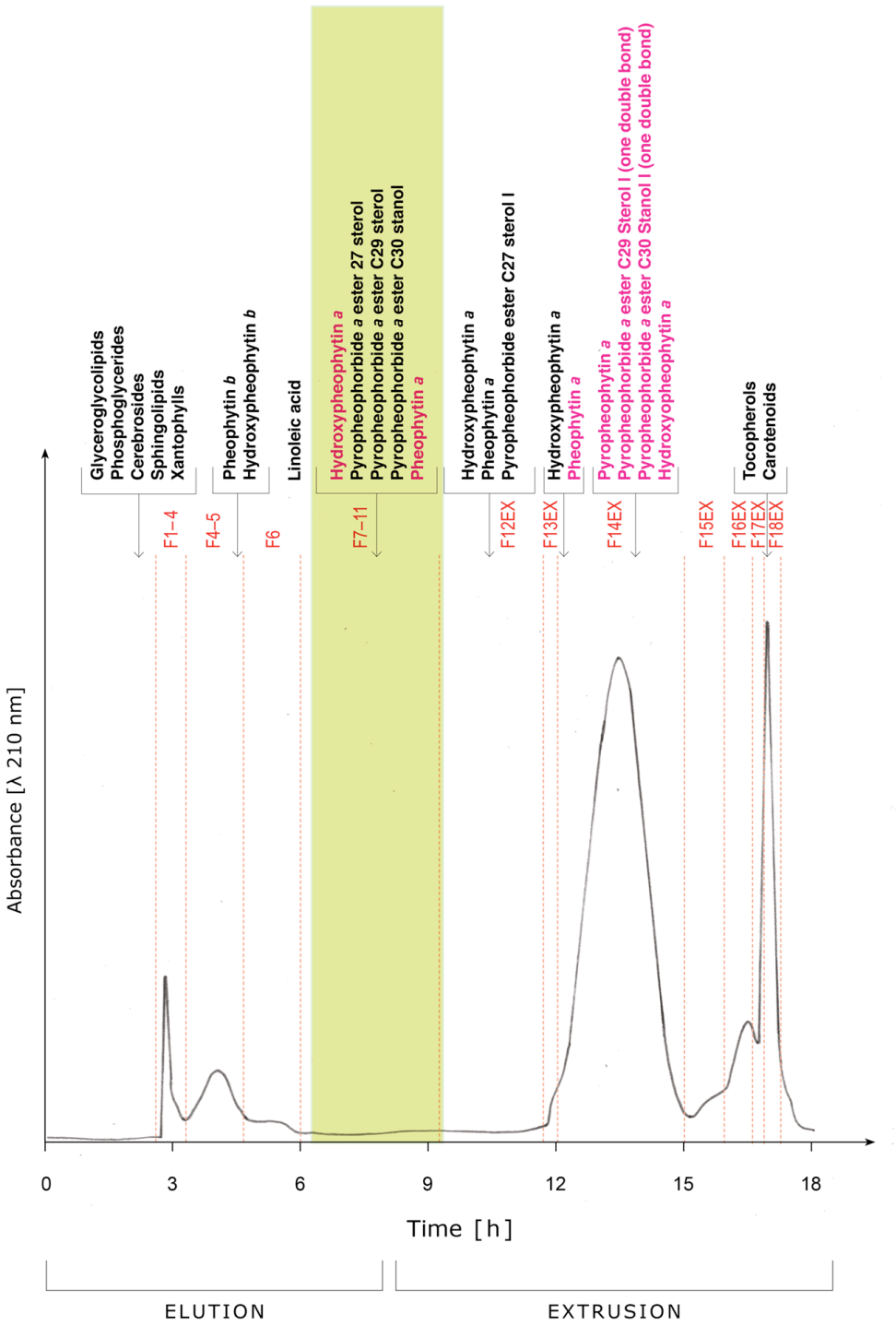

Figure 2-127. Spiral-Coil-LSRCCC chromatogram of Baby Banana peel extract shows a pyropheophytin *a ester* 27sterol *l,* 29 sterol *m*, and 30 stanol between fraction 9 to fraction 11 of elution mode, and in extrusion mode (Fraction 12, 13) pyropheophorbide *a ester* 27 sterol *l* as well as 29, 30 sterol *l,* identified by APCI-HPLC-MS-MS.

2.3.4 Spiral-Coil-LSRCCC of Baby Banana peels with hyperpigmentation: comparison with HSCCC of Baby Banana control

The comparison between the chromatograms of both separations when using the solvent system ACN/Hexane [1:1] depicts the reproducibility of the technique. The results indicate a degradation of the chlorophyll compounds, which are present only in the Baby Banana with hyperpigmentation. The identification of the pyropheophorbide *a* esterified with sterols, pheophytin *b*, hydroxypheophytin *b* and the compound with *m/z 419* reveals the type of degradation of chlorophyll in hyperpigmented Baby Banana **(Figures 2-128, 2-129, 2-130).** The pattern of compounds detected differs from the derivatives that were separated and isolated in Baby Banana control where only pheophytin *a* was found **(Figure 2-128).**

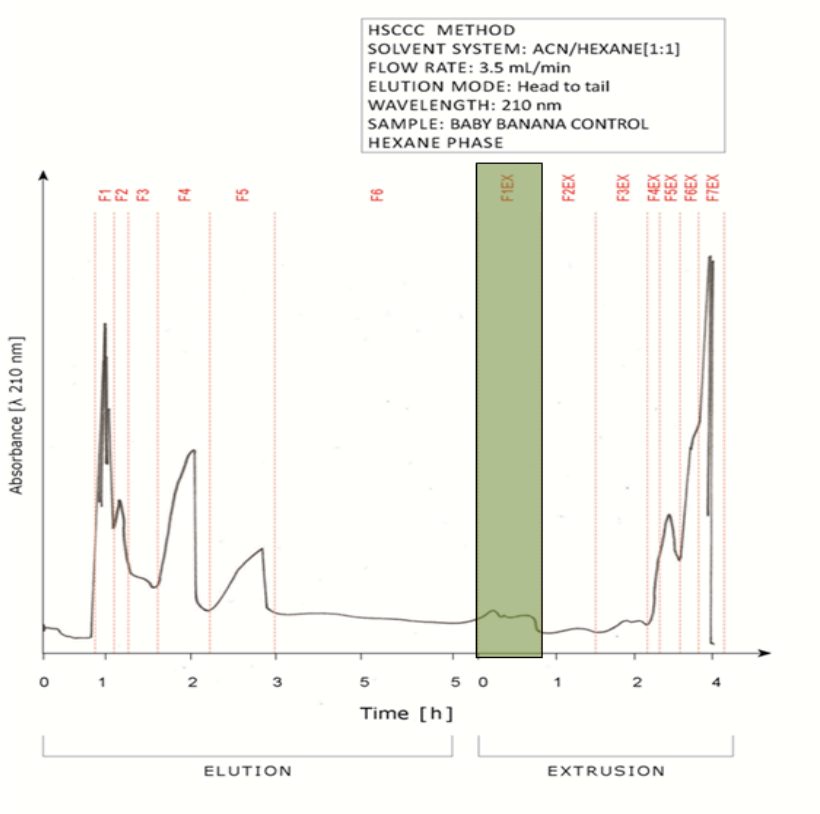

Figure 2-128. HSCCC chromatogram from Baby Banana control in elution and extrusion mode. Pheophytin *a* was separated in fraction 1 of extrusion mode.

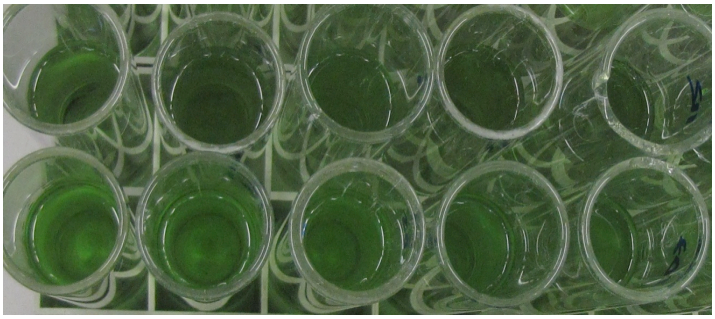

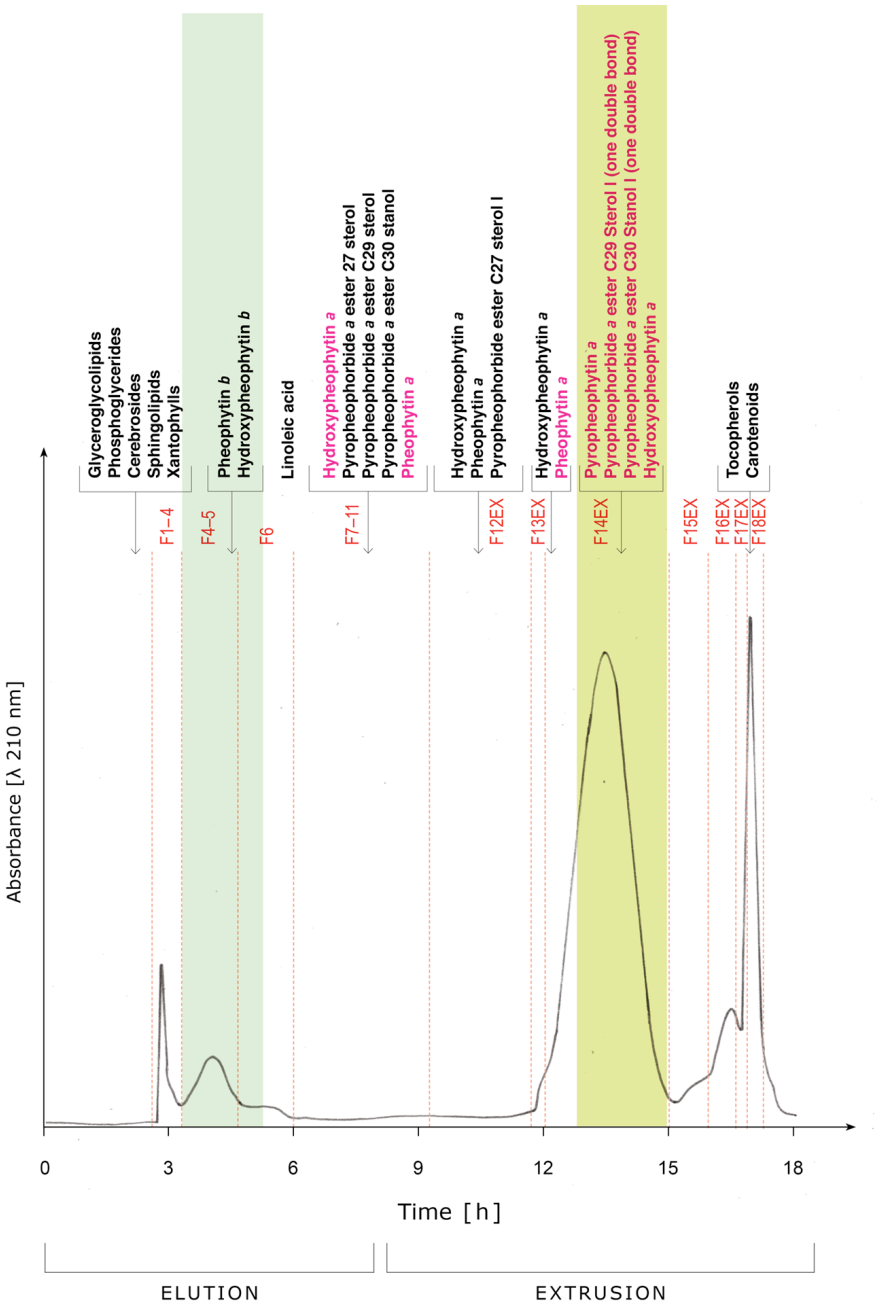

Figure 2-129. Spiral-Coil-LSRCCC chromatogram in elution mode with 1.5 g of pheophytin *b* in fraction 5_3. and 27.5 mg of hydroxypheophytin *b* in fraction 4. Additionally, pyropheophorbide *a* 27 sterol ester was identified in fraction 13 (7 mg) (below). Tubes of Spiral Coil-LSRCCC in elution mode with 27.5 mg of collected hydroxypheophytin b (above) **(Table 2-32).**

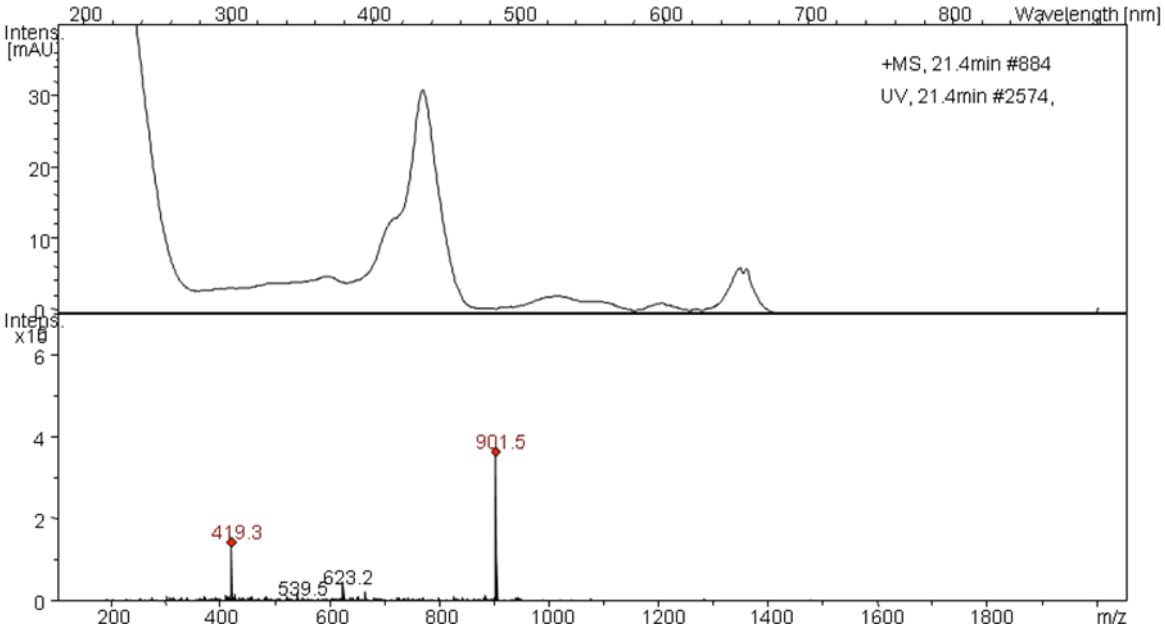

Figure 2-130. APCI-HPLC-MS-MS spectrum (*m/z* 901.5) of hydroxypheophytin *b* in fraction 4.

The APCI-HPLC-MS-MS technique was suitable for these types of compounds and gave clues to understand the degradation of the chlorophylls. For instance, **Figure 2-130** represents the APCI-HPLC spectrum of hydroxypheophytin *b* in fraction 4.

The type of fragmentation shows the tentative structure of the compounds identified at *m/z* 419 in the Spiral-Coil-LSRCCC separation. This could correspond to a sugar moiety in the structure in the case of fractions (elution mode) but in the extrusion mode the presence of a strong fluorescence at 366 nm could indicate either one fragmentation of a derivative of chlorophylls or a different compound. The elution of this compound begins in fraction 10 when the elution mode is ending but it is also detected during the extrusion mode to show a high resolution in UV-contour plot of APCI-HPLC-MS-MS in fraction 14 **(Tables 2-31, 2-32; Figure 2-131).**

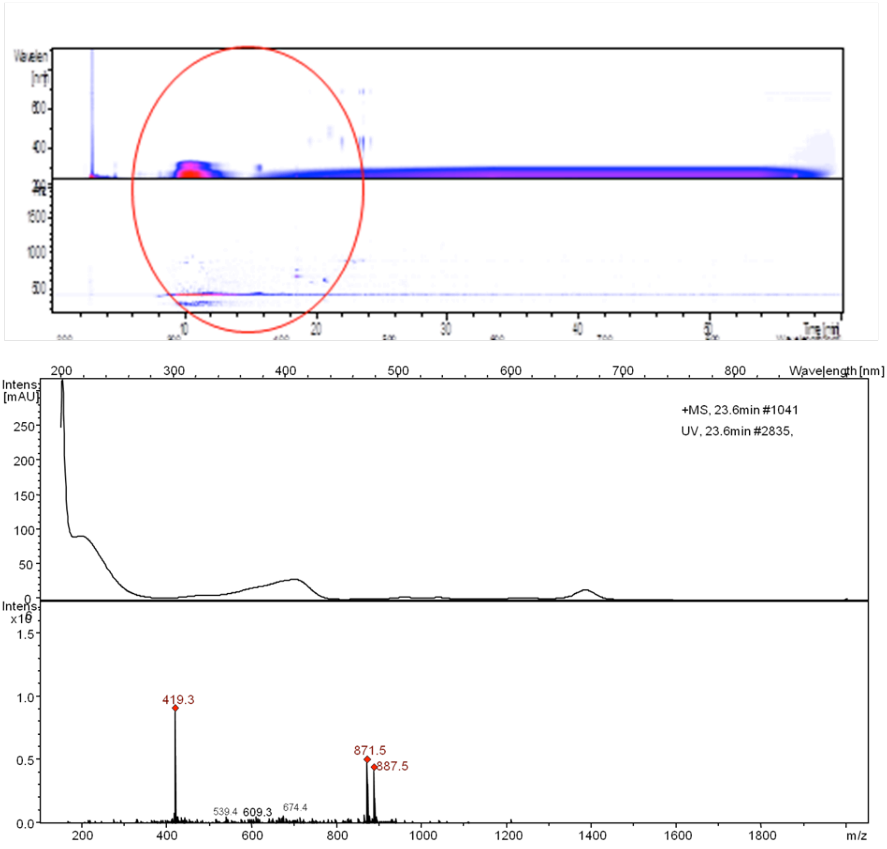

Figure 2-131. UV-Contour plot of APCI-HPLC-MS-MS of fraction 14 (above). The high fluorescence at 10.07 min corresponding to m/z 419 in contrast with the low fluorescence at 22.3 min of pheophytin a and hydroxypheophytin at m/z 871 and 887.5, respectively (below).

The analysis of the fragmentation for pheophytin *a* and pyropheophytin *a* could help to tentatively assign the structure of the fluorescent compound. The loss of phytol is represented by an ion at *m/z* 532 and 593 for pyropheophorbide *a* and pheophytin *a,* repectively.The losses of 28 and 72 u are explained as fragments of ethylene C_2H_4 or CO, and ($CH_2CHCOOH$). The loss of two consecutive fragments at *m/z* 28 could explain the fragment at *m/z* 419 and indicates the elution of pyropheophytin *a* in fraction 15 (**Figure 2-132**).

Nevertheless, this hypothesis is not supported when the analysis of the ^{1}H and ^{13}C NMR spectra of fraction 14 has been performed **(Figure 2-133).**

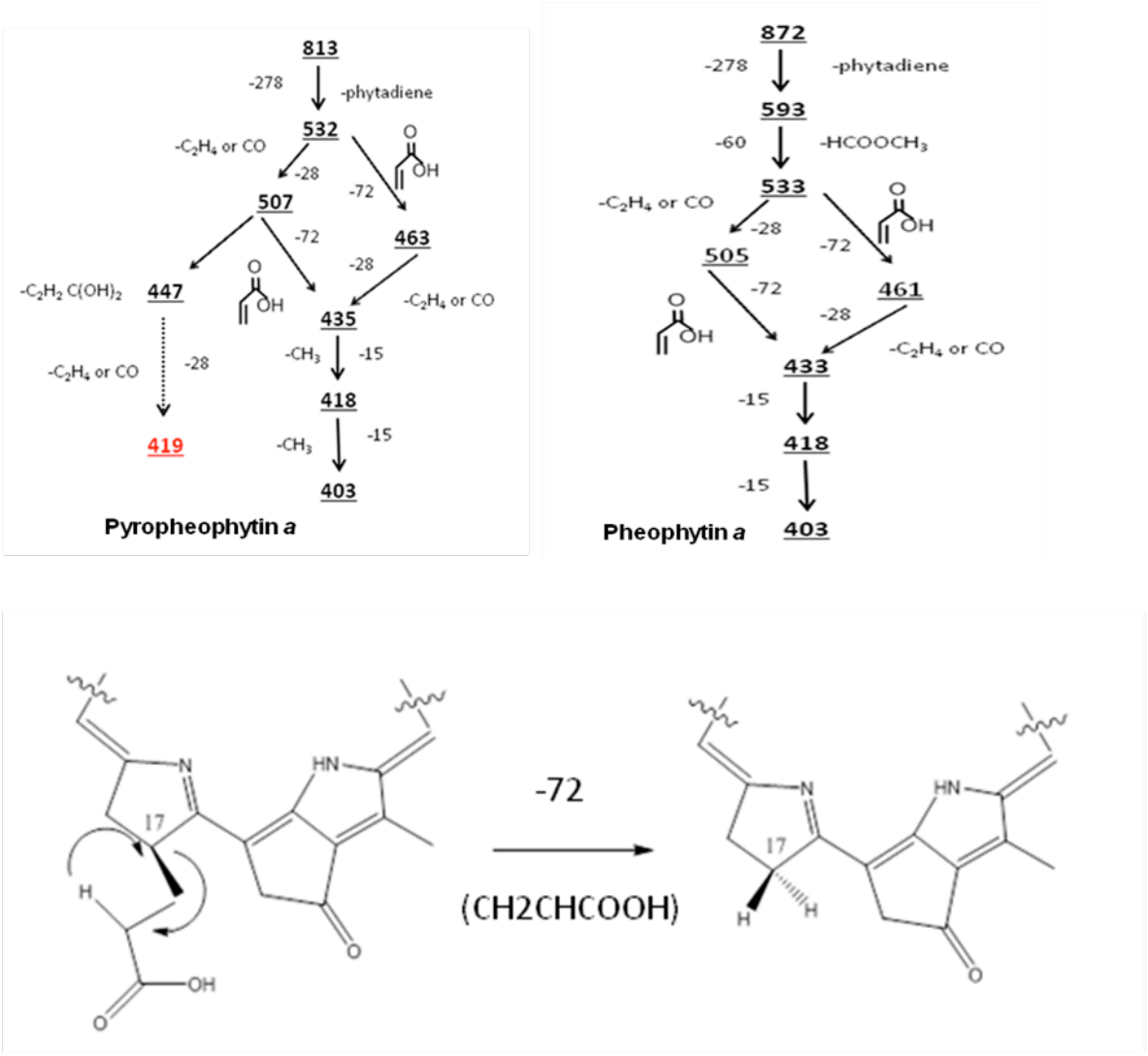

Figure 2-132. Fragmentation pathway of pheophytin *a* and pyropheophytin *a* (above). Pyropheophytin *a* structure as yield of loss of (CH2CHCOOH) fragment equivalent to *m/z* 72 (Chillier et al. 1994).

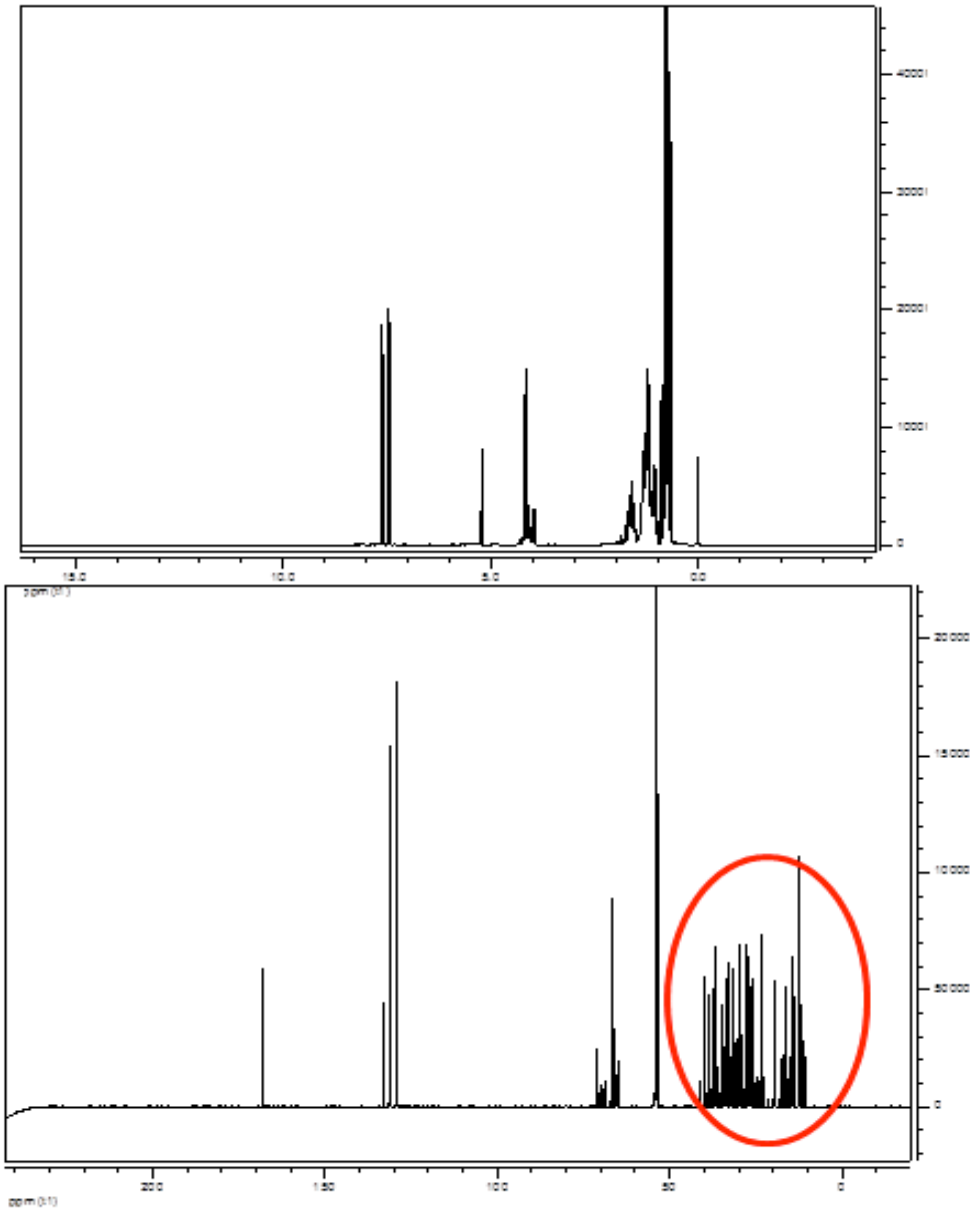

Figure 2-133. ^{1}H (above) and ^{13}C NMR spectra (below) of fraction 14 which could show the proposed structure corresponding to the fluorescent compounds in extrusion mode of the Spiral-Coil LSRCCC separation from hyperpigmented Baby Banana peels.

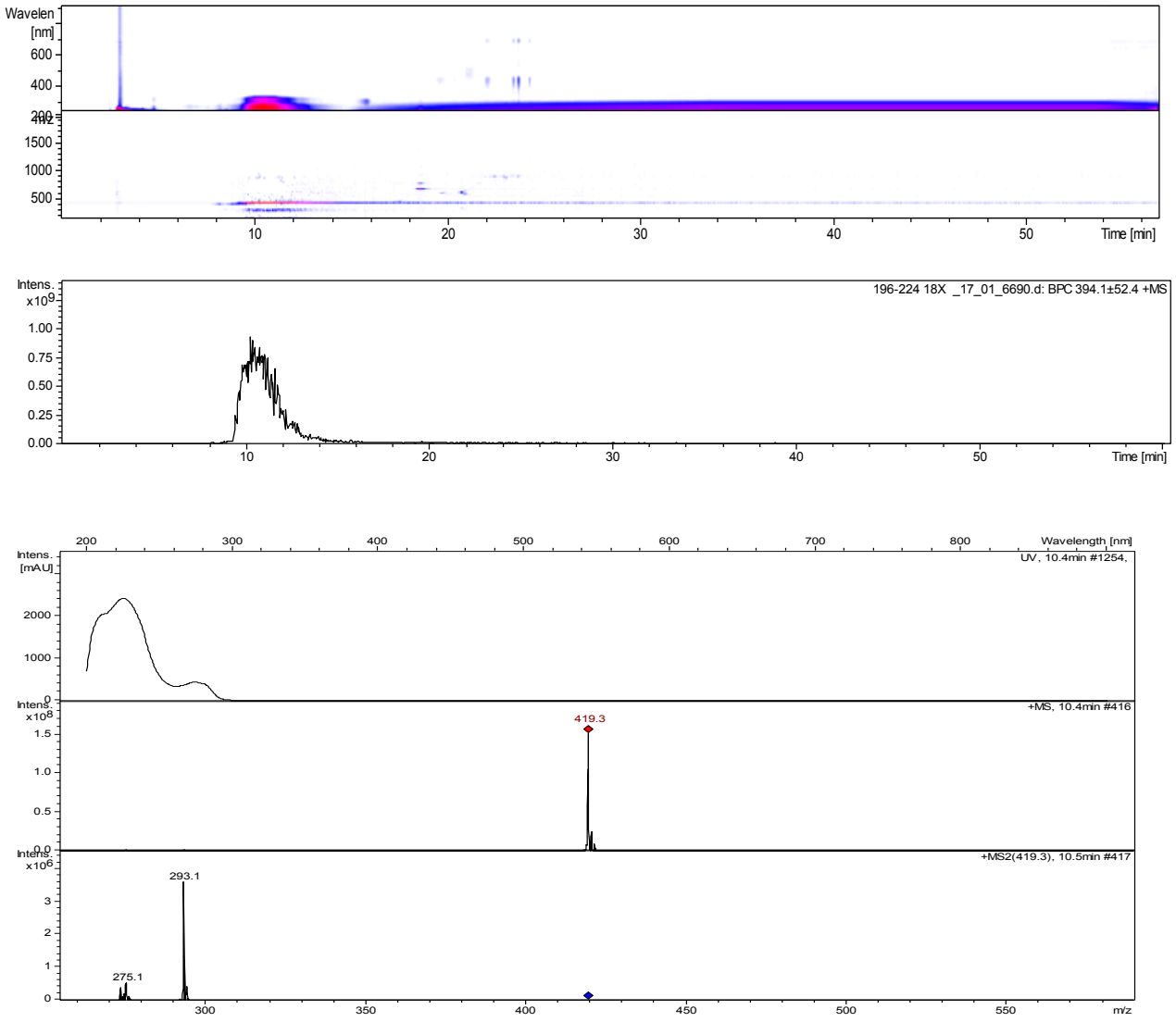

Figure 2-134. APCI-HPLC-MS-MS spectrum of fraction 14 (697.7 mg) recollected in extrusion mode during the scale-up separation of Baby Banana peels with hyperpigmentation by Spiral-Coil-LSRCCC. The mass spectrum shows a daughter peak at *m/z* 419 with a strong fluorescence between 200 to 366 nm. The low intensity of the fluorescences at 24 min correspond to hydroxypheophytin *a*, pheophytin *a* and pyropheophytin *a* identified in the fraction.

2.3.4.1 Elucidation of tocopherols and tocotrienols in Fraction 14 of Spiral-Coil-LSRCCC separation from Baby Banana peels with hyperpigmentation extract

The APCI-HPLC-MS/MS and 1D and 2D NMR data were analyzed thoroughly to identify the compound with a strong fluorescence (*m/z* 419) at 10.7 min in fraction 14 of extrusion mode **(Figure 2-134).** The HPLC-MS/MS contour plot UV spectra of fractions during the elution and extrusion mode were observed to determine that the fluorescence shows a sequence between fraction 11 in elution mode and fraction 17 in extrusion mode. The fluorescence shows an increase from fraction 12 toward fraction 15 to decrease totally in fraction 16 of extrusion mode **(Figure 2-135).**

The ^{1}H-and ^{13}C-NMR spectra of fractions were analyzed with APCI–HPLC-MS/MS to conclude that although the compound with *m/z* 419 was detected between fraction 12 and fraction 15, the ^{1}H- and ^{13}C-NMR experiments together with APCI mass data showed different results in comparison to the spectrum of fraction 14. ^{1}H-and ^{13}C-NMR spectra recorded at 600 and 150 MHz, respectively, from fraction 14 not only depicted the occurrence of one compound but also a variety of resonances with high intensity that mask low intensity chemical shifts, which play an important role in the elucidation of important compounds such as tocopherols and tocotrienols.

The clue for the elucidation of tocopherols and tocotrienols was based on a resonance at δ 167.88 and also the lack of carboxyl acid signals. ^{13}C-NMR spectrum showed between 10 and 40 ppm characteristic resonances of methylenes, methyls and methines which could be matched with a carboxyl group to figure out the presence of α fatty acid **(Figures 2-133, 2-136).**

The olefinic region showed resonances with chemical shifts at δ 132, 131 and 129 ppm which could belong to an unsaturated fatty acid but the chemical shift for a carboxyl group was not found. HSQC and HMBC data indicated that not all the chemical shifts in the carbon spectra matched each other and also the chemical shift at δ 7.4 and 7.6 revealed compounds that could contain nitrogen **(Figure 2-136).**

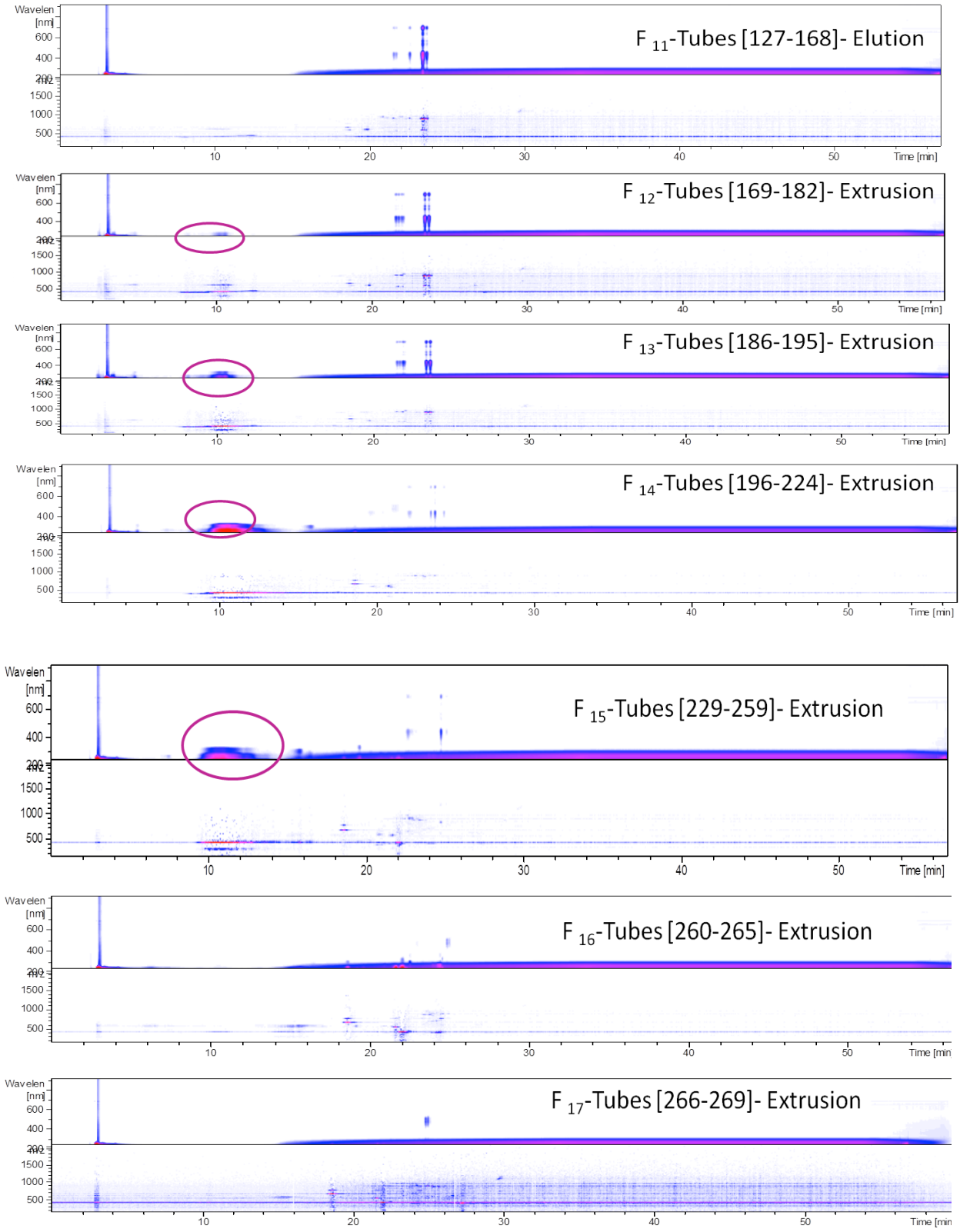

Figure 2-135. UV Contour Plot HPLC-MS/MS from fractions 11(elution) to fraction 17 (extrusion). The fluorescent compound (*m/z* 419) at 10.7 min increases from fraction 12 to fraction 15 in extrusion mode.

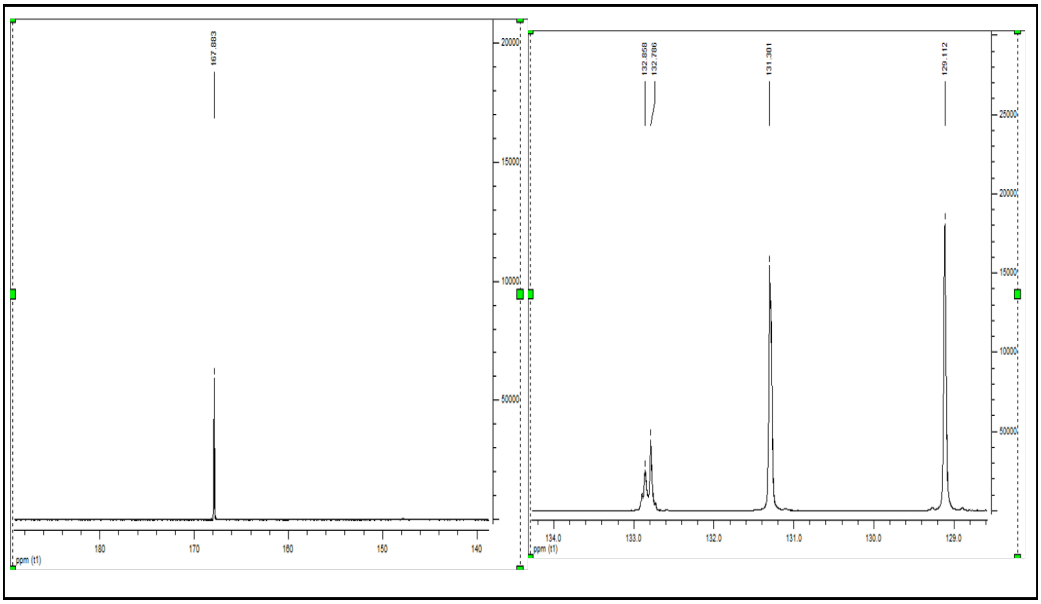

Figure 2-136. ^{13}C-NMR spectra (olefinic region) with signals at δ 132, 131,129 and a unique carboxyl resonance at δ 167 recorded in CD_2Cl_2 from Baby Banana with hyperpigmentation.

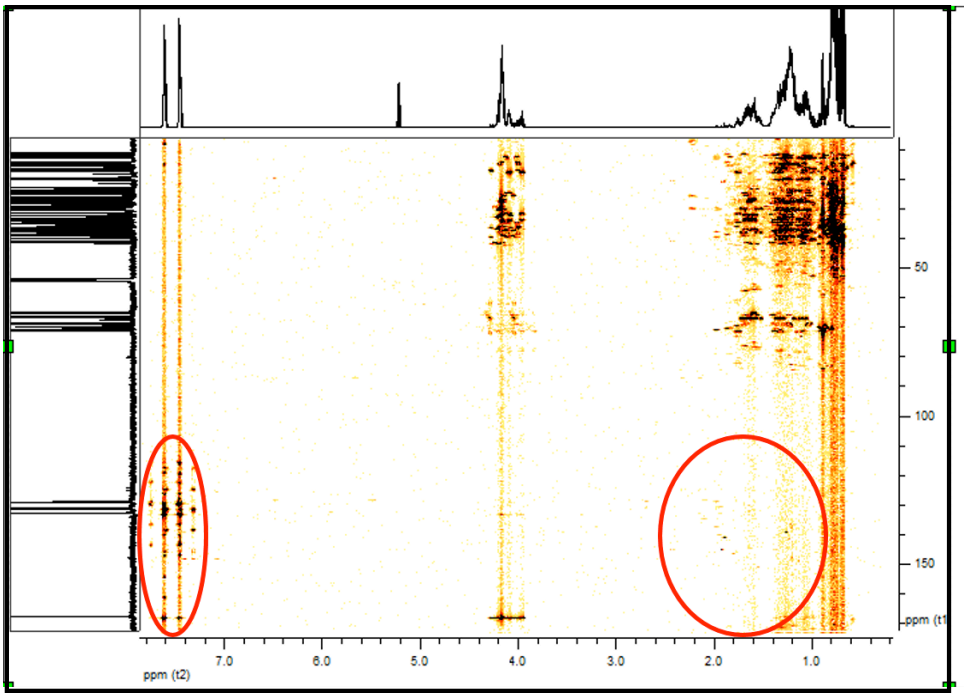

Figure 2-137. HMBC spectrum of fraction 14 (150 MHz) in extrusion mode of Baby Banana peels with hyperpigmentation.

In the HMBC spectrum **(Figure 2-137)** low intense resonances in a logic sequence were elucidated in order to reveal tocopherols and tocotrienols in the spectrum of fraction 14. The cause of the strong fluorescence in the UV contour plot was discovered.

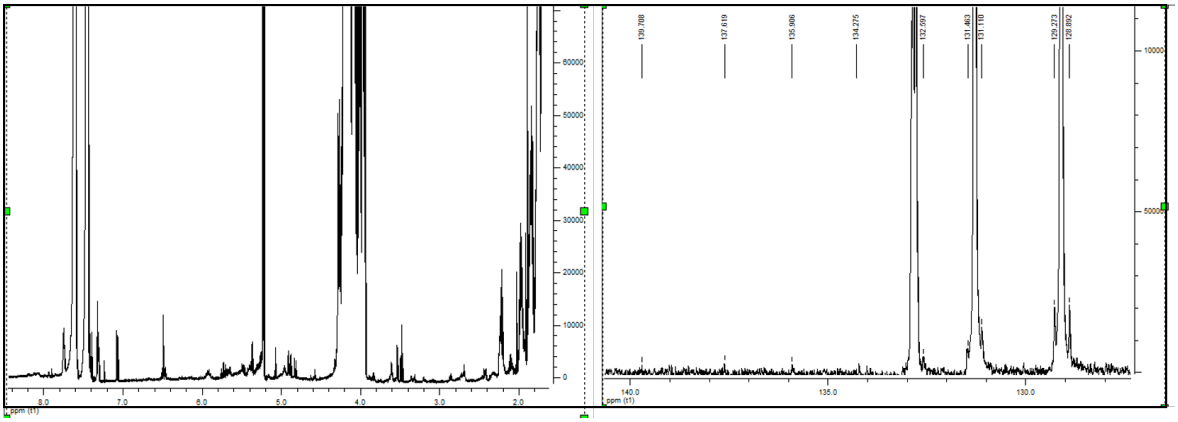

Figure 2-138. 13C-NMR spectra (olefinic region) at δ 132, 131,129 (right) and ^{1}H-NMR spectra (left) expanded. The chemical shift of low intensity corresponded to tocopherols and tocotrienols elucidated in fraction 14 in accordance with literature data (Ohnmacht et al. 2008).

In spite of the low intensity of resonances in the spectra, it was clearly distinguishable the vinyl protons (H-3', H-7', H-11') from the unsaturated side chain of tocotrienols which showed that the major component in the mixture of tocopherols and tocotrienols in fraction 14 was a tocotrienol **(Figure 2-138).**

The relevant singulet at δ 6.48 supported the structure of a ß-tocotrienol as a characteristic resonance at H-7 in comparison with δ 6.38 and 6.50 of γ-tocotrienol and δ-tocotrienol, respectively. The results were in agreement with literature data (Ohnmacht et al. 2008) **(Figure 2-139).**

The polar chromanol ring of ß-tocotrienol was defined by resonances of quaternary carbons in the ^{13}C-NMR spectrum with the support of the HSQC and HMBC experiments. The carbon peaks at δ 144.75 and 144.13 were assigned to C-10 and C-6, respectively, as well as to C-5 and C-9 at δ 119.30 and 116.63, respectively. **Table 2-33** summarizes the spectral data of the ß-tocotrienol in fraction 14.

The OH group of ß-tocotrienol was identified in ^{1}H-NMR spectrum at δ 4.57 as a major component when three peaks in this region were compared. Two adjacent peaks appear at δ 4.59 and 4.67 which shows the presence of two additional compounds. According to literature data the resonances could correspond to ß-tocopherol (δ 4.59) and γ-tocotrienol (δ 4.67) (Ohnmacht et al. 2008) **(Figure-2-140).**

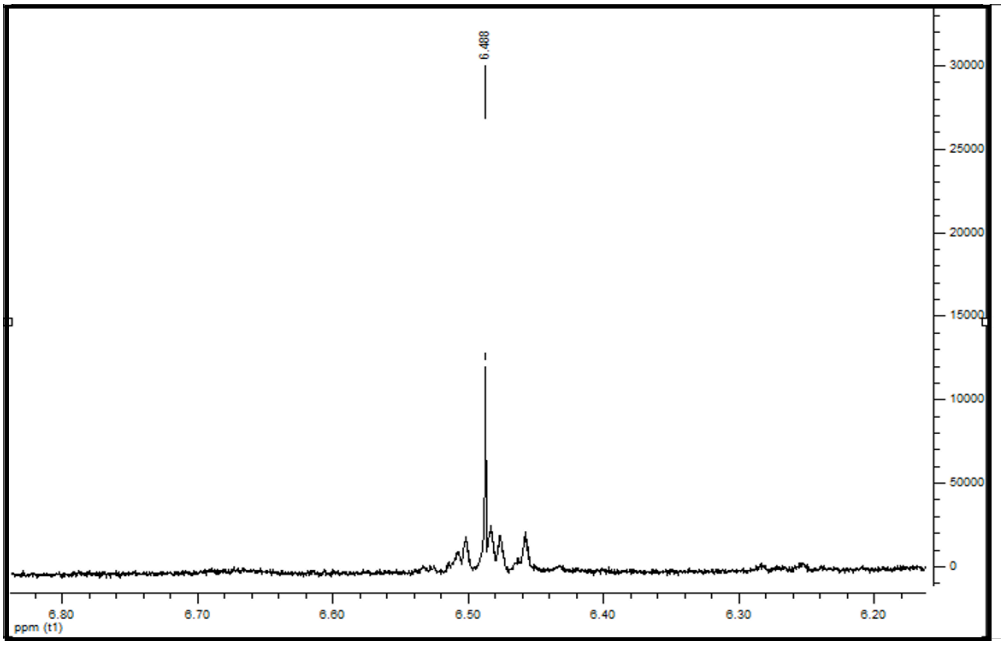

Figure 2-139. ^{1}H-NMR spectrum (600 MHz) in CD_2Cl_2 of fraction 14 from Spiral Coil LSRCCC from Baby Banana peel with hyperpigmentation. The characteristic singulet at δ 6.48 supports the assignment to H-7 of ß-tocotrienol as major component in the mixture of tocopherols and tocotrienols in fraction 14.

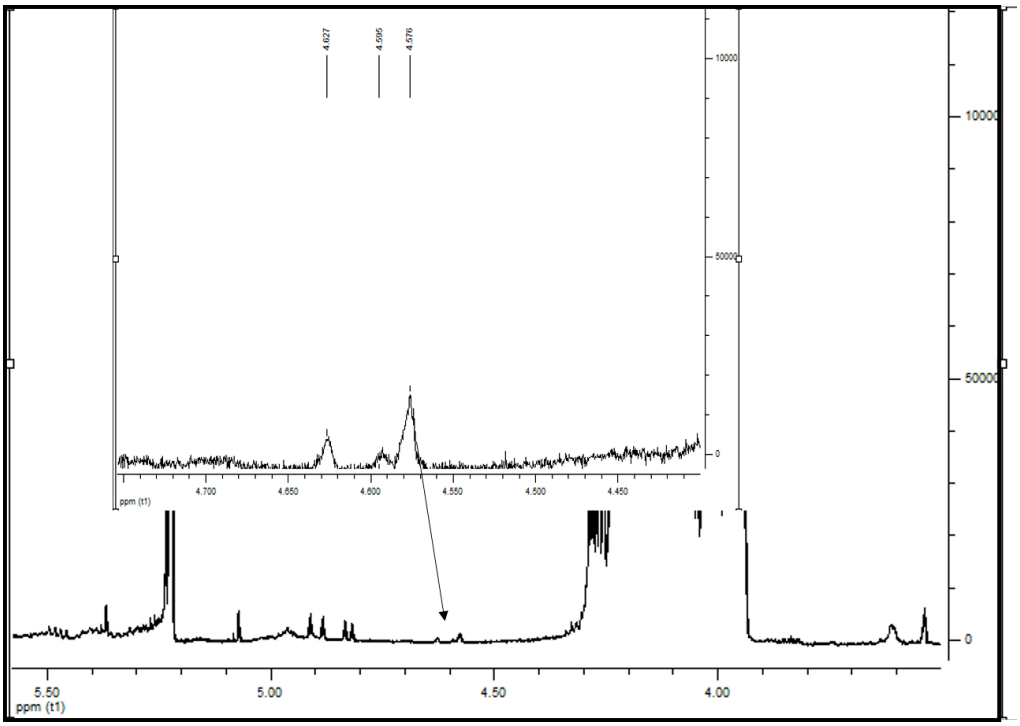

Figure 2-140. ^{1}H NMR spectrum (600 MHz) in CD_2Cl_2 of fraction 14 from Spiral Coil LSRCCC from Baby Banana peel with hyperpigmentation. The OH group for ß-tocotrienol at δ 4.57 supports the assignment to H-7 as the major tocotrienol in the mixture of tocopherols and tocotrienols in the fraction.

Although the ^{1}H- and ^{13}C-NMR spectra depict resonances of tocopherols as well as the low intensity of the chemical shift, the complete elucidation was enabled with the support of HSQC and HMBC data. The tentative chemical structure of ß-tocotrienol has been defined in **Table 2-33** and illustrated in **Figure 2-141**.

Table 2-33. ^{1}H-and ^{13}C-NMR spectroscopic data of ß-tocotrienol elucidated in fraction 14 of Spiral-Coil Low Speed Rotary Countercurrent Chromatography (Spiral-Coil LSRCCC) separation from Baby Banana peels with hyperpigmentation (Ohnmacht et al. 2008).

Assignment	δ ^{13}C (ppm)	δ ^{1}H (ppm)	DEPT
2	79.78	---	Quaternary
2-CH_3	24.46	1.34 (*s*)	CH_3
3	32.97	1.77-1.75	CH_2
4	21.39	1.33-1.22	CH_2
5	119.30	-----	Quaternary
5-CH_3	19.12	1.22 (*s*)	CH_3
6	144.13	---	Quaternary
7	114.70	---	CH
7-CH_3	---	6.48 (s)	---
8	124.44	---	Quaternary
8-CH_3	12.08	1.91 (*s*)	CH_3
9	116.63	---	Quaternary
10	144.75	---	Quaternary
1’	33.89	1.98-1.96	CH_2
2’	31.05	2.3-2.1	CH_2
3’	124.47	5.24 (*m*)	CH
4’	139.35	---	Quaternary
4’-CH_3	17.07	1.65 (*s*)	CH_3
5’	33.89	1.98-1.96	CH_2
6’	28.94	2.14-2.08	CH_2
7’	128.17	5.24 (*m*)	CH
8’	132.86	---	Quaternary
8’-CH_3	17.97	1.61 (*s*)	CH_3
9’	34.59	1.88-1.87	CH_2
10’	27.93	2.08-2.14	CH_2
11’	128.26	5.24 (*m*)	CH
12’	131.79	---	Quaternary
12’ aCH_3	24.53	1.62	CH_3
12’ bCH_3	17.57	1.63	CH_3
OH	---	4.57	---

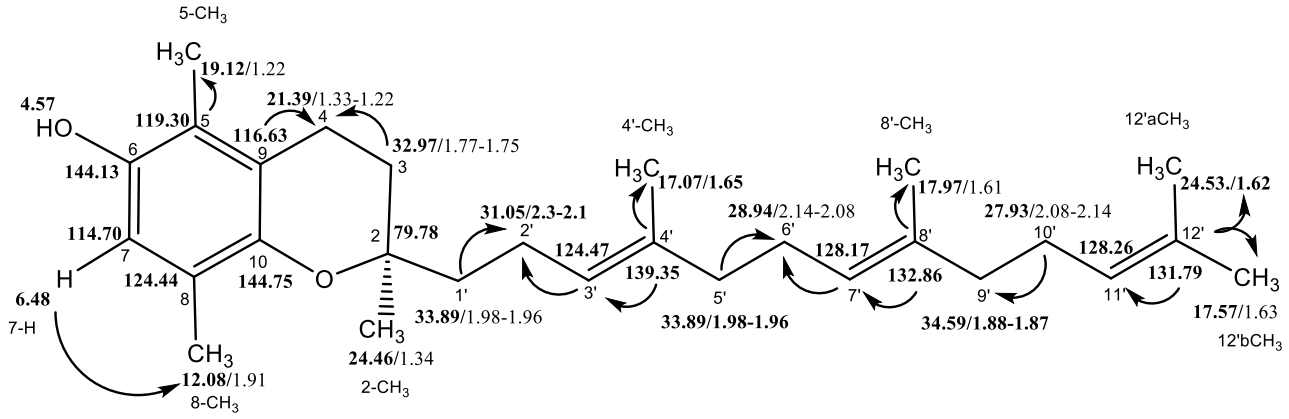

Figure 2-141. Chemical structure of ß-tocotrienol in fraction 14 from Spiral-Coil-LSRCCC. HSQC and HMBC correlations confirm the tentatively elucidated structure.

The APCI-HPLC-MS-MS data confirmed the occurrence of ß-tocotrienol as major compound in fraction 14 when the fragmentation of the spectrum was analyzed. Literature data report (*m/z*) of $[M + H]^+$ ions at *m/z* 431, 417, 417 and 403 corresponding to α-, β-, γ-, and δ tocopherols, and at *m/z* 425, 411, 411 and 397 for tocotrienols, respectively. Also, the characteristic fragment ions reported at *m/z* 205 and 165 for α-tocols, *m/z* 191 and 151 for β- and γ-tocols, and *m/z* 177 and 137 for δ-tocols (Lampi et al. 2008; Ryynänen et al. 2004).

The analysis of the APCI-HPLC-MS/MS data of fractions with red fluorescence described below was performed and a pattern of fragmentation was observed which confirms the presence of α- and β-tocols in fractions 12 -15 in extrusion mode. Although the base peak at *m/z* 419 is recurrent in the report of APCI mass data, this could be compared with *m/z* 417 reported in literature data as well as *m/z* 429. The fragmentation pattern corresponds to the values which were reported in literature data. **Figures 2-142, 2-143, 2-144** show the APCI-HPLC-MS/MS spectra of fraction 12, 13, 14 and 15.

Figure 2-145 illustrates the chemical structure of natural occurring tocopherols and tocotrienols in order to understand the pattern of fragmentation in the APCI-MS data analysis.

FRACTION 12 –Tubes [169-182] –EXTRUSION MODE

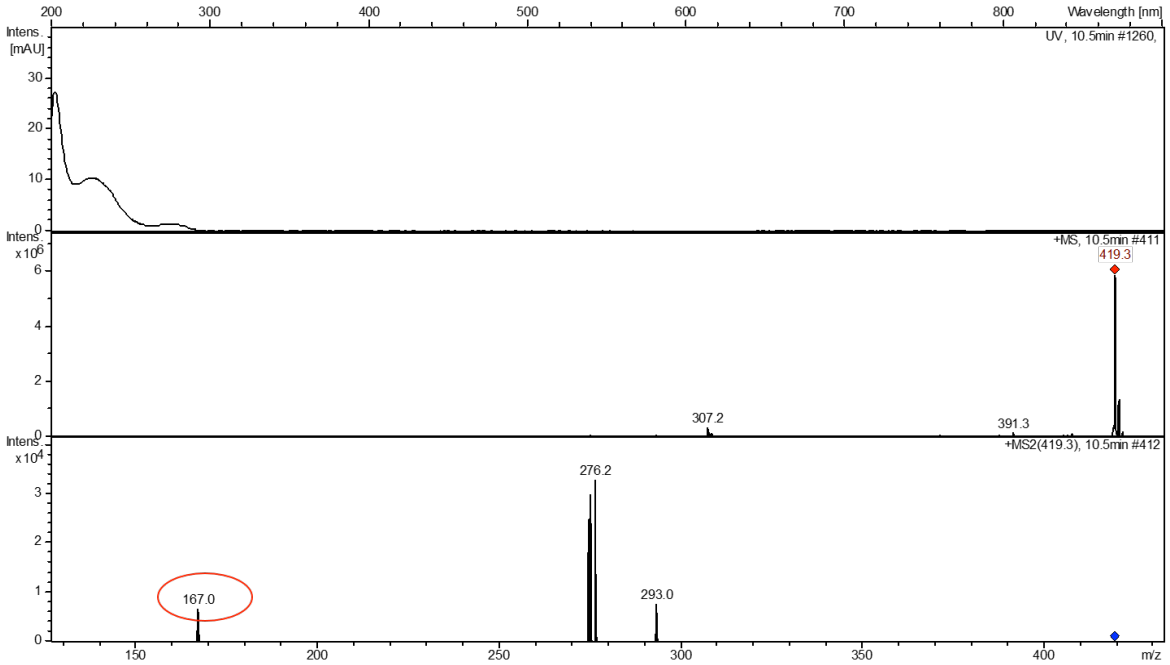

FRACTION 13 –TUBES [186-195] –EXTRUSION MODE

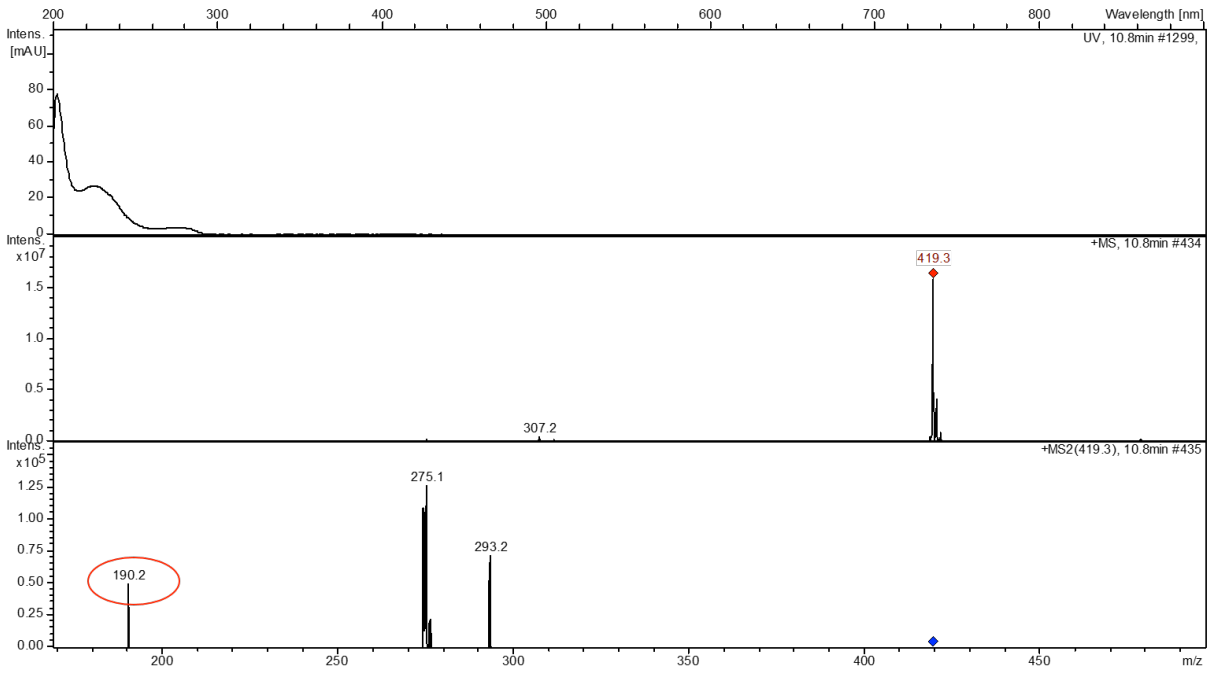

Figure 2-142. APCI-HPLC-MS/MS data for fraction 12 (above) and 13 (below) in extrusion mode.

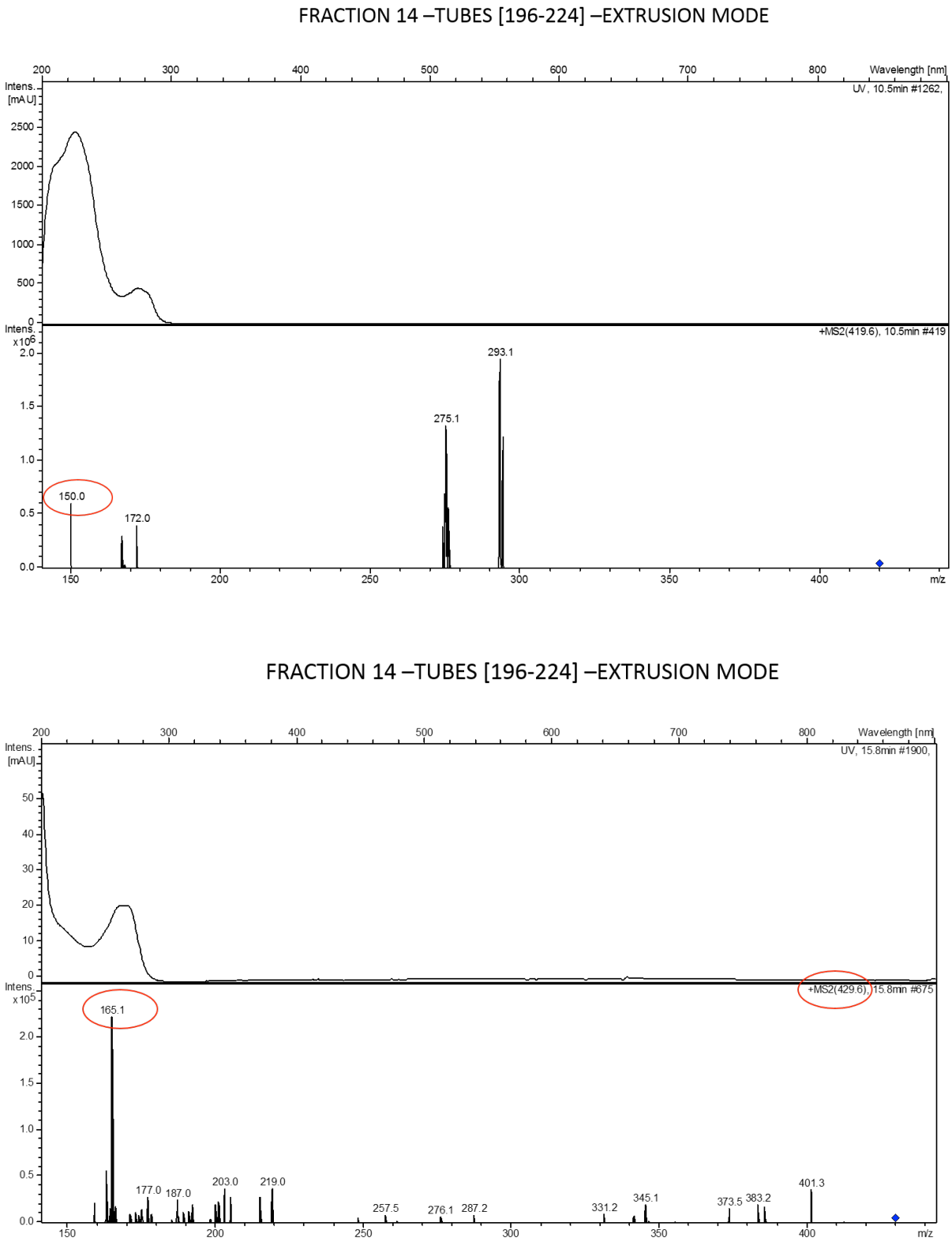

Figure 2-143. APCI-HPLC-MS/MS data for fraction 14a (above) and 14b (below) in extrusion mode.

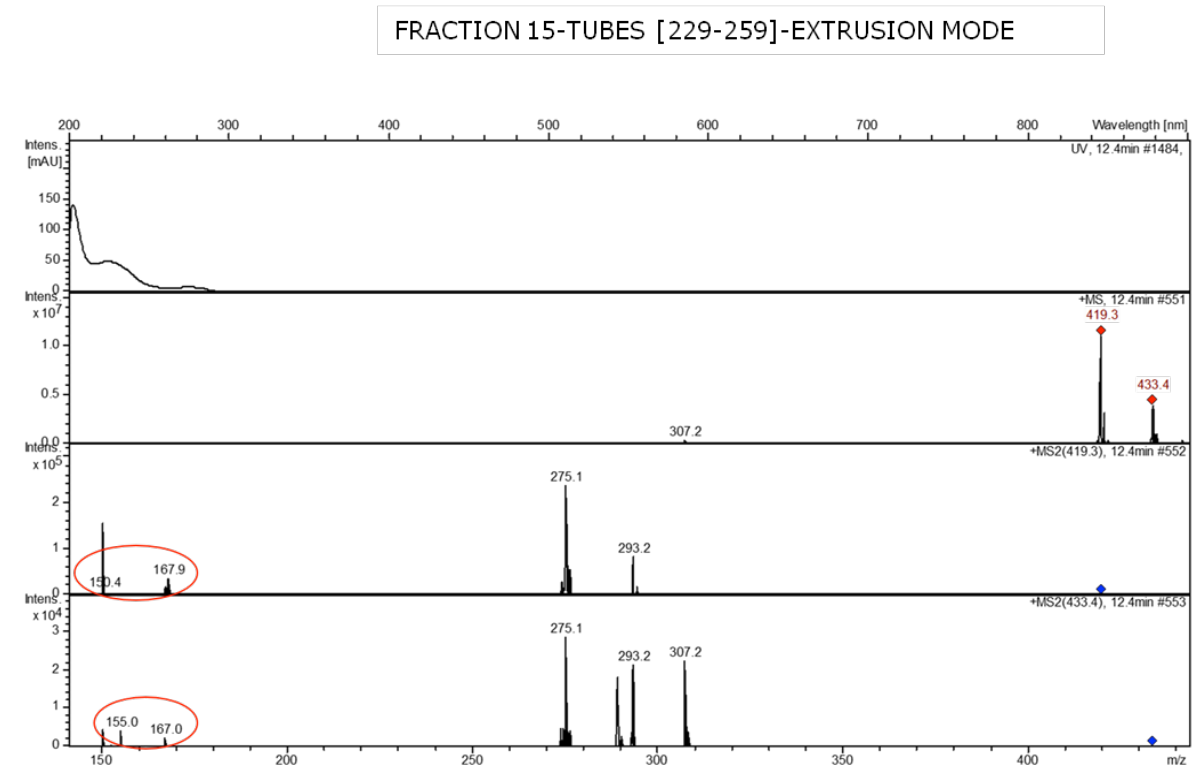

Figure 2-144. APCI-HPLC-MS/MS data for fraction 15 in extrusion mode.

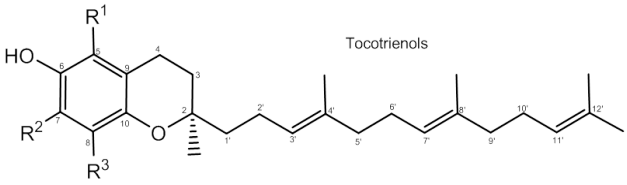

$R^1 = R^2 = R^3 = CH_3$, α-tocotrienol
$R^1 = R^3 = CH_3$, $R^2 = H$, β-tocotrienol
$R^1 = H$, $R^2 = R^3 = CH_3$, γ-tocotrienol
$R^1 = R^2 = H$, $R^2 = CH_3$ δ-tocotrienol

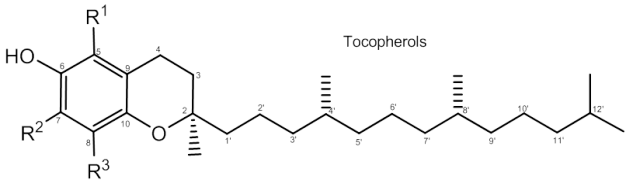

$R^1 = R^2 = R^3 = CH_3$, α-tocopherol
$R^1 = R^3 = CH_3$, $R^2 = H$, β-tocopherol
$R^1 = H$, $R^2 = R^3 = CH_3$, γ-tocopherol
$R^1 = R^2 = H$, $R^2 = CH_3$ δ-tocopherol

Figure 2-145. Structure of the naturally occurring tocopherols and tocotrienols (Ohnmacht et al. 2008).

Analytical thin layer chromatography assay was conducted by using aluminum sheets of silica gel F_{251} [Merck©] for tubes between 194 and 224 from the Spiral-Coil LSRCCC. The mobile phase CH_2Cl_2/MeOH (9.9/0.1) showed the elution for fraction 14 in the plate. The red fluorescence was identified both at 254 nm and 366 nm **(Figures 2-146, 2-147) (cf. 4.3.2.1).**

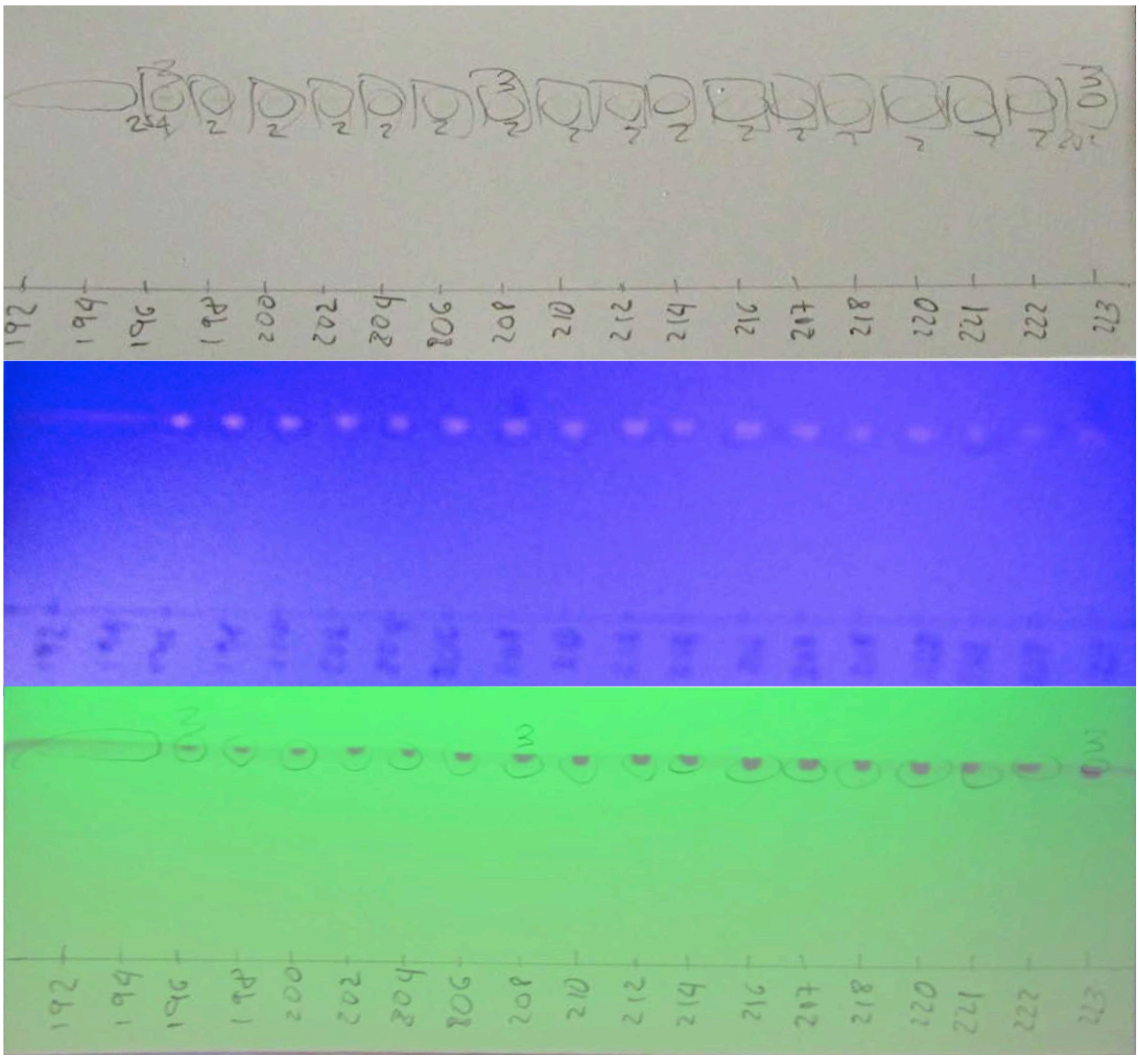

Figure 2-146. Silica gel TLC gel screening of tubes corresponding to fraction 14 in extrusion mode from Spiral-Coil LSRCCC from Baby Banana peels with hyperpigmentation (Above: silica gel TLC under white light; Middle: silica gel TLC under 366 nm; Below: silica gel TLC under 254 nm).

NOTE: Fraction 14 includes tubes between 196 and 224 in extrusion mode but the photo did not show the tube 224 due to the amplitude of the photo area.

Figure 2-147. Silica gel TLC gel screening of fraction 14 (697.74 mg) in extrusion mode from Spiral-Coil LSRCCC from Baby Banana peels with hyperpigmentation (Left: silica gel TLC under 366 nm; Middle: silica gel TLC under 254 nm; Right: after spraying with anisaldehyde).

2.3.4.2 Elucidation of triterpene alcohol ferulates in fraction 14 of Spiral-Coil-LSRCCC separation from Baby Banana peels with hyperpigmentation extract

The identification of cycloartenyl ferulate was enabled due to the noteworthy resonance at δ 167.88 in the ^{13}C-NMR spectrum of fraction 14 which was not known previously during the phytochemical study of Baby Banana peel. **Figure 2-148** illustrates the isolated peak in the carboxylic region of the ^{13}C-NMR spectrum and the high intensity of the peak in relation with the hidden resonances of tocopherols and tocotrienols in the fractions.

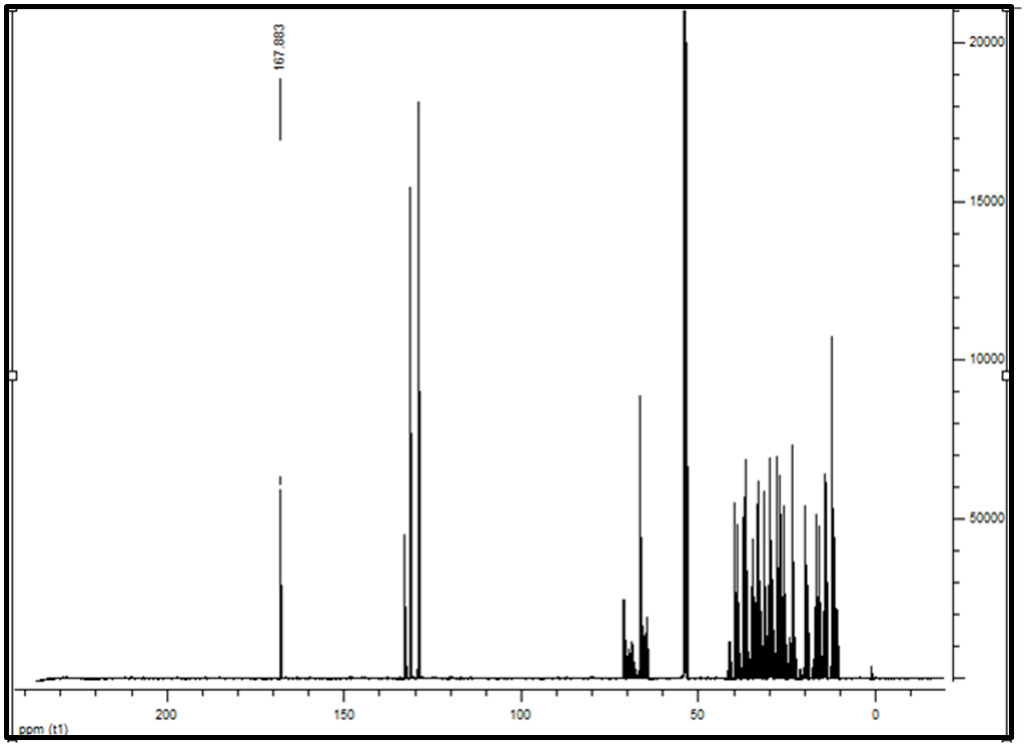

Figure 2-148. ^{13}C-NMR spectrum (150 MHz) of fraction 14 from Spiral-Coil LSRCCC of Baby Banana peel with hyperpigmentation. The chemical shift at δ 167.88 belongs to the triterpene alcohol ferulates identified in the fraction.

The HSQC and HMBC experiments data supported the assignments of protons and carbons corresponding to a ferulic acid. Once identified as ferulic acid, the elucidation of the triterpenes was enabled by comparison with the standards of sitosterol and triterpenes reported in section 2.1.10 and 2.1.11. Thus, the chemical structure for the cycloartenyl E-ferulate was elucidated and summarized in **Table 2-34. Figure 2-149** shows the chemical structure (Liu et al. 2013).

The APCI-HPLC-MS/MS spectrum was further analyzed in the positive mode. *m/z* 599.9 was assigned to the cycloartenyl *E*-ferulate and a derivative of 25-hydroxy-24-methylcycloartenyl ferulate $[M\text{-}H\text{-}OH]^-$ was detected at *m/z* 617 **(Figures 2-150, 2-151).**

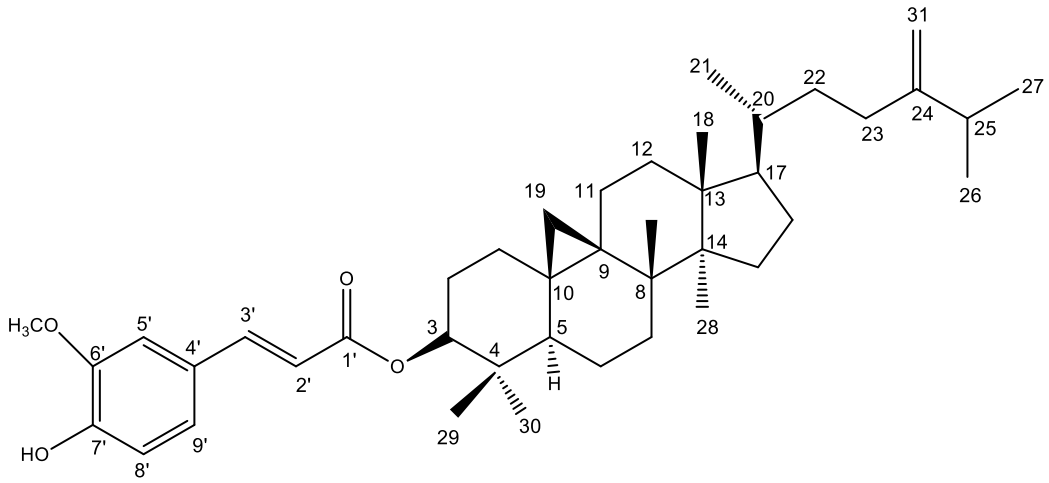

Figure 2-149. Chemical structure of cycloartenyl E-ferulate elucidated in fraction 14 of Spiral Coil-LSRCCC of Baby Banana peel with hyperpigmentation.

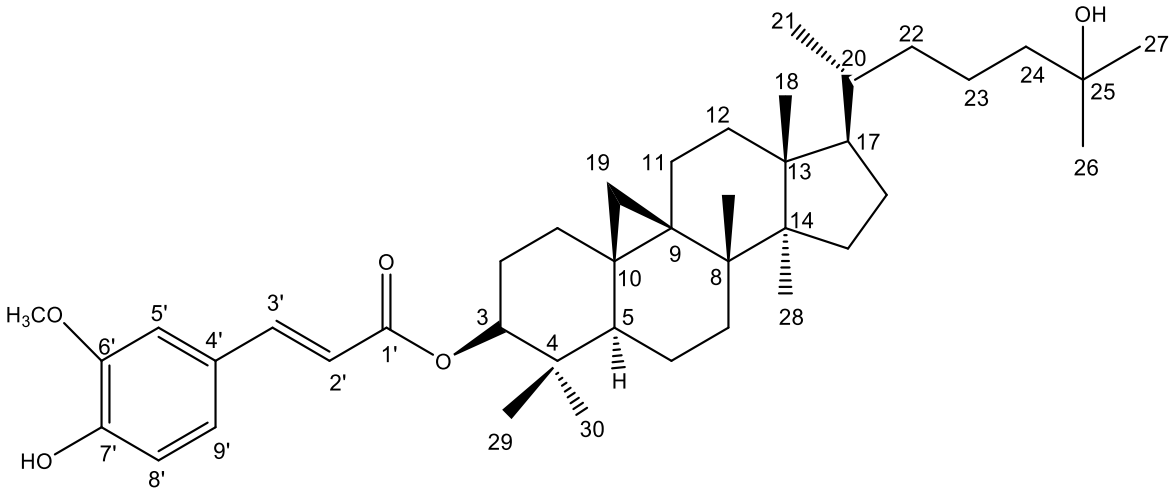

Figure 2-150. Chemical structure of a tentatively identified derivative of 25-hydroxy-24-methylcycloartenyl ferulate (*m/z* 617 [M-H-OH]-) in fraction 14 from Spiral-Coil LSRCCC of Baby Banana peels with hyperpigmentation (Fang et al. 2003).

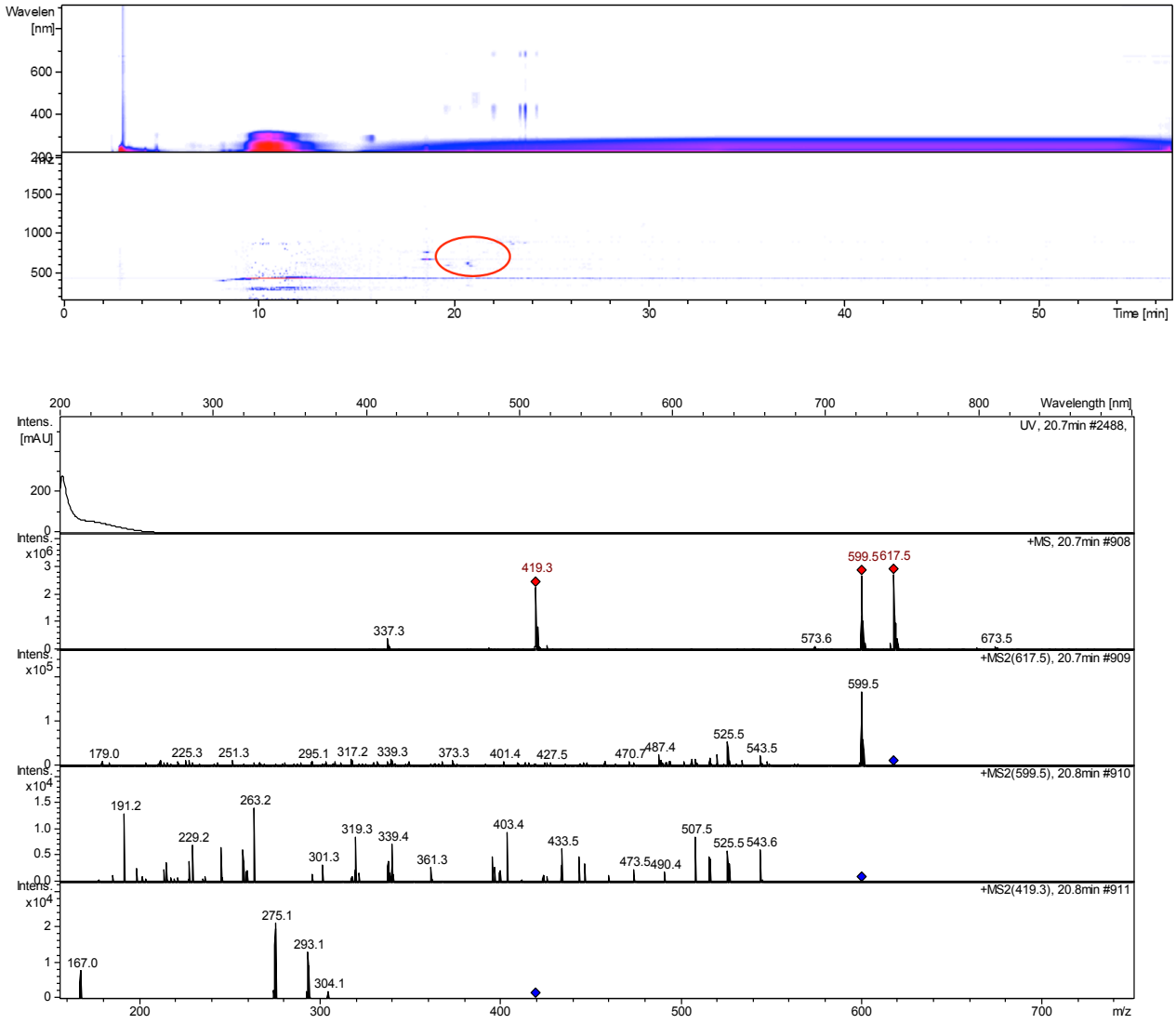

Figure 2-151. APCI-HPLC-MSMS spectra (below) and UV contour-plot (above) from fraction 14 in extrusion mode. The region of mass spectrum without UV shows at 20.7 min two peaks with *m/z* 617.5 and 599.9 corresponding to a tentavively identified derivative of 25-hydroxy-24-methylcycloartenyl ferulate and cycloartenyl E-ferulate.

Table 2-34. ^{1}H and ^{13}C-NMR spectroscopic data at 600 and 150 MHz, respectively, of cycloartenyl E-ferulate elucidated in fraction 14 of Spiral-Coil LSRCCC from Baby Banana peels with hyperpigmentation (Liu et al. 2013).

Assignment	$\delta^{13}C$ (ppm)	$\delta^{1}H$ (ppm)
1	31.80	1.66 (1H, *m*), 1.29 (1H, *m*)
2	28.80	1.84 (1H, *m*), 1.68 (1H, *m*)
3	80.13	4.7 (1H, *dd*)
4	39.80	---
5	47.30	1.44 (1H, *dd*)
6	21.10	1.60 (1H, *m*), 0.81 (1H, *m*)
7	28.30	1.90 (1H, *m*), 1.28 (1H, *m*)
8	48.00	1.53 (1H, *dd*)
9	20.25	---
10	26.30	---
11	25.80	1.34 (1H, *m*), 1.11 (1H, *m*)
12	35.70	1.29 (2H, *m*)
13	44.90	---
14	49.00	---
15	33.10	1.62 (2H, *m*)
16	26.60	2.00 (1H, *m*), 1.13 (1H, *m*)
17	54.47	n.d
18	18.10	0.97 (3H, *s*)
19	29.90	0.60 (1H, *d*), 0.36 (1H, *d*)
20	36.00	1.39 (1H, *m*)
21	18.80	0.89 (3H, *d*)
22	36.50	1.44 (1H, *m*), 1.05
23	25.1	1.63 (1H, *m*), J=6.8
24	125.00	5.10 (1H, *t,* J= *7.0* Hz*)*
25	131.00	---
26	17.80	1.61 (3H,*s*)
27	25.90	1.68 (3H,*s*)
28	19.30	0.91 (3H, *s*)
29	25.60	0.89 (3H, *s*)
30	15.50	0.97 (1H, s)
1'	**167.88**	**---**
2'	**117.00**	**7.3 (1H, *d*)**
3'	**145.00**	**7.4 (1H, *d*)**
4'	**125.09**	**---**
5'	**119.40**	**7.06 (1H, *d*), J=2.5 Hz)**
6'	**146.46**	**---**
7'	**147.90**	**---**
8'	**114.21**	**4.82 (1H, *d*), 4, 89 (1H, *d*) 4.83 (1H, *dd*), J=1.2, J=3.5, J=10.2) 4.9 (1H, *dd)*, J=1.6, J=3.8, J=17.1)**
9'	**124.35**	**7.08 (1H, *dd*), J=2.5 Hz, J= 8.6**
-OCH_3	**56.70**	**3.7 (3H, *s*)**

2.3.5 Summary

The Spiral-Coil Low Speed Rotary Countercurrent Chromatography experiment covered a broad spectrum of compounds in relation to the degradation of chlorophylls and also detected other lipids in Baby Banana peel with hyperpigmentation. Moreover, the scale-up experiment demonstrated the power of the technique with regard reproducibility and accuracy.

The results summarized for each fraction indicated a possible value as ingredients for the pharmaceutical drug industry (Subramanian et al. 2008; Neugebauer et al. 2011; Scavariello and Avellano 1998; Islam et al. 2008; Cui et al. 2010; Farag and Paré 2013; Fuchs et al. 2005; Gonzáles-Montelongo et al. 2010; Guo et al. 2002; Islam et al. 2009; Kikuchi et al. 2007; Kolesnik et al. 1991; Nakagawa et al. 2008; Potta et al. 2003; Skakovskii et al. 2007; Stoffel et al. 1972; Xu et al. 2001; Stoffel et al. 1974; Schwartz et al. 2008) Nevertheless, the main objective proposed of the research was to find an explanation for the hyperpigmentation phenomenon.

In the study of the phenomenon of hyperpigmentation by means of HSCCC and Spiral-Coil LSRCCC it became apparent that several compounds occur in larger quantities in banana peels with hyperpigmentation than in control banana peels. The main relevant results have been explained in the Spiral-Coil experiment when the elucidation of fraction 14 was performed. 1D and 2D NMR experiments enabled the identification of tocopherols and tocotrienols in the fractions. It is meaningful that the same types of NMR spectra have been obtained in different experiments of Baby Banana peels with hyperpigmentation. For example, during the separation of methanol phase from banana with hyperpigmentation by means of HSCCC, fraction 5 in extrusion mode depicted a similar spectrum, also when the acetone extract was fractionated and the fractions were analyzed.

Additionally, derivatives of chlorophylls esterified with sitosterols could play an important role in the phenomenon of hyperpigmentation. Additionally, the Ba-

by Banana with hyperpigmentation showed only chlorophyll *b* in contrast with the normal banana which contained only chlorophyll *a*.

In any case, the results should be analyzed carefully in relation with the biochemistry and physiology of the plant in order to understand the difference between banana control and banana with hyperpigmentation. The research should continue in order to elucidate the physiological behavior due to the hyperpigmentation phenomenon.

In a previous report it has been published that the lipophilic extracts of bananas residues represent a source of valuable phytosterols. Oliveira et al. 2006 studied the fatty acids, sterols and steryl esters in unripe pulp and peel of banana fruit 'Dwarf Cavendish' by gas chromatography-mass spectrometry. Fatty acids are more abundant in the banana pulp (29-90% of the total amount of lipophilic extract), with linoleic, linolenic, and oleic acids as the major compounds among the unsaturated fatty acids. Sterols represented about 49-71% of the liphophilic extract with two triterpenic ketones (31-Norcyclolaudenone and cycloeucalenone) as the major components. The detection of high amounts of steryl esters (469-24405 mg/kg) and diacylglycerols (119-878 mg/kg) is reported, mainly present in the banana peel extract (Oliveira et al. 2006).

Steryl glycosides and acyl steryl glycosides from *Musa paradisiaca* were isolated from peeled fruits of banana and identified as sitoindoside-III and sitoindoside-IV, and two new steryl glycosides, sitosterol gentiobiose and sitosterol *myo*-inosytyl-ß-D-glucoside (Ghosal 1985).

Still, this is the first report of the analysis of Banana peel by means of HSCCC and Spiral-Coil LSRCCC. Consequently, the results could be a guide for further studies in relation with other fruits.

3. SUMMARY AND OUTLOOK

The degree of greenness, attributed to chlorophyll pigment, is important in determining the quality of banana during the postharvest stage. For this reason the hyperpigmentation phenomenon observed in some peels of Baby Bananas (*Musa acuminata AA Simmonds cv. Bocadillo*) from Colombia has been studied in the current research. The visible small green bands which occur when the fruit reaches the green stage of ripening and disappear subsequently when the carotenoids are the major compounds in the peels, could be related with the degradation of chlorophyll according to the results obtained in the present phytochemical study.

Chlorophyll *a* (Chl *a*), chlorophyll *b* (Chl *b*) and pheophytin *a* (Phy *a*) were isolated from Baby banana peels by means of high-speed countercurrent chromatography (HSCCC) with the application of a novel solvent system composed of hexane/EtOH/CH_2Cl_2/H_2O (6:2:4:2 *v/v/v/v*). This suitable solvent system elaborated during the assays of optimization permitted the evaluation of chlorophylls *a/b* ratio and derivatives not only in Banana peels but also in grass and spinach. The results revealed a significant difference in the pigment composition between the baby banana with hyperpigmentation and the baby banana control. Chl *a/b* and Phy *a/b* ratios in control and hyperpigmented banana could indicate that Baby Banana control uses the reversal Chl-*b* biosynthesis during the degradation pathway to produce just Chl-*a* while banana with hyperpigmentation did not depict Chl-*a* and conversely accumulate Chl-*b.*

According to recent publications regarding chlorophyll degradation, a pathway of chlorophyll breakdown not only occurs in chloroplast/gerontoplast but also in both cytosol and vacuole via pheophorbide *a* oxigenase (PaO) to produce fluorescent (Mc-FCC) as well as nonfluorescent (NCCs) chlorophyll catabolites. The preference of PaO for pheophorbide *a* as substrate instead of pheophorbide *b* is explained by the fact that pheophorbide *b* is a competitive inhibitor of PAO. Therefore catabolism of chlorophyll *b* is required to yield chlorophyll *a.*

These results could explain the reason of the accumulation of Chl-*b* in Baby banana peels with hyperpigmentation and also its lower ratio of Phy *a/b* (0.86) in comparison with 3.06 of Phy *a/b* in control. The difference of ratios between Phy *a*/*b* is due to the lower amount of Phy *b* in Baby banana control in contrast with the high value of Phy *b* in the hyperpigmented banana.

The role of the enzymes during the degradation of chlorophylls is relevant and therefore a methodology to isolate chlorophyllase enzyme and proteins in Baby banana peel was applied **(cf. 4.3.6).** Proteins bands in SDS/PAGE were found in the range from 20 kD to 37 kD from the extract of Baby banana peel without hyperpigmentation that could correspond to the chlorophyllase enzyme of Baby Banana peels in concordance with both the 25 kDa protein band and molecular weight of the heated enzyme protein with 35 kDa reported in the literature (Harpaz-Saad et al. 2007; Trebitsh et al. 1993). Further studies are necessary to compare these results with the protein screening of a Baby banana extract with hyperpigmentation.

Spiral-coil LSRCCC fractionated 17 g of an hexane extract of Baby banana peels with hyperpigmentation by using the solvent system acetonitrile/hexane (1:1 *v/v*). Chlorophyll derivatives were eluted (polar→unpolar) in elution and extrusion mode. The extraction method used increases the pheophytinization and APCI-HPLC-MS method showed that it is suitable for these type of compounds with polar and unpolar moieties.

Further studies with Spiral-coil LSRCCC should be performed to evaluate the behavior of chlorophyll *a/b* ratios with the application of the second extraction method which avoids the total degradation of chlorophylls by using the novel solvent system hexane/EtOH/CH_2Cl_2/H_2O (6:2:4:2 *v/v/v/v*).

The elucidation of tocotrienols by 1D and 2D NMR in fraction 14 of Spiral-coil LSCCC separation of Baby Banana peel with hyperpigmentation is relevant. The control Banana does not show any presence of these compounds.

The tentative explanations could be supported by the detection of the major derivatives of chlorophyll in Baby Banana peel with hyperpigmentation during the Spiral-Coil LSRCCC experiment which were pyropheophorbides esterified with sterols **(cf. 2.3.3).** The loss of phytol in the chlorophyll molecule during the degradation would yield an accumulation of phytol which can be transformed into tocopherols and tocotrienols as it is reported by Collakowa and DellaPenna (2003) and DellaPenna and Pogson (2006). The tocopherols are synthesized exclusively by photosynthetic organisms.

The occurence of triterpene alcohol ferulates has been reported before in Rice Bran oil fractionated by means of HSCCC (Angelis et al. 2011; Liu et al. 2013). In fraction 14 from Spiral-Coil LSRCCC separation scale-up both 25-hydroxy-24-methylcycloartenyl ferulate by APCI-HPLC-MS and cycloartenyl *trans* ferulate by 1D, 2D NMR experiments have been identified **(cf. 2.3.4.1, 2.3.4.2).** The literature cited above reported that a nutraceutical edible oil from Rice bran by-product is known as γ-oryzanol which contains high amount of sterols, triterpene alcohol ferulates and vitamin E (tocopherols and tocotrienols). Therefore, Baby banana peel with hyperpigmentation contains this valuable raw material which has antioxidant and hypocholesterolemic properties (Scavariello and Avellano 1998; Islam et al. 2009).

The phytochemical analysis of Baby banana peel revealed a novel glycolipid O-α-D-Gal*p*(1''→ 6')-O-β-D-Glu*p*(1'→3)-2, 1-diacyl-L-glycerol which has not been found in higher plant before **(cf. 2.1.2).** Phosphatidylcholine (Lecithin), phosphatidyl-ethanolamine, molecular species of glucocerebroside and sulphoquinovosyl-diacylglycerol were elucidated by 1D,2D NMR experiments. Before the current research, these compounds have not been reported in banana.

It is also important to note that carotenoids do not play an important role in relation with the hyperpigmentation phenomenon since they are found in similar proportion in both types of bananas. However, the novel solvent system hexane/EtOH/$CHCl_3$/H_2O (6:2:4:2 *v/v/v/v*) enables the isolation of xanthophylls in fruit and plants which could be important for further research.

The outlook in the near future is to analyze carefully the further compounds fractionated by means of HSCCC from the methanol extract of both Baby banana peels with hyperpigmentation and control in order to clarify the occurrence of polar derivatives of chlorophyll, such as red chlorophyll catabolite (RCC), new fluorescent chlorophyll catabolites (FCCs) and nonfluorescent chlorophyll catabolites (NCCs). Afterward it would be priority to explore the hyperpigmentation phenomenon with fresh Baby bananas in Colombia by means of HSCCC and Spiral-Coil LSRCCC with the application of the methodology developed in the current research.

4. MATERIAL AND METHODS

4.1 Plant Material and Chemicals

4.1.1 Plant Material

Baby Bananas were obtained from the Colombian company CIDELA LTDA. The fruits were collected from plantations located in Cundinamarca, Colombia. The stage of ripening was green color corresponding to stage No. 2 of the color chart used in marketing. The samples were weighted and peeled to separate the peel and pulp from the fruits. Flavedo, the outer membrane of the peels, that contains plastid with chlorophylls in unripe fruit, also called "exocarp", is separated from the albedo, the inner layer of the peels, also called "mesocarp". The flavedo is weighted, gently lyophilized and stored at -20°C until the extraction is executed.

Grass material was supplied by Henkel, Germany, and spinach was purchased at a market in Braunschweig, Germany.

4.1.2 Chemicals and Solvents

Demineralised water (Barnstead, UK) and deionised water (Nanopure®, Werner, Germany) was provided for the preparations of solutions in experiments. For HPLC- and HPLC-MS- analyses solvents with HPLC-quality have been used. Extractions, HSCCC separations and Thin Layer Chromatography (TLC) were performed with p.a.–quality solvents. The chemicals and solvents were supplied by Sigma-Aldrich, Fluka (Steinheim, Germany), Roth (Karlsruhe), Merck (Darmstadt, Germany), Fisher Scientific (Loughborough, UK) AppliChem (Darmstadt, Germany), Deutero (Kastellaun, Germany) and Riedel-de Haën (Seelze, Germany) **(Table 5.1).**

Table 4-1. Chemicals used with the producer and purity information.

Chemicals	**Purity**	**Manufacturer**
Acetonitrile	p.a	Sigma-Aldrich
Acetonitrile	HPLC grade	Sigma-Aldrich
Acetone	p.a	Carl Roth
Acetone $-d_6$	99.9 % deuterated	Deutero GmbH
Acetone	Distilled	---
Anisaldehyde	p.a.	Merck
Acetic acid	p.a. (100%)	Roth
Acetic acid	p.a. (98-100%)	Merck
Chloroform	p.a.	Fluka
Chloroform-d	99.8 % deuterated	Deutero GmbH
Dichloromethane	p.a.	Fluka
Dichloromethane-d_2	99.8 % deuterated	Deutero GmbH
Diethylether	p.a	Fluka
N,N-dimethylformamide	p.a	Roth
Ethanol	p.a. (≥ 99.8%)	Sigma-Aldrich
Ethanol	Distilled	---
Ethyl acetate	p.a	Roth
Ethyl acetate	p.a (99.97%)	Fisher Scientific
n-Hexane	Distilled	---
n-Hexane	HPLC	Roth
Isopropanol	HPLC	Sigma-Aldrich
Potassium hydroxide	p.a. (≥ 85%)	Roth
Methanol	Distilled	---
Methanol	HPLC	Fisher Scientific
Methanol	HPLC-MS	VWR
Methanol-d_4	99.8% deuterated	Deutero GmbH
Magnesium carbonate	p.a.	Roth
Sodium sulfate (anhydrous)	p.a.	Merck
Sulfuric Acid	p.a (95-98%)	Roth
Tert-butylmethylether	HPLC	Merck

4.2 Equipments and Parameter

4.2.1 High-Performance Liquid Chromatography (HPLC)

4.2.1.1 Jasco-System (HPLC-DAD)

Pump:	Intelligent HPLC Pump PU-980 (Jasco, Gross-Umstadt, Germany)
Degasser:	Three-Line-Degasser DG-980-50 (Jasco, Gross-Umstadt, Germany)
Gradient mixer:	Low-pressure gradient former LG-980-02 Ternary Gradient Unit (Jasco, Gross-Umstadt, Germany)
Detector:	MD-910, Multiwavelength between 220-650 nm (Jasco, Gross-Umstadt, Germany)
Auto sampler:	Intelligent autosampler AS-950 (Jasco, Gross-Umstadt Germany)
Software:	Borwin PDA Chromatography Data System, Version 1.8.6.1 (Jasco, Gross-Umstadt, Germany)

4.2.1.2 Knauer-System (preparative) – Equipment I

Pump:	Wellchrom HPLC Pump K-1001 (Knauer, Berlin, Germany)
Degasser:	Wellchrom 4 Channel Degasser K-5004 (Knauer, Berlin, Germany)
Gradient mixer:	Solvent organizer K-1500 (Knauer, Berlin, Germany) Dynamic Mixing Chamber (Knauer, Berlin, Germany)
Injector:	Analytic: 20 µL and Preparative 500 µL (Knauer, Berlin, Germany)
Detector:	Wellchrom UV Detector K-2600 (Knauer, Berlin, Germany)
Software:	Knauer Eurochrom 2000 Windows Version 2.05

4.2.1.3 Knauer-System (preparative) – Equipment II

Pump:	Wellchrom HPLC Pump K-1500 (Knauer, Berlin, Germany)
Degasser:	Wellchrom 4 Channel Degasser K-5004 (Knauer, Berlin, Germany)
Gradient mixer:	Solvent organizer K-1500 (Knauer, Berlin, Germany) Dynamic Mixing Chamber (Knauer, Berlin, Germany)
Injector:	Analytic: 200 µL and Preparative 500 µL, 96650, (Knauer, Berlin, Germany)
Detector:	Wellchrom UV Detector K-2600 (Knauer, Berlin, Germany)
Software:	ChromGate® 3.1.7.

4.2.1.4 Analytical Columns

Luna C18 (2), 250 x 4.6 mm, 5 μm, (Phenomenex, Germany)
Hypersil C18, 250 x 2.0 mm, 5 μm (Phenomenex, Germany)

4.2.1.5 Preparative Columns

Eurosphere 5 μm 100-018 C18, 250 x 16 mm with C18 precolumn (Knauer, Germany)
Luna 5 µm C18 (2), 250 x 10 mm, with C18 precolumn (Phenomenex, Aschaffenburg, Germany)
Luna 5 µm C18 (2), 250 x 15 mm, with C18 precolumn (Phenomenex, Germany)

4.2.1.6 Solvent System and Gradients of HPLC – DAD

4.2.1.6.1

Solvent system	A:H_2O B:Methanol
Flow rate:	0.25 mL/min
Column:	Hypersil C18, 250 x 2.0 mm 5 μm (Phenomenex, Germany)
Gradient:	0 min 80% B, 7 min 85% B, 20 min 100% B, 50 min 100% B, 55 min 80% B, 60 min 80% B
Detector:	210 nm
Injection:	5 µL

4.2.1.6.2

Solvent system	A:H_2O B:Methanol 95:5 (*v*/*v*)
Flow rate:	0.25 mL/min
Column:	Hypersil C18, 250 x 2.0 mm 5 μm (Phenomenex, Germany)
Gradient:	Isocratic
Detector:	210 nm
Injection:	5 µL

4.2.1.6.3

Solvent system	Methanol 100%
Flow rate:	0.25 mL/min
Column:	Hypersil C18, 250 x 2.0 mm 5 μm (Phenomenex, Germany)
Gradient:	Isocratic
Detector:	210 nm
Injection:	5 µL

4.2.1.6.4

Solvent A:	*tert.* Butyl-methylether/Methanol/H_2O, 4/92/4 (*v*/*v*/*v*)
Solvent B:	*tert.* Butyl-methylether/Methanol/H_2O, 90/6/4 (*v*/*v*/*v*)
Flow rate:	0.8 mL/min
Column:	Luna C18 (2), 250 x 4.6 mm 5 μm, (Phenomenex, Germany).
Gradient:	0 min 0% B, 10 min 0 % B, 20 min 50% B, 30 min 100% B, 50 min 100 % B, 55 min 0% B, 60 min 0% B

4.2.1.7 Solvent System and Gradients of Preparative HPLC

4.2.1.7.1 Preparative HPLC System 1

Solvent system	Methanol/Ethanol 7:3 (*v*/*v*)
Flow rate:	3.0 mL/min
Column:	Luna 5 µm C18 (2), 250 x 15 mm, with C18 precolumn (Phenomenex, Germany).
Gradient:	Isocratic
Detector:	210 nm
Injection:	0.5 mL

4.2.1.7.2 Preparative HPLC System 2

Solvent system	Methanol 100%
Flow rate:	6.0 mL/min
Column:	Luna 5 µm C18 (2), 250 x 10 mm, with C18 precolumn (Phenomenex, Germany).
Gradient:	Isocratic
Detector:	400 nm
Injection:	0.5 mL

4.2.1.7.3 Preparative HPLC System 3

Solvent system	*tert.* Butyl-methylether/Methanol/H_2O, 90/6/4 (*v*/*v*/*v*)
Flow rate:	6.0 mL/min
Column:	Luna 5 µm C18 (2), 250 x 10 mm, with C18 precolumn (Phenomenex, Germany).
Gradient:	Isocratic
Detector:	400 nm
Injection:	0.5 mL

4.2.2 Mass spectrometry

4.2.2.1 APCI-HPLC-MS-MS

Pump:	Agilent 1200 G1329A BinPump (Santa Clara, California, USA)
Detector:	Agilent 1100 DAD G1315B (Santa Clara, California, USA)
Autosampler:	Agilent 1200 G132B ALS SL (Santa Clara, California, USA)
MS:	Bruker Daltonics Inc Ultra PTM Discovery System
Controler Unit:	Bruker Compass hystar

4.2.2.2 Column APCI-HPLC-MS-MS

ProntoSIL C18, 250 x 2 mm, 5 μm (Knauer, Germany)

4.2.2.3 Parameter Mode APCI-HPLC-MS-MS

Mass Range Mode:	Ultra Scan
Ion Polarity:	Positive
Ion Source Type:	APCI
Trap Drive:	55.6
Octopole RF Amplitude:	187.1 Vpp
Vaporizer Temp:	400°C
Capillary exit:	121.0 V
Lens 2:	-60,0 V
Dry Temp:	350°C
Dry Gas:	5.00 l/min
Nebulizer:	45,00 psi
HV Capillary:	-3500 V
HV End Plate Offset:	-500 V
Scan Begin:	150 *m/z*
Scan End:	1500 *m/z*
Average:	5 Spectra
Max. Acc. Time:	200000 µs
(Smart) ICC Target:	100000

4.2.2.4 Solvent system and gradient of APCI-HPLC-MS

Solvent A:	*tert.* Butyl-methylether/Methanol/H_2O, 4/92/4 (*v*/*v*/*v*)
Solvent B:	*tert.* Butyl-methylether/Methanol/H_2O, 90/6/4 (*v*/*v*/*v*)
Flow rate:	0.8 mL/min
Column:	ProntoSIL C18, 250 x 2 mm, 5 μm (Knauer, Germany)
Gradient:	0 min 0% B, 10 min 0 % B, 20 min 50% B, 30 min 100% B, 50 min 100 % B, 55 min 0% B, 60 min 0% B

4.2.3 High-Speed Countercurrent Chromatography (HSCCC)

Equipment:	High-Speed Countercurrent Chromatograph CCC-1000, Pharma-Tec Research (Baltimore, MD, USA)
Coil:	Triplecoil, Teflon tubing I.D. 2.5 mm
Volumen:	850 mL
Sample loop:	20 mL, 25 mL, 50 mL
Pump:	Biotronik HPLC Pump BT 3020 (Jasco, Gross-Umstadt, Germany)
Detector:	Variable Wavelength Monitor, A0293, Knauer (Berlin, Germany)
Recorder:	Servogor 120, BBC Goerz Metrawatt
Fraction collector:	LKB Bromma 2211 SuperFrac, Pharmacia (Sweden)

Parameter of HSCCC separations:

ELUTION MODE:	Head to Tail (upper phase as stationary phase)
Flow rate:	3.5 mL / min
Rotation:	800 U / min
Detector:	210 nm or/and 440 nm
Mobile phase:	lower phase
EXTRUSION MODE:	Tail to Head (lower phase as stationary phase)
Flow rate:	6.0 mL/min
Rotation:	600 U/min
Detector:	210 nm or/and 440 nm
Mobile phase:	upper phase

4.2.3.1 Solvent System of High-Speed Countercurrent Chromatography (HSCCC)

I. Hexane/CH_2Cl_2/EtOH/H_2O (4:2:6:2, *v/v/v/v*)

II. Acetonitrile/Hexane (1:1, *v/v*)

III. Hexane/Methanol/H_2O/EtOAc (10:10:1:1, *v/v/v/v*)

IV. Hexane /EtOH/ H_2O (6:5:2, *v/v/v*)

V. Hexane/Methanol (2:1, *v/v*)

VI. Hexane/Acetonitrile/$CHCl_3$ (4:6:1, *v/v/v)*

VII. Hexane/$CHCl_3$/EtOH/H_2O (4:2:6:2, *v/v/v/v*)

4.2.4 Gas Chromatography

4.2.4.1 GC-MS I

Equipment	HP 5890 Series II Plus Gas chromatograph (Agilent, USA)
Capillary column	Wax plus 0.25 mm i. D., Layer thickness 0.25 µm, length:30 m (Phenomenex, USA)
Carrier gas	Helium (1.0 mL/min)
Auto sampler	HP 6890 Series Injector with HP 7673 Controller (Agilent, USA)
Injector	Split/Splitless (1:10), 230 °C
Injection volume	1 µL
Detector	HP 5972 Series Mass selective detector (Agilent, USA)
Ionization	El 70 eV
lon source	180 °C
Scanning area	50-550 u, 1.53 Scans/s
Temperature program	70 °C for 3 min, ramp of 3 °C/min up to 220 °C and 220 °C for 10 min; transfer line temperature 220 °C

4.2.4.2 GC-MS II

Equipment	GC-2010, *Shimadzu*
Capillary column	ZB-5HT, 0.25 mm i. D., Layer thickness 0.25 µm, length:30 m, a retention gap (deactivated, 1.5 m) (Phenomenex, USA)
Carrier gas	H_2 (65.4 kPa) 40 cm/s (linear velocity mode)
Injector	Split/Splitless, 250 °C
Injection volume	1 µL
Detector	FID, H_2 (40 mL/min) and synthetic air (400 mL/min), N_2 (*make-up*-gas 30 mL/min)
Temperature program	60 °C (1 min), with 20 °C/min to 200 °C, with 4 °C /min to 250 °C, with 20 °C /min to 310 °C /min for 10 min.
Software:	GC solution Data system Version 2.3

4.2.4.3 GC-MS III

Equipment	GC-5890A, *Hewlett Packard*
Capillary column	ZB-5HT, 0.25 mm i. D., Layer thickness 0.25 µm, length:30 m, a retention gap (deactivated., 1.5 m) (Phenomenex, USA)
Carrier gas	H_2 (65.4 kPa) 40 cm/s (linear velocity mode)
Auto sampler	HP 6890 Series Injector with HP 7673 Controller (Agilent, USA)
Injector	Split/Splitless 1:20
Injection volume	1 µL
Detector	FID, H_2 (40 mL/min) and synthetic air (400 mL/min), N_2 (*make-up*-gas 30 mL/min)
Temperature program	60 °C (1 min), with 20 °C/min to 200 °C, with 4 °C /min to 250 °C, with 20 °C /min to 310 °C /min for 10 min
Software:	Amidis32 and Wsearch32

4.2.5 Spiral-Coil Low-Speed Rotary Countercurrent Chromatography (Spiral-Coil LSRCCC)

Equipment:	Prototype Spiral tube assembly of the LSRCCC Pharma-Tech Research Corporation (Baltimore, Maryland)
Coil:	"Convoluted" Teflontubing I.D 8.5 mm
Volume:	Three spiral layers 550 mL
Coil volume:	10 Spirals 5500 mL
Pump:	HPLC Pump 64 (Knauer, Berlin, Germany)
Detector:	Variable Wavelength Monitor, (Knauer, Berlin, Germany)
Recorder:	ABB Goerz SE 120, Register paper 1 cm/h
Fraction collector:	LKB SuperFrac, 10 Pharmacia, 10-12 min/fractions (Sweden)

4.2.5.1 Solvent system for Spiral-Coil LSRCCC

Solvent system:	Acetonitrile/Hexane; 1/1 (*v/v*)
Flow rate:	15.0 mL/min
Elution mode:	Head to tail
Wavelength:	210 nm
Rotation:	ca. 100 U/min

4.2.6 Nuclear Magnetic Resonance Spectroscopy

Equipment I:	AMX-300, Bruker Daltonik (Germany)
NMR frequency:	^{1}H: 300.1 MHz ^{13}C: 75.5 MHz
Equipment II:	AVII-600, Bruker Daltonik (Germany)
NMR frequency:	^{1}H: 600.0 MHz ^{13}C: 150.0 MHz

The isolated substances were dissolved in deuterated solvents: CD_3OD, CD_3Cl, CD_2Cl_2 and d_6-acetone.

4.3 Methods

4.3.1 Extraction Methods

4.3.1.1 First Extraction Method

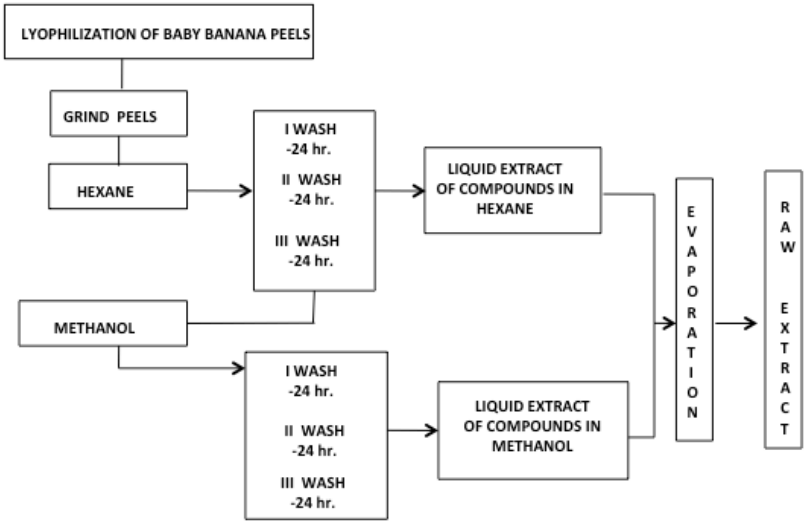

Figure 4-1. Methodology of first extraction method applied to Baby Banana peels, chlorophyllase enzyme and proteins in Baby Banana peels with hyperpigmentation (Jerz et al. 2007).

4.3.1.2 Second Extraction Method

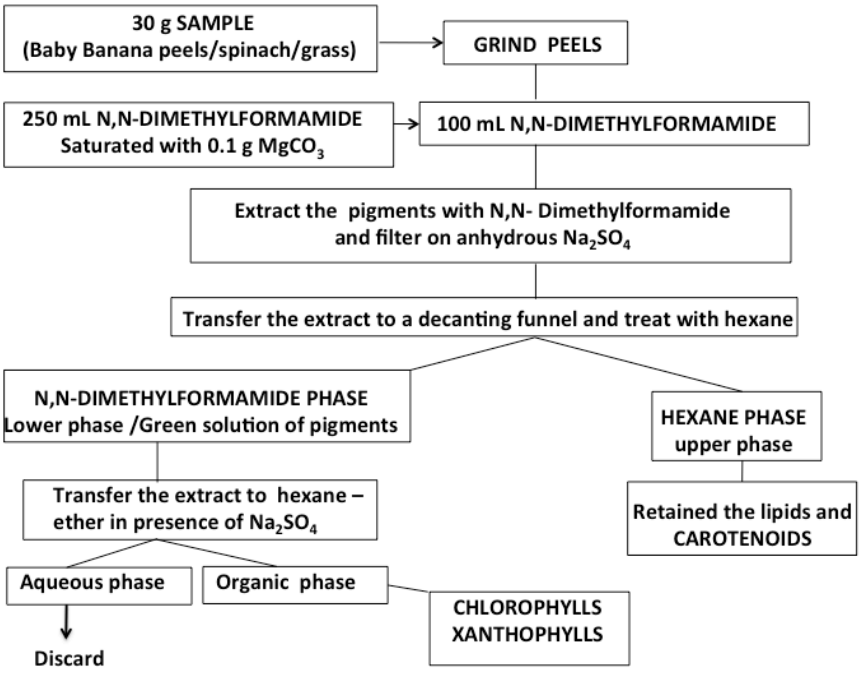

Figure 4-2. Methodology of second extraction method applied to Baby Banana peels, grass and spinach. (Minguez-Mosquera and Garrido-Fernandez 1989).

4.3.2 Thin Layer Chromatography (TLC)

4.3.2.1 System 1

TLC plate:	Silica Gel 60F_{254} TLC aluminium foils sheet 20 x 20 cm (layer 0.2 mm, MERCK)
Solvent systems:	CH_2Cl_2 /Acetone 9:1 (*v/v)* CH_2Cl_2/Acetone 9.9/0.1 (*v/v)* CH_2Cl_2/Methanol 9.9/0.1 (*v/v)* CH_2Cl_2/Hexane/Acetone 7:3:0,15 (*v*/*v*/*v*) Petroleum ether/Acetone/diethylamine 10:4:1 (*v/v/v*)
Detector:	daylight, UV 254 nm, UV 366 nm
Detection:	Spray reagent anisaldehyde-sulfuric acid according to Stahl (1967). Anisaldehyde–concentrated sulfuric acid-glacial acetic acid(1:2:97). Developing at 110°**C.**

4.3.2.2 System 2

TLC plate:	Alugram RP-18W/UV_{254} 20 x 20 cm (layer 0.2 mm, MERCK)
Solvent systems:	Acetonitrile 100% Methanol 100% Ethanol/Methanol 5:5 (*v/v*) Ethanol/Acetonitrile 5:5 (*v/v*) *tert.* Butyl-methylether/Methanol/H_2O, 4:92:4 (*v*/*v*/*v*) *tert.* Butyl-methylether/Methanol/H_2O, 90:6:4 (*v*/*v*/*v*)
Detector:	daylight, UV 254 nm, UV 366 nm
Detection:	Spray reagent anisaldehyde-sulfuric acid according to Stahl (1967). Anisaldehyde–concentrated sulfuric acid-glacial acetic acid(1:2:97). Developing at 110°**C.**

4.3.3 Compositional analysis of glycolipids

4.3.3.1 Analysis of fatty acid components by Gas chromatography–mass spectrometry (GC-MS)

Purified glycolipids (2 mg) were esterified by dissolving 1 mg of the sample in 1 mL petroleum ether in a V-vial and then 30µL from 2 mol sodium methylate solution was added. The sample should be shaked several times to obtain two phases. The upper phase (petroleum ether) contained fatty acids Me esters and the lower phase (sodium methylate and water) contained sugars and glycerol as polar components from glycolipids.

Fatty acid methyl esters were treated with ca. 100 mg of calcium chloride and were analyzed by gas chromatography–mass spectrometry (GC-MS) **(cf. 4.2.4.1)**.

4.3.3.2 Sugar composition of glycolipids (SCG)

The sugar composition of the glycolipids was determined following hydrolysis and derivatization of the sugars as their alditol acetates. 2 mg of glycolipids without acyl moiety, simultaneously, with glucose and galactose samples were treated in an 1mL V-vial, respectively, with 2M trifluoroacetic acid (TFA) (750 µL deionized water and 150 µL of concentrated TFA). After cooling to room temperature, aqueous acid was removed by repeated co-distillation with toluene in a stream of nitrogen. Hydrolyzed samples were reduced with a solution of 500 µL of 0.25 M $NaBD_4$ in 2 M NH_3 at 60 °C for 120 min. The yield of cristals into the vials reveals that the hydrolysis was carried out and the alkaline acetylation is performed (Adden et al. 2006, 2005).

After cooling to room temperature, the solution was co-evaporated with methanolic acetic acid (15%) in a stream of nitrogen to remove borate as its methyl ester. The derivatives were dissolved in 50 µL of pyridine and 200 µL of acetic anhydride was added to acetylate the sample at 90 °C for 120 min. Saturated $NaHCO_3$-solution was added and stirred until CO_2-formation ceased. The products were extracted three times with dichloromethane. The combined organic layers were first washed two time with saturated $NaHCO_3$-solution (1 mL), once with cold 0.1 M HCl (1 mL), three times with 1 mL of water, and then dried over $CaCl_2$ (Voiges et al. 2012).

Alditol acetates were prepared and analyzed by gas chromatography/mass spectrometry (GC/MS) **(cf. 4.2.4.2; 4.2.4.3).**

4.3.4 Isolation of pheophytin from methanol phase of Baby Banana peels by means of Normal Phase Chromatography

The first extraction method was applied to obtain a methanol phase from Baby Banana peels (control, without hyperpigmentation). Two HSCCC separations from the methanol phase extract were performed in elution and extrusion mode to recollect 16.34 mg of pheophytin *a* together with triterpenoids in fractions 6 of extrusion mode. Analysis was done by means of APCI-HPLC-MS **(cf. 4.2.2.4)** and TLC chromatography **(cf. 4.3.2).**

The application of normal phase chromatography onto a Silica gel mini-column (Pasteur pipette) was performed to fractionate 16.35 mg of the extract and 7 mini-fractions were eluted with the solvent system CH_2Cl_2/Hexane /Acetone, (7:3:0,2 *v/v/v*). 2.1 mg of pure pheophytin *a* was obtained from mini-fraction 3.

In order to recollect enough amount of pure pheophytin *a* for the analysis of 2D NMR experiments, preparative HPLC method **(cf. 4.2.1.7.2)** was applied to 7.8 mg from mini-fraction 2 of the normal phase chromatography. 1.2 mg of pure pheophytin *a* was obtained from fraction 7 from preparative HPLC separation and a total of 3.3 mg of pure pheophytin *a* was recollected.

4.3.5 Isolation of carotenoids from acetone extract of Baby Banana peels with hyperpigmentation by means of Normal Phase Chromatography

100 mg of fraction 12 obtained from preparative separation by HSCCC of acetone extract from Baby Banana peels with hyperpigmentation (**cf. 2.1.9**) was fractionated by means of normal phase chromatography. A chromatography column (400 mm x 30 mm i.d.) was used with a mobile phase consisting of CH_2Cl_2/Methanol (9.9/0.1) (*v/v)*. 15 fractions were eluted and monitored with TLC in order to observe the purity of the separations. Fraction 1 showed a single yellow coloured band under white light and corresponded to 27.8 mg of a mixture of carotenoids identified by APCI-HPLC-MS and 1D and 2D NMR experiments (Byrdwell 2005).

4.3.6 Partial isolation of chlorophyllase and proteins from flavedo of Baby Banana peels

A protocol was established to isolate chlorophyllase and proteins from 250 g of flavedo, the outer coloured layer of Baby Banana peels. The sample was homogenized with acetone to obtain an acetone powder and the soluble proteins were extracted with 100 mM potassium phosphate (pH 7.0) containing 50 mM KCl and 0.24% Triton–x100 from the acetone powder and centrifuged at 10,000 x *g* at 4 °C for 60 min. The supernatant was homogenized and stirred with 80% (*m/v*) of $(NH_4)_2SO_4$ for 60 min at 4 °C and centrifuged at 10,000 x *g* at 4°C for 90 min. The precipitate was resuspended in phosphate buffer and dialyzed. The dialyzed product (20%) was lyophilized to determine the proteins by Bradford assay and the remaining (80%) allowed to measure the enzyme activity and the determination of molecular mass of proteins by SDS/PAGE with the "precision plus protein standards" from Bio-Rad: 10kD, 15kD, 20kD, 25kD, 37kD, 50kD, 75kD, 100kD, 150kD and 250kD.

The Bradford assay was performed using 1.14 mg of lyophilized product from dialyzed extract and 41.56 µg corresponded to proteins with an accuracy of 99% according to the coefficient of determination (R^2) estimated (Belitz et al. 2009)The SDS-PAGE electrophoresis was carried out and molecular masses between 10kD, 15kD, 25kD and 37kD were identified from the dialyzed product of Baby Banana peels **(cf. 4.3.6.1.)**

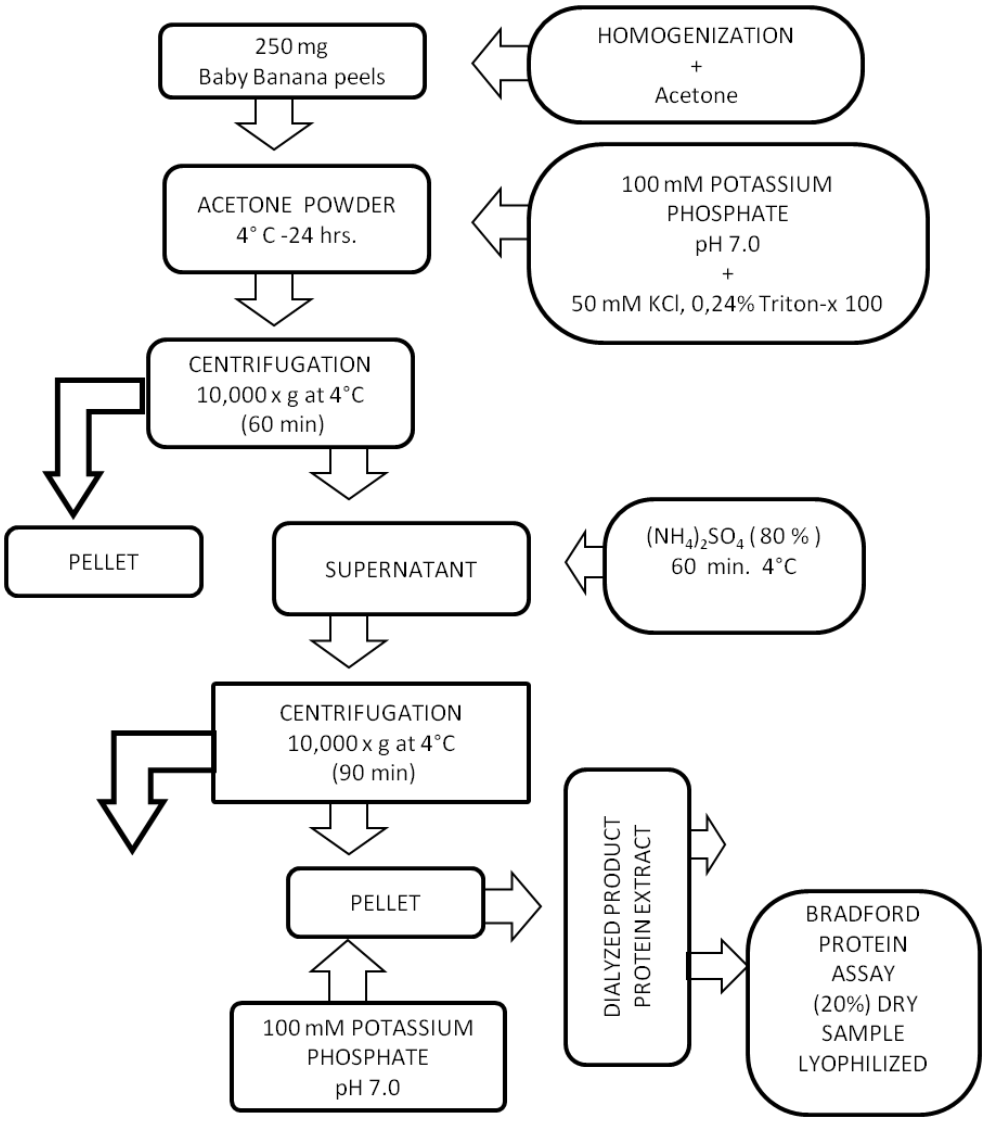

Figure 4-3. Methodology for the partial separation of chlorophyllase enzyme and proteins in Baby Banana peels with hyperpigmentation.

4.3.6.1 SDS/PAGE condition

-Gel dimensions 7.2 x 8.6 cm; 1.0 mm gel thickness.

-Stacking gel: 30% acrylamide mix (apply to 5% gel).

-Resolving gel: Mini-PROTEAN TGX gel 8-16% gradient.

-Electrophoresis Buffer:Tris-glycine.

-Sample load: 20µL.

-Sample Buffer: Laemmli Bio-Rad

-Run Conditions: 120V, 40mA

5. BIBLIOGRAPHY

Abraham, R. J., Rowan, A. E., Nuclear magnetic resonance spectroscopy of chlorophyll in: *Chlorophylls* (Hugo Scheer, ed.) CRC Press, Boca Raton, Florida, **1991**, pp. 797-834.

Abraham, R. J., Smith, K. M., Goff, D. A., Lai, J. J.: NMR spectra of porphyrins. 18. A ring-current model for chlorophyll derivatives. *Journal of the American Chemical Society,* **1982***,* 104(16), 4332-4337.

Adden, R., Mischnick, P.: A novel method for the analysis of the substitution pattern of O-methyl-α- and β-1,4-glucans by means of electrospray ionisation-mass spectrometry/collision induced dissociation. *International Journal of Mass Spectrometry*, **2005**, 242(1), 63–73.

Adden, R., Niedner, W., Müller, R., Mischnick, P.: Comprehensive analysis of the substituent distribution in the glucosyl units and along the polymer chain of hydroxyethylmethyl celluloses and statistical evaluation. Analytical Chemistry, **2006**, 78(4), 1146-1157.

Aghofack-Nguemezi, J., Manka`abiengwa, J.: Effects of exogenously applied benzylaminopurine and kinetin on the ripening of banana (*Musa acuminata Colla* var. *William*) fruits. *American Journal of Plant Physiology*, **2012**, 7(4), 154-163.

Akihisa, T., Kimura, Y., Kokke, W. C. M. C., Takase, S.-I., Yasukawa, K., Jin-Nai, A., Tamura, T.: 4-epicycloeucalenone and 4-epicyclomusalenone: two 3-oxo-28-norcycloartanes from the fruit peel of *Musa sapientum L.*, *Chemical & Pharmaceutical Bulletin,* **1997**, 45(2), 744-746.

Akihisa, T., Shimizu, N., Tamura, T., Matsumoto, T.: (24S)-14a, 24-Dimethyl-9b, 19-cyclo-5a-cholest-25-en-3b-ol: a new sterol and other sterols in *Musa Sapientum*. *Lipids*, **1986**, 21(8), 494-497.

Aman, R., Biehl, J., Carle, R., Conrad, J., Beifuss, U., Schieber, A.: Application of HPLC coupled with DAD, APcI-MS and NMR to the analysis of lutein and zeaxanthin stereoisomers in thermally processed vegetables. *Food Chemistry*, **2005a**, 92(4), 753-763.

Aman, R., Carle, R., Conrad, J., Beifuss, U., Schieber, A.: Isolation of carotenoids from plant materials and dietary supplements by high-speed counter-current chromatography. *Journal of Chromatography A,* **2005b**, 1074(1-2), 99-105.

Angelis, A., Urbain, A., Halabalaki, M., Aligiannis, N., Skaltsounis, A.-L.: One-step isolation of γ-oryzanol from rice bran oil by non-aqueous hydrostatic countercurrent chromatography. *Journal of Separation Science,* **2011,** 34, 2528-2537.

Aronoff, S., "The chlorophylls". An introductory survey, in: *Chlorophylls* (Vernon, L. P., Seely, G. R. eds.) Academic Press, New York, **1966**, p. 9.

Australian Government, Department of Health and Ageing. The Office of the Gene Technology Regulator, "The Biology of Musa L. (banana)", http: //www.ogtr.gov.au/ internet/ogtr/publishing.nsf/content/banana-3/$FILE/biologybanana.pdf, Vers. 1, **2008**.

Beck, J. G., Mathieu, D., Loudet, C., Buchoux, S., Dufourc, E. J.: Plant sterols in "rafts": a better way to regulate membrane thermal shocks. *Faseb Journal*, **2007**, 21(8), 1714–1723.

Belitz, H.-D., Grosch, W., Schieberle, P., *Food Chemistry.* Springer, Berlin, **2009**.

Benning, C., Huang, Z.-H., Gage, D.A.: Accumulation of a novel glycolipid and a betaine lipid in cells of *Rhodobacter sphaeroides* grown under phosphate limitation. *Archives of Biochemistry and Biophysics*, **1995**, 317(1), 103-111.

Berghold, J., *Chemische und biochemische Untersuchungen zum Chlorophyllabbau*, Ph. D. thesis. University of Innsbruck, Innsbruck, **2005**.

Berghold, J., Eichmüller, C., Hörtensteiner, S., Kräutler, B.: Chlorophyll breakdown in tobacco: on the structure of two nonfluorescent chlorophyll catabolites. *Chemistry & Biodiversity,* **2004**, 1(4), 657-68.

Berghold, J., Müller, T., Ulrich, M., Hörtensteiner, S., Kräutler, B.: Chlorophyll breakdown in maize: on the structure of two nonfluorescent chlorophyll catabolites. Monatshefte für Chemie Chemical Monthly **2006,** 137(6) 751-763.

Blackbourn, H. D., Jeger, M. J., John, P., Telfer, A., Barber, J.: Inhibition of degreening in the peel of bananas ripened at tropical temperatures. IV. Photosynthetic capacity of ripening bananas and plantains in relation to changes in the lipid composition of ripening banana peel. *Annals of Applied Biology*, **1990**, 117(1), 163-174.

Breithaupt, D. E., Bamedi, A.: Carotenoid esters in vegetables and fruits: A screening with emphasis on β-cryptoxanthin esters. *Journal of Agricultural and Food Chemistry*, **2001**, 49(4), 2064-2070.

Breithaupt, D. E., Schwack, W.: Determination of free and bound carotenoids in paprika (*Capsicum annuum L.*) by LC/MS. *European Food Research and Technology*, **2000**, 211(1), 52-55.

Breithaupt, D. E.: Identification and quantification of astaxanthin esters in shrimp (*Pandalus borealis*) and in a microalga (*Haematococcus pluvialis*) by liquid chromatography-mass spectrometry using negative ion atmospheric pressure chemical ionization. *Journal of Agricultural and Food Chemistry,* **2004**, 52(12), 3870-3875.

Britton, G., Liaaen-Jensen, S., Pfander, H., eds., Carotenoids, vol. 1B: *Spectroscopy*. *Birkhäuser, Basel,* **1995***.*

Britton, G., Liaaen-Jensen, S., Pfander, H.; Carotenoids Handbook, Birkhäuser: Basel, Switzerland, **2004***.*

Byrdwell, W. C., ed., *Modern Methods for Lipid Analysis by Liquid Chromatography/Mass Spectrometry and Related Techniques*, *Champaign, Ill., AOCS Press,* **2005.**

Chapman, D., Barber, J.: Polar lipids of chloroplast membranes. *Methods in Enzymology,* **1987***,* 148, 294-319.

Chapman, K.D., Ohlrogge, J.B.: Compartmentation of triacylglycerol accumulation in plants. *Journal of Biological Chemistry*, **2012**, 287(4), 2288-2294.

Chillier, X. Fr. D., van Berkel, G. J., Gülaçar, F. O., Buchs, A.: Characterization of chlorins within a natural chlorin mixture using electrospray/ion trap mass spectrometry. *Organic Mass Spectrometry,* **1994**, 29(11), 672–678.

Collakova, E., DellaPenna, D.: Homogentisate phytyltransferase activity is limiting for tocopherol biosynthesis in Arabidopsis. *Plant Physiology,* **2003** 131(2) 632-42.

Colson, P., King, R. R.: The ^{13}C-N.M.R. spectra of disaccharides of D-glucose, D-galactose, and L-rhamnose as models for immununological polysaccharides. *Carbohydrate Research*, **1976**, 47(1), 1-13.

Costantino, V., Fattorusso, E., Mangoni, A., Di Rosa, M., Ianaro, A., Maffia, P.: Glycolipids from sponges. IV. Immunomodulating glycosyl ceramides from the marine sponge *agelas dispar*. *Tetrahedron*, **1996**, 52(5), 1573-1578.

Cui, E.-J., Park, H.-J., Wu, Q., Chung, I.-S., Kim, J.-Y., Baek, N.-I.: Sterols from the Seed of Cowpea (*Vigna sinensis K.*). *Journal of Applied Biological Chemistry*, **2010**, 53(2), 77-81.

das Neves Costa, F., Guimarães Leitão, G.: Strategies of solvent system selection for the isolation of flavonoids by countercurrent chromatography. *Journal of Separation Science*, **2010**, 33(3), 336-347.

de Rosso, V. V., Mercadante, A. Z.: Identification and quantification of carotenoids, by HPLC-PDA-MS/MS, from Amazonian fruits. *Journal of Agricultural and Food Chemistry,* **2007**, 55(13), 5062–5072.

de Souza, L. M., Iacomini, M., Gorin, P. A., Sari, R. S., Haddad, M. A., Sassaki, G. L.: Glyco- and sphingophosphonolipids from the medusa *Phyllorhiza punctata*: NMR and ESI-MS/MS fingerprints. *Chemistry and Physics of Lipids*, **2007**, 145(2), 85-96.

DellaPenna, D., Pogson, B. J.: Vitamin Synthesis in Plants: Tocopherols and Carotenoids. *Annual Review of Plant Biology,* **2006,** 57, 711-738.

Dörmann, P., Benning, C.: Galactolipids rule in seed plants. *Trends in Plant Science*, **2002**, 7(3), 112-118.

Dörmann, P., Hoffmann-Benning, S., Balbo, I., Benning, C.: Isolation and characterization of an *Arabidopsis* mutant deficient in the thylakoid lipid digalactosyl diacylglycerol. *Plant Cell*, **1995**, 7(11), 1801-1810.

Dörmann, P., Hölz, G., *The role of glycolipids in photosynthesis* in: *Lipids in Photosynthesis, Essential and Regulatory Functions,* (H. Wada and N. Murata, eds.) Springer, Netherlands, **2009**, pp. 265-282.

Duarte, I. F., Legido–Quigley, C., Parker, D. A., Swann, J. R., Spraul, M., Braumann, U., Gil A. M., Holmes, E., Nicholson, J. K., Murphy, G. M., Vilca-Melendez, H., Heaton, N., Lindon, J. C.: Identification of metabolites in human hepatic bile using 800 MHz ^{1}H NMR spectroscopy, HPLC-NMR/MS and UPLC-MS. *Molecular BioSystems*, **2009**, 5(2), 180–190.

Eckardt, C.B., Keely, B.J., Maxwell, J.R.: Identification of chlorophyll transformation products in a lake sediment by combined liquid-chromatography mass-spectrometry. *Journal of Chromatography A*, **1991**, 557(1-2), 271-288.

Engel, N., Curty, C., Gossauer, A., : Chlorophyll catabolism in Chlorella protothecoides. Part 8: Facts and artefacts. *Plant Physiology, **1996,*** 1 (34) 77-83.

Englert, G., Kienzle, F., Noack, K.: ^{1}H-NMR.-, ^{13}C-NMR.-, UV.- und CD.-Daten von synthetischem (3S, 3'S)-Astaxanthin, seinem 15-cis-Isomeren und einigen analogen Verbindungen. Helvetica Chimica Acta, **1977**, 60(4), 1209-1219.

Fang, N., Yu, S., Badger, Th. S.: Characterization of Triterpene Alcohol and Sterol Ferulates in Rice Bran Using LC-MS/MS. *Journal of Agricultural and Food Chemistry,* **2003**, 51(11), 3260-3267.

Farag, M. A., Paré, P. W.: Phytochemical analysis and anti-inflammatory potential of *Hyphaene thebaica l.* fruit. *Journal of Food Science*, **2013**, 78(10), 1503–1508.

Folly, P., Engel N.: Chlorophyll b to chlorophyll a conversion precedes chlorophyll degradation in Hordeum vulgare L., *The Journal of Biological Chemistry,* **1999,** 274(31) 21811-21816.

Friesen, J. B., Pauli, G.: G.U.E.S.S. - A generally useful estimate of solvent systems for CCC. *Journal of Liquid Chromatography & Related Technologies*, **2005**, 28(17), 2777-2806.

Fuchs, B., Schiller, J., Wagner, U., Häntzschel, Arnold, K.: The phosphatidylcholine-/lysophosphatidylcholine ratio in human plasma is an indicator of the severity of rheumatoid arthritis: investigations by ^{31}P NMR and MALDI-TOF MS. *Clinical Biochemistry*, **2005**, 38(10), 925–33.

Gage, D. A., Huang, Z. H., Benning, C.: Comparison of sulfoquinovosyl diacylglycerol from spinach and the purple bacterium *Rhodobacter sphaeroides* by fast atom bombardment tandem mass spectrometry. *Lipids*, **1992**, 27(8), 632–636.

Gauthier-Jaques, A., Bortlik, J., Hau, J., Fay, L. B.: Improved method to track chlorophyll degradation. *Journal of Agricultural and Food Chemistry*, **2001**, 49(3), 1117-1122.

Geske, T., vom Dorp, K., Dörmann, P., Hölzl, G.: Accumulation of glycolipids and other non-phosphorous lipids in *Agrobacterium tumefaciens* grown under phosphate deprivation. *Glycobiology*, **2013**, 23(1), 69-80.

Ghosal, S.: Steryl glycosides and acyl steryl glycosides from *Musa paradisiaca*. *Phytochemistry*, **1985**, 24(8), 1807-1810.

Ginsburg, S., *Chlorophyllabbau in seneszenten Rapscotyledonen,* Ph. D. thesis, University of Zürich, Zürich, **1993**.

Goffman, F. D., Alonso, A. P., Schwender, J., Shachar-Hill, Y., Ohlrogge, J. B.: Light enables a very high efficiency of carbon storage in developing embryos of rapeseed. *Plant Physiology,* **2005***,* 138(4) 2269-2279.

González-Montelongo, R., Lobo, M. G., González, M.: Antioxidant activity in banana peel extracts: testing extraction conditionsand related bioactive compounds. *Food Chemistry*, **2010**, 119(3), 1030–1039.

Goodwin, T. W., Harris, J. I., Hartley, B.S., *Structure and activity of enzymes* (Federation of European Biochemical Societies Symposium). *Academic Press, London,* **1964***.*

Gross, J., Carmon, M., Lifshitz, A., Costes, C.: Carotenoids of banana pulp, peel and leaves. *Lebensmittel-Wissenschaft und Technologie*, **1976**, 9(4), 211-214.

Gross, J., Fluegel, M.: Pigment changes in peel of the ripening banana (*Musa cavendishi*). *Gartenbauwissenschaft*, **1982**, 47(2), 62-64.

Gross, J., Gabai, M., Lifshitz, A., Sklarz, B.: Carotenoids in pulp, peel and leaves of *Persea americana*. *Phytochemistry*, **1973b**, 12(9), 2259–2263.

Gross, J., Gabai, M., Lifshitz, A., Sklarz, B.: Carotenoids of *Eriobotrya japonica*. *Phytochemistry*, **1973a**, 12(7), 1775–1782.

Gunstone, F. D.: ^{13}C-NMR spectra of some synthetic glycerol esters alone and as mixtures. *Chemistry and Physics of Lipids,* **1990**, 56, (2–3), 195–199.

Gunstone, F. D.: High-resolution ^{13}C NMR spectra of long-chain acids, methyl esters, glycerol esters, wax esters, nitriles, amides, alcohols and acetates. *Chemistry and Physics of Lipids,* **1993**, 66, 189-193.

Guo, W., Kurze, V., Huber, T., Afdhal, N.H., Beyer, K., Hamilton, J.A.: A solid-state NMR study of phospholipid-cholesterol interactions: sphingomyelin-cholesterol binary systems. *Biophysical Journal*, **2002**, 83(3), 1465-1478.

Hansen, Charles, *Hansen Solubility Parameters: A user's handbook, Second Edition*. Boca Raton, Fla: CRC Press, **2007**.

Hansen, P. E.: Carbon-hydrogen spin-spin coupling constants, *Progress in Nuclear Magnetic Resonance Spectroscopy,* **1981**, 14(4), 175-296.

Hansen, P. E., Jens, J. L.: CH, CD, CC and HH coupling constants in isotopically enriched cyclobutene, **1981**, *Organic Magnetic Resonance,* 15(3) 288-293.

Happi Emaga, T., Herinavalona, A. R., Wathelet, B., Tchango Tchango, J., Paquot, M.: Effects of the stage of maturation and varieties on the chemical composition of banana and plantain peels. *Food Chemistry,* **2007**, 103(2), 590-600.

Harpaz-Saad, S., Azoulay, T., Arazi, T., Ben-Yaakov, E., Mett, A., Shiboleth, Y.M., Hörtensteiner, S., Gidoni, D., Gal-On, A., Goldschmidt, E.E., and Eyal, Y.: Chlorophyllase is a rate-limiting enzyme in chlorophyll catabolism and is posttranslationally regulated. *The Plant Cell,* **2007**, 19(3), 1007-1022.

Hatzakis, E., Agiomyrgianaki, A., Kostidis, S., Dais, Ph.: High-resolution NMR spectroscopy: an alternative fast tool for qualitative and quantitative analysis of diacylglycerol (dag) oil. *Journal of the American Oil Chemist´s Society*, **2011**, 88(11), 1695-1708.

Holčapek, M., Jandera, P., Zderadicka, P., Hrubá, L.: Characterization of triacylglycerol and diacylglycerol composition of plant oils using high-performance liquid chromatography-atmospheric pressure chemical ionization mass spectrometry. *Journal of Chromatography A*, **2003**, 1010(2), 195-215.

Hölzl, G., Dörmann, P.: Structure and function of glycoglycerolipids in plants and bacteria. *Progress in Lipid Research*, **2007**, 46(5), 225-243.

Hölzl, G., Witt, S., Gaude, N., Melzer, M., Schöttler, M. A., Dörmann, P.: The role of diglycosyl lipids in photosynthesis andmembrane lipid homeostasis in *Arabidopsis*. *Plant Physiology*, **2009**, 150(3), 1147-1159.

Hölzl, G., Witt, S., Kelly, A. A., Zähringer, U., Warnecke, D., Dörmann, P., Heinz, E.: Functional differences between galactolipids and glucolipids revealed in photosynthesis of higher plants. *Proceedings of the National Academy of Sciences of the United States of America*, **2006**, 103(19), 7512-7217.

Hörtensteiner S.: Chlorophyll degradation during senescence. *Annual Review of Plant Biology,* **2006**, 57, 55-77.

Hörtensteiner, S., Vicentini, F., Matile Ph.: Chlorophyll breakdown in senescent cotyledons of rape, Brassica napus L.: Enzymatic cleavage of phaeophorbide a in vitro. *New Phytologist,* **1995,** 129(2) 237-246.

Hörtensteiner, S.: Chlorophyll breakdown in higher plants and algae. *Cellular and Molecular Life Sciences,* **1999**, 56(3-4), 330-347.

Hu, Y., Hashimoto, H., Moine, G., Hengartner, U., Koyama, Y.: Unique properties of the 11-cis and 11, 11'-di-cis isomers of β-carotene as revealed by electronic absorption, resonance Raman and 1H and 13C NMR spectroscopy and by HPLC analysis of their thermal isomerization. *Journal of the Chemical Society, Perkin Transactions 2*, **1997**, 12, 2699-2710.

Huang, S.C., Hung, C.F., Wu, W.B., Chen, B. H.: Determination of chlorophylls and their derivatives in *Gynostemma pentaphyllum Makino* by liquid chromatography-mass spectrometry. *Journal of Pharmaceutical and Biomedical Analysis,* **2008**, 48(1), 105-112.

Hyvärinen, K., Hynninen, P. H.: Liquid chromatographic separation and mass spectrometric identification of chlorophyll *b* allomers. *Journal of Chromatography A,* **1999**, 837(1-2), 107-116.

Iida–Tanaka, N., Hikita, T., Hakomori, S.–I., Ishizukaa, I.: Conformational studies of a novel cationic glycolipid, glyceroplasmalopsychosine, from bovine brain by NMR spectroscopy. *Carbohydrate Research*, **2002**, 337(19), 1775–1779.

Inagaki, F., Kohda, D., Kodama, C., Suzuki, A.: Analysis of NMR spectra of sugar chains of glycolipids by multiple relayed COSY and 2D homonuclear: Hartman-Hahn spectroscopy. *FEBS Letters*, **1987**, 212(1), 91–97.

Islam, M. R., Aikawa, S., Midorikawa, T., Kashino, Y., Satoh, K., Koike, H.: Slr1923 of *Synechocystis sp.* PCC6803 is essential for conversion of 3, 8-divinyl(proto)chlorophyll(ide) to 3-monovinyl(proto)chlorophyll(ide). *Plant Physiology*, **2008**, 148(2), 1068-1081.

Islam, M. S., Yoshida, H., Matsuki, N., Ono, K., Nagasaka, R., Ushio, H. et al.: Antioxidant, free radical-scavenging, and NF-kappaB-inhibitory activities of phytosteryl ferulates: structure-activity studies. *Journal of Pharmacological Sciences,* **2009,** 111, (4), 328-37.

Ismaiel, O. A., Halquist, M. S., Elmamly, M. Y., Shalaby, A., Karnes, H. T.: Monitoring phospholipids for assessment of ion enhancement and ion suppression in ESI and APCI LC/MS/MS for chlorpheniramine in human plasma and the importance of multiple source matrix effect evaluations. *Journal of Chromatography B*, **2008**, 875(2), 333–343.

Ito, Y., Conway, D. (eds.) *High-speed Countercurrent Chromatography.* Wiley: New York, 1996.

Ito, Y.: Golden rules and pitfalls in selecting optimum conditions for high-speed counter-current chromatography. *Journal of Chromatography A*, **2005**, 1065(2), 145-168.

Ito, Y.: Recent advances in countercurrent chromatography. *Journal of Chromatography A,* **1991,** 538 (1), 3-25.

Jacob-Wilk, D., Holland, D., Goldschmidt, E. E., Riov, J., Eyal, Y.: Chlorophyll breakdown by chlorophyllase: isolation and functional expression of the Chlase 1 gene from ethylene-treated Citrus fruit and its regulation during development. *The Plant Journal,* **1999,** 20(6), 653-661.

Jakab, A., Héberger, K., Forgács, E.: Comparative analysis of different plant oils by high-performance liquid chromatography–atmospheric pressure chemical ionization mass spectrometry. *Journal of Chromatography A*, **2002**, 976(1), 255–263.

Jensen, N. J., Tomer, K. B., Gross, M. L.: Fast atom bombardment and tandem mass spectrometry of phosphatidylserine and phosphatidylcholine. *Lipids*, **1986**, 21(9), 580-588.

Jerz, G., Arrey, T., Wray, V., Du, Q., Winterhalter, P.: Structural characterization of 13^2-hydroxy-(13^2-S)-phaeophytin-a from leaves and stems of *Amaranthus tricolor* isolated by high-speed countercurrent chromatography. *Innovative Food Science & Emerging Technologies, **2007***, 8(3), 413-418.

Jubert, C., Bailey, G.: Isolation of chlorophylls *a* and *b* from spinach by counter-current chromatography. *Journal of Chromatography A,* **2007**, 1140(1-2), 95-100.

Kaffarnik, S., Ehlers, I., Gröbner, G., Schleucher, J., Vetter, W.: Two-dimensional ^{31}P, ^{1}H NMR spectroscopic profiling of phospholipids in cheese and fish. *Journal of Agricultural and Food Chemistry*, **2013**, 61(29), 7061−7069.

Kasumov, T., Huang, H., Chung, Y.M., Zhang, R., McCullough, A.J., Kirwan, J.P.: Quantification of ceramide species in biological samples by liquid chromatography electrospray ionization tandem mass spectrometry. *Analytical Biochemistry*, **2010**, 401(1), 154-161.

Katz, J. J., Doughterty, R. C., Boucher, L. J.: "Infrared and nuclear magnetic resonance spectroscopy of chlorophyll" in: *Chlorophylls* (Vernon, L. P., Seely, G. R. eds.) Academic Press, New York, **1966**, pp. 185-250.

Katz, J. J., Shipman, L. L., Cotton, T. M., Janson, T. R.: Chlorophyll aggregation: coordination interactions in chlorophyll monomers, dimers and oligomers in *The Porphyrins*, Dolphin, D., Ed., Academic Press, New York, Vol. 5, **1978**, 1, 405-458 (413).

Katz, J. J., Strain, H. H., Leussing, D. L., Dougherty, R. C.: Chlorophyll-ligand interactions from nuclear magnetic resonance studies, *Journal of the American Chemical Society*, **1968**, 90(3), 784-789.

Kikuchi, T., Akihisa, T., Tokuda, H., Ukiya, M., Watanabe, K., Nishino, H.: Cancer chemopreventive effects of cycloartane-type and related triterpenoids in in vitro and in vivo models. *Journal of Natural Products*, **2007**, 70(6), 918-922.

Klein, R.A.: Mass spectrometry of the phosphatidylcholines: dipalmitoyl, dioleoyl, and stearoyl-oleoyl glycerylphosphorylcholines. *Journal of Lipid Research*, **1971**, 12(2), 123-131.

Knapp, F. F., Nicholas, H. J.: Phytosterol biosynthesis in banana peel. Initial removal of the 4-methyl group of 24-methylenecycloartanol during its conversion into cycloeucalenol in *Musa sapientum*. *Journal of the Chemical Society D, Chemical Communications,* **1970**a, 7, 399-400.

Knapp, F. F., Nicholas, H. J.: The biosynthesis of 31-norcyclolaudenone in *Musa sapientum*. *Phytochemistry*, **1971a**, 10(1), 97-102.

Knapp, F. F., Nicholas, H. J.: The biosynthesis of phytosterols in *Musa sapientum*. *Phytochemistry*, **1971b**, 10(1), 85–95.

Knapp, F. F., Nicholas, H. J.: The isolation of 31-norcyclolaudenone from *Musa sapientum*. *Steroids*, **1970b**, 16(3), 329-51.

Knapp, F. F., Nicholas, H. J.: The sterols and triterpenes of banana peel. *Phytochemistry*, **1969a**, 8(1), 207-214.

Knapp, F. F., Nicholas, H. J.: The sterols and triterpenes of banana pulp. *Journal of Food Science*, **1969b**, 34(6), 584–586.

Kobayashi, M., Komeda, H., Nagasawa, T., Nishiyama, M., Horinouchi, S., Beppu, T., Yamada, H., Shimizu, S.: Amidase coupled with low-molecular-mass nitrile hydratase from *Rhodococcus rhodochrous J1*. Sequencing and expression of the gene and purification and characterization of the gene product *European Journal of Biochemistry,* **1993**, 217 (1), 327-36.

Kohler, B. E., Electronic structure of carotenoids in: *Carotenoids (G. Britton, S. Liaaen-Jensen, H. Pfander, eds.)* vol. 1B. *Birkhäuser, Basel,* **1995***, pp. 1-12.*

Köhler, N., Chou, E., Ito, Y., Winterhalter, P.: Development of a new preparative spiral-coil low-speed rotary countercurrent chromatographic (Spiral-coil LSRCCC) method. *Journal of Liquid Chromatography & Related Technologies*, **2004**, 27(16), 2547-2560.

Kolesnik, A. A., Golubev, V. N., Gadzhieva, A. A.: Lipids of the fruit of *Feijoa sellowiana*. *Chemistry of Natural Compounds*, **1991**, 27(4), 404–407.

Kosower, E. M., " An Introduction to Physical Organic Chemistry". John Wiley and Sons, New York, N.Y., **1968**, section 2.6.

Kosower, E. M., Huang, Pin-Kuei C., Tsuji, T.: Diazenes. V. Aryldiazenes. *Journal The American Chemical Society,* **1969**, 91(9) 2325-2329.

Kovganko, N. V., Kashkan, Zh. N., Borisov, E. V., Batura, E. V.: ^{13}C NMR spectra of β-sitosterol derivatives with oxidized rings A and B. *Chemistry of Natural Compounds*, **1999**, 35(6), 646-649.

Kräutler, B., Hörtensteiner, S., in *Chlorophylls and Bacteriochlorophylls: Biochemistry, Biophysics, Functions and Applications. Advances in Photosynthesis and Respiration*, vol. 25. (Bernhard Grimm, Robert J. Porra, Wolfhart Rüdiger, Hugo Scheer, eds.) Springer, Dordrecht, **2006**, pp. 237-260.

Kräutler, B., Jaun, B., Amrein, W., Bortlik, K., Schellenberg, M., and Matile Ph.: Breakdown of chlorophyll: Constitution of a secoporphinoid chlorophyll catabolite isolated from senescent barley leaves. *Plant Physiology and Biochemistry, **1992**,* 30(3), 333-346.

Kräutler, B., Jaun, B., Bortlik, K., Schellenberg, M., and Matile Ph.: On the enigma of chlorophyll degradation: The constitution of a secoporphinoid catabolite. *Angewandte Chemie International Edition in English, **1991,*** 30(10) 1315-1318.

Kräutler, B., Mühlecker, W., Anderl, M., Gerlach, B.: Breakdown of chlorophyll: partial synthesis of a putative intermediary catabolite. Preliminary communication. *Helvetica Chimica Acta,* **1997**, 80(5), 1355–1362.

Kräutler, B., Puffer, B., Müller, T.: "Was passiert, wenn's bunt wird". *Nachrichten aus der Chemie,* **2012**, 60, 1082–1086.

Kreuz, K., Tommasini, R., Martinoia, E.: Old enzymes for a new job. *Plant Physiology,* **1996,** 111, 349-353.

Krupa, Z.: The action of lipases on chloroplast membranes. III. The effect of lipid hydrolysis on chlorophyll-protein complexes in thylakoid membranes. *Photosynthesis Research*, **1984**, 5(2), 177-84.

Lacker, T., Strohschein, S., Albert, K.: Separation and identification of various carotenoids by C_{30} reversed-phase high-performance liquid chromatography coupled to UV and atmospheric pressure chemical ionization mass spectrometric detection. *Journal of Chromatography A,* **1999**, 854(1-2), 37-44.

Lago, J. H. G., Brochini, C. B., Roque, N F.: Terpenes from leaves of *Guarea macrophylla (Meliaceae)*. *Phytochemistry*, **2000**, 55(7), 727-731.

Lampi, A.-M., Nurmi, T., Ollilainen, V., Piironen, V.: Tocopherols and tocotrienols in wheat genotypes in the HEALTHGRAIN diversity screen. Journal of Agricultural and Food Chemistry, **2008**, 56, 9716-9721.

Levery, S. B., Toledo, M. S., Straus, A. H., Takahashi, H. K.: Structure elucidation of sphingolipids from the mycopathogen Paracoccidioides brasiliensis: an immunodominant β-galactofuranose residue is carried by a novel glycosylinositol phosphoceramide antigen. *Biochemistry*, **1998**, 37(24), 8764-8775.

Li, X., Sun, D.–D., Chen, J.–W., He, L.-W., Zhang, H.-Q., Xu, H.-Q.: New sphingolipids from the root of *Isatis indigotica* and their cytotoxic activity. *Fitoterapia*, **2007**, 78(7-8), 490–495.

Liaaen-Jensen, S.: Structural elucidation of carotenoids –a progress report. *Pure and Applied Chemistry*, **1973**, 35(1), 81-112.

Liu, M., Yang, F., Shi, H., Akoh, C.C. Yu, LL.: Preparative separation of triterpene alcohol ferulates from rice bran oil using high performance counter-current chromatography. *Food Chemistry,* **2013**, 139(1-4), 919-924.

Lötjönen, S., Hynninen, P. H.: Carbon-13 NMR spectra of chlorophyll *a*, chlorophyll *a'*, pyrochlorophyll *a* and the corresponding pheophytins. *Organic Magnetic Resonance*, **1983**, 21(12), 757-765.

Lötjönen, S., Hynninen, P. H.: Complete assignment of the carbon-13 NMR spectrum of chlorophyll *a*. *Organic Magnetic Resonance*, **1981**, 16(4), 304-308.

Lu, D., Singh, D., Morrow, M. R., Grant, C. W. M.: Effect of glycosphingolipid fatty acid chain length on behavior in unsaturated phosphatidylcholine bilayers: a 2H NMR study. *Biochemistry*, **1993**, 32(1), 290–297.

Lustosa, K. R. M. D., Menegatti, R., Braga, R. C., Lião, L. M., de Oliveira, V.: Microbial β-glycosylation of entacapone by Cunninghamella echinulata ATCC 9245. Journal of Bioscience and Bioengineering, **2012**, 113(5), 611-3.

Lutnaes, B. F., Bruås, L., Kildahl-Andersen, G., Krane, J., Liaaen-Jensen, S.: The charge delocalised beta, beta-carotene dication--preparation, structure elucidation by NMR and reactions with nucleophiles. *Organic & Biomolecular Chemistry*, **2003**, 1(22), 4064-72.

Luzzati, V., Spegt, P. A.: Polymorphism of lipids. *Nature*, **1967**, 215(5102), 701-704.

Maoka, T., Akimoto, N.: Structures of minor carotenoids from the Japanese common catfish, *Silurus Asotus. Chemical & Pharmaceutical Bulletin,* **2011**, 59(1), 140-145.

Maoka, T., Fujiwara, Y., Hashimoto, K., Akimoto, N.: Rapid identification of carotenoids in a combination of liquid chromatography / UV-visible absorption spectrometry by photodiode-array detector and atmospheric pressure chemical ionization mass spectrometry (LC/PAD/APCI-MS). *Journal of Oleo Science*, **2002**, 51(1), 1–9.

Martínez, A.: *Carotenoides*. Universidad de Antioquia, **2003.**

Martínez, A.: *Esteroles*. Universidad de Antioquia, **2002**.

Matile, P., Hörtensteiner, S., Thomas, H.: Chlorophyll degradation. *Annual Review of Plant Physiology and Plant Molecular Biology,* **1999**, 50, 67-95.

Mendes-Pinto, M. M., Silva Ferreira A. C., Caris-Veyrat C., Guedes de Pinho, P.: Carotenoid, chlorophyll, and chlorophyll-derived compounds in grapes and port wines. *Journal of Agricultural and Food Chemistry,* **2005**, 53 (26), 10034–10041.

Mercadante, A. Z., Britton, G., Rodriguez-Amaya, D.: Carotenoids from yellow pasion fruit (*Passiflora edulis). Journal of Agricultural and Food Chemistry,* **1998**, 46, 4102-4106.

Mercadante, A. Z., Rodríguez-Amaya, D. B., Britton, G.: HPLC and mass spectrometric analysis of carotenoids from mango. *Journal of Agricultural and Food Chemistry*, **1997**, 45(1), 120–123.

Minguez-Mosquera, M. I., Garrido-Fernandez, J.: Chlorophyll and carotenoid presence in olive fruit (*Olea europaea*). *Journal of Agricultural and Food Chemistry*, **1989**, 37(1), 1–7.

Minguez-Mosquera, M. I., Garrido-Fernandez, J.: Role of chlorophyllase in chlorophyll metabolism in olives cv. Grodal. *Phytochemistry*, **1996**, 41(3) 691-697 .

Mohammad, M. and Kosower, E. M.: Solvent polarity in electrochemical and other salt solution studies. *The Journal of Physical Chemistry,* **1970**, 74(5) 1153-1154.

Molnár, P., Deli, J., Matus, Z., Tóth, G., Steck, A., Pfander, H.: Partial synthesis and characterization of the mono-and diepoxides of β-cryptoxanthin. *Helvetica Chimica Acta*, **1997**, 80(1), 221-229.

Molnár, P., Deli, J., Ösz, E, Zsila, F., Simonyi, M., Tóth, G.: Confirmation of the absolute (3R, 3´S, 6´R)-configuration of (all-E)-3'-epilutein. *Helvetica Chimica Acta*, **2004**, 87(8), 2159-2167.

Molnár, P., Ösz, E., Tóth, G., Zsila, F., Deli, J.: Preparation and spectroscopic characterization of (9z, 9'z)-lutein (neolutein C). *Helvetica Chimica Acta*, **2006**, 89(4), 667-674.

Moreau, R.A., Young, D.H., Danis, P.O., Powell, M.J., Quinn, C.J., Beshah, K., Slawecki, R.A., Dilliplane, R.L.: Identification of ceramide-phosphorylethanolamine in oomycete plant pathogens: *Pythium ultimum, Phytophthora infestans,* and *Phytophthora capsici*. *Lipids*, **1998**, 33(3), 307–317.

Moser, S., Müller T., Holzinger, A., Lütz, C., Jockusch, S., Turro, N.J., Kräutler, B.: Fluorescent chlorophyll catabolites in bananas light up blue halos of cell death. *Proceedings of the National Academy of Sciences*, **2009b**, 106(37), 15538–15543.

Moser, S., Müller, T., Ebert, M-O., Jockusch, S., Turro, N.J., Kräutler, B.: Blue luminescence of ripening bananas. *Angewandte Chemie International Edition in English,* **2008**, 47(46), 8954–8957.

Moser, S., Müller, T., Holzinger, A., Lütz, C. and Kräutler, B.: Structures of chlorophyll catabolites in bananas (*Musa acuminata*) reveal a split path of chlorophyll breakdown in a ripening fruit. *Chemistry. A European Journal,* **2012**, 18(35), 10873-10885.

Moser, S., Müller, T., Oberhuber, M.: Kräutler, B.: Chlorophyll catabolites-Chemical and structural footprints of a fascinating biological phenomenon. *European Journal of Organic Chemistry,* **2009a,** 2009(1), 21-31

Mühlecker, W., Kräutler, B.: Breakdown of chlorophyll: constitution of nonfluorescing chlorophyll-catabolities from senescent cotyledons of the dicot rape. *Plant Physiology and Biochemistry, **1996,*** 34(1), 61-75.

Mühlecker, W., Ongania, K.-H., Kräutler, B., Matile, P., Hörtensteiner, S.: Tracking down chlorophyll breakdown in plants: elucidation of the constitution of a 'fluorescent' chlorophyll catabolite. *Angewandte Chemie International Edition in English,* **1997**, 36(4), 401–404.

Nakagawa, K., Kiko, T., Hatade, K., Asai, A., Kimura, F., Sookwong, P., Tsuduki, T., Arai, H., Miyazawa, T.: *Development of a high-performance liquid chromatography-based assay for carotenoids in human red blood cells: application to clinical studies. Analytical Biochemistry*, **2008**, 381(1), 129-134.

Neugebauer, J., Veldstra, J., Buda, F.: Theoretical spectroscopy of astaxanthin in crustacyanin proteins: absorption, circular dichroism, and nuclear magnetic resonance. *The Journal of Physical Chemistry B.,* **2011**, 115(12), 3216-3225.

Nichols, B.W. "The structure and function of plant glycolipids", in: *Plant Carbohydrate Biochemistry* (Pridham, J.B., Ed.), Academic Press, New York. **1974,** No.10, 97-108.

Oberhuber, M., Berghold, J., Mühlecker, W., Hörtensteiner, S., Kräutler, B.: Chlorophyll breakdown – On a nonfluorescent chlorophyll catabolite from spinach. *Helvetica Chimica Acta* **2001**, 84(9), 2615–2627.

Ohnmacht, S., West, R., Simionescu, R., Atkinson, J.: Assignment of the ^{1}H and ^{13}C NMR of tocotrienols. *Magnetic Resonance in Chemistry,* **2008**, 46(3), 287–294.

Oliveira, L., Freirec, C.S.R., Silvestre, A. J. D., Cordeiro, N., Torres, I.C., Evtuguin, D.: Lipophilic extractives from different morphological parts of banana plant "*Dwarf Cavendish*". *Industrial Crops and Products*, **2006**, 23(2), 201-211.

Ortiz, R., Ferris, R. S. B. and Vuylsteke, D. R.: Banana and plantain breeding, in: *Bananas and Plantains* (Gowen, S.R. ed.), Chapman & Hall, London; **1995**, pp. 110-146.

Oshio, Y., Hase, E.: Studies on red pigments excreted by cell of *Chlorella protothecoides* during the process of bleaching induced by glucose or acetate. II. Mode of formation of the red pigments*. Plant and Cell Physiology,* **1969,** 10(1), 51-59.

Potta, I., Breithaupt, D. E., Carle, R.: Detection of unusual carotenoid esters in fresh mango (*Mangifera indica* L. cv. 'Kent'). *Phytochemistry,* **2003**, 64(4), 825–829.

Pružinská, A., Tanner, G., Anders, I., Roca, M., Hörtensteiner, S.: Chlorophyll breakdown: Pheophorbide *a* oxygenase is a Rieske-type iron–sulfur protein, encoded by the *accelerated cell death 1* gene. *Proceeding of the National Academy of Sciences of the United States of America,* **2003,** 100(25) 15259-15264.

Pružinská, A., Tanner, G., Aubry, S., Anders, I., Moser, S., Müller, T., Ongania, K.-H., Kräutler, B., Youn, J.Y., Liljegren, S.J., Hörtensteiner, S.: Chlorophyll breakdown in senescent *Arabidopsis* leaves. Characterization of chlorophyll catabolites and of chlorophyll catabolic enzymes involved in the degreening reaction. *Plant Physiology,* **2005**, 139(1), 52-63.

Putzbach, K., Krucker, M., Albert, K., Grusak, M. A., Tang, G., Dolnikowski, G. G.: Structure determination of partially deuterated carotenoids from intrinsically labeled vegetables by HPLC-MS and 1H NMR. *Journal of Agricultural and Food Chemistry*, **2005a**, 53(3), 671-677.

Putzbach, K., Krucker, M., Grynbaum, M. D., Hentschnel, P., Webb, A. G., Albert, K.: Hyphenation of capillary high-performance liquid chromatography to microcoil magnetic resonance spectroscopy - determination of various carotenoids in a small-sized spinach sample. *Journal of Pharmaceutical and Biomedical Analysis*, **2005b**, 38(5), 910-917.

Ragasa, C. Y., Martinez, A. T., Chua, J. E. Y., Rideout, J.: A triterpene from *Musa errans*. *Philippine Journal of Science*, **2007**, 136(2), 167-171.

Riaz, N., Tabussum, A., Saleem, M., Ashraf, M., Nasar, R., Jabeen, B., Malik, A., Jabbar, A.: New lipoxygenase inhibitory sphingolipids from *Chrozophora plicata*. *Journal of Asian Natural Products Research*, **2013**, 15(10), 1080–1087.

Risch, N., Brockmann (JR), H.: Chlorophyll *b*. Totalzuordnung des ^{13}C-NMR-Spektrums. *Tetrahedron Letters,* **1983**, 24(2), 173-176.

Robinson, J. C.: *Bananas and Plantains*. CAB International, Wallingford, Oxon, Great Britain, **1996**.

Rodríguez-Amaya, D. B., *A guide to carotenoid analysis in foods. Ilsi Press, Washington,* **2001**.

Ruberto, G., Tringali, C.: Secondary metabolites from the leaves of *Feijoa sellowiana Berg*. *Phytochemistry*, **2004**, 65(21), 2947-2951.

Ryynänen, M., Lampi, A.-M., Salo-Väänänen, P., Ollilainen, V., Piironen, V.: A small-scale sample preparation method with HPLC analysis for determination of tocopherols and tocotrienols in cereals. *Journal of Food Compositional and Analysis,* **2004**, 17, 749-765.

Sarmientos, F., Schwarzmann, G., Sandhoff, K.: Direct evidence by carbon-13 NMR spectroscopy for the erythro configuration of the sphingoid moiety in *Gaucher* cerebroside and other natural sphingolipids. *European Journal of Biochemistry*, **1985**, 146(1), 59–64.

Sassaki, G. L., Machado M. J., Tischer C. A., Gorin, P. A., Iacomini, M.: Glycosyldiacylglycerolipids from the lichen *Dictyonema glabratum. Journal of Natural Products*, **1999**, 62(6), 844-7.

Scavariello, E. M., Arellano, D. B.: Gamma-oryzanol: an important component in rice brain oil. *Archivos Latinoamericanos de Nutrición,* **1998,** 48 (1), 7-12.

Scheer, H., ed., *Chlorophylls*, CRC Press, Boca Raton, Florida, **1991**.

Schwartz, H., Ollilainen, v., Piironen, V., Lampi, A.-M.: Tocopherol, tocotrienol and plant sterol contents of vegetable oils and industrial fats. *Journal of Food Composition and Analysis,* **2008**, 21, 152-161.

Schweiggert, U., Kammerer, D. R., Carle, R., Schieber, A.: Characterization of carotenoids and carotenoid esters in red pepper pods (*Capsicum annuum L.*) by high-performance liquid chromatography/atmospheric pressure chemical ionization mass spectrometry. *Rapid Communications in Mass Spectrometry,* **2005**, 19(18), 2617-2628.

Seo, S., Sankawa, U., Seto, H., Uomori, A., Yoshimura, Y., Ebizuka, Y., Noguchi, H., Takeda, K. J.: Biosynthesis of sitosterol in tissue cultures of *Rabdosia japonica hara* and ergosterol in yeast from [2-^{13}C, 2-$^{2}H_3$] acetate. *Journal of the Chemical Society, Chemical Communications,* **1986**, 14, 1139-1141.

Shaw, G., Apperley, D. C.: ^{13}C-NMR spectra of *Lycopodium clavatum* sporopollenin and oxidatively polymerised β-carotene. *Grana*, **1996**, 35(2), 125-127.

Simmonds, N. W.: Bananas, in: *Evolution of Crop Plants* (Smartt, J. and Simmonds, N. W. eds.) Longman Scientific & Technical, Harlow, Great Britain, **1995**, pp. 370-375.

Simmonds, N.W.: Segregation in some diploid bananas. *Journal of Genetics,* **1953**, 51(3), 458-469.

Simmonds, N.W.: The development of the banana fruit. *Journal of Experimental Botany,* **1953a,** 4(1), 87-105.

Skakovskii, E. D.; Tychinskaya, L. Yu.; Gaidukevich, O. A.; Klyuev, A. Yu.; Kulakova, A. N.; Petlitskaya, N. M.; Rykove, S. V.: NMR analysis of oils from pine nuts (*Pinus sibirica*) and seeds of common pine (*Pinus silvestris L.*). *Journal of Applied Spectroscopy*, **2007**, 74(4), 584-588.

Smith, K.M., Goff, D.A., Abraham, R.J.: The NMR spectra of porphyrins. 27 – proton NMR spectra of chlorophyll-*a* and pheophytin-*a*. *Organic Magnetic Resonance*, **1984**, 22(12), 779-783.

Sobolev, A.P., Brosio, E., Gianferri, R., Segre, A.L.: Metabolic profile of lettuce leaves by high-field NMR spectra. *Magnetic Resonance in Chemistry*, **2005**, 43(8), 625-638.

Sohn, B.-H., Park, J.-H., Lee, D.-Y., Cho, J.-G., Kim, Y.-S., Jung, I.-S., Kang, P.-D., Baek, N.-I.: Isolation and identification of lipids from the silkworm (*Bombyx mori*) droppings. *Journal of the Korean Society for Applied Biological Chemistry*, **2009**, 52(4), 336-341.

Sperling P. Heinz, E.: Plant sphingolipids: structural diversity, biosynthesis, first genes and functions. *Biochimimica et Biophysica Acta*, **2003**, 1632(1-3), 1-15.

Stahl, E.: Dünnschichtchromatographie, Berlin: Springer Verlag. **1967**.

Sticher, O.: Natural product isolation. *Natural Product Reports*, **2008**, 25(3), 517-554.

Stoffel, W., Zierenberg, O., Tunggal, B., Schreiber, E.: 13C nuclear magnetic resonance spectroscopic evidence for hydrophobic lipid-protein interactions in human high density lipoproteins. *Proceedings of the National Academy of Sciences U.S.A.*, **1974**, 71(9), 3696–3700.

Stoffel, W., Zierenberg, O., Tunggal, B.D.: ^{13}C-nuclear magnetic resonance spectroscopic studies on saturated, mono-, di- and polyunsaturated fatty acids, phospho- and sphingo- lipids. *Hoppe-Seyler's Zeitschrift für Physiologische Chemie*, **1972**, 353(2), 1962-1969.

Storm, C. B., Corwin, A. H., Arellano, R. R., Martz, M., Weintraub, R.: Stability constants of magnesium porphyrin-pyridine complexes, *Journal of the American Chemical Society,* **1966**, 88(11) 2525-2532.

Strohschein, S., Pursch, M., Händel, H., Albert, K.: Structure elucidation of β-carotene isomers by HPLC-NMR coupling using a C_{30} bonded phase. *Fresenius Journal of Analytical Chemistry*, **1997**, 357(5), 498-502.

Subagio, A., Morita, N., Sawada, S.: Carotenoids and their fatty-acid esters in banana peel. *Journal of Nutritional Science and Vitaminology*, **1996**, 42(6), 553-566.

Subagio, A., Morita, N.: Changes in carotenoids and their fatty acid esters in banana peel during ripening. *Food Science and Technology International Tokyo*, **1997**, (3)3, 264-268.

Subramanian, A., Shankar Joshi, B., Roy, A.D., Roy, R., Gupta, V., Dang, R. S.: NMR spectroscopic identification of cholesterol esters, plasmalogen and phenolic glycolipids as fingerprint markers of human intracranial tuberculomas. *NMR in Biomedicine*, **2008**, 21(3), 272–288.

Sutherland, I.: Countercurrent Chromatography. Laboratory Practice, **1987,** 36(2), 37-42.

Swain, T., *Comparative phytochemistry.* Academic Press, London, **1966**.

Talbott, C. M., Vorobyov, I., Borchman, D., Taylor, K. G., DuPré, D. B., Yappert, M. C.: Conformational studies of sphingolipids by NMR spectroscopy. II. Sphingomyelin. *Biochimica et Biophysica Acta-Biomembranes*, **2000**, 1467(2), 326–337.

Thomas, H., Bortlik, K.-H., Rentsch, D., Schellenberg, M., Matile, P.: Catabolism of chlorophyll in vivo: significance of polar chlorophyll catabolites in a non-yellowing senescence mutant of *Festuca pratensis* Huds. *New Phytologist,* **1989**, 111(1), 3–8.

Thomas, H., Ougham, H., Hörtensteiner, S.: Recent advances in the cell biology of chlorophyll catabolism. *Advances in Botanical Research,* **2001,** 35, 1-52.

Thomas, P., Janave, M., T.: Effect of temperature on chlorophyllase activity, chlorophyll degradation and carotenoids of cavendish bananas during ripening. *International Journal of Food Science and Technology,* **1992**, 27 57-63.

Toledo, M. S., Levery, S. B., Glushka, J., Straus, A. H., Takahashi, H. K.: Structure elucidation of sphingolipids from the mycopathogen *Sporothrix schenckii*: identification of novel glycosylinositol phosphorylceramides with core manα1→6ins linkage. *Biochemical and Biophysical Research Communications*, **2001**, 280(1), 19–24.

Trebitsh, T., Goldschmidt, E.E. and Riov, J.: Ethylene induces de novo synthesis of chlorophyllase, a chlorophyll degrading enzyme, in citrus fruit peel. *Proceedings of the National Academy of Sciences of the United States of America,* **1993,** 90, 9441-9445.

Tsukida, K., Saiki, K.: Isolation of sterically 'hindered' 7-cis-beta-carotene. Journal of Nutritional Science and Vitaminology, **1982**, 28(3), 311-313.

Tüting, W., Adden, R., Mischnick, P.: Fragmentation pattern of regioselectively O-methylated maltooligosaccharides in electrospray ionisation-mass spectrometry/collision induced dissociation. *International Journal of Mass Spectrometry*, **2004**, 232(2), 107-115.

Unterieser, I., Mischnick, P.: Labeling of oligosaccharides for quantitative mass spectrometry. *Carbohydrate Research*, **2011**, 346(1), 68-75.

Valsecchi, M., Mauri, L., Casellato, R., Ciampa, M.G., Rizza, L., Bonina, A., Bonina, F., Sonnino, S.: Ceramides as possible nutraceutical compounds: characterization of the ceramides of the Moro blood orange (*Citrus sinensis)*. *Journal of Agricultural and Food Chemistry*, **2012**, 60(40), 10103-10110.

van Breemen, R. B., Canjura, F. L., Schwartz, S. J.: High-performance liquid chromatography-continuous-flow fast atom bombardment mass spectrometry of chlorophyll derivatives. *Journal of Chromatography A*, **1991a**, 542, 373-383.

van Breemen, R. B., Canjura, F. L., Schwartz, S. J.: Identification of chlorophyll derivatives by mass spectrometry. *Journal of Agricultural and Food Chemistry*, **1991b**, 39(8), 1452–1456.

van Breemen, R. B., Dong, L., Pajkovic, N. D.: Atmospheric pressure chemical ionization tandem mass spectrometry of carotenoids. *International Journal of Mass Spectrometry*, **2012**, 312, 163-172.

van Breemen, R. B., Huang, Ch-R., Tan, Y., Sander, L. C., Schilling, A. B.: Liquid chromatography/mass spectrometry of carotenoids using atmospheric pressure chemical ionization. *Journal of Mass Spectrometry*, **1996**, 31(9), 975–981.

Verzegnassi, L., Riffé-Chalard, C., Gülaçar, O. F.: Rapid identification of Mg-chelated chlorins by on-line high performance liquid chromatography/atmospheric pressure chemical ionization mass spectrometry. *Rapid Communications in Mass Spectrometry*, **2000**, 14(7), 590-594.

Vicentini, F., Hörtensteiner, S., Schellenberg, M., Thomas, H., Matile, P.: Chlorophyll breakdown in senescent leaves: identification of the biochemical lesion in a stay-green genotype of *Festuca pratensis* Huds*. New Phytologist,* **1995**, 129(2), 247-252.

Vlahov, G.: C nuclear magnetic resonance spectroscopy to determine fatty acid distribution in triacylglycerols of vegetable oils with "high - low oleic acid" and "high linolenic acid". *The Open Magnetic Resonance Journal*, **2009**, 2, 8-19.

Voiges, K., Adden, R., Rinken, M., Mischnick, P.: Critical re-investigation of the alditol acetate method for analysis of substituent distribution in methyl cellulose. *Cellulose*, **2012**, 19(3), 993-1004.

Wada, H., Murata N., eds., *Lipids in photosynthesis: essential and regulatory functions,* Springer, Dordrecht, The Netherlands, **2009**.

Wade, N. L, Bishop, D.G.: Changes in the lipid composition of ripening banana fruits and evidence for an associated increase in cell membrane permeability. *Biochimica et Biophysica Acta-Biomembranes*, **1978**, 529(3), 454-60.

Weller, P., Breithaupt, D. E.: Identification and quantification of zeaxanthin esters in plants using liquid chromatography-mass spectrometry. *Journal of Agricultural and Food Chemistry*, **2003**, 51(24), 7044–7049.

Wieslander, Å., Christiansson, A., Rilfors, L., Lindblom, G.: Lipid bilayer stability in membranes. Regulation of lipid composition in *Acholeplasma laidlawii* as governed by molecular shape. *Biochemistry*, **1980**, 19(16), 3650-3655.

Wieslander, Å., Christiansson, A., Walter, H., Weibull, C.: Fractionation of membranes from *Acholeplasma laidlawii A* on the basis of their surface properties by partition in two-polymer aqueous phase systems. *Biochimica et Biophysica Acta-Biomembranes*, **1979**, 550(1), 1-15.

Wieslander, Å., Rilfors, L., Johansson, L. B.-A., Lindblom, G.: Reversed cubic phase with membrane glucolipids from *Acholeplasma laidlawii.* 1H, 2H, and diffusion nuclear magnetic resonance measurements. *Biochemistry*, **1981**, 20(4), 730-735.

Wieslander, Å., Rilfors, L.: Qualitative and quantitative variations of membrane lipid species in *Acholeplasma laidlawii A*., *Biochimica et Biophysica Acta-Biomembranes*, **1977**, 466(2), 336-346.

Wieslander, Å., Ulmius, J., Lindblom, G., Fontell, K.: Water binding and phase structures for different *Acholeplasma laidlawii* membrane lipids studied by deuteron nuclear magnetic resonance and x-ray diffraction. *Biochimica et Biophysica Acta-Biomembranes*, **1978**, 512(2), 241-253.

Williams, D. H., Bhacca, N. S., Djerassi, C.: Unusual chemical shifts in the nuclear magnetic resonance spectra of 7- and 11-keto steroids. *Journal of the American Chemical Society*, **1963**, 85(18), 2810, 2813.

Willmann, J., Thiele, H., Leibfritz, D.: Combined reversed phase HPLC, mass spectrometry, and NMR spectroscopy for a fast separation and efficient identification of phosphatidylcholines. *Journal of Biomedicine and Biotechnology*, **2011**, Article ID 385786, 8 pages.

Willstätter, R., Stoll, A.: Untersuchungen über Chlorophyll: Methoden und Ergebnisse. Berlin: Spinger, **1913**.

Xu, X., Bittman, R., Duportail, G., Heissler, D., Vilcheze, C., London, E.: Effect of the structure of natural sterols and sphingolipids on the formation of ordered sphingolipid/sterol domains (rafts). Comparison of cholesterol to plant, fungal, and disease-associated sterols and comparison of sphingomyelin, cerebrosides, and ceramide. *The Journal of Biological Chemistry*, **2001**, 276(36), 33540–33546.

Yamauchi, R., Aizawa, K., Inakuma, T., Kato, K.: Analysis of molecular species of glycolipids in fruit pastes of red bell pepper (*Capsicum annuum L.*) by high-performance liquid chromatography-mass spectrometry. *Journal of Agricultural and Food Chemistry*, **2001**, 49(2), 622-627.

Yamauchi, R., Analysis of molecular species of plant glycolipids by HPLC/APCI-MS, in: *Modern methods for lipid analysis by liquid chromatography/mass spectrometry and related techniques* (William Craig Byrdwell, ed.) *Champaign, Ill., AOCS Press,* **2005***, ch. 9, pp 431-446.*

Yang, X., Pang, X., Xu, L., Fang, R., Huang, X., Guan, P., Lu, W., Zhang, Z.: Accumulation of soluble sugars in peel at high temperature leads to stay-green ripe banana fruit. *Journal of Experimental Botany*, **2009**, 60(14), 4051-4062.

Yuan, J-P., Gong, X-D., Chen, F.: Separation and analysis of carotenoids and chlorophylls in *Haematococcus lacustris* by high-performance liquid chromatography photodiode array detection. *Journal of Agricultural and Food Chemistry*, **1997**, 45(5), 1952–1956.

Zamora, R., Gómez, G., Hidalgo, F. J.: Classification of vegetable oils by high-resolution 13C NMR spectroscopy using chromatographically obtained oil fractions. *Journal of the American Oil Chemists' Society*, **2002**, 79(3), 267-272.

Zeller, Friedrich J. "Herkunft, Diversität und Züchtung der Banane und kultivierter Zitrusarten", *Journal of Agriculture and Rural Development in the Tropics and Subtropics, Beiheft nº 81*, Kassel, Kassel Univ. Press, **2005**.

Zhou, B., Mattern, M. P., Johnson, R. K., Kingston, D. G. I.: Structure and stereochemistry of a novel bioactive sphingolipid from a *Calyx sp. Tetrahedron*, **2001**, 57(47), 9549–9554.

6. CURRICULUM VITAE

Name: Marcela Castro-Benitez
Date and place of birth: 24.7.1961, Bogotá, Colombia
Nationality: Colombian
Marital status: married with Camilo Umaña
Child: Diego Umaña

Academic Background

2007 to date. PhD student in the research group of Prof. Dr. Winterhalter.

2004. Diploma in teaching for Higher Education. Faculty of Education. Pontificia Universidad Javeriana. Bogotá, Colombia.

2001. Master of Agrarian Science, Area of Special Emphasis: Plant Physiology and Biochemistry of tropical fruits. Faculty of Agronomy, National University of Colombia, Bogotá.

1992-1994. Master Student. Institute of Plant Sciences and Genetics in Agriculture. Faculty of Agriculture, Food and Environment. The Hebrew University of Jerusalem, Israel.

1978-1984. Food Engineering. School of Natural Science and Engineering. Jorge Tadeo Lozano University. Bogotá, Colombia.

Professional Experience

2001 to date. Assistant Professor. Full time work. Biochemistry and Nutrition Department. Faculty of Science. Javeriana University. Higher Educational Institution. Bogotá, Colombia.

2004-2008. Academical and Technical Coordinator. Chemistry and Technological Network of Latin America Agribussines. LAGROTECH. ALFA -America Latina Academical Formation-programme of cooperation between Higher Education Institution of the European Union and Latin America. Development and Cooperation-EuropeAid, European Comission.

1998-2001. Researcher. Study of Chemistry and Biochemistry changes in fresh and processing food. Research group of Prf. Patricia Restrepo. Department of Chemistry. National University of Colombia, Bogotá.

1992-1994. Researcher. Postharvest Physiology. Research group of Dr. Edna Pesis. Department of Postharvest Science of Fresh Product. The Agriculture Research Organization of Israel. ARO. Bet Dagan, Israel.

1992-1994. Researcher. Plant Science in Agriculture. Research Group Prf. Dr. Emeriti Eliezer Goldschmidt. Institute of Plant Science und Genetics in Agriculture. Faculty of Agriculture, Food and Environment, The Hebrew University of Jerusalem. Israel.

1990-1991. Coordinator. Food Engineering Programm. Regional Center of Distance and Virtual Education. CREAD. Cartagena University. Cartagena, Colombia.

1988-1989. Quality Control Assistant. Industry of Food Mundy. LTDA. Bogotá, Colombia.

1986-1987. Assistant consulting. Asesorias Industriales S. A. Dr. Alvaro Iregui Borda. Food Technology Consulting. Bogotá, Colombia.

1984-1986. Assistant Coordinator. Interscience Programme of Biological Resources in Latin America. PIRB. Instituto Colombiano de la Ciencia y la Tecnologia. COLCIENCIAS. Bogotá, Colombia.

Awards and Grants

Awards and grant by German Academic Exchange Service (DAAD) for Doctoral Studies in Germany. Institute of Food Chemistry – Technische Universitat zu Braunschweig, 2007.

Awards and grant by the Programme ALFA-European Commission-EuropeAid Office for good results of the ALFA LAGROTECH Project and financial support to attend the Conference "*Good Practice and Results of ALFA II Projects*" (LAGROTECH International Network). Mexico, 21-22, May 2007.

Grant from The Agricultural Research Organization (ARO)-Ministry of Agriculture and Rural Development Center for International Agricultural Development Cooperation to attend the *International workshop on formulating policy national and regional agricultural research.* Tel-Aviv, Israel- September 2003.

Meritorious qualification to Master dissertation awarded by Academic Committee Resolution of Agronomy Faculty. National University of Colombia. Bogotá, Colombia. 2001.

Schooling

1976-1977 High School II- Colegio Santa Mariana de Jesús in
1972-1975 High School I -Colegio La Consolacion in Bogotá
1966-1971 Primary School -Colegio Reyes Castenblanco in Bogotá